

VOLCANIC EVOLUTION OF THE OTOWI MEMBER OF THE BANDELIER TUFF,
JEMEZ MOUNTAINS, NEW MEXICO

By

GEOFFREY WILLIAM COOK

A dissertation submitted in partial fulfillment of
the requirements for the degree of

DOCTOR OF PHILOSOPHY

WASHINGTON STATE UNIVERSITY
School of Earth and Environmental Sciences

DECEMBER 2009

To the Faculty of Washington State University:

The members of the Committee appointed to examine the dissertation of
GEOFFREY WILLIAM COOK find it satisfactory and recommend that it be accepted.

John A. Wolff, Ph.D., Chair

Peter B. Larson, Ph.D.

Dennis Geist, Ph.D.

VOLCANIC EVOLUTION OF THE OTOWI MEMBER OF THE BANDELIER TUFF,
JEMEZ MOUNTAINS, NEW MEXICO

Abstract

by Geoffrey William Cook, Ph.D.
Washington State University
December 2009

Chair: John A. Wolff

The 1.61 Ma Otowi Member of the Bandelier Tuff is a compositionally-zoned, high-silica rhyolite tuff showing internal upward decreases in the concentrations of incompatible trace elements. It is associated with the first major episode of collapse at the Valles caldera. Using a comprehensive methodology, the minimum eruptive volume of the Otowi Member has been recalculated at 335 km³ DRE. The plinian phase has been calculated at 45 km³ DRE. Based on these minimum calculations, it is likely that the original volume of the deposit was greater than 500 km³ DRE.

Prior studies suggested that the Otowi eruption began with a single, central vent and transitioned quickly to multiple ring vents as collapse ensued. This model has been evaluated by comparing vertical profiles in pumice chemistry and lithic abundances in outflow sheet sections around the caldera. Lithic distributions are surprisingly uniform around the caldera. Thus, a new model for eruption of the Otowi Member is presented here in which a single, central vent was responsible for the majority of the eruption. Lithic and chemical evidence indicate a vent shift late in the eruption towards the northeast as collapse ensued. However, multiple ring vents are not evident in the data. In addition, volume calculations of chemical types in the Otowi ignimbrites indicate a roughly equal tri-part distribution. This volume-constrained chemical data may prove useful in future petrogenetic studies on the Otowi Member.

TABLE OF CONTENTS

	Page
ABSTRACT.....	iii
LIST OF TABLES.....	vi
LIST OF FIGURES.....	vii
CHAPTER	
1. INTRODUCTION.....	1
Review of Caldera-Related Studies.....	1
Experimental Studies.....	36
Summary and Discussion.....	42
2. GEOLOGIC BACKGROUND.....	53
The Jemez Mountains Volcanic Field and the Valles Caldera.....	53
Purpose of the Study.....	57
Overview of Regional Geology.....	58
Volcanism in the JMVF.....	64
Overview of JMVF Stratigraphy.....	66
Petrogenetic History of the JMVF.....	75
3. VOLUME CALCULATIONS.....	88
Prior Studies and Rationale.....	88
Methods.....	94
Volume Calculations.....	104
Estimation of Errors.....	114

4. A LITHIC STUDY OF THE OTOWI MEMBER.....	130
Background.....	130
Results.....	141
Discussion.....	151
5. CORRELATION OF LITHIC DATA AND NB CONCENTRATIONS	174
Purpose.....	174
Background: Stratigraphy, geochemistry and zoning in the OM	176
Nb variations and comparisons to lithic population data.....	184
Summary	195
6. ERUPTIVE SEQUENCE AND CONCLUSIONS.....	217
Eruptive Sequence	217
Conclusions.....	225
BIBLIOGRAPHY.....	232
APPENDIX	
A. DACITE LITHIC GEOCHEMISTRY	248

LIST OF TABLES

3.1. Volume calculations for Zones A-M	118
3.2. Volume calculations for pre-Otowi paleostructures	119
3.3. Volume calculations for hypothesized Otowi outflow sheets.....	120
3.4. Final volume calculations	120
4.1. Lithic count data summarized by sample locality.....	157
4.2. XRF major element oxide geochemical data for unknown dacites	169
4.3. XRF trace element geochemical data for unknown dacites.....	170
4.4. Distribution of unknown dacite samples per sample locality	171
5.1. Proportions of Otowi chemical types.....	212
5.2 Chart of volumes and proportions of chemical types in the Otowi ignimbrite.....	213
5.3 Proportions of Otowi chemical types present in the plinian phase.....	214
5.4 Chart showing volumes of chemical types in the Otowi plinian phase	215

LIST OF FIGURES

1.1. Mechanisms of cauldron subsidence at Glen Coe Scotland	44
1.2. Adaptation of Cell theory of Wing Easton	45
1.3. Evolution of a caldera of the Krakatau type	46
1.4. The seven stages of resurgent caldera development (Smith and Bailey, 1968).....	47
1.5. Various caldera types proposed by G. P. L. Walker	48
1.6. Two stage eruptive model of Druitt and Sparks	49
1.7. Caldera components.....	50
1.8. Models of caldera subsidence	51
1.9. Experimental apparatus of Marti et al. (1994)	52
2.1. Map of the Rio Grande Rift and the JMVf	77
2.2. Study location map	78
2.3. Map of the Valles Caldera	79
2.4. Cross-sections of Nielson and Hulen (1984) and Heiken et al. (1986)	80
2.5a. Geophysical model (SW-NE cross-section) of the Valles caldera.....	81
2.5b. Cross-sections illustrating the development of the Valles caldera	81
2.6. Interpretation of the Lower Bandelier Tuff eruptive sequence.....	82
2.7. Map of the JMVf and surroundings	83
2.8. Revised stratigraphy for the JMVf (Goff and Gardner, 2004).....	84
2.9. Distribution of major stratigraphic groups in the JMVf	85
2.10. Diagram illustrating temporal ranges of JMVf units	86
2.11. TAS plot of intermediate to silicic pre-caldera rocks of the JMVf.....	87
3.1. Isopach maps of selected intracaldera units.....	121
3.2. Ignimbrite morphologies of Wilson (1991)	122

3.3.	Pre-caldera paleotopographic map of Potter and Oberthal (1987)	123
3.4.	Map of pre-Otowi paleosurface	124
3.5.	Map of zones used in volume calculations	125
3.6.	Isopach map for Guaje fall unit A.....	126
3.7.	Isopach map for Guaje fall units B-E	127
3.8.	Close-up view of isopach map for Guaje fall units B-E	128
3.9.	Calculations and plots used to determine plinian volumes.....	129
4.1.	Lithic distribution map of Potter and Oberthal (1987)	154
4.2.	Map of pre-Otowi geology.....	155
4.3.	Map showing locations used for sample collection across the JMVf	156
4.4.	Lithic distributions on pre-caldera geologic map	160
4.5.	Pie charts showing overall lithic fragment proportions	161
4.6.	Stratigraphic column for Guaje Canyon	162
4.7.	Stratigraphic columns for Pueblo Mesa, NE section, and Cebolla Canyon.....	163
4.8.	Stratigraphic column for Cat Mesa	164
4.9.	Stratigraphic column for Wildcat Canyon	165
4.10.	Stratigraphic column for Dixon Ranch.....	166
4.11.	Stratigraphic columns for Upper Cochiti Canyon and the Airport section.....	167
4.12.	TAS diagram comparing dacite lithic geochemistry	168
4.13.	Selected geochemical data used in determining dacite lithic provenance.	172
4.14.	Hypothetical lithic distributions based on the ring-vent hypothesis.....	173
5.1.	Sample locations for geochemical analyses of whole pumices	199
5.2.	Volumes and compositions of magma erupted from known caldera systems	200
5.3.	Nb versus height in stratigraphy at Guaje Canyon	201
5.4.	Nb versus height in stratigraphy at Cat Mesa A	202
5.5.	Nb versus height in stratigraphy at Cat Mesa B	203
5.6.	Nb versus height in stratigraphy at Wildcat Canyon	204

5.7. Nb versus height in stratigraphy at Pueblo Mesa	205
5.8. Nb versus height in stratigraphy at Seven Springs	206
5.9. Nb versus height in stratigraphy at Dixon Ranch (Location 14)	207
5.10. Nb versus height in stratigraphy at Upper Cochiti Canyon	208
5.11. Nb versus height in stratigraphy at the Airport Section.....	209
5.12. Nb versus height in stratigraphy at Locations 13 and 27	210
5.13. Nb versus height in stratigraphy at Location 17	211
5.14a. Pie chart showing proportions of chemical types in the Otowi ignimbrite.....	216
5.14b. Pie chart showing proportions of chemical types in the Otowi plinian	216
6.1. Eruptive sequence stage one	227
6.2. Eruptive sequence stage two.....	228
6.3. Eruptive sequence stage three.....	229
6.4. Eruptive sequence stage four	230
6.5. Eruptive sequence stage five.....	231

Dedication

This dissertation is dedicated to my wife, Heather.

Without her endless emotional and intellectual support this work would not have been possible

CHAPTER ONE

INTRODUCTION TO CALDERA STUDIES

Large pyroclastic eruptions and associated caldera collapses are among the most catastrophic events in geologic history. The largest known calderas can have dimensions of up to 80 km, such as Toba caldera in Indonesia. Volumes of erupted materials can range from hundreds to thousands of cubic kilometers; examples include the 5000 km³ of material that emanated at approximately 27.8 Ma from the La Garita caldera in the San Juan volcanic field of southwestern Colorado (Lipman et al., 1984), the 2500 km³ erupted from the Yellowstone caldera at approximately 2 Ma as the Huckleberry Ridge Tuff (Boyd, 1961), and the 600 km³ of material that erupted approximately 760 ka from Long Valley caldera as the Bishop Tuff (Hildreth, 1979; Hildreth and Mahood, 1986; Wilson and Hildreth, 1997).

During the past century, significant advances have been made in comprehending the nature of large volcanic eruptions and consequent caldera collapse. Despite this, there is still a great deal to be learned about caldera eruptions and collapse processes. The general mechanism is well understood: eruptions of large ignimbrites lead to the evacuation of a magma chamber that causes the unsupported overlying crust to collapse downward. The most common model invoked in this scenario is the “piston” or “plate” collapse in which a disc-shaped plug of crust settles neatly into the void vacated by the erupting material. However, the processes responsible for caldera formation may be far more complex and thus the aforementioned model simply represents an end-member process (Walker, 1984). There is a great deal of information that has yet to be learned regarding the mechanisms and timing involved in large caldera-forming eruptions.

The term “caldera” comes from the Spanish word for kettle or cauldron. Its roots lie in the Latin word ‘calderia,’ which translates to ‘boiling pot.’ Initially, the term was used in the Canary Islands to describe bowl-shaped topographic depressions. The definition has changed with time, but it is generally used to describe large, circular collapse structures associated with volcanic eruptions. Typically, the term caldera is used to define a geomorphologic feature resulting from collapse or subsidence associated with an eruption. The term cauldron is now used to define a structural feature that represents the eroded remnant of a past caldera-collapse event (Komuro et al., 2006), where most of the eruptive material associated with caldera collapse has been removed, exposing older rock units beneath the former caldera floor (Cole et al., 2005).

The first studies on calderas were conducted in the late 18th and early 19th centuries. The majority of early studies assumed that calderas and volcanic craters were created solely by explosive fragmentation of a volcanic edifice. In the early 19th century Leopold vön Buch, a student of Abraham Werner and a Neptunist, examined the Caldera de La Palma (now known as Caldera de Taburiente) and described it as an ‘ehbungskratere’—an elevation crater. Based on his studies vön Buch proposed two classes of volcanic craters including one in which craters form through explosion and one in which craters are formed by uplift. The first class was in keeping with prevailing doctrine at that time, which revolved around the concept that ejecta from explosive eruptions and more passive lava flows accumulated around vents to create a volcanic mountain; the second class was attributed to growth of the volcano by inflation from below. The latter concept was referred to as craters of elevation theory by vön Buch (1820) and it was based mainly on studies that he conducted in the Auvergne region of France and in the Canary Islands (MacDonald, 1972). The craters of elevation hypothesis stated that volcanoes were not formed by accumulation of volcanic products around a vent; rather, it was suggested that upward

pressure from molten material at depth caused up-warping of formerly horizontal lava flows to create the volcano. Two observations were made by von Buch at La Palma that led him to develop this idea: First, he observed coarse-grained granitoid rocks in the summit crater. To von Buch, this implied elevation since granitic rocks were believed, in the Neptunian way of thinking, to represent the lowest or primary portion of rock sequences. Second, he believed that the slopes of the volcano were too steep to allow flows to accumulate on them and thus must have been uplifted (von Buch, 1820; translated in part by Macdonald, 1972).

Many geologists of the time, including Charles Lyell, Charles Darwin, and George Poulett-Scrope were opposed to craters of elevation theory. Poulett-Scrope conducted field work on numerous volcanoes in Italy, France, and elsewhere in Europe, and published one of the first major volcanological studies *Considerations on Volcanos* (Poulett-Scrope, 1825). In this work Poulett-Scrope challenged the theory of craters of elevation, arguing that volcanoes were not ‘craters of elevation,’ but instead ‘craters of eruption’ formed from accumulation of lavas on steep slopes. Poulett-Scrope pointed out that all of the layers of rock exposed in volcanic vents were ejected from the vent itself, and that volcanic cones did not exhibit evidence of significant uplift such as cracking and swelling (Macdonald, 1972). Thus, volcanic cones could not be formed by uplift alone as the craters of elevation hypothesis suggested.

Lyell was also highly skeptical of von Buch’s theory that the summit crater at La Palma was formed through upheaval of lavas and suggested instead that it was likely related to explosion. In *Principles of Geology* (Lyell, 1830 and later editions) Lyell used observations from Mt. Etna, Stromboli, and Mt. Vesuvius in an attempt to discredit “craters of elevation.”

Despite this opposition, two French geologists, Pierre Armand Dufrenoy and Jean-Baptiste Élie de Beaumont, embraced the concept. In particular, de Beaumont offered evidence

supporting the theory in his 1836 study of Mt. Etna in Sicily (de Beaumont, 1836). In this paper (published in French and later summarized by McBirney, 1990), de Beaumont pointed out that lava flows on the flanks of the volcano were uniform in thickness and resting at angles of nearly 30 degrees. He wondered how it was possible for these flows to accumulate in such a manner on such steep slopes when it was common knowledge that lava flows will move downhill under the influence of gravity on slopes of as little as 3 degrees. Furthermore, he noted that the volcano had only added approximately 1.25 meters to its height in 2000 years. De Beaumont concluded that the volcano grew not by accumulation of erupted materials but through uplift (de Beaumont, 1836). Lyell later used observations from Etna to challenge the conclusions of de Beaumont and von Buch. However, it took until 1859 before the arguments of Lyell and Poulett-Scrope took hold and craters of elevation was largely discredited (Macdonald, 1972). Throughout the debate, Lyell was careful to note that de Beaumont was, in fact, a meticulous field geologist and that his study of Etna was a valuable and well written contribution to the literature (Chester et al., 1985).

The fundamental idea that calderas are formed through collapse was first suggested in 1879 by Ferdinand Fouqué (Fouqué, 1879 and later translated by A.R. McBirney). In a study of the Greek isles of Santorini, Fouqué determined that the prominent central bay existing between the isles of Thera and Therasia must have resulted from collapse of a large central block associated with a large eruption. He vehemently rejected the “craters of elevation theory” and dismissed the concept that the caldera had been blown out. Fouqué identified several key pieces of evidence to support a collapse origin. First, it was necessary to estimate the total volume of erupted material, which he determined to equal approximately 60 km^3 . Within the erupted material, accidental fragments only accounted for a small (1-10%) proportion of the overall volume. In addition, significant tephra deposits were not found on nearby islands. Fouqué

concluded that if all the missing material in the bay were explosively removed, the amount of ejecta should be several orders of magnitude larger. By his calculations, the erupted volume could range from 600-6000 km³. Consequently, he suggested a new idea, one in which a large eruption was followed by a collapse of the volcanic edifice (Fouqué, 1879).

Fouqué proposed two potential mechanisms for collapse. The first was that compaction of marine sediments allowed for subsidence of the volcano. The second was that downward collapse of a coherent central block in the volcano caused a large crater. Of all the theories relating to caldera formation until this point in time, only the collapse model could account for the steep slopes of the crater and the distinct lack of accidental fragments in pyroclastic deposits (Fouqué, 1879). Fouqué even went as far as to suggest that collapse events could trigger large-scale eruptions and not the converse. The idea that discharge of magma in calderas is a consequence and not a cause of collapse is a concept that was only revived over 100 years later (Druitt and Sparks, 1984).

Another major caldera study (Verbeek, 1885) was conducted soon after the eruption of Krakatoa in 1883. This eruption was catastrophic, killing approximately 36,000 on the Indonesian islands of Java and Sumatra, primarily by the large tsunami that was created. Although the 1815 eruption of Tambora was significantly larger, the 1883 Krakatoa eruption garnered far more attention and ranks as one of the best-studied caldera events of all time. Two factors contributed to this increased scrutiny: First, communication technology in 1883 had advanced to the point where news of the eruption was broadcast around the world almost instantaneously. Second, by 1883 there existed a significantly heightened sense of scientific curiosity in the west about natural phenomena.

In his 1885 study, Dutch geologist R.D.M. Verbeek dismissed explosive coring as a primary mechanism and identified collapse as the likely cause of caldera formation. Verbeek recognized that the volume of lithics in the erupted materials was far less than the volume of material missing in the caldera. He concluded, like Fouqué before him, that the bulk of the volcano had collapsed downward into a void space created by the evacuation of magma during the eruption. Verbeek also suggested that re-melting within the volcano may have weakened the edifice, thereby contributing to collapse (Verbeek, 1885).

The late 19th century and early 20th centuries saw several significant studies of calderas. Dutton (1884) conducted a study on the origins and evolution of volcanism and the formation of craters in Hawaii. In this investigation, Dutton introduced the term caldera in American scientific literature to describe collapse structures in the Hawaiian Islands. Diller and Patton (1902) described the history and geology of Crater Lake in Oregon. The geology of the caldera, including its structure, petrology, and petrography was examined in detail. The overall goal was to reconstruct Mount Mazama, the stratovolcano that was present prior to caldera formation approximately 7700 years before present.

A major milestone in caldera study was in 1909, when Clough and his colleagues presented a paper focusing on the evolution of Glen Coe Cauldron in Scotland (Clough et al., 1909). Glen Coe in western Scotland is a deeply dissected caldera approximately eight kilometers in diameter that erupted roughly 420 Ma (Clough et. al, 1909). The cauldron, as Clough and co-workers called it, was interpreted as having formed via subsidence of a coherent, piston-like block along steeply dipping ring faults (Clough et al., 1909; Moore and Kokelaar, 1998). The ring faults were found to be steeply dipping on the surface and it was assumed that they behaved in similar fashion at depth (Clough et al., 1909). The general sequence is shown in

Figure 1.1; although, it is interesting to note that the ring faults in this diagram are drawn nearly vertical. The authors state, however, that they do not regard the diagram as “anything more than diagrammatic” (Clough et al., 1909).

In addition, it was envisioned that simultaneous intrusion of magmas into the ring faults accompanied caldera subsidence, thereby forming a complex series of ring dikes around the cauldron (Clough et al., 1909). Ring fault controlled subsidence became a simple and easily evoked caldera collapse model that was applied to not only deeply dissected calderas but to younger volcanic systems as well. Later in the 20th century, it would become increasingly evident that a greater diversity in processes exists at many calderas worldwide (Roberts, 1974; Walker, 1984; Scandone, 1990; Branney, 1995; Lipman, 1997; Moore and Kokelaar, 1998)

From 1909 to the early 1940’s the concept of collapse as a caldera-forming mechanism was becoming more established, but the literature lacked a well-defined classification scheme for the variety of caldera types. The studies that surfaced during this time dealt mainly with exploration and recognition of previously unknown calderas and the development of a classification scheme (McBirney, 1990). Daly (1914), Walker (1928), Tanakadate (1930), Reck (1936), and Van Bemmelen (1939) all proposed classification systems for calderas. Burbank et al. (1933) examined the evolution of the San Juan Volcanic Field in Colorado. In addition to providing a classification, Van Bemmelen (1939) recognized Toba in Indonesia as a large caldera. The absence of a unified classification scheme effectively ended in 1941, when Howell Williams of the University of California wrote a seminal treatise on caldera evolution entitled *Calderas and their Origins* (Williams, 1941).

In *Calderas and their Origins*, Williams provided an in-depth literature review of the ideas available up to that time. He enthusiastically attacked the stale concept that the explosive

shattering of vents was the main process involved in the creation of volcanic depressions.

Williams also proposed a universal classification scheme for different types of calderas.

Although this scheme has been modified over the past 65 years, it is still significant and deserves recognition as the first attempt to organize the taxonomy of calderas.

Williams's first task was to address confusion relating to nomenclature. He pointed out that in the science of volcanology no term had undergone more changes in meaning and usage than caldera. Williams noted that originally the term 'caldera' was used in the Canary Islands to describe natural depressions. On this subject, it is interesting to consider that some Canarian 'calderas' are actually not calderas in the modern sense of the word. A classic example of this is Caldera de Taburiente on La Palma, which represents a lateral avalanche scar and not a vertical collapse. The Valle del Bove on Mt. Etna is another example of a lateral landslide scar that has been associated with the term caldera (Walker, 1984). Early researchers such as von Buch thus used the term caldera for features that were not necessarily associated with an eruption. The confusion between lateral and vertical collapse continues to cause nomenclature problems to this day.

In his discussion, Williams noted that Dutton (1884) later used the term caldera to describe collapse structures in the Hawaiian Islands. He suggested that most geologists in the early 20th century had varied opinions on the meaning of the term. For example, Sandberg (1927) proposed that there was no difference between a caldera and a crater and that size was the only distinguishing structural factor. Others, including Escher (1929) maintained that for a structure to truly represent a caldera, it must have a flat floor and steep inner walls (Williams, 1941). Regarding the definition of the word caldera, it is evident that in *Calderas and their Origins*, Williams was influenced a great deal by German geologist Hans Reck. In 1936, Reck

proposed the following interpretation of the term caldera in which he delineates seven specific criteria: 1) Calderas are related to volcanic topography. 2) Calderas are characterized by their “centric structure.” In other words, regardless of whether the edifice is vented outward or collapses inward, the structure remains roughly circular. 3) Calderas are different from craters not only in size but also because craters are directly associated with the magmatic conduits of a volcano. To clarify, craters are typically situated directly above a conduit, whereas large portions of calderas may be far from eruptive vents. 4) A fundamental difference is that a crater is an eruption vent; whereas, a caldera is never a vent but it may contain vents within its structure. 5) Calderas are the result of changes (either state or volume) in the underlying magma reservoir. 6) Craters form within the tops of constructional features (i.e. positive features) such as cones and domes; calderas are collapse features (i.e. negative features) and are associated with an emptied magma chamber. 7) Craters are associated with active, young phases of volcano growth, whereas, calderas are a mark of “decadence and age” regardless of whether a later renewal of activity takes place (Reck, 1936).

Williams’s own summary defined a caldera as “a large, circular volcanic basin produced by engulfment.” He also went so far as to differentiate between calderas and craters, which he later described as constructional features forming from accumulation of tephra around a vent (Williams, 1941).

The next segment of the discussion is a review of five prominent, pre-1941 caldera classification schemes. The first, proposed by Daly (1914), divided calderas into four main morphological types: true calderas, sinks, sunken calderas, and volcanic rents. True calderas were related to explosion and may either be simple or nested. Sinks were ascribed to collapse that was not associated with an explosion. Sunken calderas were related to post-explosion

subsidence. Finally, volcanic rents were explained as resulting from the horizontal tearing apart of cones (Daly, 1914).

Walker (1928) divided calderas into two types: explosion calderas and subsidence calderas. Explosion calderas were classified as “volcanic depressions more than a mile across.” Subsidence calderas were subdivided into Kilauea type and Katmai type. Kilauea type calderas were designated as those formed via engulfment following recession of lava in the conduit. Katmai type calderas were classified as those formed through explosion of silica-rich magmas and subsequent collapse of the crater (Walker, 1928).

The third system, proposed by Tanakadate (1930), suggested that all calderas were fundamentally related to collapse. Three classifications were proposed: crater-type, depression-type, and *conca*-type. Crater type calderas were defined as circular or oval-shaped calderas situated at the summit of a volcano. Examples given were Aso and Hakone in Japan. Depression type calderas were defined by Tanakadate as basins without distinct rims, many of which are modified by erosion. Examples given included Sikots, Towada, and Koya calderas of Japan. *Conca* type calderas (*conca* is an Italian term used to describe a depression) were defined as shallow depressions that have gently-sloping inner walls. A classic example— Lago di Bolsena, Italy was given, and it was noted that Akan and Inawasiro in Japan were similar (Tanakadate, 1930). Tanakadate also distinguished central from lateral calderas. As the names imply, in the former, engulfment occurs about a central vent; while in the latter depressions are created due to escape of magma from adjacent volcanoes. Williams noted, perhaps a bit harshly, that few will agree to Tanakadate’s use of terms since “crater-caldera is contradictory” and “depression caldera is redundant” (Williams, 1941).

In the fourth classification scheme, Van Bemmelen (1939) subdivided what he terms “negative volcanic forms” into two groups. The first group included depressions caused by explosion, such as craters and maars. The second group included depressions caused by collapse, which were tentatively termed calderas. Of the calderas, he further subdivided them into three types, including central, depression, and conca type (Van Bemmelen, 1939).

Finally, Williams reviewed Hans Reck’s classification (Reck, 1936) which was comprised of two main groups: calderas formed by endogenous forces and those formed by exogenous forces. The endogenous grouping included four subdivisions: explosion calderas, rückflussskalderen, intrusion calderas, and collapse calderas. Explosion calderas, such as Krakatoa and Santorini were attributed to collapse brought on by partial emptying of magma chambers during violent explosive eruptions. This concept is similar to Daly’s (1914) sunken calderas, and it is also quite similar to the modern view of caldera collapse in which engulfment is related to loss of magmatic support. Rückflussskalderen (rückfluss means ‘a withdrawal’) were explained as collapse forms in which loss of support was initiated by an internal melting process. Intrusion calderas were related to either cryptovolcanic activity or deep-seated movement of magmas. Cryptovolcanic activity is characterized by subterranean volcanic explosions where little or no magmatic material is erupted on the surface, and thus the activity is hidden or largely unknown. Examples given include the Bosumtwi caldera of West Africa and the Steinheim basin of Germany. Collapse calderas, such as Kilauea and Askja were related to magma withdrawal and subsequent loss of crustal support.

The exogenous grouping includes erosion calderas, such as La Palma and deflation calderas, such as those found in Southwest Africa. Williams (1941) noted that all of the endogenous calderas of Reck (1936) were related in some way to engulfment. He also suggested

that it would be more appropriate to group all of the exogenous calderas as ‘erosion calderas’ because some had been modified by wind and others by water (Williams, 1941).

Based in part on the previous work of others, and in part on his own ideas, Williams presented his preferred classification for calderas. He delineated six categories (A-F) of caldera types. Those grouped in category A were termed explosion calderas. These calderas are formed through explosive shattering of a volcanic edifice, a concept that had been suggested for nearly 150 years. Williams noted that these types of calderas are not only rare but are typically very small (2-3 km) in diameter.

Category B included the so-called collapse calderas. Williams sub-divided this category into six models named primarily for type localities including Krakatau type, Kilauea type, Katmai type, cryptovolcanic type, Glen Coe type, and what he described as miscellaneous collapse types. Krakatau type calderas were described as being formed by engulfment followed by a small eruption of juvenile material. Kilauea type calderas were associated with shield volcanoes. They were described as having undergone rapid effusion of lava from flank vents that causes foundering of the central vent, thus creating a small central caldera. Katmai type calderas were suggested to be formed through internal melting of pre-existing lavas beneath a volcano that enlarges the magma chamber and subsequently forces the edifice to collapse inward. Cryptovolcanic type calderas were suggested to be formed through “muffled” volcanic explosions in which there is little or no escape of magma on the surface. These eruptions were considered to represent “products of more or less abortive attempts to blast diatremes and produce surficial explosion maars” (Williams, 1941). Glen Coe type examples, named for Glen Coe in Scotland (Clough et. al, 1909), were described as collapses of a coherent roof block along well-developed ring fractures. This is the so-called “stopping” discussed by Clough et al. (1909).

Finally, the miscellaneous calderas are an assortment of collapses produced by changes in the shapes or volumes of magma chambers beneath the volcano.

Williams' category C included erosion calderas. These are described as calderas forming from erosion of pre-existing caldera types. It is also suggested that they may represent enlargement of craters within existing calderas. Examples given are Papenoo in Tahiti and the Banks Peninsula of New Zealand.

Categories D and E are calderas that are associated with structural deformation of a volcanic edifice that is not necessarily related to eruption. Calderas in Category D were termed volcanic grabens. These structures were described as trench-like valleys on the slopes of volcanic cones. They may exist as summit grabens found at the peak of the edifice, or, as sector grabens found on the flanks of the cones. Haleakala Crater on Kilauea Volcano in Hawaii is an example of the former. Examples of the latter include Stromboli and the Somma on Mt. Vesuvius, Italy.

Category E consisted of volcanic rents or fissure troughs. Daly (1933) suggested the use of the term "volcanic rents" to describe depressions formed on volcanic cones in response to lateral magma displacements. An example given is the island of St. Helena, where it is suggested that a cone was torn apart due to the injection of dikes. Other examples given include the Bandoeng ridge (entertainingly termed a "geotumor" by Van Bemmelen) and the Tengger massif, both of Java, Indonesia (Williams, 1941). Williams supports Daly's (1933) assertion that these structures form via horizontal movements that literally "tear apart" the edifice (Williams, 1941).

In a modern discussion of caldera types, categories D and E are more appropriately considered to represent structural deformation associated with magma movement, intrusion, or

withdrawal in the shallow subsurface. Examples include flank collapse scars and slump scarps, such as those observed at Pu'u O'o on Hawaii and sector collapses associated with vent shifts such as those that have occurred at Stromboli. As such, they are not necessarily calderas.

The final category (F) in Williams's classification is termed "major volcano-tectonic depressions." This classification includes subsidence structures that are associated with fissure eruptions instead of those emanating from central vents. Examples include a portion of the North Island of New Zealand that lies between two major structural axes and is home to late-Tertiary to recent volcanism, and the Barisan Rift Zone of Sumatra, Indonesia (Williams, 1941).

In the final portion of his paper, Williams shifted the focus from classification of caldera types to an examination of physical mechanisms involved in creation of calderas. He addresses a number of key theories, providing a criticism for each, and eventually offers his own synthesis of the issue.

The first reviewed was von Buch's craters of elevation theory. Williams makes short work of the idea, claiming that it was "short-lived" and that within a few years of its inception, Lyell and Scrope had "given it the coup de grace" based on their studies on volcanoes such as Mt. Etna and those elsewhere in Europe (Williams, 1941).

The next theory discussed is the long-standing explosion hypothesis in which a caldera is directly related to a large explosive eruption, and its size is proportional to the intensity of the eruption. Williams pointed out that the theory is inadequate because more often than not, there is a disparity between the amount of observed ejecta and the amount of missing material in a caldera. Furthermore, the relative scarcity of lithic fragments in many eruptions, such as at Krakatoa where only 1/20th of the ejecta are lithics, discredits the explosion theory. Williams

stated, “Clearly these volcanoes did not blow their heads off; on the contrary, they were disemboweled and their heads caved in” (Williams, 1941).

The gas coring theory of Escher (1929) proposed that in some eruptions, large cylinders are drilled out by explosion and subsequently, the walls of the structure slide in, thus creating a depression. The idea was developed from his study of Perret’s work on the 1906 Vesuvius eruption. Escher’s contention was that the processes operating at Vesuvius are a small-scale analogue of larger caldera forming processes. Furthermore, he concluded that more violent eruptions would produce progressively larger funnel-shaped cylinders. Escher utilized artificial, scale-model volcanoes and through his experimentation determined that the radius of the proposed cylinder is a direct function of gas velocity in the conduit. He also derived a formula capable of determining the maximum attainable depth of the cylinder. Williams immediately discredited the gas coring concept, arguing that huge volumes of lithics would need to be erupted prior to caldera formation in order to accommodate the theory. He concluded that the gas coring mechanism may in fact account for moderate craters but cannot explain caldera formation (Williams, 1941). It is significant to note that despite Williams’s objections, Escher’s gas coring theory does provide a good description of the processes that form diatremes. Diatremes are small, funnel-shaped collapse structures typically less than 2 km in diameter.

The mantle pipe hypothesis of Sandberg (1928) suggested that calderas and craters are fundamentally formed in similar fashion and that the only difference between them is their size. This theory proposed that magmatic conduits of volcanoes are initially very large (of caldera proportions) and that they shrink progressively with time as they are filled in with eruptive material. An example is Mt. Vesuvius, where the Somma is presumed to represent the initial conduit and volcanic activity since the A.D. 79 eruption represents subsequent narrowing of the

vent (Williams, 1941). Four significant problems are associated with this theory. The primary objection is that if conduits are opened by explosion, there should be extremely high lithic proportions in the erupted products. This is simply not the case at the majority of the world's calderas. Williams's second objection stated that "no known volcanic neck has the diameters of a caldera and no known caldera is active over its entire surface." A third issue pointed out is that the theory cannot account for straight-sided volcanic grabens and calderas bordered by non-volcanic rocks. Finally, Williams pointed out that in order to form huge vertical conduits, the explosions would (out of necessity) be emanating from great depths and would be of "quite improbable magnitude" (Williams, 1941).

An interesting theory addressed is that of internal solution in volcanic conduits. First suggested by von Hochstetter in 1871, the concept that internal melting of the volcano could lead to its collapse was later adopted by Verbeek in his study of Krakatau. Verbeek (1885) concluded that the collapse at Krakatau was brought about in the following sequence of events: First, internal melting of old lavas results in enlargement of the magma chamber; next, foundering of the cone into the void space occurred; finally, seawater rushed in and was followed by explosions (Williams, 1941). In stark contrast, Fouqué dismissed the concept of internal solution citing a lack of field evidence to support it. Later, Fenner (1920) and Griggs (1922) would support internal solution to explain eruptive processes at the eruption of Mt. Katmai in 1912 (Williams, 1941).

It is interesting to note that internal solution is fundamentally related to modern ideas regarding magma chamber growth and formation. It is now acknowledged that silicic magmas can be generated relatively quickly prior to an eruption. This is accomplished through crustal melting related to the heat associated with basaltic intrusions. Bindeman and Valley (2003) and

Bindeman et al. (2006) have used oxygen isotope data and U-Pb zircon geochronology to demonstrate that magmas in the southwestern Nevada volcanic field (SWNVF) were derived quickly through crustal melting and assimilation of hydrothermally-altered country rock beneath the volcanoes.

Daly (1914) envisioned vertical-sided magma chambers in most volcanic systems. Easton (1916) challenged this notion, reasoning that in a vertical-walled magma chamber where conduits to the surface feed from the top of the chamber, drawdown during eruptions would soon make it impossible for eruptions to continue, and consequently the volcano would soon become extinct. This reasoning led him to propose that magma chambers in all volcanoes except for the Hawaiian type must be either inclined or of “wide vertical extent,” which presumably means both deep and broad in cross-section. In these asymmetric chambers, he suggested that conduits to the surface must tap lower levels on the roof of chambers as seen in Figure 1.2 (Easton, 1916). An eruptive scenario in this type of chamber would proceed as follows: An initial eruption from the conduit *C-E* forces magma drawdown to the *A-A* level. Gas pressure builds up in the overlying vacated space and pushes out more magma from the conduit, thus drawing magma levels down to the *B-B* level. This process is repeated, with volcanism becoming more explosive and less effusive as the edifice on the surface builds up, until magma levels reach the *C-C* level, essentially even with the conduit *C-E*. At this point, the system enters the solfataric stage in which the conduit is effectively plugged, thus forcing gases to escape to the surface through fissures in the roof. During gas escape, Easton suggested that the fissures would be widened and that melting occurs, thus creating new magmas that would percolate downward. Easton stated that “the lowest part of the volcano will consist at last of a solid skeleton with an infinite number of cells, differing greatly in size and shape, while the feeding chamber is gradually infilled with

magma and the gases above the magma attain ever increasing tension.” As gases are rising vertically in this scenario, the cells are thought to assume cylindrical forms. Easton termed this overall scenario “cell” theory, and two potential outcomes of the process were identified. First, the weight of the overlying volcano is too much for the “honeycombed” cell structure and collapse ensues. Because the cell structures are vertical, so is the collapse structure. Second, gas tension may increase until magma is forced explosively from the conduit and the cell structure. Massive engulfment ensues, and a vertical-walled caldera structure is formed.

In response, Van Bemmelen (1929) and Williams (1941) provided a number of pieces of evidence to discount cell theory: 1) No dissected volcanic structure has been found that shows cell structure; though, it is unlikely that the structure would be preserved. 2) The theory requires all calderas be eccentric with respect to their cones, and that they should occur near the bases of the cones to be in keeping with Easton’s diagram in Figure 1.2. 3) Extensive solfataric and fumarolic activity should be found on the flanks of cones that would be particularly active prior to eruption, and this has not been observed. 4) Large volumes of the lower portions of the volcanic edifice and the country rock beneath the volcano would be melted and would thus contaminate the magma, which has not been observed. (Note: see earlier discussion of Bindeman and Valley, 2003, and Bindeman et al., 2006, where this phenomenon has been verified in large silicic calderas such as Timber Mtn. Nevada and Yellowstone, Wyoming) 5) As the conduit became blocked when magma levels were drawn down sufficiently, eruptions would be expected to occur at the base of the edifice where the roof of the magma chamber is thinnest. This is not commonly observed. 6) The theory cannot account for straight-walled summit grabens. 7) Most calderas have simple outlines that do not agree with the idea of collapse of a complex “cellular” roof block.

After presenting his preferred classification system and examining the multitude of theories on caldera formation available at the time, Williams discussed the mechanism that he believed to be most significant in caldera formation: Collapse involving withdrawal of magmatic support. He stated, “It is primarily the rapid evisceration of the magma chamber which leads to crustal foundering and the production of calderas, summit, and sector graben, and the still larger volcano-tectonic depressions discussed in this paper” (Williams, 1941). Figure 1.3 is a schematic diagram modified from Van Bemmelen (1929) illustrating the aforementioned processes in a Krakatoan caldera (Williams, 1941). What is essential in the processes is that replenishment of magma from beneath is too slow to cope with evisceration and consequently a void space and collapse is inevitable (Williams, 1941). This is easily justified when we consider that volatiles rapidly decrease in concentration in the residual (non-erupted) magma and hydrostatic pressure in the chamber decreases significantly following violent eruptions. The residual magma is under less pressure and is likely more crystal-rich. Thus, it is more viscous than the erupted material (depending on the degree to which it has crystallized) and is less capable of replenishing the chamber fast enough to support the overlying crust.

In *Calderas and their Origins* Williams makes two main assertions, the first being that calderas formed by the explosive shattering of an edifice are typically small (< 1 km) and rare. The second is that the fundamental cause of caldera formation is engulfment following loss of magmatic support. Several causes for loss of magmatic support are proposed, including degassing and contraction of cooling magma, rapid outpouring of lavas from fissures such as at Kilauea, and large-scale plinian eruptions in which vast quantities of pumice and ash are ejected into the atmosphere. Although essentially a literature review, Williams’ work was strongly influenced by his vast field experience and years of intense study. It is a landmark effort in that

it analyzed and organized nearly all ideas relating to caldera formation up to the 1940's. Most aspects of his work are still valid today, and it continues to be respected as a major contribution.

The 1960s and 1970s saw a resurgence of interest in calderas and publications on caldera forming processes. Significant new work on the evolution of calderas was advanced by a number of researchers. Boyd (1961) investigated the nature of volcanic deposits at Yellowstone Caldera in Wyoming. Although the work is chiefly concerned with description and interpretation of ignimbrites in the region, it provided significant insight into volcanism at Yellowstone. This, coupled with the fact that Yellowstone is one of the largest resurgent calderas on the planet makes the study worthy of mention in a review of caldera studies.

Yokoyama (1963) and McCall (1963) illustrated the use of geophysical data (gravimetry) in delineating the structure of collapse calderas. Yokoyama's study used gravity anomalies to estimate total erupted material from a volcanic edifice. A total of eight calderas and three stratovolcanoes in Japan were used in the study, which found that low gravity anomalies commonly occur in calderas where large ignimbrites have been erupted (Yokoyama, 1963). McCall examined several calderas in the East African rift valley, also discovering significant gravity anomalies marking collapse structures (McCall, 1963).

Yokoyama (1966) alluded to an explosion hypothesis for caldera formation based on gravimetric, geologic, geomagnetic, and seismic surveys of Japanese calderas. In this study, smaller calderas were found to have large gravity anomalies, while larger calderas (those with a diameter > 20 km) were typically characterized by low-gravity anomalies. The small calderas with high gravity anomalies were attributed to upheaval of basements beneath the calderas (Yokoyama, 1966). The author proposed that the bigger calderas represented highly-explosive events in which large amounts of ejecta were blasted out of the vent. In essence, it was implied

that the larger calderas were eviscerated structures formed by explosion. This idea is akin to the explosive gas coring hypothesis proposed by Escher (1929) and it would later form the basis for establishment of the funnel-shaped caldera morphology of Yokoyama (1981; 1983).

Of particular note are the contributions of R.L. Smith, R.A., Bailey, and C.S. Ross, who wrote a number of landmark papers relating to caldera evolution and ash flow magmatism. Their work focused primarily on the Valles caldera, New Mexico. Their accomplishments are significant and include providing a framework for the study of ash flows, creating a model for the evolution of resurgent calderas, investigating the petrologic origins of large silicic magma chambers associated with calderas, and describing in great detail the geology of the Valles caldera in New Mexico.

Although they are not strictly focused on calderas, the contributions of Smith and Ross during the early 1960s on the subject of ash-flow tuffs are notable. Smith, (1960a, b) provided a sorely-needed and well-documented explanation of ash flows and depositional mechanisms. Later, in 1961 Ross and Smith published “Ash flow tuffs, their origin, geologic relations, and identification” (Ross and Smith, 1961). In the introduction to the 1979 GSA special paper on Ash Flow Tuffs, editors Chapin and Elston note that “the documentation in these papers was so thorough—including a large number of excellent photographs of outcrops, hand specimens, and thin sections—that even a beginning student could easily grasp the subject” (Chapin and Elston, 1979). Certainly, these papers are invaluable to anyone studying silicic calderas and their associated products, and they continue to be useful to this day.

Smith and Bailey (1968) established the term *resurgent caldera*, which was defined as a cauldron within which the subsided block is uplifted after initial subsidence, usually as a structural dome. In this influential work, the authors compared various well-known caldera

systems, emphasized the cyclical nature of calderas, and for the first time clearly defined individual stages in the development of resurgent systems. Smith and Bailey (1968) were enthusiastic in their praise of the work of Howell Williams. Smith in particular noted that Williams' 1941 paper "caught him, in 1942, at an impressionable age" and that it had "influenced his thinking ever since (Smith and Bailey, 1968). The authors did note, however, that in the twenty-seven years since *Calderas and their Origins* was published, many new calderas had been described thereby adding to the overall knowledge base. Consequently, they set out to re-evaluate caldera-related theories (Smith and Bailey, 1968).

The stated purpose of the paper was to introduce and amplify the authors' concept of resurgent calderas. The authors use the term caldera in the same fashion as did Williams—to describe a large, circular, volcanic depression that is typically larger than a volcanic crater and is usually associated with some form of collapse (Smith and Bailey, 1968). The authors use the term cauldron as a generic term to describe all volcanic subsidence structures regardless of shape, size, erosion, or association with surface volcanism. This includes tectonically-controlled, irregular-shaped collapse structures such as Toba where the genetic processes are similar to those involved in caldera formation. Smith and Bailey were clear to explain that it was not their intention to revise current terminology, but that for the sake of simplicity in describing similar caldera structures with common genetic characteristics the term cauldron was the most convenient available to them (Smith and Bailey, 1968). The term ring fracture was used by the authors to describe the fractures and faults that bound or are associated with the collapsed mass.

Smith and Bailey (1968) briefly described the geology and evolution of seven calderas: Valles NM, Creede CO, San Juan-Silverton-Lake City CO, Timber Mtn. NV, Long Valley CA, and Toba, Indonesia. These case studies were provided with the intent of identifying key pieces

of evidence for caldera resurgence. A number of similarities were identified between the various calderas, including comparable structural features, eruptive patterns, and (with the exception of Long Valley) centrally-located resurgent domes. Based on their observations, the authors identified a systematic sequence of seven eruptive stages. It is important to note that the model of resurgence was based mainly on the Valles caldera as this was the system with which the authors were most familiar.

Six of the seven stages of development in resurgent activity are shown in Figure 1.4. Stage I represents general regional tumescence and generation of ring fractures. Regional tumescence was defined as doming of an area larger than that defined by the outer ring fractures of a caldera. Smith and Bailey proposed that this swelling leads to initiation of fractures along which “catastrophic ash flow eruptions eventually take place” (Smith and Bailey, 1968). Stage II is marked by major caldera-forming eruptions that typically produce voluminous ash flow tuffs. The duration of this stage was a source of uncertainty for the authors, who recognized that large volumes of ash flows could be erupted in a very short time. Using the 1883 Krakatoa, 1912 Katmai, A.D. 79 Vesuvius, 1815 Tambora, and the 1.61 Ma and 1.22 Ma Bandelier eruptions as examples, a very short time was defined as representing anywhere between a few days to less than 10 years (Smith and Bailey, 1968).

Stage III represents caldera collapse in which large-scale subsidence occurs. Based mainly on their evidence from Valles N.M., Smith and Bailey separated Stages II and III. However, they noted that in some calderas eruption of large volumes of materials and collapse may in fact be concurrent. This concept is required by the observation of thick caldera fills in some systems. Druitt and Sparks (1984) examined this phenomenon in detail and this study will be discussed later in the chapter.

Stage IV is represented by pre-resurgence volcanism and intra caldera sedimentation. Smith and Bailey (1968) proposed that the period following collapse would be a time of “extreme disequilibrium” in the caldera and in the magma chamber. Within the caldera they suggested that caving, avalanching, and gravity collapse of the weakened caldera walls, and formation of intra caldera lakes would dramatically increase rates of sedimentation. In addition, they believed that minor eruptions of pyroclastic material and lava flows would occur as the magma chamber attempted to re-establish itself.

Stage V represents the resurgent doming phase in which a typically well-defined central structural dome is emplaced within the collapse zone. Smith and Bailey (1968) pointed out that resurgent domes are frequently structurally deformed; they may contain distension faults or exhibit various types of grabens. It was also suggested that resurgent doming may be accompanied by small amounts of volcanism, typically occurring along ring-fractures (Smith and Bailey, 1968).

Stage VI is represented by major ring-fracture volcanism, identified as a ubiquitous and long-lasting process in all of the calderas examined by Smith and Bailey (1968). The authors suggested that Stage VI is the second longest of the seven stages, with only Stage I having a longer duration. Stage VII (not shown in Figure 1.4) represents solfataric and hydrothermal activity. The authors argued that this stage (like stage VI) may be long-lived and could perhaps overlap other stages. However, they also suggested that it only becomes unique after all eruptions have ceased, and at that point it constitutes a “terminal” phase of activity. Valles and Long Valley are identified by Smith and Bailey (1968) as silicic resurgent calderas that currently are in either Stage VII or late Stage VI.

There is no doubt that Smith and Bailey (1968) represents a major contribution to our understanding of large, long-lived, caldera-forming volcanic systems. In many ways it is as important as the work of Williams (1941). The authors, for the first time, emphasized the cyclical nature of calderas and set out to clearly define stages of development in these large, explosive systems. One major criticism, however, is that the authors appear to have been a little too heavily influenced (perhaps understandably) by their excellent work on Valles caldera; their I-VII resurgent sequence is identical to the sequence of events that has occurred in the Jemez Mountains for the 1.22 Ma Tshirege eruption of the Bandelier Tuff. It is unrealistic to expect that all resurgent calderas would behave identically to Valles; although, the general theme of resurgence is certainly applicable to many systems worldwide. One other criticism of Smith and Bailey (1968) is their confusing use of the terms caldera and cauldron. There are several places in the paper where nearly simultaneous usage of both terms is somewhat cumbersome and potentially confusing to the reader. Although the authors justify their broad usage of the term cauldron, as it is currently understood a cauldron represents an eroded caldera. Consequently, the modern reader may become slightly disoriented. This in no way, however, invalidates the broad contributions of the work.

Williams and McBirney (1979) redefined the term *caldera*, using it to indicate “a large volcanic collapse depression, more or less circular or cirquelike in form, the diameter of which is many times greater than that of any included vent.” They also revised Williams’s prior classification scheme, abandoning all but the collapse calderas (category B) from the 1941 system. The terms Krakatoan, Katmai, Valles, Hawaiian, Galàpagos, Masaya, and Atitlàn types were retained. Categories A and C-F (explosion-related calderas, erosion-related calderas, volcanic grabens, volcanic rents and fissure troughs, and major volcano-tectonic depressions)

were abandoned by Williams and McBirney; although, some of these terms continued to be used by others. Volcano-tectonic depression in particular was used throughout the 1980's and remains in use.

During the 1980's and 1990's interest in caldera studies was again revived. During this period, and continuing through to the present, much more attention has been paid to caldera-forming processes rather than to the classification of calderas. This is no doubt due in part to advances in technology, in part due to increased interest in the potential of geothermal energy as an alternative energy resource, and also in part due to an increased awareness of the need to understand the workings of large volcanic systems from a geologic hazards perspective.

Yokoyama (1981) introduced the concept of the funnel-type caldera, suggesting that it represented a large debris-filled explosion crater that was cored out during an eruption. Gravity anomalies at Krakatoa were correlated to an "inverted circular cone (or a funnel)" structure with a maximum radius of 8 km and a depth of 1 km (Yokoyama, 1981). Yokoyama (1983) studied four low gravity anomaly calderas in Japan including Aso, Kuttyaro, Nigorikawa, and Hakone calderas. The study incorporated gravimetric survey data and various drilling studies to evaluate caldera collapse mechanisms. Three significant findings were highlighted that challenged conventional ideas of caldera collapse at that time. The first noted that coarse materials (termed 'fall-back' by the author) are usually found accumulated as deposits situated between one to four kilometers in depth beneath calderas. The second suggested that caldera boundaries are not always faults, and that they typically dip inward at shallow angles with a few steeply-dipping exceptions. The third, and perhaps most significant, suggested that the basement rock beneath some calderas assume a funnel-shaped morphology, and that they are neither piecemeal nor chaotic in nature.

Yokoyama (1983) used this evidence in support of the explosive coring hypothesis for caldera formation in general, and more specifically for the 1883 Krakatoa eruption. He rejected the idea of Williams (1941), which proposed that Krakatau-type calderas were formed by collapse of a pre-caldera volcano into a magma reservoir. In contrast, Yokoyama stressed that pre-caldera volcanoes could not collapse into a magma reservoir through narrow central vents.

The major issue with explosive excavation as a major caldera-forming mechanism is that the proportions of lithic fragments in ignimbrites associated with the eruption are too low to account for the caldera subsidence (Self and Rampino, 1981). Since Yokoyama (1981; 1983) the continuum of caldera collapse morphologies has been significantly refined. Funnel calderas have been identified as end member morphologies associated with either small or deep magma bodies (Lipman, 1997). More recently, it was proposed that funnel morphologies may not represent an end-member, and instead they reflect a variety of processes including the breakup and collapse of weak or fractured materials (Marti et. al, 1994; Lipman, 2000a; Roche et al. 2000). Roche et al. (2000) suggested that some small calderas with lithic-rich ejecta may have been formed through explosive reaming and are thus best interpreted as large vents.

Walker (1984) proposed the concept of downsag, in which stratigraphic layers warp downward, as an important mechanism in caldera subsidence. Walker recognized that not all calderas conformed to the favored collapse model at the time—the so-called piston model in which a cylindrical block subsides along well-defined, steeply-dipping ring faults. Walker cited six pieces of evidence that conflicted with the piston subsidence model: a) subsidence at some calderas occurs via broad down-sagging of the land surface; b) vent rings (which may be indicative of a larger ring fracture) are scarce at many calderas; c) vent rings may occur outside as many calderas as inside and may also occur where a caldera is lacking; d) most cauldrons are

larger than most calderas, signifying that small calderas may not be linked with cauldron subsidence; e) ring dikes are a feature of Precambrian (cratonic) crust; whereas, most modern calderas occur in younger continental crust; f) not all calderas are generated by catastrophic eruption and some may form incrementally with several phases of collapse. In addition, Walker noted that evidence from some Japanese calderas indicated that subsidence could be constrained in a small funnel-shaped collapse zone in the center of the caldera (Aramaki, 1984).

Walker concluded that no single genetic model could account for the variations in caldera collapse; and thus, a spectrum of morphologies must exist. He stressed that downsag was a significant process in caldera collapse, and that even in circumstances where subsidence occurred along ring faults downsag accounted for “at least as much of the total subsidence as downfaulting” (Walker, 1984). Downsag was defined as “a gradual inward slope of the ground toward the center of the depression coupled with a lack of tangential fault scarps, and the centripetal dip of a depositional feature that can be deduced originally to have been horizontal or nearly so” (Walker, 1984). A number of localities were identified where downsag could be readily observed, including Taupo and Lake Rotorua in New Zealand and the Lake Bolsena depression within the Vulcini volcano, Italy. Walker also noted that ring fracture subsidence and downsagging are not mutually exclusive, citing Glen Coe Scotland and the Ossipee Mountains (New Hampshire, USA) as examples where the down-faulted collapse blocks demonstrate basin-like structures with inward dipping layers. At Glen Coe it was estimated that at least half of the collapse could be attributed to simple downsag; at Ossipee over half of the subsidence was related to down-warping. Walker suggested that faulted monoclinical folds could be used as analogies, and noted that downward flexuring of caldera rocks would be expected to occur prior to failure and faulting. Thus, he stated that perhaps calderas should be regarded as faulted down-

warps. Figure 1.5 is an illustration showing a variety of caldera types that have been influenced by downsag.

In addition to establishing downsag as an important caldera collapse process, Walker (1984) also conducted a literature survey of 160 Quaternary calderas to investigate the locations of post-caldera vents. In 89 young calderas, vent locations were assigned to one of five categories: C, in which a single vent occupies a central location (20 examples); L, where vents are located along a linear trend (39 examples); M, where a single vent is located along the margin of the collapse (7 examples); R, in which vents are located in an arcuate ring roughly co-located with the caldera margin (8 examples with another 5 possible); and S, in which vents are randomly scattered (10 examples) (Walker, 1984). The key finding was that post-caldera vents are seldom co-located with peripheral ring faults; they more commonly occupy a central or near-central location. The implication of this is that the pre-collapse vent system is not necessarily altered by caldera collapse. Walker suggested that most ring fault systems were observed in Precambrian crust and thus the piston style of collapse may operate best in rigid and strong crust. He proposed that in weaker and younger crust downsag and other types of collapse would predominate (Walker, 1984).

Marsh (1984) investigated the mechanisms involved in caldera resurgence using a numerical modeling approach. A series of mathematical models were created to evaluate the applicability of a variety of physical processes thought to influence resurgent activity. Based on the results, regional detumescence following eruption and magmatic pressure associated with vesiculation were cited as the most significant causes of resurgence. Detumescence and vesiculation similarly serve to compress a magma chamber, causing doming of the caldera block. Marsh noted that in most cases, regardless of the mechanism responsible, the times of

detumescence and doming of the caldera block are inversely proportional to the size of the magma chamber (Marsh, 1984).

Mahood (1984) conducted a survey of calderas associated with strongly peralkaline magmatism. The author concluded that numerous differences exist between calderas related to peralkaline rocks and those found in calc-alkaline settings. Peralkaline calderas are typically smaller in diameter (2-8 km), are derived from moderately-sized explosive eruptions with relatively low eruptive columns, and have smaller-volume pyroclastic deposits associated with them. In addition, because of lower magma viscosities, pyroclastic deposits (including fall deposits) are commonly welded and may be subjected to processes such as rheomorphism and re-vesiculation.

Druitt and Sparks (1984) provided an intriguing investigation of the timing of large-scale caldera forming eruptions with caldera collapse. Previously, it was assumed that massive, explosive eruptions of pyroclastic material emptied a magma chamber, thus causing collapse due to withdrawal of support. Inherent in this sequence is the concept that eruption occurs first and that collapse occurs second only after a major portion of the eruption has occurred. Based on their analysis of pressure variations in magma chambers during explosive eruptions, Druitt and Sparks proposed that caldera forming events may occur in two well-defined stages (Figure 1.6). Stage one involves eruption of magma from an initial vent while the magma chamber remains over pressurized. In stage two, chamber pressure falls below lithostatic pressure and collapse of the overlying crust occurs as the magma chamber attempts to re-establish lithostatic pressure, and as a consequence, large volumes of magma (hundreds to thousands of km³) may be expelled (Druitt and Sparks, 1984). Their main contention is that only small to moderate volumes of magma may be erupted while high pressures exist in the chamber.

In the 1990's the continuum suggested by Walker (1984) became much more clearly defined. In what was essentially a reiteration of discoveries made earlier by Walker and others, Scandone (1990) examined the Krakatoa-type calderas of Williams (1941) and re-assessed the plausibility of explosive decapitation of vents. He determined that so-called Krakatoa-type eruptions are more likely formed through what was termed chaotic collapse (also referred to as "noncoherent collapse" by Roche et al., 2000). Scandone proposed that the energy required to create a caldera through straight explosive coring is not normally available in natural circumstances (Scandone, 1990). These conclusions were based on an analysis of crater formation by high explosives (both nuclear and conventional). Scandone also noted (as have many of his antecedents) that deposits in calderas rarely (if ever) contain lithic proportions that can account for lost volumes in the caldera. The conclusion was that chaotic collapse is marked by extensive brecciation of the caldera floor. Depending on the aspect ratio of the magma chamber (tall, vertically-oriented magma chambers are more likely to produce chaotic collapse; flat, horizontally-oriented magma chambers are more likely to produce large volume eruptions), chaotic collapse may occur following depressurization of a magma chamber (Scandone, 1990). However, Scandone failed to recognize that the scale differential between nuclear explosion cavities and large calderas (2-3 orders of magnitude) is significant and damages the credibility of his analogy (Roche et al., 2000).

Branney and Kokelaar (1994) conducted a study on the Scafell caldera in the Lake District of England (Branney and Kokelaar, 1994). Scafell is one of the best-described examples of chaotic or highly fragmented collapse. During collapse, the floor at Scafell broke up into multiple 0.1 to 2 km blocks separated by faults. The authors use the term "piecemeal caldera" as a substitute for the chaotic or Krakatoan type and they apply it to calderas with block-faulted

floors such as Scafell or those with indiscrete caldera floors that have been transformed into meso/mega-breccias such as Aira in Japan (Branney and Kokelaar, 1994). Their main conclusion was that subsidence in calderas where the floor is highly fragmented likely occurs via “successive localized events, each affecting small fault-bounded areas rather than the entire caldera floor” (Branney and Kokelaar, 1994).

Lipman (1997) presented a paper on caldera types in which the breadth of diversity in caldera types is recognized, and a summary is provided of the continuum of morphologies that had been developed since the early 1980’s (Lipman, 1997). In the first part of the paper, a general review of the major structural elements present in a caldera was presented. The author noted that these are not intended to represent relations at any specific caldera but rather to provide a general framework for examining caldera collapses. The elements (Figure 1.7) include the following: topographic rim, inner topographic wall, collapse collar, bounding faults, intra-caldera fill, caldera floor, sub-caldera magma chamber (Lipman, 1997).

In the second portion of the paper, Lipman identified five caldera end-members that can be expected to result from the majority of subsidence processes found at calderas. These types can be seen in Figure 1.8 and include plate or piston-type collapse, piecemeal collapse, trap-door collapse, downsag collapse, and funnel-shaped collapse (Lipman, 1997). The author is careful to note that the aforementioned collapse morphologies are end members and that collapse may frequently involve combinations of the proposed end-members.

Moore and Kokelaar (1998) undertook a complete reassessment of the Glen Coe cauldron in Scotland. In this study, the authors refuted the conclusions of Clough et al. (1909) and Roberts (1963; 1966) by interpreting Glen Coe caldera as an example of piecemeal subsidence and not coherent-block collapse. The primary evidence for this interpretation was the discovery

that the ring-faults identified by Clough et al. (1909) actually formed after a long, drawn-out collapse process and were not associated with an immediate collapse (Moore and Kokelaar, 1998).

Since the turn of the century, several significant caldera studies have been published. Troll et al. (2000) produced a study of the Rum central igneous complex, Scotland. They suggest that caldera collapse may have preceded large-scale eruptions, thus echoing the sentiments of Komuro et al., 1984. Komuro originally conducted several experimental studies on calderas in the 1980s on 1:200,000 scale models. The results from multiple experiments indicated that calderas may collapse prior to an eruption as a result of inflation of the magma chamber and expansion of the volcanic edifice. These experimental findings will be discussed in greater detail in a section to follow. More recently, Komuro and co-workers presented field evidence for a transitional type of caldera at the Sakurae cauldron in southwest Japan (Komuro et al., 2006).

Lipman (2000a) provided a review of calderas and caldera-forming processes in the *Encyclopedia of Volcanoes* (Sigurdsson, 2000). This review included an overview of historical work on calderas (including Lipman's own efforts), a bibliography of significant papers, tables of important caldera eruptions, and a discussion of societal implications of large volcanic eruptions. In addition, four stages of caldera development were designated: pre-collapse volcanism commonly associated with tumescence; caldera subsidence associated with eruption and withdrawal of magmatic support; post-collapse magmatism and resurgence; hydrothermal activity and mineralization.

Cole et al. (2005) published a review of calderas and caldera structures. The review incorporated many of the newer studies that had been completed during the preceding fifteen years, such as that of Branney and Kokelaar (1994), Lipman (1995, 1997, 2000a, 2000b), Moore

and Kokelaar (1998), and Troll et al. (2000). Several revisions to terminology were suggested; the stated intent being to more clearly distinguish between well-defined calderas and older eroded structures. The term *caldera* was defined as “a volcanic structure, generally large, which is principally the result of collapse or subsidence into the top of a magma chamber during or immediately following eruptive activity.” A *caldera complex* was defined as “spatially and structurally associated nested or overlapping calderas of different ages.” A *cauldron* was defined as “an eroded caldera in which most of the eruptives accompanying caldera collapse have been removed by erosion, and older volcanic or sedimentary units below the caldera floor are now exposed.” Finally, a *ring structure* was defined as “a magma chamber or chambers, exposed by deep erosion (generally > 2 km), beneath an inferred caldera structure.”

The review provides an overview of caldera structures, collapse morphologies, and examples of different calderas. This draws mainly on the work of previous authors. In the latter section, examples are organized according to eruptive compositions, including basaltic, peralkaline, andesitic-dacitic, and rhyolitic types. Cole et al. (2005) suggest that eruptive composition may serve as a useful way of grouping calderas. However, they note that some calderas may erupt multiple compositions, and therefore this is not intended as a classification.

The final portion of the review is a summary of ideas. Chief among them is the recognition of the “individuality” of caldera collapse structures. The authors assert that calderas form from a variety of processes and that “in many ways, each caldera is unique.” Furthermore, they suggest that it is inappropriate to classify them into overly-specific types such as was attempted by Williams (1941) and his predecessors.

The work of Cole et al. (2005) is a solid contribution to the literature on calderas, primarily because a significant volume of caldera-related studies are reviewed, including some of

the more recent studies from the previous decade. The discussion regarding nomenclature is helpful and informative, and the point about distinguishing between well-defined structures and eroded, older calderas is well-taken. In addition, an important and valid theme emphasized in the beginning and end of the review is that calderas are unique—they form from a spectrum of collapse processes and exhibit a multitude of features; and thus, they should not be pigeonholed into well-defined types.

A criticism of Cole et al. (2005) is their somewhat confusing and disappointing use of eruptive compositions as a means of grouping calderas. A significant portion of the review is devoted to the description of calderas that have been grouped based on eruptive composition. To be completely fair, the authors are careful to note early on that their use of eruptive compositions is not intended as a classification. Furthermore, they note that “there is not a direct relationship between composition of the eruptives and ‘types’ of calderas” (Cole et al., 2005). Having said this, in their conclusion, they contradict themselves in stating that “composition of erupting magma at a caldera-forming volcano is a useful criteria (sic) for subdividing calderas for descriptive purposes” (Cole et al., 2005). Based on their initial commentary, this is a confusing and misleading way to end the review. As has been demonstrated by numerous studies in the past, many of which have been reviewed in this work, collapse styles, mechanisms, and structures are a far better means of characterizing calderas. Despite the disclaimer to the contrary, many readers may still come away with the vague notion that magma composition is an acceptable means of classifying calderas. It is therefore somewhat frustrating that the authors chose to use this ‘technique’ in their work.

Experimental Studies

A number of interesting experimental methods have been developed to better constrain the nature of caldera collapse. Ramberg (1981) used a centrifuge with putty as a magma chamber placed under a roof of clay to simulate collapse. In this experiment, preexisting fractures were created in the clay that served as a guide for the subsiding clay block (Ramberg, 1981). Komuro et al. (1984) used 1:200,000 scale models with balloons placed in boxes of powdered material to simulate the expansion and collapse of a volcanic edifice. Using finite element analysis performed as plane strain problems, they determined that the depth of a magma chamber is proportional to the diameter of an associated uplifted pre-eruptive dome (Komuro et al., 1984). They also concluded that in some cases, caldera collapse may precede large explosive eruptions. They suggested that uplift directly related to the inflation of a magma chamber could produce a pre-eruption caldera (Komuro et al., 1984). Komuro (1987) refined the experiments in 1:200,000 scale to include dry ice balls placed in a mixture of dry sand and powdered clay. Evaporation of the dry ice simulates eruption of the “magma body.” As evaporation continues, it was found that collapse of the overburden becomes inevitable. From the experimentation, Komuro concluded that pre-caldera doming will typically form polygonal cauldrons. Conversely, catastrophic eruptions are expected to form circular cauldrons. Since the two eruption events are not mutually exclusive, he acknowledged that a spectrum of caldera collapse morphologies must exist with the polygonal and circular types as end members (Komuro, 1987).

Marti et al. (1994) presented an experimental study on caldera collapse using an apparatus consisting of a balloon placed within a box filled with fine alumina powder. The depth of the powder was 40 cm, and the balloon was attached to a pump system allowing it to be inflated and deflated. The model (Figure 1.9) was built to a scale of approximately 1:100,000.

Thus, the 10 cm experimental caldera equates to a natural caldera with a diameter of 10 km. Inflation of both spherical and elongate balloons within the powder led to structures exhibiting varied morphologies, depths, and sizes (Marti et al., 1994). A number of significant conclusions were derived from this experimental study. Caldera sizes were found to be related to the size of their associated magma chamber—essentially, larger magma chambers result in larger calderas. Shallow experimental magma chambers were found to create calderas with larger areas than deeper magma chambers with the same dimensions. Subsidence shapes were found to reflect the shape of the projected area of the associated evacuated magma chamber responsible for collapse. Radial fractures and normal faults created during tumescence and doming were found to be open to re-activation during collapse to form reverse faults. The wide spectrum of deep caldera morphologies was attributed to the degree to which country rock has been affected by tumescence. Funnel collapse morphologies were suggested to result from the collapse of weak or fractured materials; while, coherent piston-type collapses were proposed to reflect a lack of disruption of the collapsing material. The experiments also indicated that migration of magma bodies beneath a volcanic edifice may result in multiple, overlapping collapses. Similarly, it was predicted that rejuvenation of magma chambers could result in nested calderas that utilize the same collapse structural elements, such as ring faults. This notion has a particular relevance to the Valles caldera, where the individual Bandelier eruptions at 1.61 and 1.22 Ma yielded caldera collapses that appear to be nested within one another (Heiken et al., 1986).

On the subject of scaled balloon collapse experiments, Roche et al. (2000) noted that a limitation of these experiments is that the balloon preserves its convex-upward shape during subsidence and thus continues to affect the deformation pattern in the roof block. In a real-life caldera, it seems logical that the opposite is far more likely to be true. As the roof block

collapses, it will apply a force on the magma chamber beneath it, deforming the magma and making it impossible for the magma to retain a convex shape as does the balloon in the scaled experiments. Thus, the magma chamber should not continue to have a deformational influence on the subsiding roof block as is observed in the scaled models.

Branney (1995) conducted an investigation of caldera-like structures using data from mining-subsidence models, scaled analogue subsidence experiments, ice-melt collapse pits from the 1991 eruption of Volcán Hudson in Chile (Branney and Gilbert, 1995), and data from over 50 calderas. The goal was to determine which types of structures are formed during caldera collapse where the only mechanism is withdrawal of magmatic support in the absence of tumescence or regional tectonic/structural control. Commonalities were drawn between downsag collapse events at calderas and the ice-melt pit, mining subsidence, and experimental models, including outward-dipping extensional fractures and inward tilting strata. The general conclusion is that complex patterns of deformation may form directly from subsidence in lieu of a more intricate deformational history (Branney, 1995). The author is careful to note the wide diversity in caldera types and that factors important in the structural development of many types of calderas are not represented using the subsidence models employed in the study.

Roche et al. (2000) conducted scaled caldera-collapse experiments in two and three dimensions using dry sand as analogue rock and silicone as analogue magma. A range of roof aspect ratios likely to form in calderas (thickness/width = 0.2, 1.0, 2.0, and 4.5) were utilized in the experiments. To achieve correct scaling, the models were built to be geometrically and dynamically similar to the real thing—each physical parameter in the model was realistically scaled to natural physical parameters. Critical parameters considered in the calculations include density, gravity acceleration, typical length, stress, angle of internal friction, and viscosity. In

earlier experimental models such as that of Komuro et al. (1984), Komuro (1987) and Marti et al. (1994) scaling was achieved by defining pi-numbers (dimensionless products) that include ratios such as external force to gravity force and internal friction to resistant forces.

The authors compared their experimental results with field observations and also with data from mining subsidence models. A limitation inherent in the latter comparison is that the ratio of subsidence to roof thickness is 10 to 100 times greater in calderas than in mines and therefore the stresses involved in caldera collapse are significantly higher (Roche et al., 2000).

The experiments revealed that for calderas not influenced by pre-existing faults, a general mechanism of subsidence exists that is only slightly influenced by the shape of the magma reservoir (Roche et al., 2000). Variations in collapse morphology were found to represent diverse roof aspect ratios. For low roof aspect ratios (≤ 1) the dominant collapse morphology was piston-type along vertical or reverse faults. For high roof aspect ratios (>1) it was discovered that multiple reverse faults break up the roof into large pieces resulting in a chaotic or noncoherent collapse.

Walter and Troll (2001) conducted scaled analogue experiments in order to better understand the nature of caldera faults and their relations to magma chamber dynamics. The authors evaluated several scenarios that typically result in caldera-related faults and fractures, including doming (radial and circumferential fractures), pure evacuation collapse (concentric fault systems), and a combination of the two that represents cyclical resurgence. The experimental apparatus involved a glass tank filled to a depth of several tens of centimeters with 'granular analogue material,' in this case sieved quartz sand with a mean diameter of 500 μm , mixed with clay (Walter and Troll, 2001). A balloon was placed in the center of the tank and a mound was constructed with the intent of simulating a volcanic cone. The geometry of the

apparatus was changed over 30 times by adjusting the shape and size of the simulated magma chamber and the volcanic edifice. The experiments were geometrically scaled to represent ocean-island volcanoes using parameters derived from Hubbert (1937), Sanford (1959), and Komuro et al. (1984).

Based on their experiments, Walter and Troll (2001) concluded that the geometry and arrangement of caldera-related faults and fractures are linked to specific mechanisms of formation. Doming (inflation) of an edifice was found to generate a compressive stress regime on the periphery of the dome and a tensile stress regime at the apex of the dome. This resulted in propagation of fractures and dikes in a radial fashion, over-steepening of the outer slopes, and the formation of a polygonal apical graben. Pure evacuation collapse was found to generate outward-dipping faults that circle the subsided block. These faults were sharply defined and curved in nature. Multi-stage caldera collapses were found to generate complex networks of intersecting dikes and faults both in the central caldera and on the periphery of the caldera.

Troll et al. (2002) examined the often confusing relationship between extracaldera (peripheral) faults and the central regions of multicycle caldera volcanoes. The study was based on field data collected from the Tejeda caldera on Gran Canaria and analogue experiments scaled to the island of Gran Canaria. The experimental setup used (in 1:100,000 scale) was similar to that of Walter and Troll (2001) in which balloons were immersed in sand and repeatedly inflated and deflated to simulate multicyclic caldera collapse.

Troll et al. (2002) found that data collected from experiments on multiple collapse cycles in scale models were quite similar to that observed in the field at the Tejeda caldera on Gran Canaria. The authors observed complex crosscutting radial and concentric dikes on the periphery and within the intracaldera zone of the Tejeda caldera. In addition, this complex

crosscutting relationship was similarly observed in the experimental models. The main conclusion was that multicycle calderas (such as Tejedá) are unlikely to have undergone simple piston collapse (Troll et al., 2002). The authors instead proposed that “discrete block subsidence (i.e. piecemeal)” is a far more likely subsidence mechanism in long-lived multicycle calderas. Based on the agreement observed between field observations and scaled analogue experiments, they also inferred that peripheral fault systems may yield significant information about the nature and mechanisms of caldera collapse (Troll et al., 2002).

Holohan et al. (2008) investigated vent migration at Long Valley using scaled analogue models. Prior studies revealed that eruptive vents migrated in concert with lateral propagation of ring fractures during the 760,000 yr B.P. eruption. Lithic fragment studies were previously used by Hildreth and Mahood (1986) and Wilson and Hildreth (1997) to establish that vent locations migrated throughout the course of the Bishop Tuff eruption. The so-called ‘unzipping’ pattern of ring fractures was noted by previous workers such as Wilson and Hildreth (1997), who hypothesized that pre-existing structural weaknesses may have provided an impetus for the phenomenon; however, the reasons for it remained unclear.

Holohan et al. (2008) used analogue modeling to provide an explanation for ‘unzipping’ at Long Valley and identified other localities where their mechanical explanation was applicable. The experimental apparatus used a reservoir of creamed honey situated within a 4:1 sand/gypsum mixture. Four magma (honey) chamber morphologies were used, each with a different plan-view elliptical shape defined by the ratio of their long/short axes. The A/B ratios used were 1, 1.33, 1.5 and 2.0. In the models one cm was equal to 2 km in nature. Thus, for Long Valley a 14 x 7 cm model approximates the 32 x 16 km collapse area, and a depth of 3 cm

approximates the ~5-6 km depth to the Bishop magma chamber (Holohan et al., 2008). Each chamber was run (collapsed) five times.

Based on the analogue experiments, Holohan et al. (2008) determined that vent migration and ring fracture unzipping at Long Valley resulted from two main factors: (a) the highly elliptical nature of the pre-collapse chamber roof, and, (b) the effects of pre-failure shear strain along the short axis of an elliptical roof block (Holohan et al., 2008). In addition, examples of smaller calderas that have experienced syncollapse vent migration were provided as examples. These included Laacher See (Germany), Campi Flegrei (Italy), Rabaul (Papua New Guinea) , Suswa (Kenya), and Alcedo in the Galapagos Islands (Holohan et al., 2008).

It is interesting to note that Marti et al. (1994) had previously suggested that the shape and size of magma bodies affect caldera collapse morphology. Based on the results of Holohan et al. it appears even more likely that the shape of a magma chamber roof is influential in the collapse process. At elliptical calderas, the introduction of pre-failure shear strain, coupled with the elliptical shape of the pre-eruptive magma chamber may result in the ‘unzipping’ phenomenon of ring fractures and consequently, vents may migrate during the eruption.

Summary and Discussion

Overall, this review demonstrates that calderas are complex geologic entities and that our current thinking regarding them has advanced significantly over the past 200 years. Some important conclusions can be drawn: 1) Calderas are collapse features related to volcanic activity; cauldrons represent eroded calderas. 2) Calderas form via collapse or subsidence resulting from removal of support in the crust. This loss of support is frequently caused by removal of magma beneath a volcanic structure. Explosive coring has been used to explain the origins of some small calderas. However, explosive coring is not a genetic process common to

most calderas. 3) Subsidence mechanisms (and the nature of caldera collapse) are dependent on a number of physical characteristics including the intensity of an eruption, the shape, size, and depth of the magma chamber associated with the collapse, and the presence (or absence) of pre-existing faults or other tectonic influences. 4) Some calderas are resurgent and thus erupt and collapse multiple times in a cyclical fashion, similar to the Valles Caldera in New Mexico. 5) Several end-member morphologies can be applied to caldera collapses, including piston, downsag, trapdoor, and piecemeal. Chaotic and funnel morphologies have also been proposed in past literature. However, Lipman (1997, 2000a) noted that chaotic collapse is not well documented in nature and can be explained instead by alternative processes such as piecemeal collapse. Likewise, Lipman (2000a) also suggested that “funnel calderas” do not represent an end member and instead reflect a variety of processes. It is also very important to recognize that some calderas may exhibit characteristics from multiple end-member morphologies. 6) Most importantly, calderas form from a variety of processes; they may contain a variety of structures, and a single system may erupt multiple magma compositions. Consequently, not all calderas are alike. Thus, the application of a generic caldera template or classification scheme is not always appropriate, and it should be recognized that many calderas will exhibit behaviors or characteristics that fall on a continuum between end-member types. Ideally, a holistic approach to caldera classification is best, taking into account significant features and characteristics including collapse geometry, number of collapse events, resurgence in the system, deformation of the collapse floor, and the type of magma erupted. In this way, caldera research will continue to advance into the 21st century.

Figure 1.1. Several diagrams illustrating mechanisms of cauldron subsidence along ring faults at Glen Coe Scotland, (Clough et al., 1909)

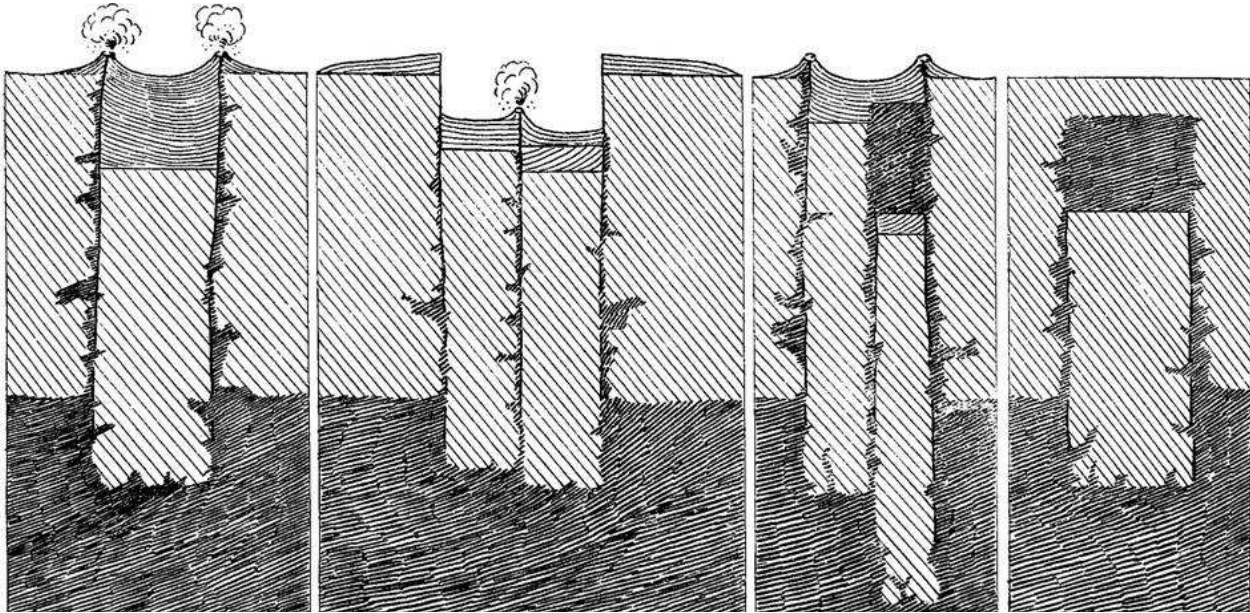


Figure 1.2. Adaptation of Cell theory of Wing Easton, as presented in *Calderas and their Origins* by Howell Williams (1941). Easton pointed out that all non-Hawaiian type magma bodies must be either asymmetric or of wide extent, otherwise drawdown during an eruption would quickly starve the volcano of magma, effectively shutting off the eruption prematurely. The cell theory suggested that during an eruption, magma is progressively withdrawn from the chamber in stages. With each successive magma removal, the level in the chamber drops. Gas pressure increases in the vacated spaces, which continues to drive the eruption. When the magma levels reach the level at which the conduit (*C-E*) sits, the volcano enters a solfataric stage where the conduit is plugged and gases escape upward through fissures. This gas escape process forms numerous cylindrical and vertically-oriented “cells” in the lower half of the volcano. This in turn weakens the structure and was proposed as a means for caldera collapse to occur. This theory was rejected by Van Bemmelin and Williams for a number of reasons.

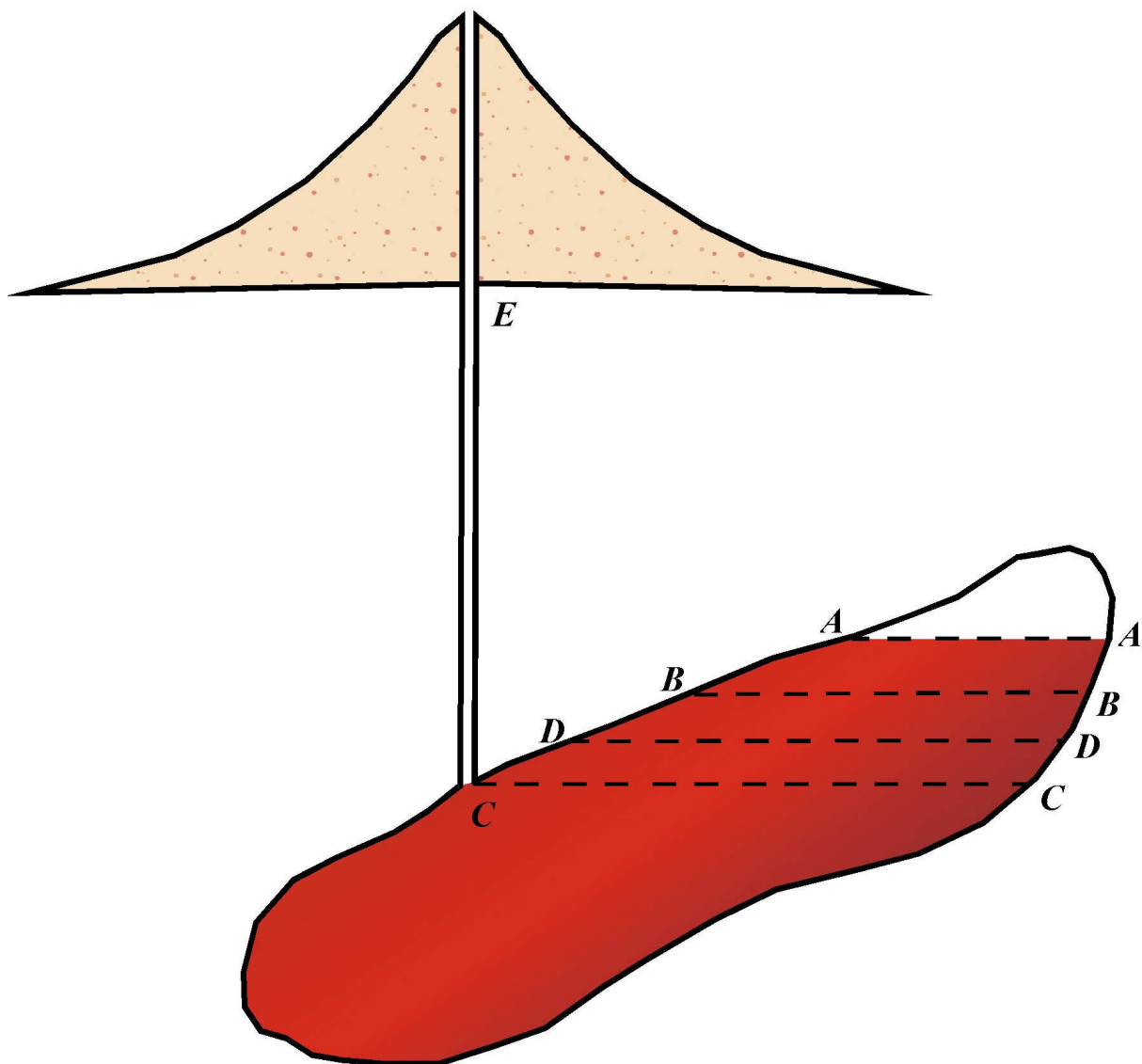
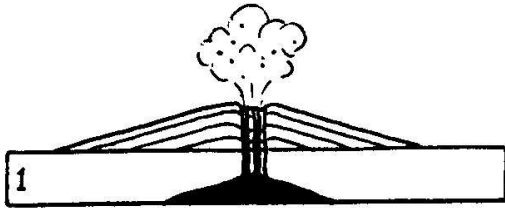
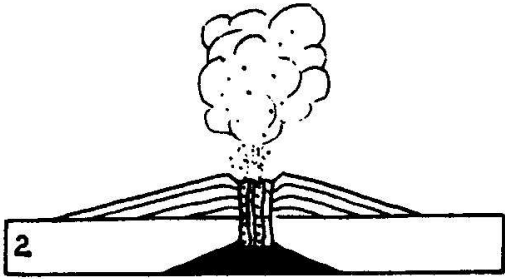


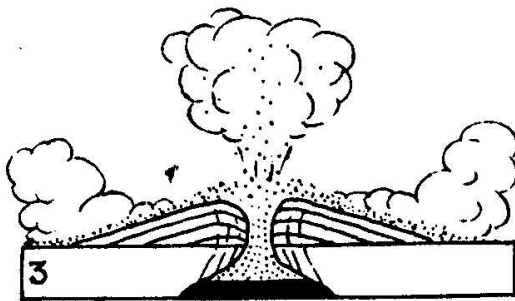
Figure 1.3. Evolution of a caldera of the Krakatau type. Drawing has been modified from *Calderas and their Origins* by Howell Williams (1941)



Stage 1: Mild explosions of pumice. Magma stands high in conduit



Stage 2: Explosions increase in violence. Magma level falls into main chamber



Stage 3. Culminating explosions. Ejecta are projected into the atmosphere and also down the flanks of the caldera as pyroclastic flows. Magma level is deep. Fracturing of roof begins.



Stage 4. Collapse of volcano into magma chamber due to a lack of support from beneath.



Stage 5. Resurgent magmatic activity begins.



Stage 6. Young cones build above caldera rim and vent lavas down the flanks of the caldera

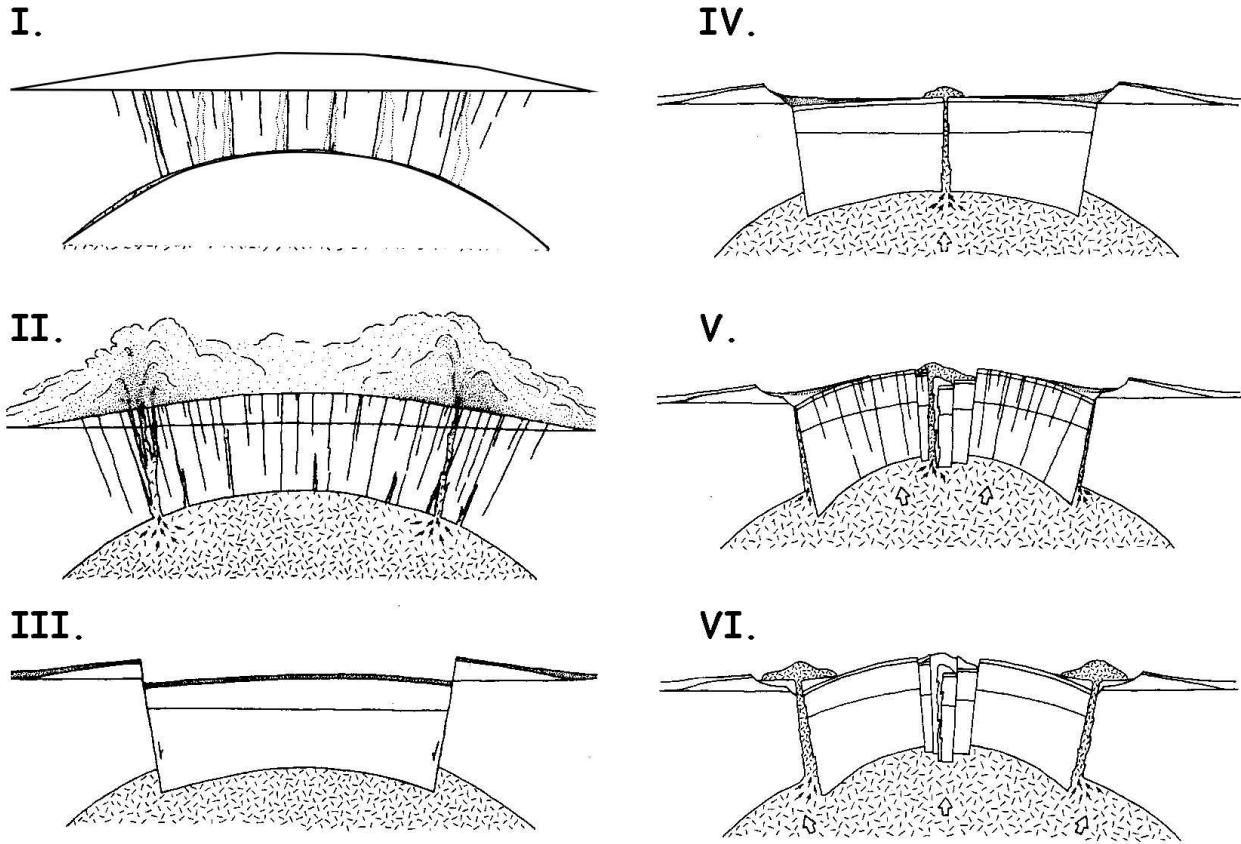


Figure 1.4. The seven stages of resurgent calderas as defined by R. L. Smith and R. Bailey: I. Regional tumescence and doming. II. Caldera-forming eruption. III. Collapse. IV. Pre-resurgent volcanism and sedimentation. V. Resurgent doming. VI. Ring fracture volcanism. VII. Solfataric and hydrothermal activity (not shown). Adapted from Smith and Bailey, 1968

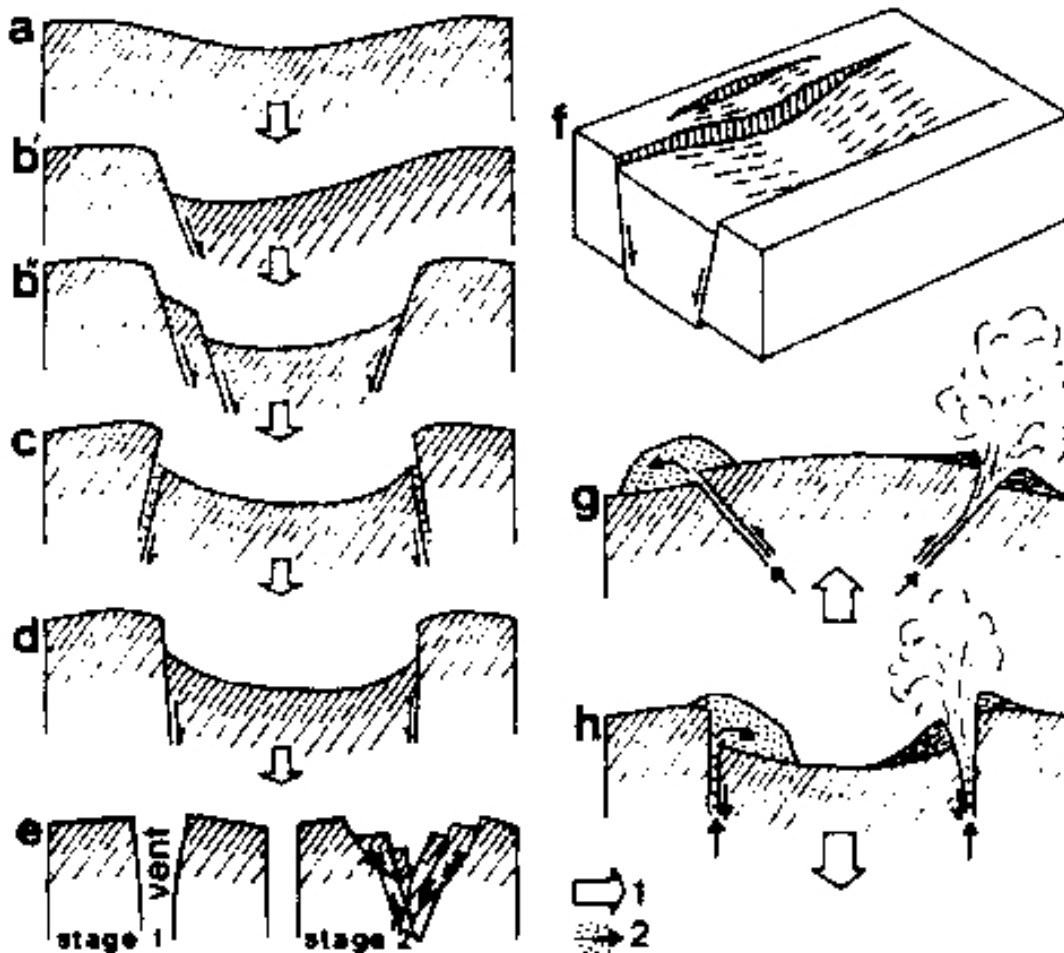
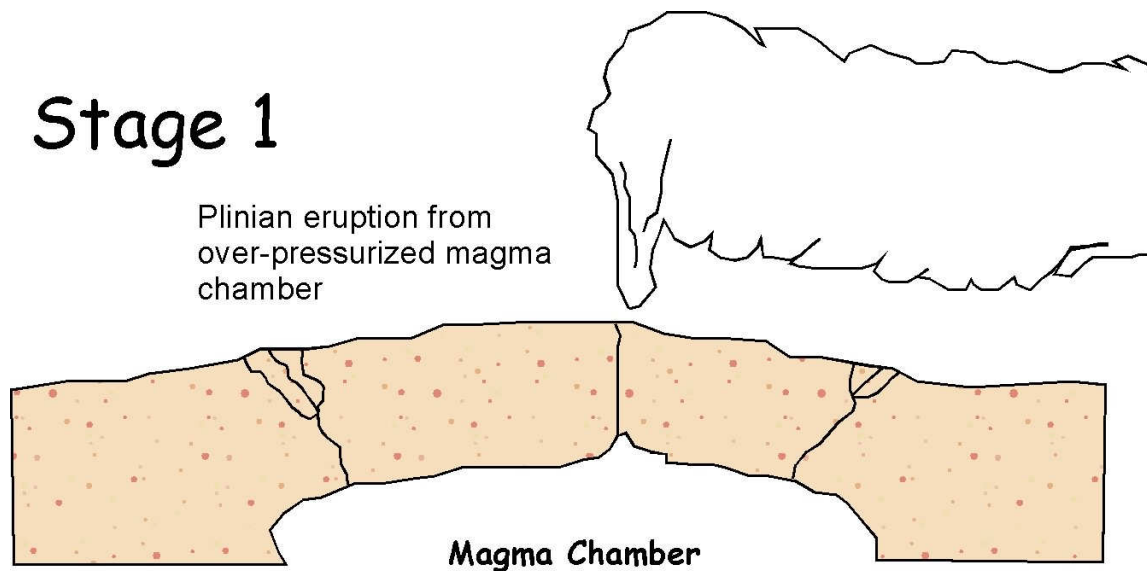


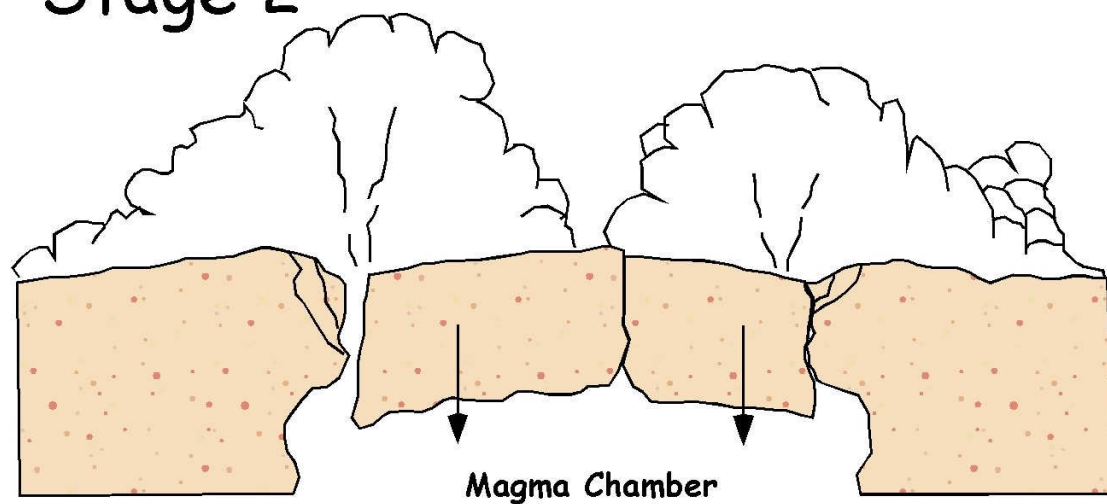
Figure 1.5. Various caldera types as proposed by G. P. L. Walker. A) downsagged, B) normal-faulted downsag, C) subsidence via Anderson-type ring fault, D) subsidence with a steep, inward-dipping ring fault, E) cored out explosive vent of Escher (1929), F) block diagram of downsagged graben. G-H represent two scenarios in which ring vents may form. Taken from Walker (1984)

Stage 1

Plinian eruption from
over-pressurized magma
chamber



Stage 2



Depressurization allows large-scale eruption and collapse to occur

Figure 1.6. A simplified diagram of the two-stage eruption model proposed by Drutt and Sparks. In stage one the magma chamber is over-pressurized, allowing only a small fraction of magma to erupt from a central vent. In stage two, chamber pressure has decreased significantly below the lithostatic pressure of the overlying rock. This allows large scale eruptions and caldera collapse to occur. Modified from Drutt and Sparks (1984)

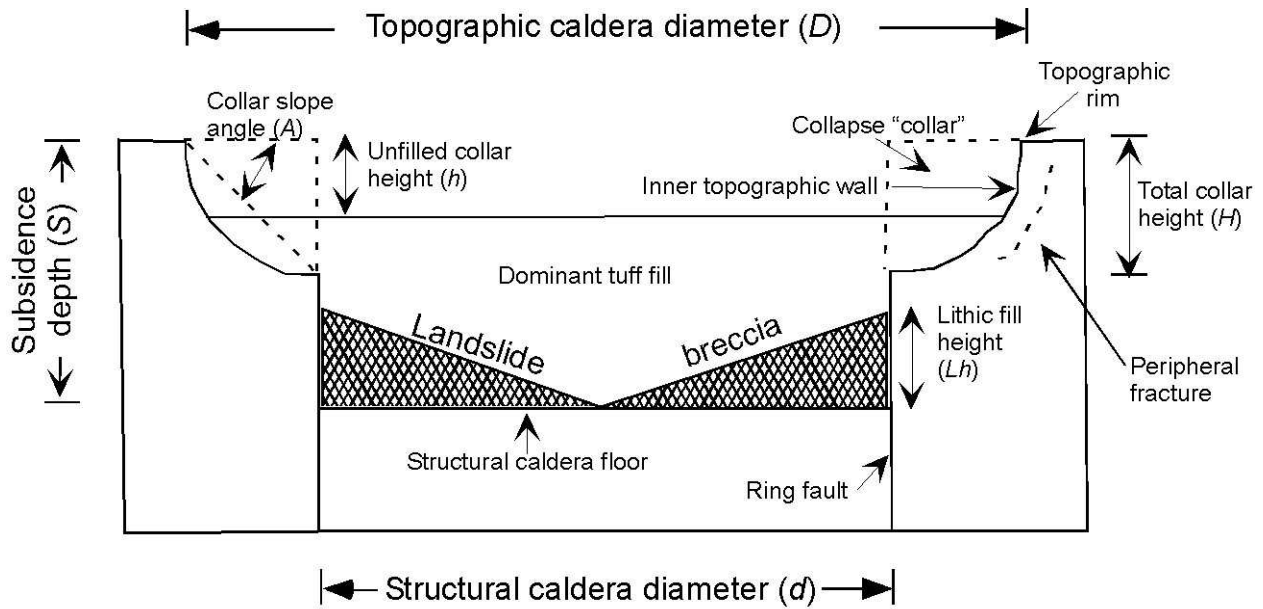


Figure 1.7. Diagram showing the components of a typical caldera, and the features that result from subsequent caldera collapse. Re-drawn from Lipman (1997).

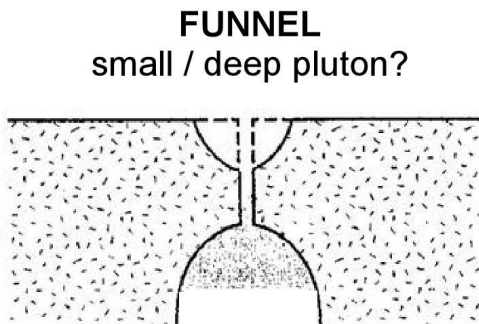
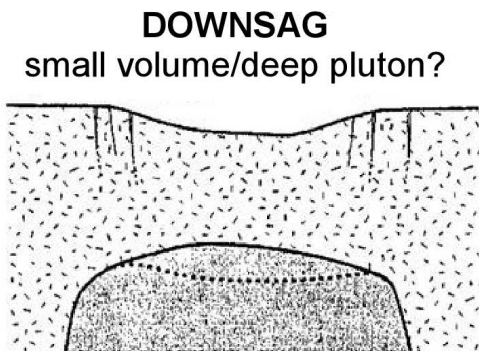
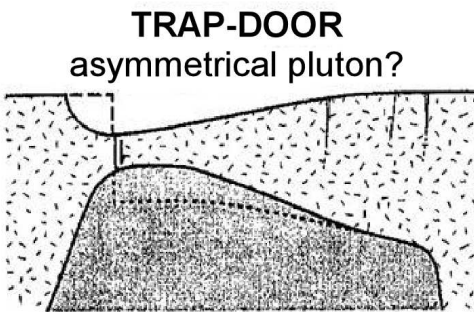
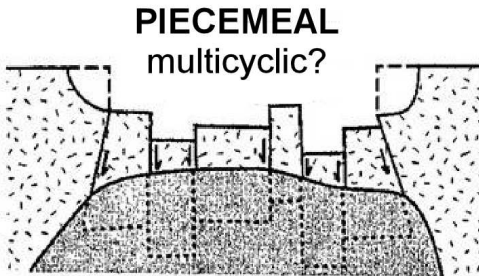
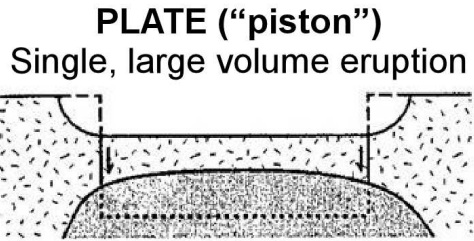


Figure 1.8. Various models of caldera subsidence (Lipman 1997) showing both end-member models and intermediate collapse morphologies.

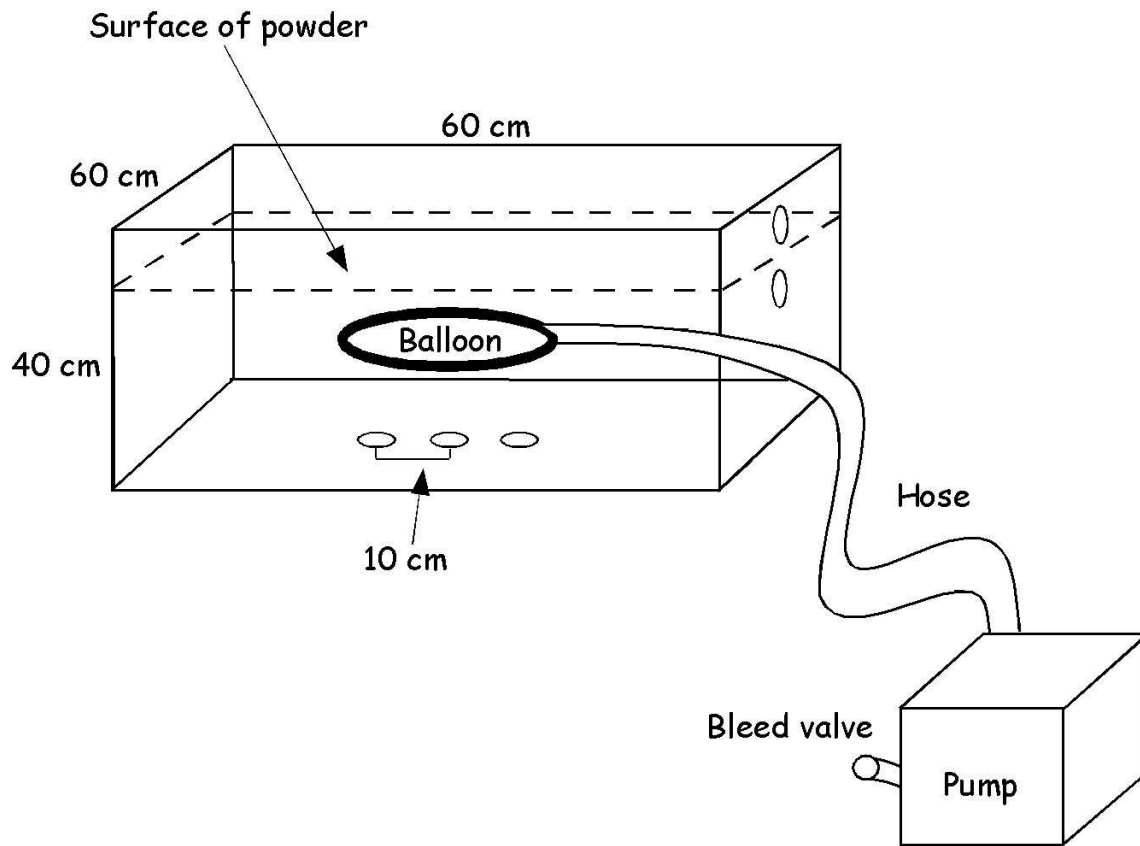


Figure 1.9. Experimental apparatus of Marti et al. (1994) in which a balloon immersed in powder is alternately inflated and deflated to simulate tumescence and subsequent collapse in a caldera-forming eruption. Note that three holes have been drilled in the sides and bottom of the tank that are spaced at 10 cm distances from one another. These are used to perform multiple inflations and deflations simultaneously.

CHAPTER TWO

GEOLOGIC BACKGROUND

Introduction to the Jemez Mountains Volcanic Field and The Valles Caldera

The Valles caldera situated in the Jemez Mountains Volcanic Field (JMVF) in north-central New Mexico, is one of three major Quaternary silicic calderas in the United States. The others are Yellowstone caldera in Wyoming and Long Valley caldera in California. The JMVF is situated on the western edge of the Rio Grande rift (Figure 2.1), a major north-south trending Cenozoic extensional feature that runs from Colorado in the north to Mexico in the south. In addition to the Rio Grande Rift, the JMVF is also directly associated with a structural feature known as the Jemez Lineament. The lineament (Figures 2.1 and 2.2) is a NE-SW trending zone of lithospheric weakness marked by a series of volcanic centers on the surface and is believed to control volcanism in the Jemez Mountains (Wolff et al., 2005).

Although volcanic activity in the JMVF area dates back to approximately 25 Ma, the best known unit in the field is the Pleistocene Bandelier Tuff, which is subdivided into the lower (Otowi) member erupted at approximately 1.61 Ma and the upper (Tshirege) member erupted at approximately 1.24 Ma (Izett and Obradovich, 1994; Spell et al., 1996a; Winick et al., 2001; Phillips et al., 2006). Both members of the Bandelier Tuff are compositionally-zoned, high-silica rhyolitic tuffs exhibiting overall upward decreases in incompatible trace element concentration. The products are the result of progressive sampling of compositionally-zoned magma chambers. Basal plinian fall beds are present for both members around the caldera in various locations and are overlain by ignimbrite deposits. The Guaje pumice bed, found to the

east and southeast of the caldera, is associated with the Otowi eruption. The Tsankawi pumice bed, found mainly to the northeast of the caldera, is associated with the Tshirege eruption.

Each of the two Bandelier eruptions is associated with a caldera collapse event. The Otowi eruption resulted in formation of the Toledo caldera, while the Tshirege eruption created the current Valles caldera. It is believed that the Valles caldera (Figure 2.3) is nested in the remnants of the earlier Toledo caldera (Self et al., 1986). The Otowi collapse structure is believed to be roughly similar in size, shape, and location to the later Valles collapse (Self et al., 1986). The Toledo embayment (Figure 2.3) is a separate, 9 km circular depression overlapping the northeast corner of the main Valles caldera. A ring of lava domes are found within the Valles caldera (Figure 2.3) and are associated with resurgent activity following the Tshirege eruption (Self et al., 1986).

Since the earliest descriptions of the geology in the region, nomenclature has been continually evolving. Initially, Smith and Bailey (1966) introduced the term 'Toledo caldera' to describe the collapse feature associated with the Otowi eruption. This collapse was identified with the Toledo embayment (Figure 2.3), the aforementioned prominent depression located in the NE corner of the present-day Valles caldera. Self et al. (1986) relocated the Otowi collapse structure to a more centrally-located position coincident with the Valles collapse. This was based in large part on age determinations from the outer ring of lava domes in the northern section of the caldera (Figure 2.3). The original name Toledo was retained from Smith and Bailey (1966) but was now used to describe the 'new' Otowi collapse structure. The original Toledo caldera of Smith and Bailey became the Toledo embayment. Gardner and Goff (1996) suggest that the embayment may have formed during the Otowi eruption. In this study, the model of Self et al. (1986) will be used. Thus, the collapse associated with the Otowi eruption

will be referred to as the Toledo caldera, and the collapse associated with the Tshirege will be called the Valles caldera. The smaller depression in the northeast part of the present-day Valles caldera will be referred to as the Toledo embayment.

In prior studies the Valles caldera has been identified as a type locality for piston-style collapse (Smith and Bailey 1968; Lipman, 1997). However, geophysical and stratigraphic studies suggest that the combined results of the two collapse events associated with eruption of the Bandelier Tuff are too asymmetric to represent simple piston-style collapse. Nielson and Hulen (1984) and Heiken et al. (1986) proposed a trapdoor collapse hypothesis for both the Toledo and Valles calderas. Nielson and Hulen (1984), Hulen et al. (1991), and Nowell (1996) found that the Valles caldera is filled with a wedge-shaped body of intra-caldera tuff (Figures 2.4, 2.5). The tuff wedge is thickest in the east and is bounded on the eastern side by a major, NE-trending fault system that lies parallel to the Rio Grande Rift. The hinge of the collapse resides in the west, where the tuff wedge is thinnest. Collapse is interpreted to have occurred predominantly in the eastern part of the caldera, directly associated with rift-bounding faults. The hinge overlies topographically high Paleozoic sedimentary rocks and Precambrian plutonic and metamorphic rocks. Heiken et al. (1986), Self et al. (1986), and later Nowell (1996) proposed that the Toledo and Valles calderas collapsed in similar trapdoor fashion, had similar centers, and that the collapses are 'nested' in roughly the same location. Nowell (1996) reinterpreted the gravity data of Seagar (1974) to determine that the Valles caldera is an asymmetrical structure containing 760 m of caldera fill in the west and over 4570 m in the east. Three dimensional gravity modeling showed that the caldera floor is broken into pieces, offset by a series of discontinuous faults and not smooth as would be expected in a typical trapdoor

collapse (Nowell, 1996). Thus, Nowell concluded that the Toledo and Valles calderas may represent a transitional morphology between chaotic and trapdoor.

As one of the best-studied caldera systems in the world, a large number of papers have been written on the Valles on a wide range of topics including stratigraphy, petrology, structural geology, geophysics, volcanology, geochemistry, hydrology and economic geology. A number of geothermal and scientific drilling studies starting in the early 1960's and ending in the late 1980's yielded an enormous amount of information on the structural, stratigraphic, geophysical, and hydrothermal nature of the caldera (Neilson and Hulen, 1984; Goff et al., 1986; Hulen et al., 1991). The Bandelier Tuff itself is also one of the best studied ignimbrite units in the world. Despite this, many studies go unpublished and therefore a great deal is still to be learned about the specific nature of the eruptions.

The pioneering work conducted by R.L. Smith and colleagues provides a valuable foundation for information on the volcanic evolution of the Jemez Mountains Volcanic Field (JMVF) and the subsequent catastrophic caldera-collapse events associated with the Bandelier Tuff (Bailey et al., 1969; Smith, 1979; Smith et al., 1961; Smith and Bailey, 1966; Smith and Bailey, 1968; Smith et al., 1970). Self et al. (1986) provide an interpretation of the eruptive sequence for the Otowi (lower) member of the Bandelier Tuff, which can be seen in Figure 2.6. The eruptive cycle shown represents a sequence in which an initial Plinian eruption from a central vent is followed by ring fractures and collapse of a coherent, central piston. In this scenario, the vents are believed to have shifted to the periphery along the ring-fractures as the eruption progressed.

Purpose of this study

This study deals specifically with the eruption of the lower (Otowi) member of the Bandelier Tuff and uses lithic distribution data and associated geochemical data of the host tuff to delineate the nature and progression of the eruption. Only two studies have focused on Bandelier lithic fragments in the JMVF. Eichelberger et al. (1979) examined lithic geochemistry in the Otowi Member, and Potter and Oberthal (1987) used lithic counts from the Otowi Member to assist in identification of vent localities. In this study, lithic distributions have been used to help identify vent locations and shifts throughout the eruption. In addition, a recalculation of the total eruptive volume and a calculation of chemical volume types in the Otowi Member has been undertaken. The overall goal is to evaluate the applicability of the currently accepted eruptive model of Self et al. (1986). In this model, the Otowi eruption is presumed to have begun as a large central vent eruption with a plinian phase, and then later to have migrated outward to ring vents on the periphery of the caldera.

This study will represent a significant improvement on prior lithic fragment studies for several reasons. First, this study is more comprehensive and better organized than prior attempts (Potter and Oberthal, 1987; Self et al., 1986; Eichelberger et al., 1979). Specifically, bulk samples of ignimbrite were collected in the field and brought back to the lab where they were sieved to separate various fractions (matrix, lithics, and pumice), washed (a vital step), and then all lithics greater than 0.5 cm in diameter were identified and counted. Prior studies, such as that of Potter and Oberthal (1987) counted lithics in-situ, using a grid placed over the face of the outcrop in the field. While this methodology is not necessarily flawed, it does allow for the distinct possibility that lithic fragments will be misidentified due to difficult field conditions. Even under the best of circumstances, identification of small fragments of aphanitic volcanic

rock can be difficult. The inherent problems associated with this procedure will be further explored in Chapter 4. A number of factors that may be present in the field can all lead to misidentification including lighting conditions, the absence of proper magnification equipment, time constraints, and perhaps most significantly, the overall ‘cleanliness’ of a given sample. Because bulk ignimbrite samples were collected in the field and then processed in a controlled lab setting, this study will undoubtedly benefit from greater accuracy and success in the identification and counting of samples.

A second improvement offered by this study is that it attempts to link the chemistry of the host tuff with the lithic fragment population data. The goal associated with connecting the chemical and lithic data is to link magmatic processes with volcanic processes operating on the surface, including vent transitions and shifts and changes in the intensity of the eruption. An example of successful use of this methodology is at Long Valley caldera, where Hildreth and Mahood (1986) and Wilson and Hildreth (1997) have used chemical stratigraphy and lithic fragments in the Bishop Tuff to link eruptive events with magmatic processes.

A third improvement brought forth by this study is that it includes chemical and lithic data from all regions of the Jemez Mountains Volcanic Field, including some of the more remote and previously under-studied regions such as the Jemez Plateau in the western portion of the field. The geographic extent of the data allows for the overall spatial understanding to be far more comprehensive than in previous studies.

Overview of Regional Geology

Geology of the Rio Grande Rift

The Rio Grande rift is a major late Cenozoic extensional feature located east of the Colorado plateau in the southwestern United States (Figure 2.1). It consists of a series of en-

echelon right-stepping sedimentary basins extending from central Colorado southward through New Mexico and into Chihuahua, Mexico (Keller and Cather, 1994). The rift is the easternmost expression of the Basin and Range province. Rifting began at approximately 30 Ma although the most rapid extension occurred later in the Miocene (Aldrich et al., 1986). Chapin (1971) found that a significant increase in extension occurs from the San Luis Basin in the north (8-12%) to the Socorro Basin in the middle (50%). Opening of the rift is thought to be via clockwise rotation about an Euler pole located in northeastern Utah (Chapin, 1971). However, Cordell (1982) suggests clockwise rotation around a pole at 41° N in north-central Colorado.

In its entirety, the rift stretches more than 1000 km in length and widens significantly from approximately 5 km in the north to greater than 200 km in the south (Chapin, 1971). The majority of the sedimentary basins found within the rift are half-grabens bounded by steeply-dipping normal faults. Basin asymmetry alternates from one side of the rift to another along the axis of the rift. Faulting in the rift is complex and episodic with both high and low angle faults common. Topographically, the eastern rim of the rift sits higher than the western. Topographic relief throughout the rift averages approximately 2400 meters (Chapin, 1971). Bedrock relief ranges from several hundred meters to nearly 11,000 meters within the San Luis basin. Alluvial fill ranges from approximately 120 meters in the Estancia Basin to an estimated 9150 meters in the San Luis Basin. Lithologic assemblages vary considerably on opposite sides of the rift. On the eastern margin, Precambrian and Paleozoic rocks predominate; whereas on the western margin, Tertiary volcanics and sediments are more common (Chapin, 1971). Galusha and Blick (1971) described a number of the sedimentary units in the northern Rio Grande Rift and in the Española Basin, including the Tesuque Formation. The Tesuque Formation contains significant ash beds and Miocene fossils that have been useful in constraining tectonic events in the region.

It should be noted that the Miocene mammal fossils from this area are significant, and rank as one of the premier occurrences in North America.

The majority of work done on the Rio Grande Rift has focused on the northern and central portions (Colorado and New Mexico). Bryan (1938) is credited with the earliest description of the rift in the literature. He described the rift as the Rio Grande depression. He went on to delineate eight significant basins within the rift including the San Luis, Española, Santo Domingo, Albuquerque, Belen, Socorro, Engle, Rincon, and Mesilla. Later studies by Kelley (1952, 1954, and 1956) investigated the structural geology and tectonics of the rift. The definitive account of the RGR was published by Chapin (1971) in which a number of revisions to the pioneering work of Bryan and Kelley were made. Most significantly, the boundaries of the rift were re-defined and re-delineated. In addition, index fossils and potassium-argon (K-Ar) dates were used to better constrain the initial onset of rifting at approximately 18 Ma (Chapin, 1971). The onset of rifting has since been moved back in time to approximately 30 Ma by Aldrich et al. (1986).

Recent investigations have better constrained the sequencing of events in the evolution of the Rio Grande Rift. With an abundance of fieldwork, new radiogenic dating techniques, and geophysical techniques such as teleseismic imaging, the tectonic evolution of the Rio Grande rift is more clearly understood.

Evolution of the RGR

Prior to initiation of Rio Grande extension, the southwestern region of the U.S. underwent at least two significant episodes of deformation. During the Pennsylvanian, the ancestral Rockies were formed, and during the late Cretaceous through the early Tertiary the Laramide orogeny occurred (Ingersoll et al., 1990). It has been suggested that Rio Grande

extension is partly controlled by pre-existing structural features from these earlier episodes (Chapin and Seager, 1975). Laramide compression continued until approximately 50 Ma in the northern portion of the rift and 40 Ma in the southern region (Lucas, 1984; Seager and Mack, 1986). This compression is likely related to the subduction of an oceanic slab beneath the western coast of North America. The evolution of the rift during the Cenozoic is fundamentally associated with tectonism along the western margin of North America (Ingersoll et al., 1990).

Studies by Aldrich et al. (1986) suggest two phases of rift extension in and around the Española Basin. Phase one began during the Oligocene (30 Ma) and continued until the mid-Miocene (18 Ma). This period was characterized by low-angle faulting, formation of broad, shallow basins, and regional extension of approximately 30-50%. It is estimated that the axis of extension during this time was NE-SW. Next, a period of relative quiescence occurred until approximately 15 Ma, during the middle Miocene. At this point, phase two was initiated, lasting as late as 7 Ma. Clockwise rotation of the Colorado plateau increased in rate during this period and changed orientation to E-W (Aldrich and Laughlin, 1984). This period was marked by higher angle faulting and regional uplift of approximately 1 km.

Extension has slowed overall since 10 Ma and has been characterized as weak to moderate (Keller and Cather, 1994). Sedimentation began during the late Oligocene and has resulted in thick sedimentary sequences. For example, in the San Luis Basin, alluvial fill has reached 9.1 kilometers in thickness (Chapin, 1971).

In the Jemez Mountains region fault activity has migrated eastward, roughly parallel to the Jemez lineament (Aldrich, 1986). Several major fault systems developed (Figure 2.7) as the western edge of the Española Basin shifted eastward (Aldrich, 1986). The Sierrita and Jemez fault zones (Figure 2.7) were active during the late Oligocene and early Miocene during a period

of extreme extension in the Rio Grande rift, and they likely served as the western boundary of Española Basin (Lipman, 1981; Aldrich, 1986). Gardner and Goff (1984) suggested that the Jemez Fault Zone, resurgent and subsurface structures in the Valles-Toledo caldera complex, and the Toledo embayment are manifestations of the Jemez Lineament.

Following a period of quiescence in the early Miocene from 21-15 Ma, a revival of rifting and volcanic activity occurred that resulted in an eastward shift of the western boundary of the Española Basin. This shift formed the Cañada de Cochiti fault zone (Figure 2.7) sometime before 13 Ma (Gardner and Goff, 1984). Intense tectonic activity from 13 to 10 Ma was accompanied by basalt and rhyolite eruptions along the Cañada de Cochiti fault zone (Goff et al., 1989). Between 7 and 4 Ma the western margin of the Española Basin once again shifted eastward, this time forming the Pajarito fault zone (Gardner and Goff, 1984). The Cañada de Cochiti, Sierrita, and the Jemez fault zones remained active because they are adjacent to the Albuquerque and Santo Domingo basins and thus are still influenced by activity in the Rio Grande rift (Aldrich, 1986). Golombek (1983) and Golombek et al. (1983) proposed that Pajarito fault system initially formed at 5 Ma. Activity continues to the present with the fault system having offset the Bandelier Tuff as much as 100 m in the past 1.1 million years (Golombek, 1983). The total displacement across the Pajarito fault zone over its 5 million year history is between 200 to 600 m. The position and trend of the Pajarito fault zone is thought to be controlled by mechanics associated with abrupt facies changes between older volcanic complexes and volcanoclastic sediments from the Jemez Mountains (Golombek, 1983).

On the northeast side of the caldera is the Embudo fault zone (Figure 2.7), which strikes northeast into the Española Basin and is coincident with the Jemez lineament. The fault zone separates two segments of the Rio Grande rift and thus acts as a transform fault (Muehlberger,

1979). During the Pliocene, the Embudo fault zone underwent major right lateral strike-slip motion (Dungan et al., 1984), but since 2.5 Ma movements along the fault system have slowed (Aldrich, 1986).

The Jemez Lineament

The Jemez lineament is a northeast-southwest trending structural feature that stretches through Arizona and New Mexico and extends across three major tectonic provinces including the Colorado Plateau, the Rio Grande Rift, and the Great Plains (Aldrich, 1986). On the surface, the Jemez lineament manifests itself as a northeast-southwest trending group of Cenozoic volcanic fields stretching from southeast Arizona to northeast New Mexico (Figure 2.1). This includes the Jemez Mountains, Mt. Taylor, Raton-Clayton, Ocate, Zuni-Bandera, and Springerville volcanic fields. Beneath the surface, the lineament is a crustal flaw that is thought to control volcanic and tectonic activity in the Jemez Mountains (Aldrich, 1986).

Seismic studies such as the CD-ROM project have suggested that the lineament may correspond to a suture between the 1.65 Ga Mazatzal Island Arc, the 1.8-1.7 Ga Yavapai proto-North American continent, and a transitional terrane that lies between the two (Shaw and Karlstrom, 1999; Dueker et al., 2002; Karlstrom et al., 2002; Magnani et al. 2004). Seismic data obtained from the CD-ROM Project indicate a southward-dipping crustal reflector projecting towards a southward-dipping mantle layer that is coincident with the Jemez Lineament. This boundary, which has been interpreted as the Southern Yavapai-Mazatzal suture, extends beneath 200 km depth and is marked by a division between high-velocity mantle to the south and low-velocity mantle to the north (Karlstrom et al., 2002). Wolff et al. (2005) propose that the fertile mantle trapped in the suture is the source for magma erupted in the JMVF. Migratory pathways to the surface are provided by Rio Grande Rift-related extension.

Volcanism in the JMVF

The Jemez Mountains Volcanic Field (JMVF) is the largest and most diverse volcanic field with respect to erupted products found along the Jemez lineament (Goff and Gardner, 2004). The JMVF contains approximately 2000 km³ of erupted material ranging from lava flows to ignimbrites and encompassing a compositional spectrum from nephelinite to high-silica rhyolite (Wolff et al., 2005). The JMVF is built upon a series of Upper-Paleozoic rift-fill sediments that in turn rest on Proterozoic basement rocks (Brookins and Laughlin, 1983). These Precambrian rocks have been dated between 1.62-1.44 Ga (Brookins and Laughlin, 1983).

Previous work

Early descriptions of the stratigraphy and volcanic evolution of the JMVF began in the late 19th century with the work of Iddings (1890) and Flood and Vincent (1885, republished by Powell in 1961). Later, Ross (1938) authored a study on what he termed the Valles Volcano. Comprehensive study of the region began in the mid 20th century, as evidenced by the abundance of publications produced in the 1960's and 1970's (Ross et al., 1961; Smith et al., 1961; Griggs, 1964; Smith and Bailey, 1966; Smith and Bailey, 1968; Bailey et al., 1969; Smith et al., 1970). The majority of these studies combined geologic mapping, borehole analysis, and stratigraphic observations. Early K-Ar age determinations were provided by Dalrymple et al. (1967), Doell and Dalrymple (1966), and Doell et al. (1968).

Griggs (1964), Bailey et al. (1969) and Smith et al. (1970) introduced the first formal stratigraphic framework for the JMVF. They divided the rocks of the field into three groups including, from oldest to youngest, the Keres, Polvadera, and Tewa groups. These authors believed the individual groups to be temporally and petrologically distinctive (Goff et al., 1989). Subsequent work, including more detailed mapping, more accurate geochronology, and borehole

data has determined that both temporal and petrologic overlap exists between all groups (Gardner and Goff, 1986; Loeffler, 1988; Goff et al., 1989). The work of Gardner et al. (1986) in particular served as a significant landmark in the ongoing re-evaluation of the JMVf stratigraphy. A more recent revision to JMVf stratigraphy is that of Goff and Gardner (2004) shown in Figures 2.8 and 2.9. It is significant in that it recognizes not only temporal overlaps between groups, but also geographic distributions among the erupted groups.

JMVf stratigraphy as currently understood

The stratigraphic framework of Bailey et al. (1969) and Smith et al. (1970) has been substantially modified as new geochronological and stratigraphic data have become available. Notable revisions have been published by Gardner et al. (1986), and later by Goff and Gardner (2004). However, a major issue with the stratigraphic nomenclature in the JMVf is that researchers now recognize that the subdivisions of Keres and Polvadera groups are not particularly useful (Rowe et al., 2007). The two groups are not temporally distinct and significant overlaps exist in the ages of many formations. In particular, the Polvadera Group rocks as defined by Bailey et al. (1969) and Smith et al. (1970), represent wide-ranging ages and petrologic origins (Rowe et al., 2007). Wolff et al. (2005) described the petrogenesis of pre-caldera mafic lavas using a modified stratigraphy from Gardner et al. (1986). More recently, Rowe et al. (2007) provided a description of the pre-caldera intermediate and silicic rocks in which usage of the terms Keres and Polvadera is largely abandoned and units are described independently. This improved temporal scheme is illustrated in Figure 2.10. In this paper, a combination of the revisions of Goff and Gardner (2004), and modifications by Wolff et al. (2005) and Rowe et al. (2007) will be used to describe the stratigraphy of the JMVf. It is hoped

that in the near future a new stratigraphic framework will be developed for the JMVf that ties together the advances made by the above mentioned researchers.

Overview of JMVf Stratigraphy

Santa Fe Group Lavas

The oldest volcanic rocks exposed in the JMVf are a series of sporadic basaltic lavas found interbedded with Santa Fe Group basin-fill sediments beneath the Keres Group in the Saint Peter's Dome region, to the north and northeast of the field, and in the northern Española Basin (Goff et al., 1990; Gardner et al., 1986; Woldegabriel et al., 2003). These lavas have been dated at 25-16.5 Ma (Bailey et al., 1969, Smith et al., 1970, Gardner et al., 1986, Woldegabriel et al., 2003). The Santa Fe lavas fall in two chemical groups (Wolff et al. 2005): strongly silica-undersaturated nephelinites and basanites, and tholeiites and quartz-normative basaltic andesites. It has been proposed that the Santa Fe Group lavas erupted during an early extensional phase (one that preceded activity in the JMVf) that resulted in a small-volume, late Oligocene to middle Miocene volcanic episode in the Española Basin (Gardner et al., 1986; Gibson et al., 1993; Woldegabriel et al., 2003)

Keres Group of Bailey et al. (1969)

As originally defined by Bailey et al. (1969), the Keres Group contained four formations: Paliza Canyon, Canovas Canyon Rhyolite, Bearhead Rhyolite, and the Basalt of Chamisa Mesa. The Basalt of Chamisa Mesa has been largely discredited as a unit as it is chemically, temporally, and petrographically indistinguishable from Paliza Canyon basaltic lavas (Gardner et al., 1986). Gardner et al. (1986) also included the Cochiti formation, a series of volcanoclastic rocks as a part of the Keres Group. Rocks of the group are generally found in the southern JMVf but also crop out in a small area along the northern rim of the Valles caldera (Figure 2.9).

The group contains volcanic rocks of the entire compositional spectrum from basalt to rhyolite, but it is dominated by andesite of the Paliza Canyon Formation (Gardner et al., 1986). Based on K/Ar and $^{40}\text{Ar}/^{39}\text{Ar}$ dates, the Keres Group is thought to span the time period from 13-6 Ma (Luedke and Smith, 1978; Gardner, 1985; Gardner et al., 1986; Goff et al., 1990; McIntosh and Quade, 1995; Justet, 1996; Chamberlin et al., 1999; Justet and Spell, 2001).

Paliza Canyon Formation

The Paliza Canyon Formation consists of mainly of trachyandesites, trachydacites, and dacites, with subordinate mafic lavas, andesites, and low-silica rhyolites erupted between 13-7 Ma (Rowe et al., 2007). The approximately 1000 km³ of lava flows, domes, tuffs and minor intrusives are exposed mainly in the southern portion of the JMVf. However, well data (Hulen et al., 1991), mapping (Smith et al., 1970; Gardner and Goff, 1996), and lithic fragment data show that Paliza Canyon rocks extend under the caldera and underlie the Tschicoma Formation in the north central Jemez Mountains. On the basis of age and geochemical affinity, the dacite of Los Cerritos found in the northeastern JMVf (originally Polvadera Group) has been included as a part of the Paliza Canyon Formation.

Figure 2.11 is a TAS plot showing the intermediate to silicic pre-caldera rocks of the JMVf (Rowe et al, 2007). This plot shows that the Paliza Canyon compositions are weakly alkaline. Therefore, most Paliza Canyon lavas in the 57-63% SiO₂ range are classified as trachyandesite and the remainder as andesite. Lavas in the range 63-69% SiO₂ are more evenly distributed between trachydacite and dacite (Rowe et al., 2007). Phenocryst assemblages for the trachyandesites and andesites are plagioclase (An₃₀-An₆₀) + augite + hypersthene + opaque oxides ± hornblende ± olivine. Reaction rims and resorption textures are common among the olivine and plagioclase phenocrysts respectively (Rowe et al., 2007). For the dacites, plagioclase

(An₁₆-An₅₃) is the most common phenocryst with hornblende, biotite, clinopyroxene, opaque oxides, and small quantities of apatite also present (Rowe et al., 2007).

The mafic lavas of the Paliza Canyon Formation (seen in the TAS plot in Figure 2.11) include olivine tholeiites, olivine basalts, hawaiites, mugearites and benmoreites that have the same petrographic and trace-element groupings as the Cerros del Rio lavas (Wolff et al., 2005). The lavas have distinctively high La/Nb and Th/K ratios, and plagioclase phenocrysts (An₃₀₋₆₀) exhibit complex zoning and resorption textures. Wolff et al. (2005) suggest that these textures represent varying degrees of magma mixing and hybridization.

Canovas Canyon Rhyolite

The Canovas Canyon Formation is comprised of low and high silica rhyolite and rhyodacite lava flows, domes, plugs, and pyroclastic deposits found interbedded within the Paliza Canyon Formation (Bailey et al., 1969; Rowe et al., 2007). A tuff has been dated at 12.4 Ma by Gardner and co-workers (1986). The TAS plot in Figure 2.11 shows that the rhyolites are split between two types: a low-silica (69-72 % SiO₂) variety that is very similar petrographically and geochemically to Paliza Canyon rocks mapped as 'biotite dacite' by Goff et al. (1990) and a high-silica (76-78% SiO₂) variety that is sparsely porphyritic (Rowe et al., 2007). The latter contains phenocrysts of sanidine + quartz + opaque oxides ± plagioclase ± pyroxene ± hornblende ± biotite (Rowe et al., 2007).

Bearhead Rhyolite

The Bearhead Rhyolite and associated Peralta Tuff consist of a series of high-silica rhyolite (Figure 2.11) domes, flows, tuffs, and shallow intrusions. These rocks have been described in detail by Smith (1989) and Gay and Smith (1993), and have been dated at 7.06 – 6.1

Ma by Justet and Spell (2001). Bearhead rhyolite lavas have been described by Rowe et al., (2007) as being nearly aphyric and similar to the Canovas Canyon rhyolites.

Lobato Basalt

The Lobato basalt is the only mafic unit in what was formerly the Polvadera Group of Bailey et al. (1969). It is mainly comprised of lava flows and cinder deposits. The majority of the basalts appear to have been erupted between 10.8 -7.8 Ma, based on mapping and geochronology by Manley (1982) and Goff et al. (1989). Aldrich and Dethier (1990) reported K/Ar ages of 13.9 ± 0.4 to 9.6 Ma and Gardner et al. (1986) reported a voluminous pulse of volcanism dated at 10.8 ± 0.3 to 9.1 ± 0.2 Ma. Several flows found inter-bedded with Santa Fe Group sediments in the northern JMVf were dated at 14.05 ± 0.33 Ma using K/Ar techniques (Dethier et al., 1986; Aldrich and Dethier, 1990). Goff et al. (1989) and Wolff et al. (2005) state that the Lobato basalts are predominantly tholeiitic in nature. These rocks are typically olivine-phyric and are comparable in composition (Figure 2.11) to tholeiitic lavas from the later Cerros del Rio and El Alto basalts (Wolff et al., 2005).

Tschicoma Formation

The Tschicoma Formation is a major unit in the northern portion of the JMVf. It is comprised of approximately 500 km^3 of domes and lava flows ranging in composition from andesite to rhyodacite (Gardner et al., 1986). Dacite is by far the predominant composition (Figure 2.11) with subordinate amounts of trachyandesite, andesite, and rhyolite (Rowe et al., 2007). Ages range from 6.9 ± 0.3 to 2.96 ± 0.27 Ma with the majority of the dacites erupted from 5-2.7 Ma (Dalrymple et al., 1967; Leudke and Smith, 1978; Gardner et al., 1986); Goff et al., 1989; Goff and Gardner, 2004).

Tschicoma dacites are coarsely porphyritic and contain 15-20% phenocrysts with the assemblage plagioclase \pm clinopyroxene \pm orthopyroxene (resorbed) \pm hornblende \pm biotite + opaque oxides (Rowe et al., 2007). Disequilibrium textures in plagioclase and hornblende phenocrysts are common, as are mafic enclaves composed of basaltic andesite, andesite and trachyandesite up to 25 cm in diameter (Rowe et al., 2007).

The Cerro Rubio quartz latites consist of two small plugs on the east side of the Toledo embayment on the northeast side of the current Valles caldera (Gardner et al, 1986). They are rhyodacitic in composition and have been dated by K/Ar at 2.18 ± 0.09 Ma and 3.59 ± 0.36 Ma respectively (Heiken et al., 1986). Rowe et al. (2007) include the Cerro Rubio quartz latites in the Tschicoma Formation on the basis of similar age and chemistry.

The lavas of the La Grulla Plateau in the northern JMVf are separated from the main body of the Tschicoma Formation by the Mesa del Medio, which consists of Bandelier Tuff occupying a deep paleovalley system (Rowe et al., 2007). It consists of andesite lavas (Figure 2.11) that are capped by domes and flows of dacite and trachydacite (Singer and Kudo, 1986). The suite has been dated at 7.9-7.4 Ma (Singer and Kudo, 1986), a timeframe that overlaps late activity in the Paliza Canyon Formation. The La Grulla Plateau rocks share major element, trace element, and isotopic characteristics with both the Paliza Canyon Formation and the main body of the Tschicoma Formation (Rowe et al., 2007). However, one dacite dome contains mafic enclaves that are chemically similar to those found in the more easterly Tschicoma dacites (Rowe et al., 2007).

Puye Formation

The Puye formation is a 15 km^3 volcanoclastic alluvial fan derived from Tschicoma Formation domes and lavas (Waresback and Turbeville, 1990). It is situated on the eastern side

of the JMVf, covers nearly 200 km² and has an estimated total thickness of at least 110 m (Waresback and Turbeville, 1990). Fallout deposits equivalent in composition to Tschicoma dacite are found interbedded throughout the Puye. The Puye ignimbrite, exposed in the middle of the formation, has been dated at 2.53 ± 0.1 Ma with K/Ar techniques (Waresback and Turbeville, 1990). High silica rhyolite pyroclastic fall deposits are found in the upper Puye, one of which is correlative to the San Diego Canyon ignimbrites erupted at 1.85 Ma (Turbeville and Self, 1988). These deposits are noteworthy because they represent the first eruptive products from the Bandelier magma system.

El Rechuelos Rhyolite

El Rechuelos Rhyolite (Figure 2.11) is a group of six small rhyolite domes and plugs found in the northern JMVf (Smith et al., 1970; Loeffler et al., 1988). They are thought to represent three phases of volcanism at 7.5 Ma, 5-6 Ma, and 2 Ma (Loeffler et al., 1988). The two older groups are similar in age to the Bearhead Rhyolite (7.06-6.1 Ma) but they share more chemical similarities with the Tschicoma rhyolites (Rowe et al., 2007). The younger group is composed of high-silica rhyolite with sparse microphenocrysts of sanidine, plagioclase (Na-rich), and quartz.

San Diego Canyon (SDC) Tuff

The SDC Tuff underlies the Bandelier Tuff in Cañon de San Diego on the southwest side of the present-day caldera, and it has also been found in core holes drilled within the caldera (Hulen et al., 1991). Like the Bandelier, the SDC Tuffs are high-silica rhyolite (Figure 2.11) between 75-78% SiO₂ and consist of fall, flow, and surge deposits. Turbeville and Self (1988) divided the SDC rocks into two informal units, an older ignimbrite termed unit A, and a younger unit B. Unit A is lithic-rich and non-welded while unit B is stratified, non-welded to weakly-

welded, and pumice-rich (Turbeville and Self, 1988). Spell et al. (1996) determined $^{40}\text{Ar}/^{39}\text{Ar}$ ages of 1.85 ± 0.07 Ma and 1.85 ± 0.04 Ma for SDC ignimbrite units A and B respectively. The SDC ignimbrites share many geochemical similarities with the Bandelier Tuffs and have been identified as early products of the Bandelier magma chamber (Spell et al., 1990).

Bandelier Tuff

The Bandelier Tuff is one of the best known ignimbrite units in the world and has been extensively studied (Ross et al., 1961; Smith and Bailey, 1966; Bailey et al., 1969; Smith et al., 1970; Smith, 1979; Gardner et al., 1986; Self et al., 1986; Potter and Oberthal, 1987; Goff et al., 1989; Spell et al., 1990; Wolff et al., 1999; Wolff et al., 2002; Wolff and Ramos, 2003). The Bandelier Tuff consists of two units, the Otowi (lower) and Tshirege (upper) Members that represent the products of two major caldera-forming eruptions. Izett and Obradovich (1994) cite $^{40}\text{Ar}/^{39}\text{Ar}$ ages of 1.61 ± 0.01 Ma for the Otowi and 1.22 ± 0.02 Ma for the Tshirege. Winick et al. (2001) cited $^{40}\text{Ar}/^{39}\text{Ar}$ ages using melt inclusion-bearing quartz phenocrysts of 1.629 ± 0.022 Ma and 1.235 ± 0.032 Ma for the Otowi and Tshirege respectively. More recently, Phillips et al. (2006) cite ages of 1.68 Ma for the Otowi and 1.21-1.25 Ma for the Tshirege. Each member consists of basal plinian fall beds overlain by ignimbrite deposits. The Guaje pumice bed is the plinian deposit associated with the Otowi Member, and the Tsankawi pumice bed is the plinian deposit associated with the Tshirege Member. Both members are compositionally-zoned, high-silica rhyolite tuff sheets showing internal upward decreases in the concentrations of incompatible trace elements. The Otowi Member is generally less welded than the Tshirege and is more lithic-rich. Smith and Bailey (1966) provided an early volume estimate for the Otowi Member of approximately 200 km^3 dense rock equivalent (DRE). Later, Self and Lipman (1989) estimated the total erupted volume to be approximately 400 km^3 DRE.

The approximately 390,000 year interval between the Otowi and Tshirege Members is referred to as the Cerro Toledo interval (Heiken et al., 1986; Stix et al., 1988; Spell et al., 1996). The Cerro Toledo Rhyolite is found within the present-day Valles caldera and consists of domes, lava flows, and pyroclastic deposits. In addition, Cerro Toledo pyroclastic rocks are found sandwiched between Bandelier Tuff members on the Pajarito Plateau (Griggs, 1964; Gardner et al., 1986). Cerro Toledo rhyolites are typically aphyric, which contrasts with the highly porphyritic pumice of the Bandelier Tuff (Goff and Gardner, 2004). Heiken et al. (1986) defined seven cycles of explosive activity in the Cerro Toledo Rhyolite, some of which erupted through an intracaldera lake located in the eastern portion of the Toledo caldera. This hypothesis was based on the presence of phreatomagmatic tuffs in the Cerro Toledo Rhyolite deposits. Spell et al. (1996) used $^{40}\text{Ar}/^{39}\text{Ar}$ geochronology to suggest that five major tephra-producing eruptions occurred in pulses at 1.59, 1.54, 1.48, 1.37, and 1.23 Ma. Cerro Toledo domes have been interpreted as representing resurgent activity associated with the last remnants of Otowi magmatism (Gardner et al., 1986; Stix et al., 1988, Spell et al., 1996).

Valles Rhyolite

The Valles Rhyolite was first described by Griggs (1964) and was later subdivided into six members by Bailey et al. (1969) and Smith et al. (1970). It includes domes, lava flows, and pyroclastic deposits, all of which represent intra-caldera volcanism postdating the creation of the Valles Caldera. From oldest to youngest the members are the Deer Canyon, Redondo Creek, Valle Grande, Battleship Rock, El Cajete, and Banco Bonito. They are divided into two compositional groupings, including the high-silica rhyolites of the Valle Grande and Deer Canyon members and the lower-silica rhyolites of the Redondo Creek, Battleship Rock, El Cajete, and Banco Bonito members (Bailey et al., 1969). El Cajete, Battleship Rock, and Banco

Bonito members are commonly referred to as the southwestern moat rhyolites (Wolff and Gardner, 1995; Wolff et al., 1996). These rocks are the youngest eruptive products in the JMVF.

Hydrothermal Activity

Two episodes of significant hydrothermal activity are recognized in the JMVF: a period lasting from approximately 8.5 to 5.5 Ma associated with Keres Group volcanism and a second period that began 1.6 Ma and continues to the present. The current phase of activity is associated with formation of the Toledo and Valles calderas and with younger Tewa Group volcanism (Woldegabriel and Goff, 1989; 1992). Considerable study has been devoted to understanding the active nature of the Valles geothermal system (Goff and Grigsby, 1982; Hulen and Nielson, 1986; Goff et al., 1989; Goff and Gardner, 1994; Woldegabriel and Goff, 1989; 1992).

Associated Mafic Volcanism

Three mafic volcanic fields exist on the periphery of the JMVF along its border with the Rio Grande Rift (Figure 2.4). From north to south these fields are El Alto, Cerros del Rio, and Santa Ana Mesa (Smith et al., 1970). The three fields consist mainly of small mafic shields, lava flows, cinder cones, and maars. The TAS diagram of Rowe et al. (2007) in Figure 2.11 shows the compositional ranges for the El Alto and Cerros del Rio groups. The Cerros del Rio is the largest of the fields and contains lavas of two compositional groups: tholeiites and a continuum of *ne-hy* normative hawaiiites-mugearites (Wolff et al., 2005). The tholeiites in White Rock Canyon were erupted between 2.48 and 2.33 Ma and the hawaiiite-mugearite series between 2.57 and 2.46 Ma (Woldegabriel et al., 1996). El Alto field is smaller but its lavas are petrographically and chemically similar to those found in the Cerros del Rio (Wolff et al., 2005). Gardner et al. (1986) indicated a minimum duration of 4.6 to 1.45 or 1.12 Ma for eruption from the three fields. This was based on a single K/Ar age of 4.62 ± 0.12 Ma and the recognition of

lavas inter-bedded between the Tshirege and Otowi members of the Bandelier Tuff (Gardner et al., 1986).

Petrogenetic History of the JMVF

Pre-caldera mafic lavas

Wolff et al. (2005) proposed that the lithospheric mantle represents a significant source for JMVF parental mafic magmas. The Proterozoic suture zone beneath the JMVF constitutes a major crustal weakness, and ancient oceanic lithosphere associated with the suture has been identified as a likely source for primary magmas. Seismic and geophysical evidence presented by previous workers (Shaw and Karlstrom, 1999; Duecker et al., 2001; Karlstrom et al., 2002; Magnani et al. 2004) supports this theory. Two types of parent magmas have been identified including a K-depleted, silica-undersaturated parent derived from partial melting of lithospheric mantle and a tholeiitic parent derived from either lithospheric or asthenospheric mantle (Wolff et al., 2005). From these parental compositions, two types of JMVF mafic lavas have resulted, including hawaiite-mugearites and tholeiites. Wolff et al. (2005) suggest that these magmas have been derived primarily through a combination of partial melting of lithospheric mantle and subsequent contamination with variable amounts of continental crust.

Pre-caldera intermediate to felsic rocks

Rowe et al. (2007) provided a review of the petrogenesis of the pre-caldera intermediate to silicic rocks in the JMVF and the caldera-related silicic rocks. A significant process in the petrologic evolution of the JMVF appears to be mixing of mantle-derived mafic compositions with crustal melts. Most notably, hawaiites, mugearites, and basaltic andesites of the Cerros del Rio and some of the Paliza Canyon Formation are attributed to mixing of crustal melts with the K-depleted, silica-undersaturated parent material identified by Wolff et al. (2005). The majority

of the Paliza Canyon, Canovas Canyon, Bearhead, and La Grulla Plateau (Tschicoma) volcanic products between 63-73% SiO₂ formed from a diverse set of petrogenetic processes including fractional crystallization, assimilation-fractional crystallization (AFC), and simple mixing of mafic magmas with crustal melts (Rowe et al., 2007). The large dacite domes of the Tschicoma Formation formed through near-complete crustal melting of granitoid rocks and mixing with mafic magmas. Pre-caldera rhyolites in the JMVf, such as the Bearhead and Canovas Canyon are isotopically distinct and appear to be generated by melting of Proterozoic crust (Rowe et al., 2007).

The Caldera Rhyolites (SDC, Bandelier, Valles)

The caldera rhyolites, like their predecessors, are thought to represent crustal melts. However, unlike the Bearhead and Canovas Canyon rocks, they represent partial re-melting of 'hybridized' crust as opposed to more 'pristine' Proterozoic crust (Rowe et al., 2007). Repeated basalt intrusions beneath the JMVf after approximately 2-3 Ma led to rejuvenation of young, warm intrusive rocks beneath the surface. The products associated with this melting formed the Bandelier magma system, which first erupted as the San Diego Canyon ignimbrites at 1.85 Ma and later as the Bandelier Tuff and Valles Rhyolite (Rowe et al., 2007). The residual heat from the basaltic intrusions is thought to have resulted in a reduced thermal "penalty" during the melting process and allowed for the generation of greater quantities of crustal melts (Rowe et al., 2007). In other words, less thermal energy was required to heat the crust as part of the melting process, and thus this extra energy was available for increased crustal anatexis. This may help to explain why the caldera rhyolites are more voluminous than their predecessors.

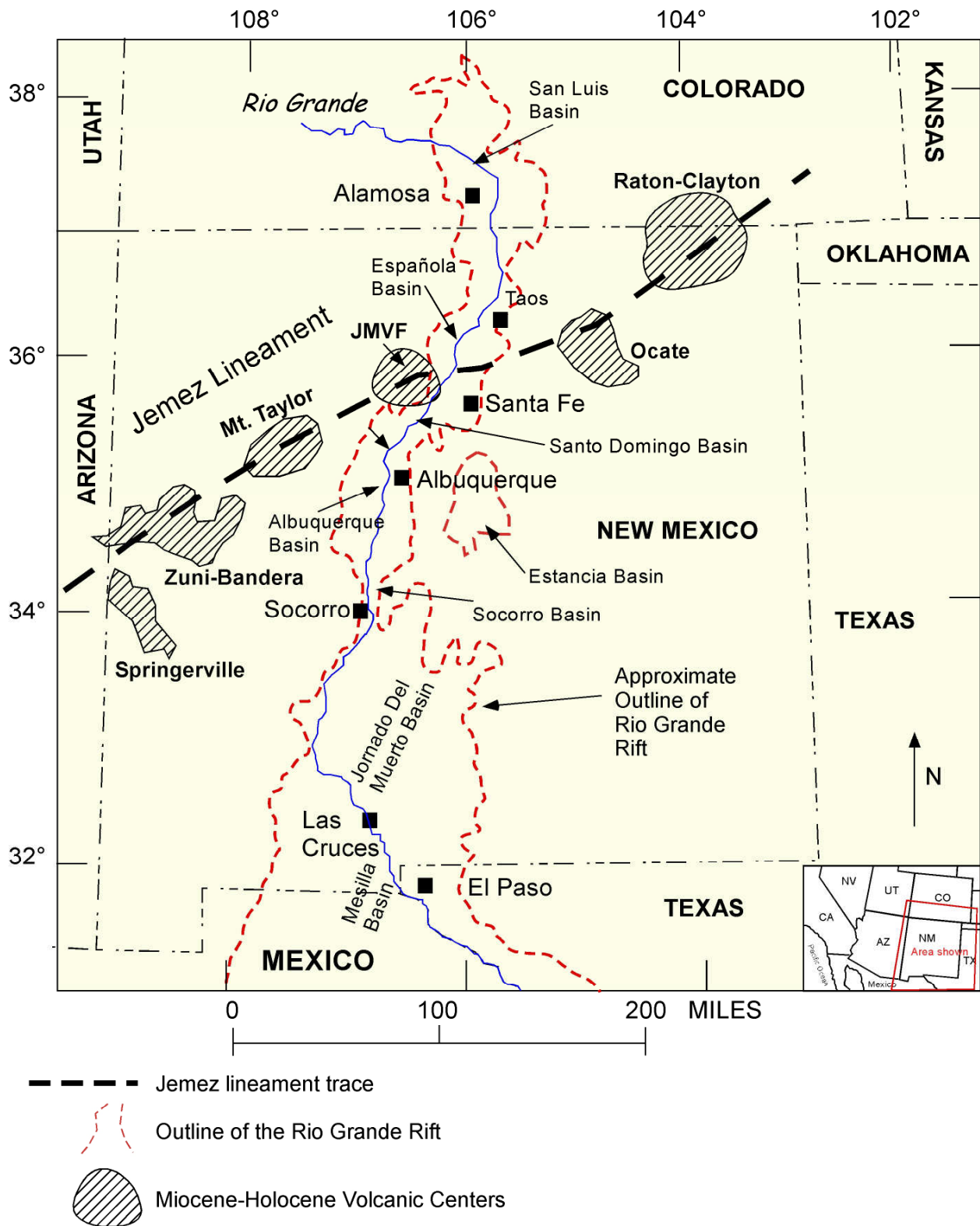


Figure 2.1. Map showing the Rio Grande rift, the Jemez Mountains Volcanic Field (JMVF), other major Cenozoic volcanic centers, major rift-related basins, and the Jemez lineament.

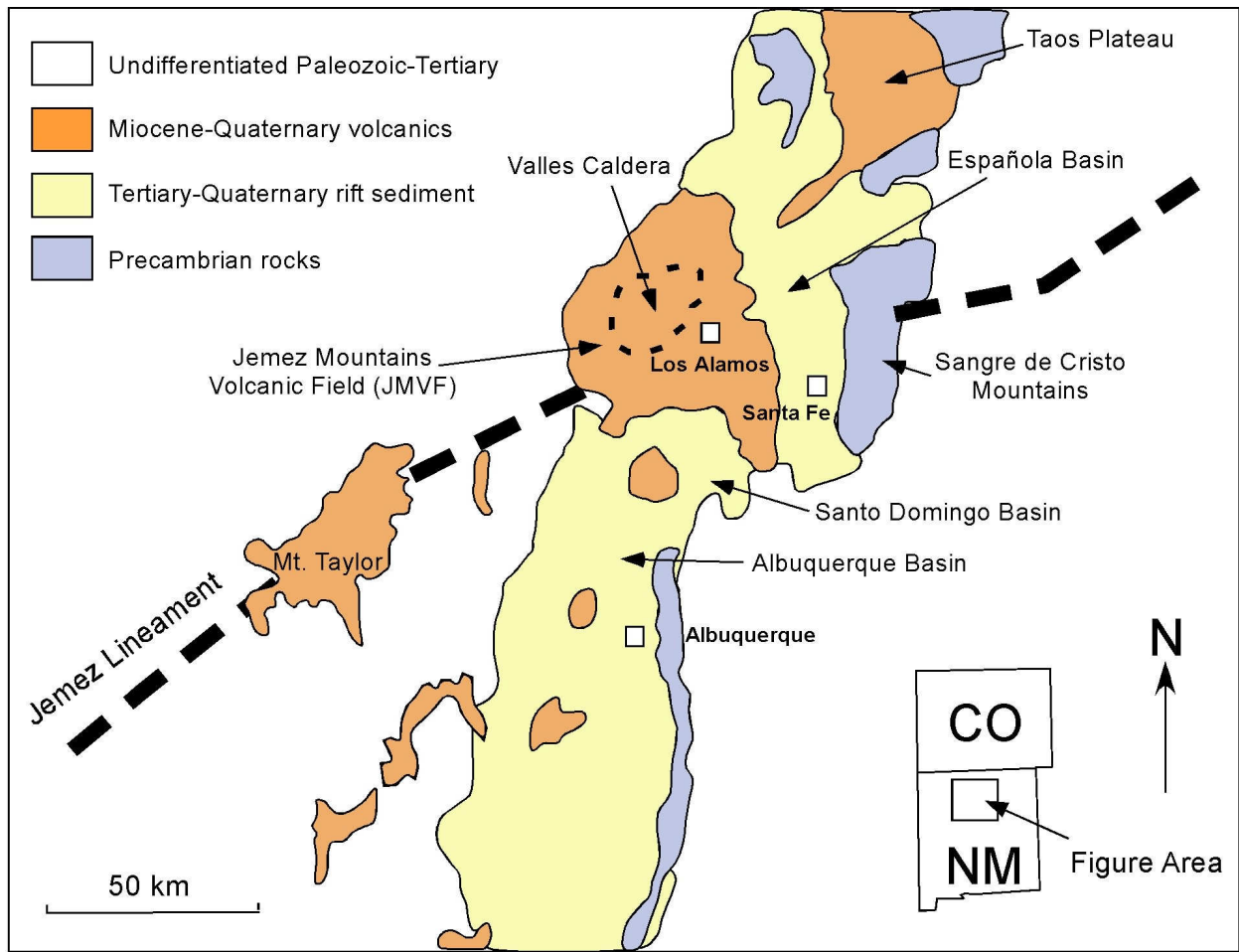


Figure 2.2. Location map showing the northern Rio Grande Rift, the Jemez Lineament, and the Jemez Mountains Volcanic Field (JMVF). (Modified from Gardner et al., 1986)

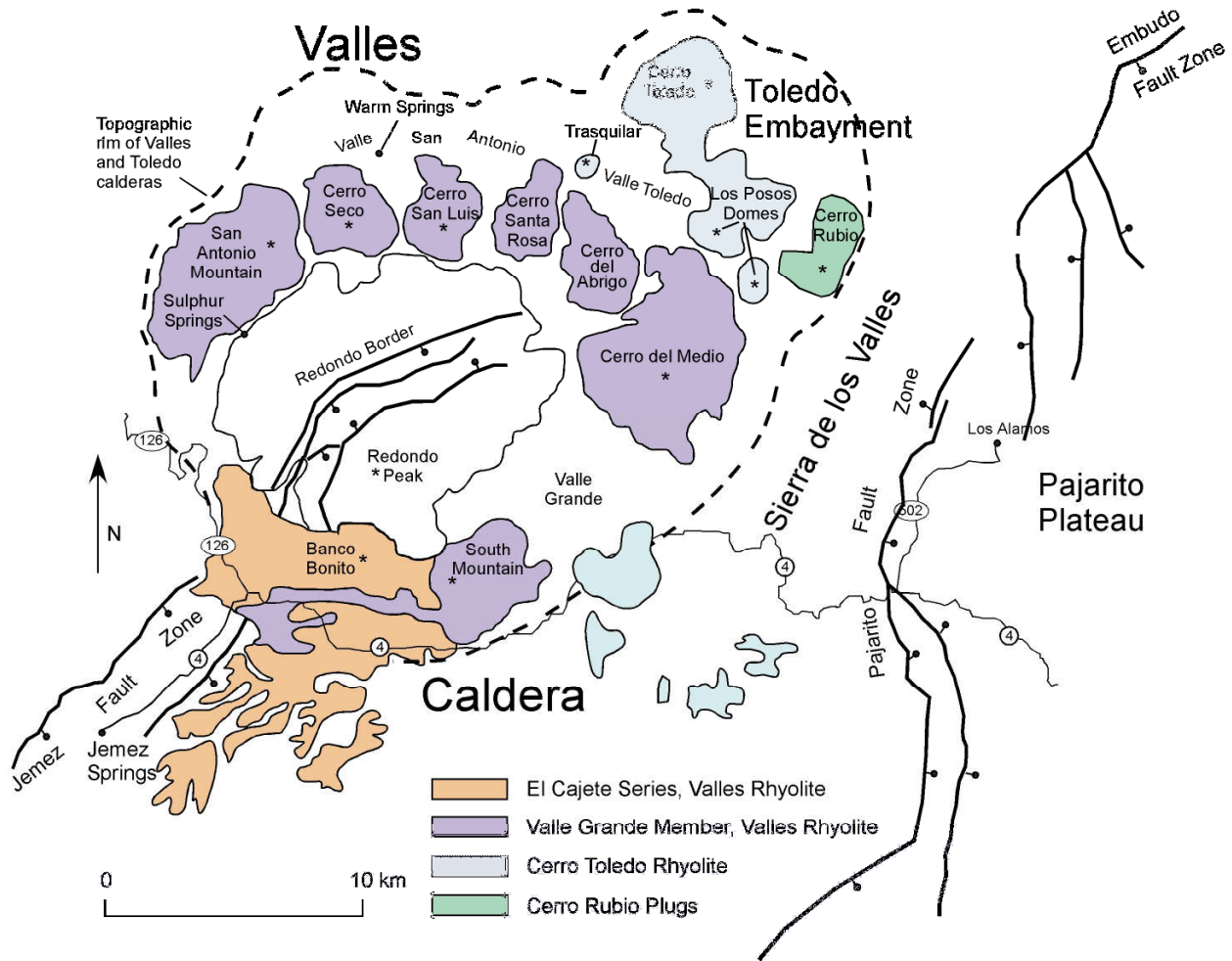
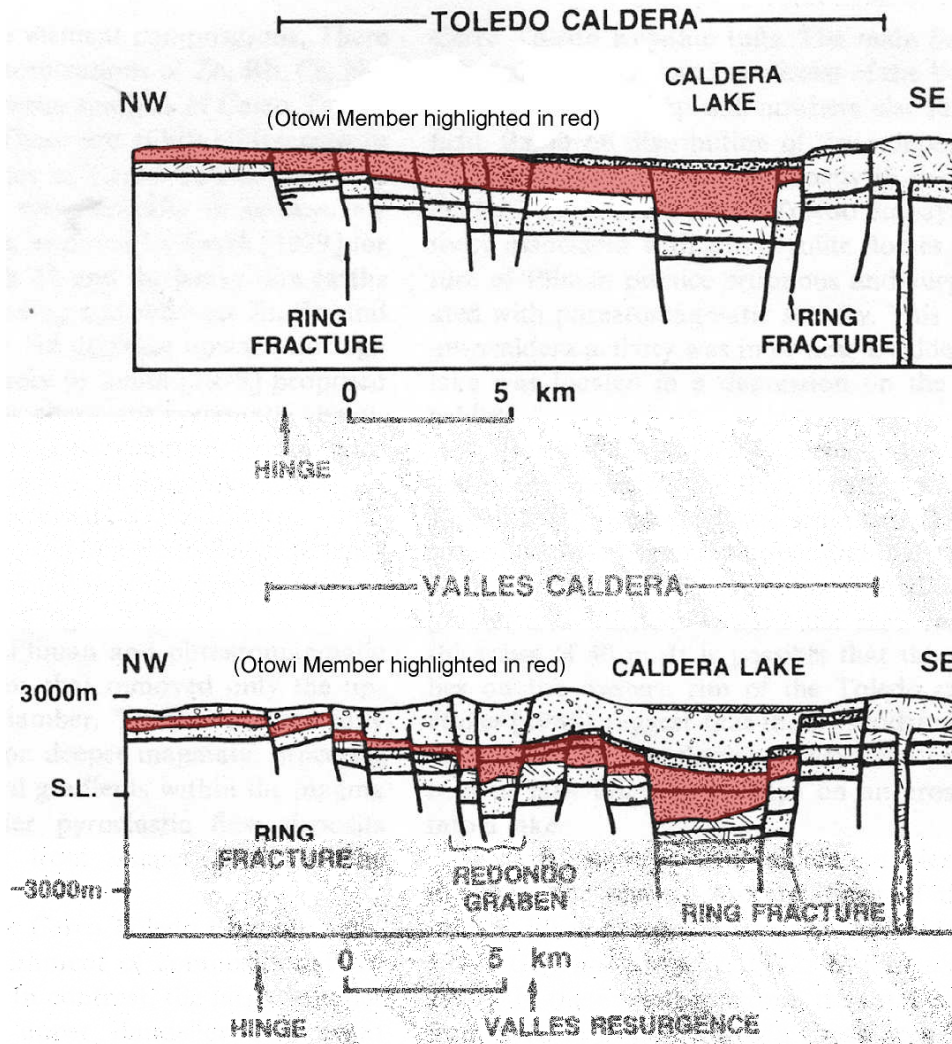


Figure 2.3. Map of the Valles caldera showing the outline of the current caldera, the Toledo embayment, and various resurgent domes and peaks. Modified from Goff and Gardner, 2004.



Key to Lithologies

- White** - Precambrian basement, Paleozoic and Mesozoic sedimentary rocks
- Fine stipple** - sedimentary rocks of the Rio Grande rift
- Double dashes with red background** - pre-Bandelier tuff volcanic rocks
- Dark, short dashes** - Otowi Member, Bandelier tuff
- Coarse stipple and cross-hatch** - intracaldera tuffs and lake deposits
- Dots and circles** - Tshirege Member, Bandelier tuff

Figure 2.4. Cross-sections illustrating geophysical models proposed by Nielson and Hulen (1984) and Heiken et al. (1986) that support a trap-door style collapse origin for both caldera-forming eruptions of the Bandelier Tuff (Heiken et al., 1986).

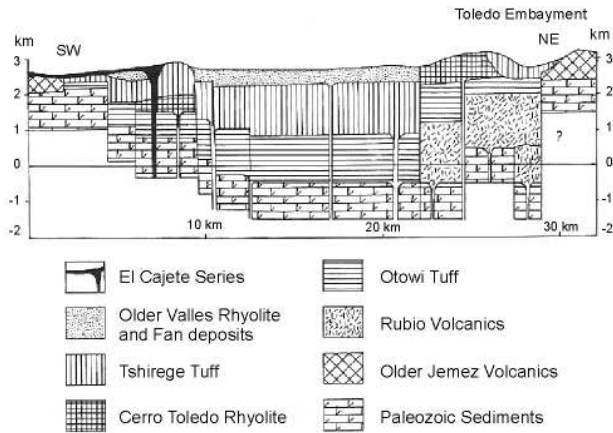


Figure 2.5a. Geophysical model (SW-NE cross-section) of the Valles caldera by Nowell (1996) illustrating major rock units, thicknesses, and basic structure

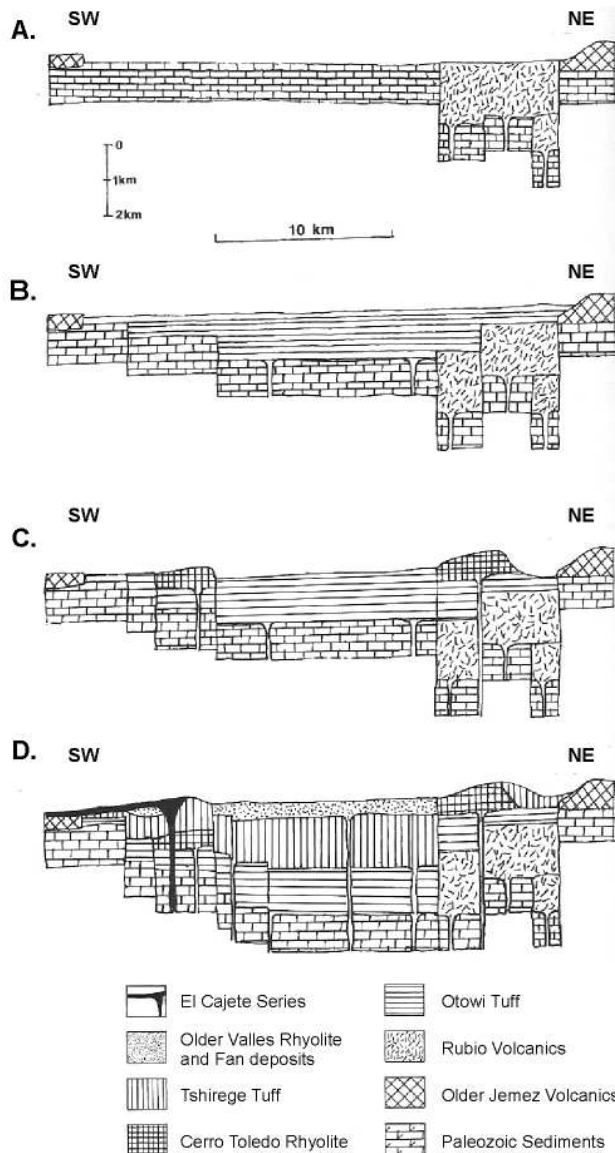


Figure 2.5b. Sequence of SW-NE cross-sections showing the development of the Valles caldera based on geophysical modeling of Seagar (1974) and Nowell (1996). **A.** Volcanism associated with the Rubio volcano in the NE (4 Ma to 1.78 Ma); **B.** Formation of the Toledo caldera (1.61 Ma); **C.** Intracaldera volcanics; **D.** Collapse of the Valles caldera and post-caldera volcanics (1.22 Ma to 53 Ka).

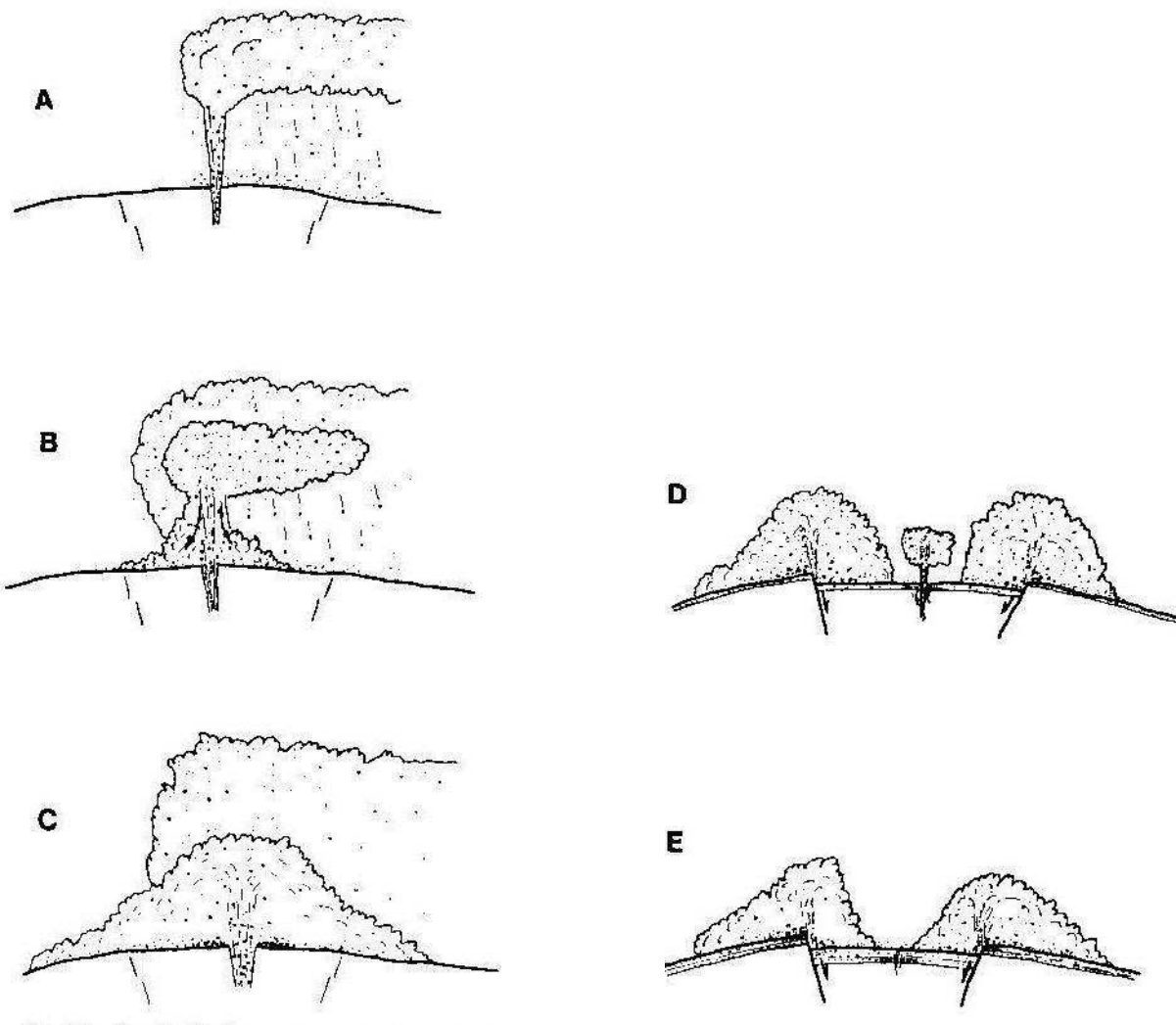
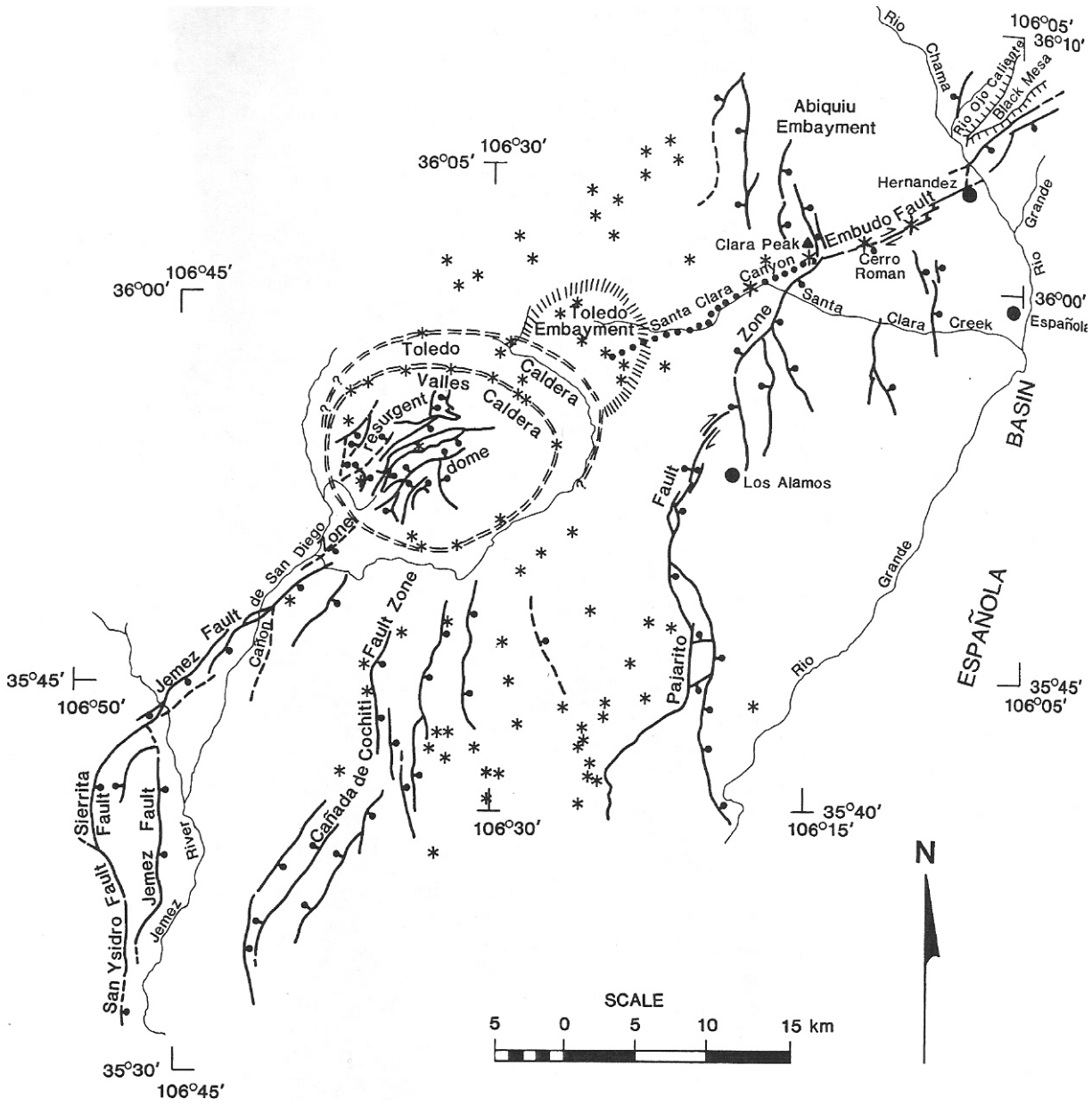


Figure 2.6. Interpretation of the Lower Bandelier Tuff eruptive sequence. A = initial Plinian eruption from central vent, B = initial collapse of central eruption column produces thin pyroclastic flow and surge deposits, C = wholesale collapse of central column leads to development of large-scale pyroclastic flow deposits, D = caldera collapse (magma chamber under-pressurized), transition of vents to ring fractures, E = continued collapse and ring fracture eruptions. From Self et al. (1986)









- EXPLANATION**
-  Caldera ring fracture
 -  Structural depression
 -  Volcanic vent
 -  Mesa edge
hachures on slope
 -  High angle fault
dumbbell on downthrown side
arrows show relative offset
 -  Structural discontinuity

Figure 2.7. Map of the JMVF and surroundings showing the Valles caldera, major Neogene fault systems, and locations of volcanic vents. Compiled by Aldrich (1986) using data from Kelly (1978), Smith et al. (1970) Woodward and Ruetschilling (1976), Woodward et al. (1977), Goff et al. (1984), Gardner and Goff (1984), Dethier and Manley (1986), and unpublished maps from F. Goff (1984).

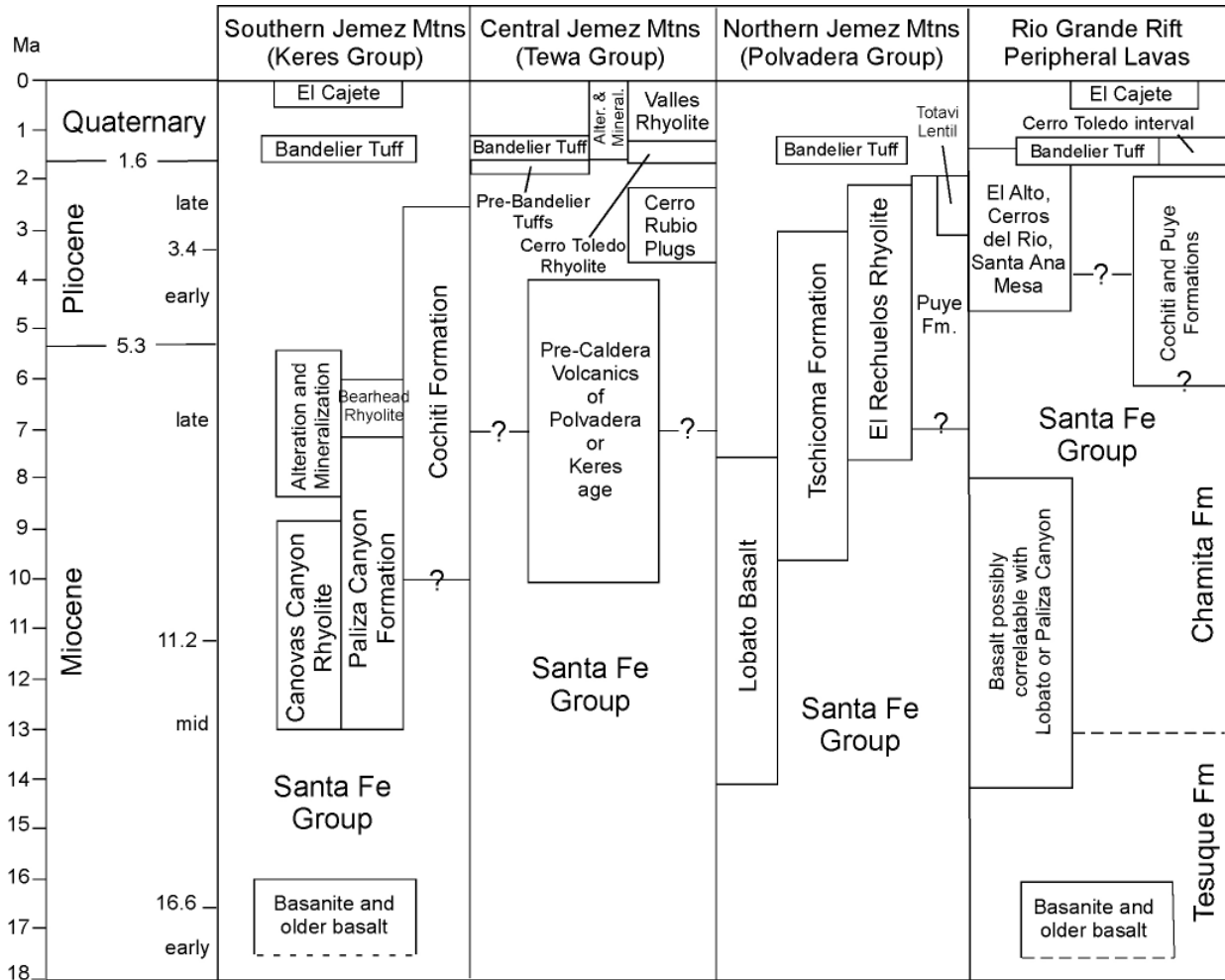


Figure 2.8. Revised stratigraphy for the JMVf showing stratigraphic relationships in the Jemez Mountains by area. (Adapted from Goff and Gardner, 2004)

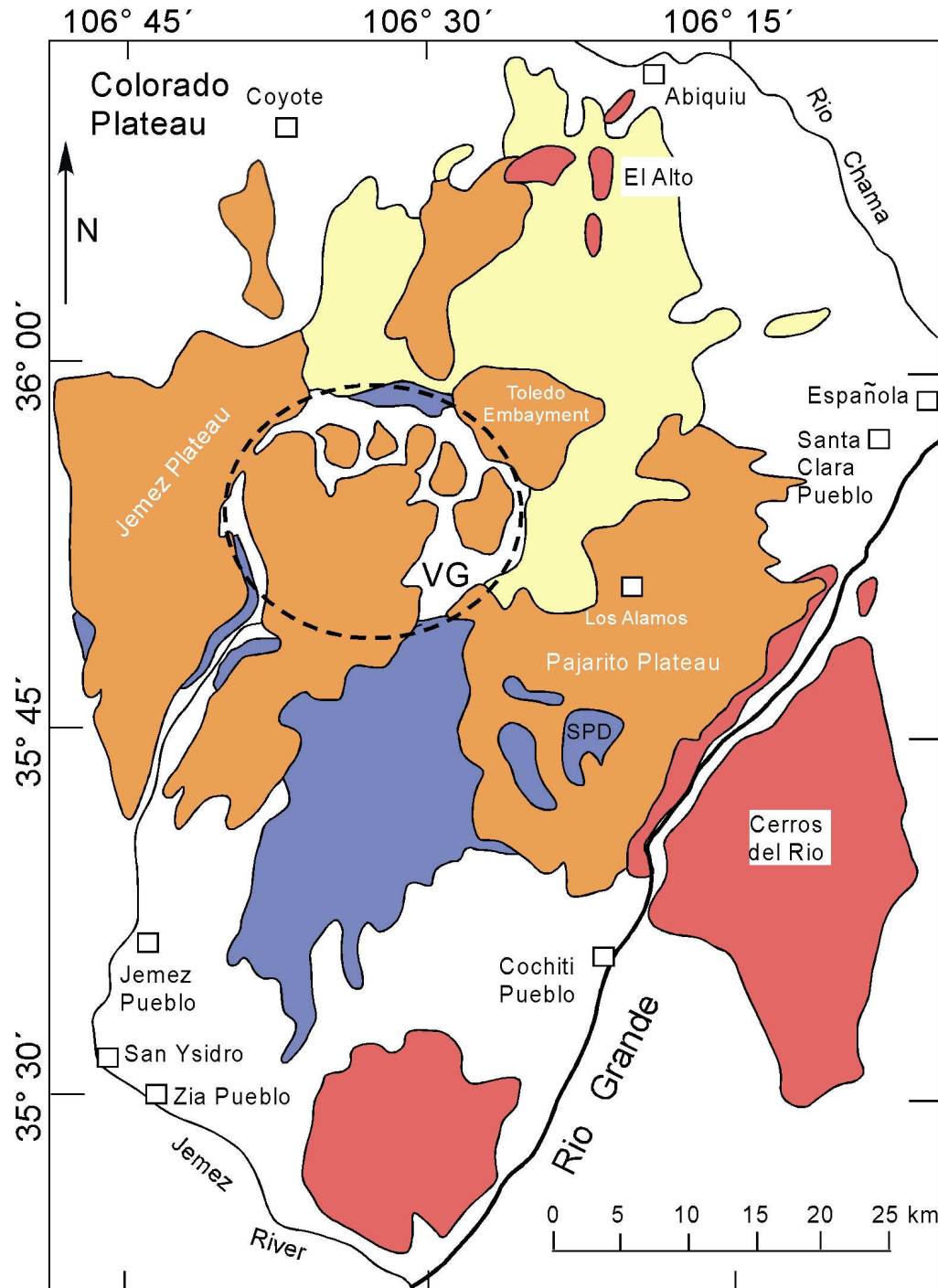


Figure 2.9. Map Showing the approximate distribution of major stratigraphic groups in the JMVF and associated mafic volcanic fields. (Modified from Goff et al., 2004)

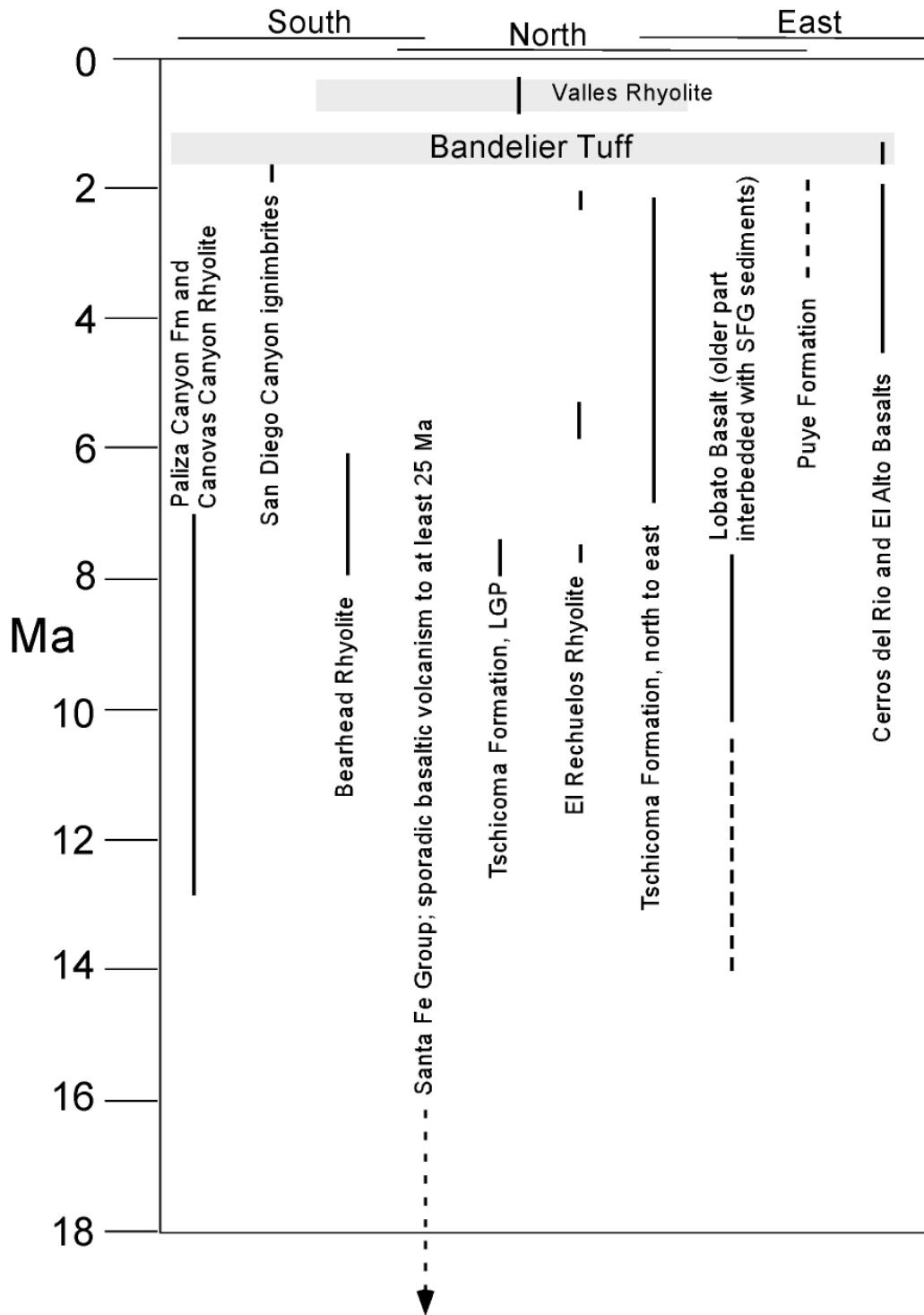


Figure 2.10. Diagram illustrating temporal ranges of JMVF units. SFG = Santa Fe Group; LGP = La Grulla Plateau. From left to right units are arranged according to areas of maximum exposure (i.e. southern, northern, and eastern portions of the JMVF). Dashed lines indicate interbedded volcanic and sedimentary units. Taken from Rowe et al. (2007) and originally modified from Goff and Gardner (2004).

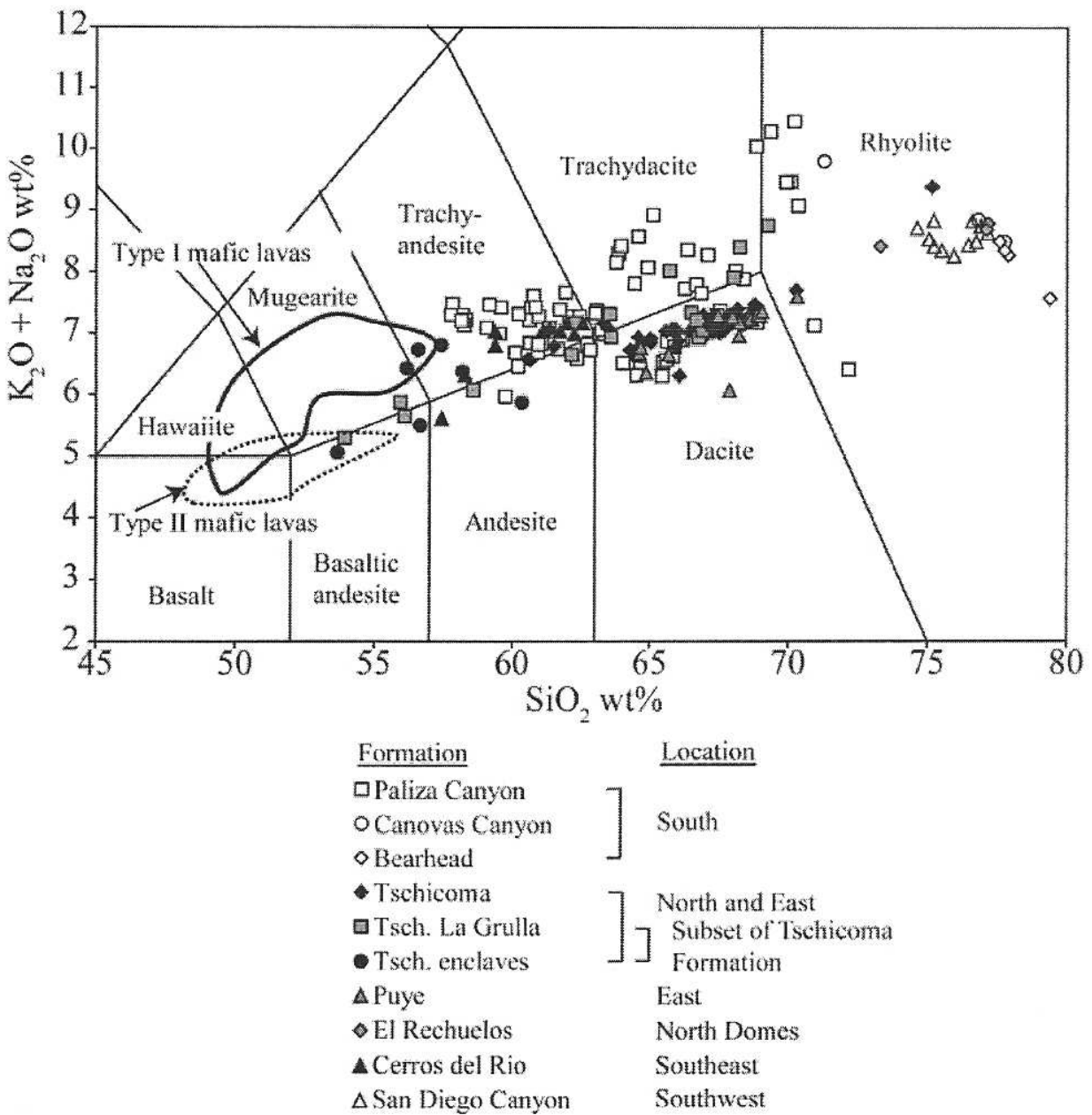


Figure 2.11. Total alkali-silica plot of pre-caldera intermediate to silicic rocks of the JMVF. Diagram from Rowe et al. (2007).

CHAPTER THREE

CALCULATION OF ERUPTIVE VOLUME OF THE OTOWI MEMBER

Prior Studies and Rationale

Calculations published thus far for the total erupted volume of the Otowi Member of the Bandelier Tuff have been estimates, largely based on the distribution of existing Otowi outcrops and also on the distribution of the younger Tshirege Member. Smith and Bailey (1966) provided the first estimate, based on an assumption of similarity between the Tshirege and Otowi members. Their data suggests that the Tshirege originally covered an area of approximately 2200 km², and had a volume of approximately 200 km³; although, it is not stated whether this volume estimate is a dense rock equivalent (DRE). They inferred that the Otowi area and volume must be very similar to Tshirege values but note that pre-Tshirege erosion and subsequent burial by the Tshirege flows have reduced its present outcrop area (Smith and Bailey, 1966). The logic behind using a younger unit to describe an older one is easily understood—the Otowi Member has been significantly eroded and is covered by younger units, and thus the Tshirege presents itself as a reasonable analogue for the Otowi based on similarities between the two. Several parallels can be drawn between the Upper and Lower Bandelier eruptions. Each Bandelier ignimbrite was erupted explosively from similarly located centers in the JMVf. The source material for each ignimbrite originated in the same magmatic system, albeit 390,000 years apart. In addition, each eruption produced plinian fall deposits followed by ignimbrite flow units, and each eruption resulted in a trapdoor-style caldera collapse. Based on these similarities, it seems logical that Otowi and Tshirege distributions should be comparable, and this is the assumption made by early researchers such as Smith and Bailey (1966). Despite the similarities,

the eruptions are not identical, and it is obviously desirable to more rigorously estimate the volume of the Otowi.

More recent volume estimates for the Otowi Member include that of Self and Lipman (1989), who inferred a total erupted volume of 400 km³ DRE. This estimate was based on the distribution of ignimbrites and fall deposits around the JMVf. Self et al. (1996) reaffirmed the total volume of 400 km³ DRE, and calculated the Guaje plinian volume to be 20 km³ DRE based on isopach maps constructed from the deposit.

This study attempts to systematically re-calculate the total erupted dense rock equivalent (DRE) volume of the Otowi Member. The overall aim is to calculate an accurate minimum volume. This has been accomplished using three sources of information: drill-core data, stratigraphic thicknesses (both observed in the field and taken directly from maps), and three-dimensional reconstructions of eroded material on the periphery of the field. In addition, published studies on the JMVf and the Pajarito Plateau and knowledge of pre-Otowi eruptive topography has been used extensively.

The 1:125,000 scale geologic map of Smith, Bailey, and Ross (1970), the 1:500,000 scale New Mexico Geological Map (2003), 1:24,000 scale geologic maps published by the New Mexico Bureau of Mines and Mineral Resources, and 1:250,000 USGS topographic maps were used as base maps for calculations. Two significant problems inherent in the geologic data make these calculations difficult. First, the Otowi Member has been extensively eroded and subsequently covered over by younger volcanic rocks. This makes it difficult to determine the true extent of the original deposit. Second, the paleotopographic surface onto which the Otowi was erupted is covered by the deposit itself and is thus poorly constrained in most areas. The notable exception is the Pajarito Plateau where well and corehole coverage is excellent due to the

fact that Los Alamos National Lab sits atop the plateau. Despite the difficulties involved in discerning paleotopography, there are some areas that are deeply dissected, and thus a reasonable idea of the pre-Otowi paleosurface can be inferred. The following sections will describe the background and methodology used for the calculations.

Geologic Background

Geothermal drilling has been conducted by the Union Oil Company (UOC) and Los Alamos National Lab (LANL) within the Valles Caldera. In addition, a variety of wells have been drilled for water (Griggs, 1964), environmental remediation, and seismic hazard studies by LANL on the Pajarito Plateau. These studies have provided a great deal of stratigraphic and thickness data for the Otowi Member. In the 1960's drilling was undertaken by UOC; in what was termed the Baca project, nearly 42,000 meters of drill-hole data was produced from within the caldera (Neilson and Hulen, 1984). In a study of the Redondo Dome, Nielson and Hulen provided thickness data for the Otowi member from 25 individual wells. This data shows a maximum thickness of 833 meters and a minimum of 176.8 meters, with an average of 400 meters. As the rock sampled is situated within the caldera walls, the Otowi Member encountered in each of these drill cores consists almost exclusively of densely welded tuff (Nielson and Hulen, 1984).

The Continental Scientific Drilling Program (CSDP) has drilled three deep core holes in the Valles Caldera. The first, VC-1, was drilled in August and September of 1984 on the southwest side of the Valles caldera and measures 856 meters in depth (Goff et al., 1986). The second, VC-2A, was drilled to a depth of 527.4 meters inside the caldera in the vicinity of Sulphur Springs during 1986 (Hulen et al., 1991). The third core, VC-2B, was drilled approximately 600 meters from VC-2A to a depth of 1762 meters in 1988 (Hulen et al., 1991).

The initial results from core VC-1 were reported by Goff et al. (1986) and later revised by Self et al. (1991). More recently, Wolff et al. (1996) used the VC-1 core in an examination of El Cajete and southwestern moat rhyolites. Goff et al. (1986) reported an approximately 85 meter thickness of Otowi in VC-1. However, a reassessment of core VC-1 by Self et al. (1991) refuted the presence of Otowi in VC-1. Otowi thicknesses in cores VC-2A and VC-2B were reported as 136.9 meters and 226.9 meters respectively (Hulen et al., 1991).

Hulen et al. (1991) used the CSDP coreholes in addition to UOC geothermal boreholes to conduct a more comprehensive study of the geology of the western Valles caldera. Earlier studies, such as that of Nielson and Hulen (1984) on the Redondo Dome used drill cuttings rather than core. Drill cuttings typically produce much smaller samples that may obscure larger-scale textural features. These textural features may yield valuable information about depositional environments and modes of emplacement (Hulen et al., 1991). Hulen et al. (1991) is an improvement on previous attempts, such as that of Nielson and Hulen (1984), to interpret the intracaldera geology.

An important finding of Hulen et al. (1991) is their reiteration of the importance of the S_3 beds (also known as the S_3 sandstones from Nielson and Hulen, 1984). These beds represent an important marker horizon that separates the upper and lower Bandelier tuffs within the Valles caldera, and thus they are useful in identification and interpretation of the Bandelier units in cores. Hulen et al. (1991) proposed a phreatomagmatic origin for the S_3 beds; previously these sediments were interpreted as a simple epiclastic caldera apron.

Of even greater significance to this study are the isopach maps derived for various intracaldera units by Hulen et al. (1991). Isopach maps were created (Figure 3.1) using thickness data from core studies for the lower (San Diego Canyon) tuffs, the Otowi Member of the

Bandelier Tuff, the aforementioned S₃ beds, and the Tshirege Member of the Bandelier Tuff within the western Valles caldera. The isopach map for the Otowi Member delineates a thinning towards the east. This eastward-thinning is problematic, as prior research has shown the Toledo caldera to represent a trapdoor collapse structure that has subsided on the eastern margin (Segar, 1974; Nielson and Hulen (1984); Heiken et al. (1986); Nowell, 1996). Based on the asymmetric nature of the caldera, we would expect the Otowi to thicken to the east. This inconsistency will be discussed in more detail later in this chapter.

Numerous core-drilling studies on the Pajarito Plateau east of the caldera have been undertaken by Los Alamos National Lab. As part of the Lab's Seismic Hazards Program and continuing environmental remediation efforts, wells have been drilled in technical areas TA-55 (well SHB-1), TA-3 (well SHB-2), TA-16 (well SHB-3), and TA-18 (well SHB-4). LANL studies LA-12460-MS (Gardner et al., 1993) and LA-13831-MS (Gardner et al., 2001) summarize the findings of well-drilling operations in these technical areas. Broxton and Reneau (1995, 1996) have published a comprehensive compilation of core data from LANL in order to delineate the pre-eruptive and post-eruptive surfaces of the Otowi Member on the Pajarito Plateau. These studies proved invaluable resources for calculation of Otowi volume on the Pajarito Plateau.

Morphology as a means of describing ignimbrites

Ignimbrite morphology has traditionally been expressed using aspect ratios. Walker et al. (1980) and Wilson and Walker (1981) used aspect ratio (defined as the ratio of the average thickness of the deposit to the diameter of the circle which has the same area as the deposit) to quantify whether an ignimbrite is relatively thin and widespread (low aspect ratio) or thick and localized (high aspect ratio) for a given volume of tuff. Examples of high aspect ratio

ignimbrites ($< 1:1000$) include the Valley of Ten Thousand Smokes ignimbrite (1:400) and the Bishop Tuff (1:250). Examples of low aspect ratio ignimbrites ($> 1:1000$) include Taupo (1:70,000) and Rabaul (1:7000) (Wilson and Walker, 1981).

Variations in aspect ratio reflect different eruptive rates and inferred violence of emplacement of deposits (Wilson and Walker, 1981). Low aspect ratio ignimbrites have high eruption rates, high transport velocities, and are violently emplaced. High aspect ratio ignimbrites have low eruption rates, low velocities, and are more gently emplaced (Wilson and Walker, 1981). In addition, low aspect ratio ignimbrites tend to consist of a single flow unit over most of their extent, while high aspect ratio ignimbrite deposits tend to be composed of multiple flow units (Wilson and Walker, 1981). More recently, the applicability of the latter rule has been brought into question. Some low-aspect ratio ignimbrites such as the Rattlesnake Tuff (Streck and Grunder, 1995) and the Abrigo Ignimbrite on Tenerife (Pittari et al., 2006) have been found to contain multiple flow units. This rule needs further examination, particularly as more examples of LARI are found with multiple flow units.

Wilson (1991) noted that aspect ratios of ignimbrites are “coarse-scale measurements” and stressed the need for a more detailed approach to investigating ignimbrite morphology. Wilson therefore used physical parameters such as thickness, volume, and area to more accurately describe the size and shape of an ignimbrite. The Oruanui ignimbrite in New Zealand was used as an example, first to illustrate a new classification of morphologies and second to demonstrate the usefulness of erosion models in reconstruction of an original ignimbrite deposit.

The study provided two theoretical end-member ignimbrite morphologies (Figure 3.2) including a slab (uniform thickness) model and an exponential-decay model in which thickness decreases exponentially with distance from a maximum (Wilson, 1991). These models were not

necessarily linked to any particular aspect ratio values, but simply represent two possible morphologies. Violently emplaced, low aspect ratio ignimbrites were found to more closely approach the exponential decay model. More gently emplaced, intermediate to high aspect ratio ignimbrites were found to more closely approach the slab model (Wilson, 1991).

These models were then ‘eroded’ in two fashions: even removal in which a specific thickness of ignimbrite is evenly removed from the entire area and preferential erosion in which a physical attribute of the ignimbrite (such as welding) allows only certain areas to be removed. The study found that for low to intermediate aspect ratio ignimbrites, the area of the deposit (pre-erosion) can be best estimated by drawing an envelope around known exposures instead of summing the areas of the exposures themselves. For high aspect ratio ignimbrites a close approximation of original area may be obtained by summing existing exposures. It was determined that for all aspect ratios, a best estimate of original volume may be obtained by multiplying existing outcrop areas by inferred original thicknesses (Wilson, 1991).

Methods

Using the logic set forth by Walker et al. (1980), Wilson and Walker (1981), and Wilson (1991) the Otowi Ignimbrite can be classified as a high aspect ratio ignimbrite (HARI). Using thickness data derived from this study (Table 3.1), an average thickness of 111 m was calculated for the Otowi. The geologic map of Smith et al. (1970) was used to estimate a maximum diameter of 90 km for the entire deposit. These variables yield an aspect ratio of 1:811, which classifies the Otowi as a HARI.

Wilson (1991) showed that high-aspect ratio ignimbrites have inherently less variation of area with erosion. Therefore, estimates of original area and volume based on present day outcrops and inferred original thicknesses may be close to the true value. Thus, the most

appropriate method of estimating the area and volume for a HARI is to sum the areas and volumes of present day outcrops.

The findings of Wilson (1991) provide us with a simple and very practical set of guidelines for use in estimation of ignimbrite volumes. Ignimbrite volume estimates are by no means easy to calculate—numerous physical variables may thwart estimation attempts. For example, eruptive units are frequently covered by younger ones; they can be eroded or deeply incised through a variety of natural means, and they may be dispersed hundreds to thousands of kilometers from the vent as plinian fall and distal ash. Wilson (1991) showed that by multiplying existing outcrop areas by inferred original thicknesses, the original volume of an erupted unit can be accurately estimated. Although valid, this method can be substantially improved upon if more detailed geologic data is incorporated into the calculations. By taking into account a variety of sources of information, including core data (if available), field and map observations of unit thicknesses, paleotopographic features, and more complete calculations of distal ash, a much more accurate volume estimate can be derived.

In this study a rigorous approach was used for an improved estimate of the Otowi Member volume. Rather than simply summing up large areas of the Otowi deposit and multiplying by an inferred original thickness, a piecemeal approach was adopted. The outline of the deposit was defined using its current outcrop area. Then, the deposit was broken down into numerous ‘zones’ in which individual volumes were calculated and later summed to derive a total volume. These zones were constrained based on their geologic characteristics. Plinian and distal ash deposits were calculated using pre-existing and newly developed isopach maps. Even though the volume derived from this study is an estimate, it is the most systematic and accurate

estimation of the Otowi Member volume to date. The hope is that it will serve as a model for calculation of large-volume ignimbrites at localities other than Valles.

To define the extent of the deposit, three pieces of information were used. First, in accordance with guidelines set forth by Wilson (1991), the area for the Otowi Member was outlined using present exposures. The USGS 1:125,000 Smith, Bailey, and Ross geologic map of the Jemez Mountains (1970), the 1:500,000 New Mexico Geological Map (2003) published by the New Mexico Bureau of Mines and Mineral Resources (NMBMMR), and several 1:24,000 scale geologic maps also published by the NMBMMR were used. Second, in regions where the Tshirege and Otowi Members are both present, the Tshirege Member was used as a guide to help identify the Otowi extent. This was based on the assumption of Smith et al. (1966) that the Otowi and Tshirege eruptions were at least in some part similar and thus must have covered similar areas. Third, paleotopographic information was used to assist in estimation of the original (pre-erosion) extent of outflow sheets, to determine the location of topographic features such as canyons, and to make reasonable hypotheses about where Otowi ignimbrites would likely have flowed during the eruption. Figure 3.3 is a map illustrating the calculated pre-Otowi paleosurface by Potter and Oberthal (1987). Figure 3.4 is a reconstruction of the pre-Otowi Member paleosurface on the Pajarito Plateau by Broxton and Reneau (1996). These maps were invaluable in both delineation of the Otowi deposit and in volume calculations. Figure 3.5 shows the results of the volume calculation exercise in which thirteen individual zones labeled A-M have been subdivided based on geologic constraints.

Additionally, in Figure 3.5, in the Santo Domingo Basin south of the caldera and in the Española Basin east of the caldera, two distal ignimbrite outflows have been added onto the periphery of the Otowi envelope. Based on the topography (there are relatively unrestricted

“lanes” of travel into each of these basins), it is likely that Otowi flows would have extended far to the east and south. Unfortunately, erosion has removed much of the outcrop evidence. In two localities, however, isolated Otowi ignimbrite exposures support the hypothesis that the outlying basins once held flow deposits. Specifically, a small outcrop of Otowi ignimbrite is found associated with fall deposits near Truchas, New Mexico on the far eastern side of the Española Basin. Also, in the Santo Domingo Basin, limited exposures of Otowi ignimbrites up to 15 m thick have been mapped in tributaries along Galisteo Creek near Santo Domingo Pueblo (Smith and Kuhle (1998). Based on the presence of these deposits, it is reasonable to assume that flows would have continued far into the Rio Grande rift basins. Thus, distally-thinning outflow sheets have been extended into the Española and Santo Domingo Basins to account for eroded deposits. Their significance will be discussed in a later section.

An interesting aspect of Figure 3.5 is the large-scale discontinuity of areas of the Otowi outcrop distribution. Several gaps appear to the north and northeast of the caldera, and it appears that flows extended farther to the south than in any other direction. A plausible explanation for this pattern is that pre-existing topographic features influenced deposition of Otowi pyroclastic flows. One major example of this control is a series of obstructions situated on the northern and northeast rim of the caldera. In this area, large domes of Tschicoma dacite appear to have significantly impeded pyroclastic flows. Consequently, Otowi deposits are conspicuously absent to the northeast of the caldera and also in a corridor consisting of the La Grulla Plateau located between zones F and G. Otowi flows reappear to the east of the caldera in an eroded remnant at Puye Cliffs in the north-central portion of zone H. To the west of this exposure, pyroclastic flows from both the Otowi and Tshirege eruptions were funneled down Guaje and Santa Clara

Canyons (Figure 3.5). In all likelihood, Otowi flows extended out from these canyons and then proceeded to spread out over the Puye Formation surface on their way into the Española Basin.

To the southeast of the caldera several topographic features presented an obstacle to pyroclastic flows. For example, it is unlikely that significant Otowi thicknesses were deposited on the site of what is now St. Peter's Dome and the San Miguel Mountains in zone B (Figure 3.5). Farther to the southeast of the caldera is the Cerros del Rio volcanic field. The hills formed during these basaltic and intermediate eruptions provide a possible obstacle to Otowi flows. Several pieces of evidence support this hypothesis. Most significantly, reconnaissance geologic mapping in the Cerros del Rio by USGS and UNM researchers have uncovered Otowi (Guaje) fall deposits but no ignimbrites (Gary Smith, personal communication; Mark Hudson, personal communication). Assuming that Otowi flows originally travelled through the Cerros del Rio and covered the majority of the fall deposits located there, it is extremely unlikely that the flows would be completely eroded away, leaving only the highly erodible fall deposits behind. A more likely scenario is that the Otowi ignimbrite never made it that far, and only Guaje fall was deposited there. Another piece of evidence in support of this hypothesis is the deflection and capture of Otowi flows in the White Rock Canyon area in zone B of Figure 3.5. There, a thick sequence (approximately 130 m on the map) is present within the canyon but is not observed to overwhelm topographic features further southeast into the Cerros del Rio volcanic field.

Another potential obstacle lies to the south of the caldera at Santa Ana Mesa, which is a significant topographic feature. The mesa is relatively low— approximately 1835 meters at its summit. However, there is sufficient relief between it and the surrounding area (approximately 130 meters) to assume that Otowi flows would have been forced (at least in some part) to flow around to the east and west of the mesa.

Finally, on the southeast side of the caldera, there is no evidence of Otowi flows to the southeast (outboard) of the Cerros del Rio. If the 15 m Otowi exposures of Smith and Kuhle (1998) are used as a rule of thumb for the farthest point of advance for the outflow sheet on the south-southeast side of the caldera, then Otowi ignimbrite should also be observed southeast of the Cerros del Rio. However, no such exposures have been found. The distal edge of zone L has been conservatively drawn through the center of the Cerros del Rio to account for any flows that may have possibly made it into the hills but have been eroded.

On the western side of the JMVf, Otowi and Tshirege flows are constrained along a roughly N-S trending line by the Laramide-age uplift known as the Sierra Nacimiento.

The greatest Otowi outflow thicknesses are found on the western side of the JMVf on the Jemez Plateau in zone E. In this region it is likely that Otowi flows were funneled through a breach in the western rim of the caldera into a broad paleocanyon in the vicinity of the present-day Cebolla Canyon and Telephone Canyon areas. This paleostructure will be discussed in more detail in a later section.

The individual zones labeled A-M in Figure 3.5 were subdivided based on the available geologic data. However, it should be noted that on the periphery of the outflow sheet, outcrop coverage is poor to non-existent. Consequently, some boundaries on the periphery are not as well constrained as those where outcrop coverage is more widespread. In these areas, boundaries were drawn based on the available data. A prime example of this can be observed along the distal edges of zones J, K, and M where outcrops are spotty due to extensive erosion (zone J in particular is dissected by a major watershed). The distal boundaries in these areas are based on sparse exposures—the up to 15 m-thick outcrops of Otowi ignimbrite found at approximately 5400 ft in the southeastern portion of zone K near Santo Domingo Pueblo (Smith and Kuhle,

1998). Because these localities are the most distal outcrops on the south side of the caldera, they have been used to represent the farthest point of advance. Accordingly, the southern boundaries of zones J and K have been defined using a common topographic contour corresponding to the 15 m exposures. It should be noted that there is no paleotopographic feature at this point in the Santo Domingo basin that could explain a sudden end to the Otowi pyroclastic flows.

Obviously, it is highly likely that the Otowi flows continued out further into the Santo Domingo Basin from this topographic line. To account for this, in a later section hypothetical distally-thinning wedges were extended out into the Santo Domingo Basin from this boundary.

Zone A covers the Pajarito Plateau, which is a particularly well-studied region thanks to the extensive work of LANL scientists including the paleotopographic studies of Broxton and Reneau (1995, 1996). Thicknesses are very well constrained due to borehole and drill core data, and the geologic map shows that the Otowi thins out closer to the caldera rim. Zone B contains the area directly to the south and extending to the Rio Grande in White Rock Canyon. This segment is deeply dissected by several canyons, most notable among them Canyon de Cochiti.

Zone C encloses the outflow sheet south of the caldera and includes Cat Mesa (a notable Bandelier Tuff stratigraphic section) and part of Cañon de San Diego on the southwest side of the caldera. Zone D includes Virgin Mesa, Wildcat Canyon, and part of Cañon de San Diego on the southwest side of the Caldera. Zone E encloses the majority of the Jemez Plateau and includes the thickest Otowi outflow deposits, most of which are densely welded. Zones F and G represent prominent alleyways through which Otowi flows were funneled north to Mesa Ojitos and Mesa Pinebetosa in zone F and Pueblo Mesa and Cañones Mesa in zone G. These segments are located on either side of a topographic barrier formed by dacite domes of the Tschicoma Formation in what is now called the La Grulla Plateau. At the north end of zone G are two small

paleocanyons, seen in Figure 3.5. Zone H encloses the region to the north of Guaje Canyon, including Santa Clara Canyon, through which Otowi flows were funneled northeast into the Española Basin. Zone I represents the intracaldera fill. The Otowi in this zone is densely-welded and up to 833 m thick, averaging approximately 400 m. (Nielson and Hulen, 1984).

Zones J and K enclose a broad area on the south and southeast side of the caldera, extending into the Santo Domingo Basin. Much of the Otowi is eroded in these segments, but several key outcrops near Santo Domingo Pueblo (Smith and Kuhle, 1998) provide evidence of Otowi flow deposition at least to the outer boundaries of these segments. The distal boundary in Zone J has been fitted around the northern edge of Santa Ana Mesa (Figure 3.5). Santa Ana Mesa sits approximately 130 m higher than the surrounding land surface, and thus constitutes a definite topographic barrier. It is unlikely that thick flows (similar to the 15 m thicknesses observed at Santo Domingo Pueblo) would have inundated the Mesa and flowed over its top. Thus, the distal boundary of zone J was drawn around the base of the north side of Santa Ana Mesa following a smoothed 5400 foot contour. To account for significantly thinner Otowi flows that may have gone up over parts of the Mesa, it has been included within the distally-thinning Santo Domingo wedge to the south.

Zone L is a very rough estimate of Otowi that may have been present within the Cerros del Rio volcanic field. As previously mentioned, no Otowi outflow is found in the Cerros del Rio volcanic field. Zone M is also a very conservative estimate of outflow on the southwest side of the caldera, and it is bounded on the west by the Sierra Nacimiento. Thicknesses in zones L and M were derived by averaging thicknesses from the distal ends of adjacent zones (C and D for Zone M; B for zone L).

Paleotopography

The pre-Otowi land surface is characterized by a complex series of deep canyons and broad valleys that extend radially away from the current caldera. Wherever possible, every effort has been made to consider paleotopography in the volume calculations. The pre-Otowi topographic surface is not well constrained in every region of the JMVF. Given the fact that the Otowi deposit covers its own pre-eruptive surface and that erosion has stripped away an indeterminate amount of geologic evidence, the true nature of the original paleosurface is clouded in many areas. The best source of paleotopographic information has been drill-core data. On the Pajarito Plateau (zone A in Figure 3.5), the pre-eruptive and post-eruptive Otowi surfaces are very well constrained. Broxton and Reneau (1996) used outcrop data and an extensive core data set (much of it from LANL sources) to reconstruct the Otowi paleotopography on the Pajarito Plateau (Figure 3.4). They determined that the pre-Otowi surface consisted of a broad, SSW-draining valley approximately 4 miles wide and at least 6.2 miles long. On the northern boundary of the valley lies a low-relief, ESE-dipping surface that represents the upper limit of an alluvial fan complex, most likely the Puye Formation (Broxton and Reneau, 1996).

An uncertainty arises with the modern canyons incised into the plateau and whether they represent paleo-structures or simply more recent fluvial erosion. In localities where consecutive layers of ignimbrite have been deposited, it is common for drainages to be incised into the approximate locations of pre-existing drainages. However, Broxton and Reneau (1996) noted that as the Otowi is largely non-welded in this region, the pre-Tshirege surface likely lacked “the sharp mesa-canyon topography” present today. Thus, it is possible, but unlikely that the current canyons on the Pajarito Plateau represent pre-Otowi paleocanyons.

In a similar fashion to the Pajarito Plateau, UOC drill core data and CSDP holes VC-2A and VC-2B have allowed for a much clearer interpretation of the caldera (zone I in Figure 3.5). Paleotopographic information and thickness data derived from these studies have been used extensively to augment the volume calculations in these regions.

Unfortunately, outside of the Pajarito Plateau and the caldera, core data is limited. As a result, researchers have reconstructed paleosurfaces using geologic maps and field observations. Potter and Oberthal (1987) reconstructed the pre-Otowi paleosurface in Figure 3.3 using the Smith et al. (1970) geologic map as a guide to draw structural contours at the base of the Otowi. The contour interval is 100 ft in areas where the Otowi is well exposed. In areas where exposures are limited, generalized contours were derived by smoothing out current surface contours of pre-Otowi units (Potter and Oberthal, 1987). In these regions the contour interval is 500 ft. Using this technique Potter and Oberthal (1987) were able to derive the minimum topographic relief for the pre-Otowi paleosurface. The authors acknowledge that the map is not perfect but assert that the general slopes and major topographic features (such as paleocanyons) are reliable. I concur with this assessment and will use this data to help discern major paleotopographic features.

Seven pre-Otowi paleocanyons have been identified using information obtained from the maps of Smith and Bailey (1970) and Potter and Oberthal (1987). To account for the volumes of Otowi ignimbrites likely contained within these structures, a series of inverted triangular prisms have been created to 'fit' each paleovalley. The prisms are based primarily on dimensions taken from the reconstructed paleosurfaces of Potter and Oberthal (1987). Thicknesses were obtained by comparing differences in elevation between the base of current Otowi outcrops and the paleotopographic data. These prisms are represented in Figure 3.5 as dashed outlines, and their

volumes are provided in Table 3.2. Calculations for these prisms will be discussed later in this chapter.

The first major structure is a broad valley running parallel to the western rim of the caldera in zone E on the Jemez Plateau. This paleo-valley is roughly centered in the same areas as the present-day Telephone Canyon and Cebolla Canyon and contains some of the thickest Otowi outflow deposits. Potter and Oberthal (1987) estimated that this wide paleo-valley had an axial gradient of 12 m/km and likely channeled pyroclastic flows emanating from a breach in the western caldera wall to the southwest (Figure 3.3).

Another large paleostructure existed beneath what is now Cañon de San Diego, on the southwest edge of the caldera. The axis of this valley is generally coincident with the modern Cañon de San Diego and had a gradient of approximately 36 m/km (Potter and Oberthal, 1987). A trace for this paleovalley is found at Jemez Springs and Wildcat Canyon, and the canyon is filled with a significant thickness of Otowi Tuff as determined from well data.

In zones C and B in Figure 3.5, three deep, narrow paleocanyons (labeled CC1, CC2, and CC3) exist in the area that is now dominated by Cochiti Canyon. These paleocanyons are each approximately 300 m deep and vary in width from 2-8 km and length from 4-8.5 km. In zone G (Figure 3.5) two small paleocanyons are present near Pueblo Mesa. The western one measures approximately 2 km wide by 7 km long. The eastern canyon measures approximately 3 km wide by 8 km long

Volume Calculations

Volume calculations for zones A-M

For zones A-M, a template ten kilometers square with demarcations for each square kilometer on tracing paper was created. The template was produced in 1:125,000 scale, which is

the scale of the map by Smith et al. (1970). Areas for each zone were determined in square kilometers using this template. Zones B through E are particularly large in area, and thus these zones were further subdivided into multiple subdivisions to enhance accuracy in the calculations (see Table 3.1).

For each lettered zone or subdivision, as accurate an average thickness as possible was calculated using drill core data and available stratigraphic thicknesses. For subdivisions containing areas with zero Otowi thickness (parts of sections B, C, D, and E), a zero was entered into the average to account for the lack of deposit. The overall average thickness was then multiplied by the area of the zone or subdivision to determine volume. The individual results were added together to determine a total volume for each lettered zone. For all zones except E and I, which are densely welded, a porosity of 50% was used to determine dense rock equivalent. This porosity was determined by measuring the volume displacements of fragments versus crushed samples of Otowi ignimbrite in beakers filled with water.

To calculate the intracaldera fill volume in Zone I, core data from CSDP VC-2A and VC-2B, along with geothermal well data from the Baca project were used. An average thickness of 436 m for the intracaldera fill was derived by averaging thicknesses from 22 Baca wells of Nielson and Hulen (1984) and the two CSDP cores. As previously noted, gravity surveys have shown that the Toledo and Valles calderas are asymmetric and collapsed farther down in the east. Therefore, it would seem logical that the intracaldera fill would thicken to the east. However, the isopach map of Hulen et al. (1991) seen in Figure 3.1 indicates a thinning of the Otowi Member to the east. Unfortunately, neither core nor well data is available from the eastern portion of the caldera, and thus the nature of the Otowi in this region is uncertain. In the absence of verified thickness data from the eastern portion of the caldera, it seems irresponsible to

assume either thickening or thinning to the east. Thus, the average thickness (436 m) attained from available data in the west was deemed the safest approximation of intracaldera thickness. Potential errors incurred in calculating the intracaldera volume will be discussed later in the chapter.

The data for the zone A-M volume calculations can be seen in Table 3.1. The calculated intracaldera volume is 149 km³ DRE, and the calculated outflow is 120 km³ DRE.

Volume calculations for paleocanyons

The inverted triangular prisms in Figure 3.5 have been used to account for extra thicknesses of tuff that filled in the deeper paleocanyons. A summary of these calculations can be seen in Table 3.2. On the Jemez Plateau a triangular prism was created to account for the paleovalley that underlies the area running from the NE to SW. The shape is 25 km long, 7.9 km wide, and an estimated 30 m in depth. In examining the differences between the base of the Otowi Member on the Smith et al. (1970) map and the reconstructed paleocontours of Potter and Oberthal (1987), very little difference is evident between the two. On average approximately one contour of difference (approximately 30 m) is observed, so 30 m has been used as the depth of the triangular prism. This shape yields a volume of 2.96 km³. Because the ignimbrite in this region is densely welded the DRE equivalent is 2.96 km³.

In Cañon de San Diego a triangular prism 23.1 km long and 11.5 km wide was established to account for extra thicknesses of Otowi deposited in the paleo (pre-Otowi) Cañon de San Diego. For the depth of this triangular prism, the average difference between the observed base of the Otowi and the bottom of the paleocanyon (as determined from paleocontours)—approximately 50 m—was used. The resulting dimensions (23.1 km long, 11.5 km wide and .05 km deep) yield a volume of 12.1 km³ (6.05 km³ DRE).

In the Cochiti Canyon area, three paleocanyons are present and have been accounted for in the volume calculations with inverted triangular prisms labeled CC1, CC2, and CC3. CC1 is the westernmost and measures approximately 1.9 km in width and 5.9 km in length. CC2 is the central of the three and measures 2.7 km in width and 5.9 km in length. CC3 is the easternmost and measures approximately 4.0 km in width and 10 km in length. Depths for these triangular prisms were determined by averaging the differences observed between the elevation of the current exposed base of the Otowi and the bottom of the paleocanyon as determined by the paleotopographic map. In the Cochiti Canyon area, the depths are fairly small, averaging approximately one contour or 30 meters. For CC1 this yields a volume of $.17 \text{ km}^3$ ($.09 \text{ km}^3$ DRE). For CC2 this yields a volume of $.24 \text{ km}^3$ ($.12 \text{ km}^3$ DRE). For CC3 this yields an estimated volume of $.60 \text{ km}^3$ ($.30 \text{ km}^3$ DRE).

At Pueblo Mesa, two paleocanyons have been modeled using inverted triangles. The western paleocanyon measures approximately 2.1 km wide and 7.7 km long. The depth of this canyon beneath the current base of the Otowi is approximately 60 m. These dimensions yield an estimated volume of $.50 \text{ km}^3$ ($.25 \text{ km}^3$ DRE). The eastern paleocanyon measures approximately 4.4 km wide and 10.3 km long. The depth of this canyon beneath the current base of the Otowi is approximately 50 m. These dimensions yield an estimated volume of 1.13 km^3 ($.57 \text{ km}^3$ DRE).

Volume calculations for distal ignimbrite wedges

In examining the pre-Bandelier geology it is evident that there are few topographic obstacles that would have impeded Otowi pyroclastic flows to the south and east of the caldera. Consequently, a reasonable assumption is that flows would have extended further out into these regions. However, because of the effects of erosion over the past 1.61 million years in the

Española and Santo Domingo Basins, very little of the Otowi ignimbrite is preserved. In the Española Basin there is one known outcrop of Otowi ignimbrite found east of the Rio Grande. An exposure on NM route 76 near Truchas, NM on the far eastern boundary of the basin (approximately 42 km from the eastern Valles Caldera rim) is the only instance of Bandelier preservation outside of the present ignimbrite distribution (Self and Lipman, 1989). At this locality, a thin (~ 1-2 meter) flow unit is preserved at approximately the 8000 foot contour.

In the Santo Domingo Basin, the approximately 15 m-thick exposures of Otowi ignimbrite found near Santo Domingo Pueblo (discussed on page 10) are the most distal exposures of ignimbrite found in the Santo Domingo Basin. These tuffs were deposited on a generally broad fan surface and lie unconformably upon gravels of the Lookout Park formation or directly on paleosols derived from eolian sands resting on the gravel (Smith and Kuhle, 1998). Based on the fairly substantial thickness of the ignimbrite here, it is reasonable to hypothesize that Otowi flows would have continued farther south from this point into the rift basin.

Thus, two ignimbrite wedges have been added onto the periphery of the field and can be seen as dashed outlines in Figure 3.5. In the Española Basin, the wedge is 20 m thick at the proximal end and zero meters at the distal end. The proximal thickness of 20 m represents an average of thicknesses along the distal edges of zones A and H. In the Santo Domingo Basin, the 15 m exposures of Smith and Kuhle (1998) were used for the proximal thickness.

In the Española Basin, the Truchas exposure has been taken as the farthest point of advance. Accordingly, the distal end of the ignimbrite wedge has been extended out to this exposure situated approximately at the 8000 foot contour, and then was traced north and south along the far edge of the basin using this contour as a guide. The edge has been smoothed out to remove the effects of post-1.61 Ma stream erosion. On the northern and southern edges of the

basin, the boundary was wrapped back towards the caldera following contours and using the topography as a guide.

In the Santo Domingo Basin, a similar methodology was employed in which the distally-thinning wedge was extended out into the basin to a common contour line (in this case the 1700 meter contour). This contour was chosen based on two criteria. First, major topographic features present south of the caldera such as the Sandia Mountains would provide a barrier to any pyroclastic flows. Second, plausible rates of thinning were considered for a distally-thinning ignimbrite wedge 15 meters thick at the proximal edge and 0 meters thick at the distal end. This exercise found 0.06 degrees to be the most realistic angle that could account for the outflow sheet. At this angle, the wedge extends out 14.5 kilometers into the basin. For comparison, a slope angle of 1 degree using the same dimensions yields a wedge only 859 m in length, and a slope angle of .01 degrees yields a wedge 86 km long. The 1 degree and .01 degree slopes are particularly unrealistic—the former yields a wedge that is unrealistically ‘stubby’ while the latter (out nearly 90 km) does not fit in the basin. Thus, the wedge was theoretically extended out 14.5 kilometers, and this was found to correspond with the 1700 meter contour. It should be noted that the wedge boundary follows this contour but has been smoothed out to account for post-emplacement stream erosion.

It should be noted that the proximal edge of the Santo Domingo wedge fits into the embayment formed in zone J around Santa Ana Mesa. This area was not included in the volume calculation for zone J, as it is likely that thicker Otowi flows were directed around Santa Ana Mesa. However, the relief on the mesa is not so large that thinner flows could not flow over the top of it. As a result, the distally-thinning Santo Domingo wedge was extended over the mesa in

an attempt to account for volumes of thinner Otowi flows that may have overwhelmed this topographic feature.

With the boundaries defined, a series of rectangular and triangular polygons were used to determine volumes enclosed within the distal wedges. The results of these calculations are shown in Table 3.3. For the Santo Domingo Basin side of the caldera, an ignimbrite wedge with a volume of 7.98 km^3 (3.99 km^3 DRE) was calculated. For the Española Basin an ignimbrite wedge with a volume of 14.21 km^3 (7.11 km^3 DRE) was derived.

Note that these are conservative, minimum estimates, and it may very well be that these regions once held larger quantities of Otowi outflow, particularly in the centers of the basins where flows tend to pond. However, based on the available geologic evidence these estimates are intended to establish a reasonable minimum volume. In all likelihood, Otowi ignimbrites in the Española and Santo Domingo basins would have ponded in the center of the basin. However, since these distal deposits have been so extensively eroded, there isn't enough information to incorporate this phenomenon into the calculations. Hence, the usage of thinning wedge shapes as representations of Otowi deposition in these regions.

Volume calculations for distal ash

Self et al. (1986) calculated a volume of 20 km^3 DRE for the Otowi Member plinian deposit. Later, Self et al. (1996) estimated that the bulk volume of plinian unit A could be as little as 7 km^3 or as much as 30 km^3 (bulk volume). The authors estimated that units B-E could represent as much as 65 km^3 (bulk volume).

Sparks and Walker (1977) demonstrated that some outflow volumes (O) are equal to plinian/co-ignimbrite ash volumes (A). Lipman (1984) suggested that DRE intracaldera deposit volumes (I) are approximately equal to outflow deposit volumes (O). Mason et al. (2004) used

this information to summarize the volume relationship between caldera fill, outflow, and distal ash in large pyroclastic eruptions. They compared two eruptions for which it has been possible to calculate all three components—the ~74 ka Younger Toba Tuff eruption and the 26.5 ka Oruanui eruption. For each of these eruptions, the rule that $I \approx O \approx A$ is valid. At Toba $I:O:A = 1000:1000:800 \text{ km}^3$ (Rose and Chesner, 1987), and for the Oruanui $I:O:A = 420:320:430 \text{ km}^3$ (Wilson, 2001). Mason et al. (2004) noted that the balance between caldera fill and outflow may depend on the timing of caldera collapse. However, based on the Toba and Oruanui eruptions and a comparison of 47 large explosive eruptions, the authors adopted the assumption that $I \approx O \approx A$.

Based on this work, we may assume roughly equal volumes for caldera fill, reconstructed outflow, and distal ash in large ignimbrites such as the Otowi. In Table 3.4, zone I (149 km^3 DRE) is taken as the intracaldera volume (I), and the remainder ($290 \text{ km}^3 - 149 \text{ km}^3 = 141 \text{ km}^3$ DRE) is calculated to represent the total outflow value (O). These values are consistent with the model set forth by Mason et al. (2004), and the result justifies further application of the model to assume an equivalent volume of distal ash (A). Accordingly, the distal ash volume was determined in Table 3.4 by averaging intracaldera and outflow values. The calculated distal ash volume (A) is 145 km^3 (DRE). This value represents a discrepancy as it is significantly greater (over 7 times) than the 20 km^3 DRE calculated by Self et al. (1986).

In light of the discrepancy, an attempt has been made to estimate the volume of the Otowi fall deposit using the technique of Pyle (1989). Total thickness for the Guaje is reasonably well constrained near to the caldera (Self et al., 1986; Self et al., 1996). However, only one significant distal Guaje outcrop has been positively identified—Mt. Blanco, Texas, located approximately 22 km southeast of Floydada, Texas (Izett et al., 1972). There a 30-60 cm bed of

ash was measured and attributed to the 1.61 Ma Otowi eruption based on chemical and petrographic attributes (Izett et al., 1972). In addition, Holliday (1988) later measured and described a 30 cm Guaje ash bed at Mt. Blanco. The Guaje ash at Mt. Blanco is partially reworked, and the likely original thickness of the ash is approximately 12 cm (Self, personal communication). A detailed chemical stratigraphy of the ash beds at Mt. Blanco was not worked out by these authors. Consequently, there is uncertainty regarding which Guaje fall units are present there. Most likely, the deposit is dominantly fall units B and C. Unit C represents the period of highest eruptive intensity and thus likely has the greatest dispersal. Clearly, however, fall unit A is not exposed there as it is constrained to regions immediately east of the vent. Units D and E may be exposed; although, they are much thinner and more difficult to discern. A more detailed chemical stratigraphic analysis of the Guaje ash at Mt. Blanco would be useful in future studies.

Consequently, this calculation is an estimate based on available data. Isopachs were constructed using fall thicknesses measured by Self et al. (1986), Self et al. (1996), Izett et al. (1972), and Holliday (1988). Fall unit A has been calculated separately from units B-E because it is very small in volume and was deposited in a limited region along a narrow eastward dispersal axis. Because of this, fall unit A is thick (~ 10 m) in some areas close to the caldera, but its area of distribution is decidedly vent-proximal. Using thicknesses from fall unit A in volume calculations for the entire deposit (A-E) dramatically skews the total apparent thickness of the deposit and results in an overestimate. Fall units B-E, however, are more widely distributed (at least 12 cm thick 550 km from the vent in the Texas panhandle). Because there is a lack of thickness data for the individual fall units, units B-E have been grouped together.

Figure 3.6 is an isopach map constructed for fall unit A using thicknesses from Self et al. (1996). Thicknesses for unit A are fairly well constrained, and reasonable closures for isopachs were used. Figure 3.7 is an isopach map for fall units B-E showing ash distribution across the southwest. Figure 3.8 is a blown-up view of the region around the caldera with thicknesses for units B-E (from Self et al., 1996). Pyle (1989) stated that many tephra fall deposits are characterized by simple exponential decay. Therefore, to assist in the placement of isopachs for units B-E, a plot of thickness versus distance was made using a number of points close to the caldera and the distal locality at Mt. Blanco (550 km, 12 cm). Assuming that the Guaje deposit follows an exponential thinning trend, an exponential trend line was fitted to the data. This provided a means to determine the approximate distances from the vent that specific isopachs should be situated.

The Pyle (1989) technique was used to calculate volumes for fall unit A and units B-E (Figure 3.9). Calculations are shown with the graphs used to determine half distance (B_1). For fall unit A, T_0 equals 10.5 m and for fall units B-E T_0 is 2.5 m. A total volume of 2.3 km³ (bulk) and 1.2 km³ (DRE) was calculated for plinian fall unit A. A total volume of 88 km³ (bulk) and 44 km³ (DRE) was calculated for fall units B-E. Together, this results in a total plinian volume of 85.2 km³ (bulk) and 44 km³ (DRE).

Results

Using the methodology described, a total volume of 350 km³ was calculated for zones A-M, including caldera-fill and outflow (Table 3.1). Assuming 50% porosity in Otowi ignimbrite, and taking into consideration that zones E and I are densely welded, this yields a DRE volume of 269 km³. The paleostructures in Table 3.2 yield a total volume of 17.7 km³ and a DRE equivalent of 10.3 km³. In Table 3.3, the distal ignimbrite wedges yield a total volume of 22.2

km³ and a DRE equivalent of 11.1 km³. The total calculated intracaldera plus outflow volume is 290 km³ DRE (Table 3.4).

Using the I:O:A assumption, a value of 145 km³ DRE was calculated for the Otowi fall deposits. Using isopach data, a volume of 45.2 km³ DRE was determined for the Otowi fall deposit. Total erupted volumes of 435 km³ and 335 km³ can thus be derived for the Otowi Member; these values were calculated using fallout estimates from the I:O:A scheme of Mason et al. (2004) and the Pyle (1989) technique respectively. Both estimates are considerably greater than the approximately 200 km³ volume estimated by Smith and Bailey (1966). Furthermore they are similar to the 400 km³ DRE estimate of Self and Lipman (1996) and therefore validates their estimate. However, the volumes derived from this study are intended as minimum estimates. Large quantities of the Otowi ignimbrite and fall deposits have undoubtedly been eroded, and thus the potential exists that the Otowi eruption yielded a DRE volume equal to or greater than 500 km³.

Estimation of Errors

As this volume calculation represents a minimum estimate, a variety of uncertainties may be inherent in the data and need to be discussed and clarified. Clearly, over the past 1.61 million years the Otowi Member has been subjected to varying amounts of erosion but it is difficult to estimate how much has actually been removed. It is unlikely that an even removal scenario (Wilson, 1991) can be used for the Otowi ignimbrite because it is strongly welded in portions. Therefore, a preferential erosion scenario (Wilson, 1991) is far more likely. In those regions where the ignimbrite is significantly welded (such as the Jemez Plateau in zone E, and in the intracaldera fill in zone D), the volume estimates are probably quite accurate. However, in all of the other regions where the tuff is not densely welded, we must assume that portions have been

removed. This is particularly true in the rift basins, where erosion has removed any trace of Otowi ignimbrites.

Dethier et al. (1988) estimated rates of erosion in the western Española Basin for a variety of local rock types. From 1.1 Ma to the present the denudation rate for tuff in the White Rock quadrangle was estimated at 4 cm/1000 yr. Using this as a rough approximation for erosion rates, we can make an attempt to calculate lost volumes. The Cerro Toledo interval between the Otowi Member and Tsankawi fall deposits of the Tshirege Member spans approximately 390,000 years. Based on the erosion rate from Dethier et al. (1988) during this timeframe, as much as a 156 meter thickness could have been eroded from the exposed Otowi Member. Excluding the densely welded Zones E and I and the paleocanyon deposits (which were covered), then as much as 391 km³ (196 km³ DRE) could conceivably have been eroded from the ignimbrite outflow sheet. This would raise the total volume of the ignimbrite from 290 km³ to 486 km³ DRE. If the erosion rates are correct, and the Otowi ignimbrite was being eroded over the entire 390,000 yr interval (which in some places it clearly was not), then the maximum missing volume (196 km³ DRE) represents approximately 40% of the ignimbrite deposit lost to erosion. Including fall volumes derived from isopach data (45 km³), this theoretically increases the original (pre-erosion) volume estimate for the Otowi Member from 335 km³ to approximately 531 km³ DRE—a change of 158%.

While these numbers are significant, it is important to recognize that they are very difficult to calculate reliably. A reasonable statement would be to say that erosion has likely removed significant quantities of the Otowi Member ignimbrites, and thus its true original volume is likely much larger than the 290 km³ DRE calculated. However, the exact amount lost to erosion is difficult to determine.

Goff et al. (1989) suggested that the intracaldera fill in the undrilled eastern half of the caldera complex could possibly be as much as twice the 800 m maximum thickness observed in the west. Despite the proposals by some researchers that the intracaldera Otowi thickens to the east due to the asymmetric caldera collapse structure, there is no stratigraphic evidence for this phenomenon. Furthermore, the isopach maps of Hulen et al. (1991) suggest that the Otowi thins towards the east. In the absence of stratigraphic data, the average intracaldera thickness (436 m) calculated in this study is a reasonable and prudent minimum estimation based on the available data.

As a matter of interest, however, increasing the average thickness to 600 m increases the intracaldera volume to 205 km³ (a 138% change). An extreme scenario—one in which we assume that the entire eastern caldera averages 1600 m in thickness—would increase the average thickness to 1000 m; this maximum volume would theoretically increase the intracaldera volume to 341 km³ (a change of 229%). These modified volumes would increase the overall Otowi volume to 427 km³ and 563 km³ respectively.

The hypothesized ignimbrite aprons proposed for the Española and Santo Domingo Basins in Figure 3.5 may or may not have existed. Either way, they do not exert significant leverage on the overall calculations. If they did once exist, then the calculations provided for them in Table 3.3 indicate a reasonable minimum volume. However, if they did not exist and their volumes are removed from the outflow totals, the difference in volume is small, with a net change of 2.5% of the total outflow. An important consideration in this case is that Otowi ignimbrites would have likely ponded in the middle of basins, thus resulting in greater thicknesses of tuffs. Thus, it is safe to include the distal wedges in a low-end volume estimate. However, with so little outcrop evidence available, it is difficult to rationalize increasing the

estimate to account for ponding of flows. Consequently, as they have been calculated, the distal wedges are most likely a reasonable and justifiable addition to the total volume calculations.

It is important to remember that these calculations, while they have been geologically constrained and made to be as accurate as possible, still represent a minimum volume.

Therefore, the 335 km³ DRE may have once been much larger—perhaps over 500 km³. It is unlikely that the actual Otowi volume is less than this number for the simple reason that the calculations are a conservative estimate based solely on the available geologic data.

Wilson (1991) noted that volume estimates of old ignimbrites may be reasonably accurate even after strong erosion, provided the original thicknesses of ponded/landscape-forming material can be inferred. In this case, a plethora of thickness and paleotopographic data has been used in this study to derive as accurate an estimate of volume as possible. For a minimum calculation, the total erupted volume of 335 km³ DRE found in this study is quite reasonable and based solidly on the existing data.

<u>Zone</u>	<u>Area (km²)</u>	<u>Ave. Thickness (km)</u>	<u>Volume (km³)</u>	<u>Volume (km³ DRE)</u>
<u>A</u>	247.3	0.071	17.6	8.8
<u>B</u>				
B1	122.0	0.146	17.8	
B2	122.0	0.067	8.2	
B3	17.1	0.046	0.8	
B4	8.5	0.046	0.4	
B5	64.7	0.094	6.1	
B6	75.6	0.057	4.3	
B7	21.5	0.107	2.3	
			39.9	19.9
<u>C</u>				
C1	87.3	0.094	8.2	
C2	113.7	0.137	15.6	
C3	110.6	0.072	8.0	
C4	78.6	0.073	5.7	
			37.5	18.7
<u>D</u>				
D1	99.0	0.046	4.6	
D2	50.5	0.065	3.3	
D3	68.3	0.027	1.8	
			9.7	4.8
<u>E</u>				
E1	220.9	0.095	21.0	
E2	184.6	0.095	17.5	
			38.5	38.5
<u>F</u>	73.7	0.067	4.9	2.5
<u>G</u>	161.9	0.079	12.8	6.4
<u>H</u>	67.1	0.037	2.5	1.2
<u>I</u>	340.8	0.436	148.6	148.6
<u>J</u>	377.6	0.023	8.7	4.4
<u>K</u>	193.7	0.026	5.0	2.5
<u>L</u>	239.4	0.091	21.8	10.9
<u>M</u>	129.3	0.023	3.0	1.5
	3255 km ²	Totals:	350 km³	269 km³ (DRE)

Table 3.1. Volume calculations for Zones A-M. Zone E (Jemez Plateau) and zone I (caldera fill) are densely welded.

<u>Paleocanyon</u>	<u>Length (km)</u>	<u>Width (km)</u>	<u>Thickness (km)</u>	<u>Volume (km³)</u>	<u>Volume (km³ DRE)</u>
Jemez Plateau	25	7.9	0.03	2.96	2.96
Cañon de San Diego	23.1	11.5	0.05	12.1	6.05
CC1 (Cochiti Canyon)	5.9	1.9	0.03	0.17	0.09
CC2 (Cochiti Canyon)	5.9	2.7	0.03	0.24	0.12
CC3 (Cochiti Canyon)	10	4	0.03	0.6	0.3
Pueblo Mesa (western)	7.7	2.1	0.06	0.5	0.25
Pueblo Mesa (eastern)	10.3	4.4	0.05	1.13	0.57
TOTAL:				17.7 km³	10.3 km³ (DRE)

Table 3.2. Volume calculations for pre-Otowi paleostructures. Note that Otowi ignimbrite from the Jemez Plateau is densely welded.

<u>Basin</u>	<u>Total Volume</u>	<u>Volume (DRE)</u>
Española	14.21 km ³	7.11
Santo Domingo	<u>7.98 km³</u>	<u>3.99</u>
Total:	22.2 km³	11.1 km³

Table 3.3. Volume calculations for Otowi outflow sheets that may have existed at one time to the south (Santo Domingo Basin) and east (Española Basin) of the caldera. These sheets are represented as thinning wedges with a proximal thickness of 20 m (Española) and 15 m (Santo Domingo) and a distal thickness of 0 m.

<u>Totals:</u>		
Zones A-M	269 km ³	
Paleocanyons	10.3 km ³	
Distal Wedges	<u>11.1 km³</u>	
	290 km³ (DRE)	
Caldera Fill (I) =	149 km ³	
Total Outflow (O) =	141 km ³	
Distal Ash (A) =	<u>145 km³</u> (Mason et al. 2004)	<u>45 km³</u> (Pyle method)
TOTAL =	435 km³ (DRE)	335 km³ (DRE)

Table 3.4. Final volume calculations, including all zones and segments. Distal ash is calculated on the left as an average of outflow and caldera fill (Mason et al. 2004), and on the right using isopach maps (Pyle, 1989).

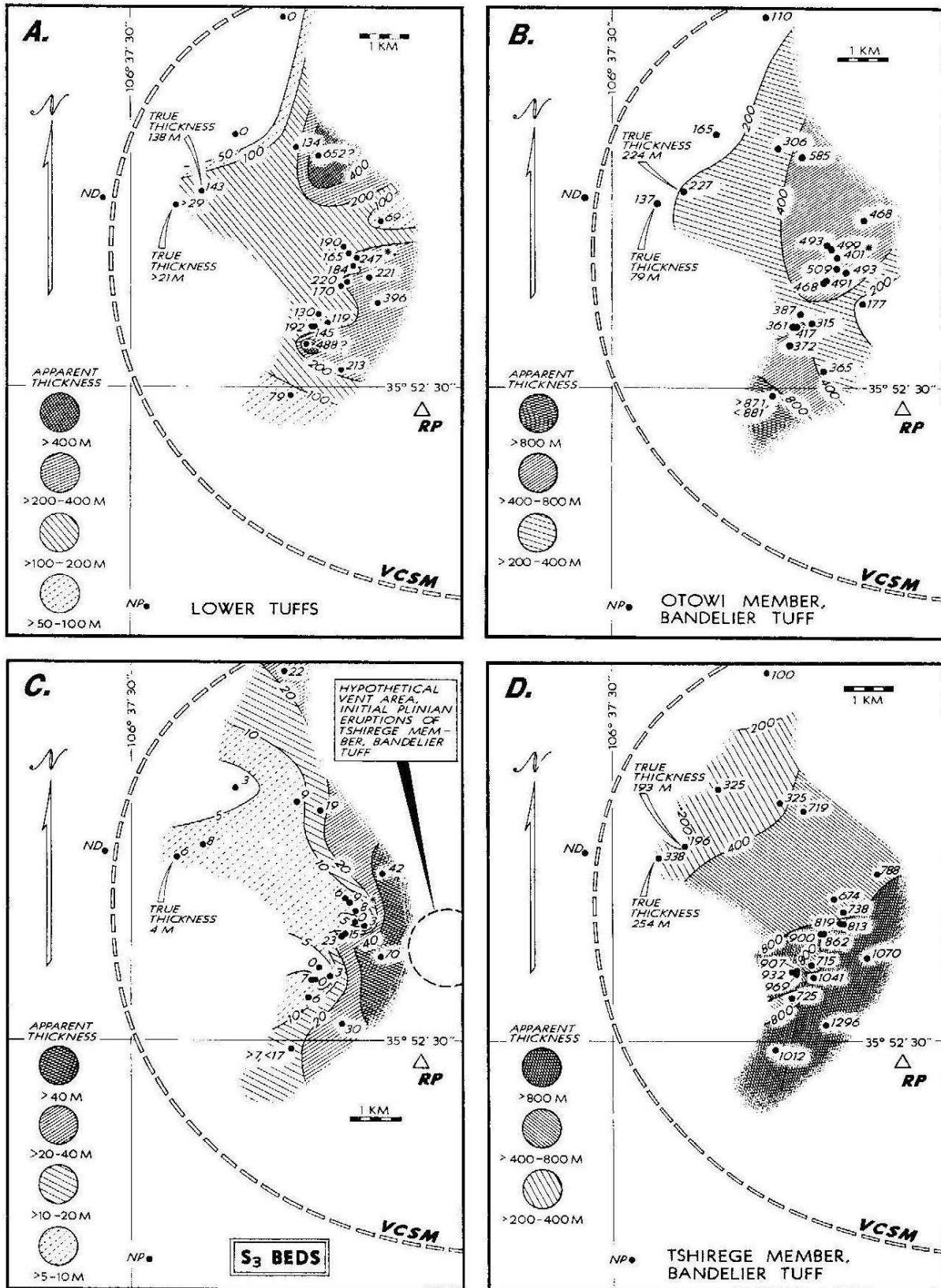


Figure 3.1. Isopach maps of selected intracaldera units (Hulen et al., 1991)

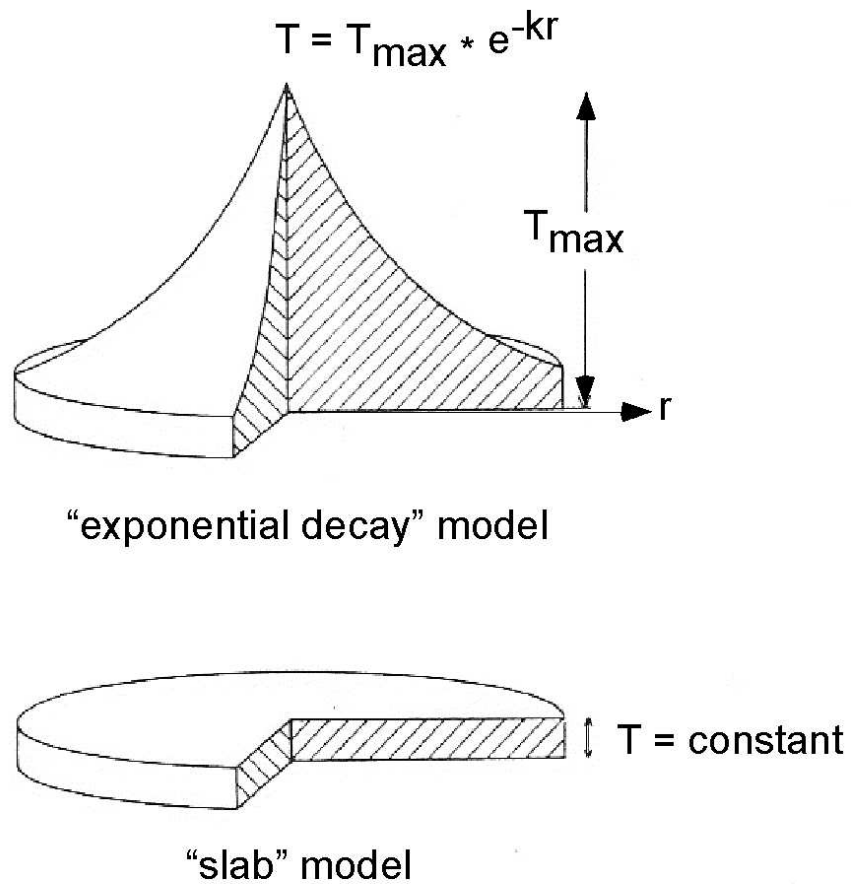


Figure 3.2. Sketch illustrating the “exponential decay” and “slab” model ignimbrites of Wilson (1991). In the exponential decay model thickness is seen to decrease exponentially with increasing distance from a maximum at the center. The equation for this morphology is $T = T_{\max} * e^{-kr}$ where T = thickness, T_{\max} = maximum thickness, k = the rate of thickness decay, and r = the distance from where $T = T_{\max}$. For the slab model, thickness is constant.

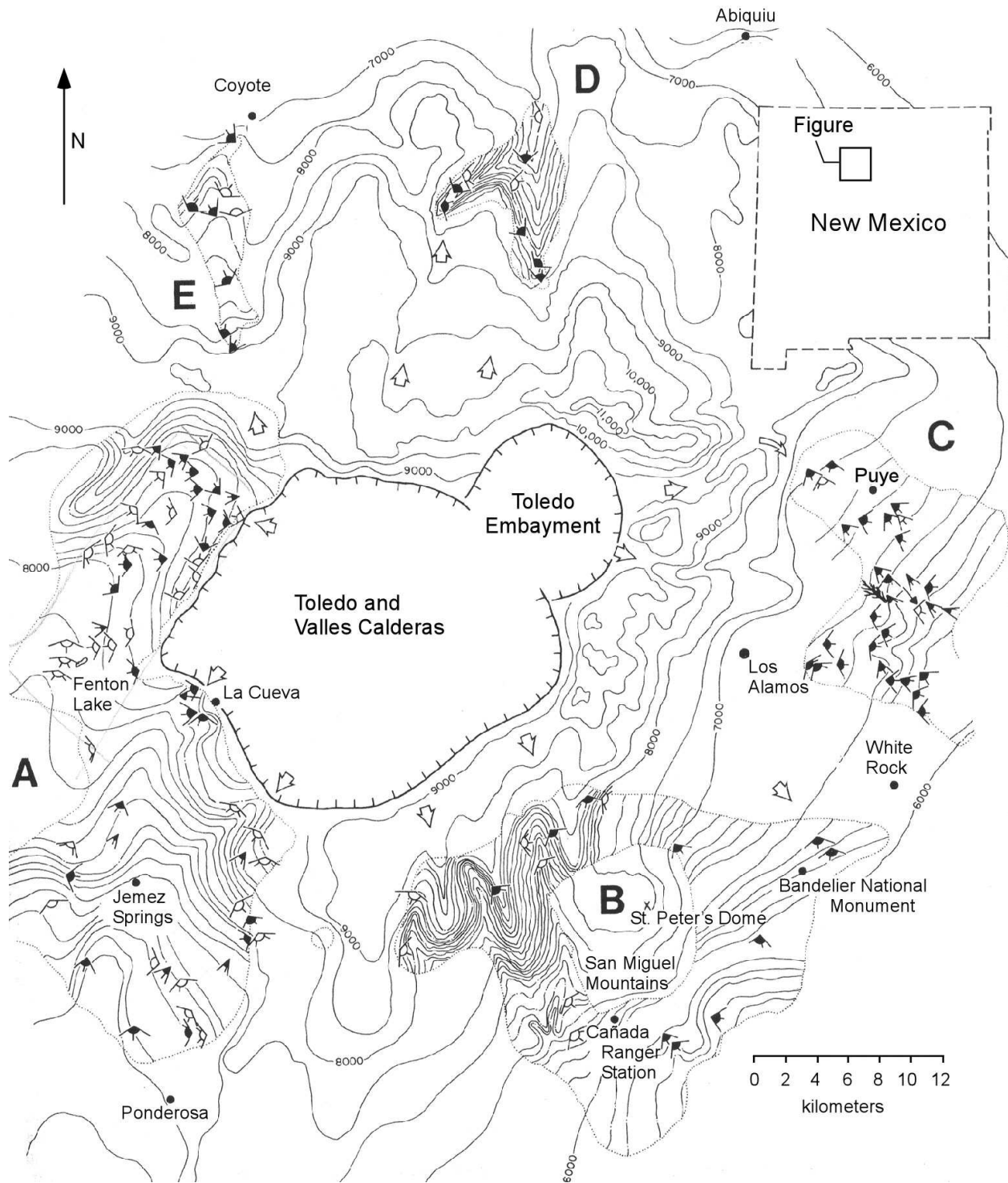


Figure 3.3. Map from Potter and Oberthal (1987) showing a reconstructed paleotopography for the pre-Otowi topographic surface. Contour interval is 100 feet in areas with significant stratigraphic and core data (labeled as areas A-E) and 500 feet in areas where data is scarce.

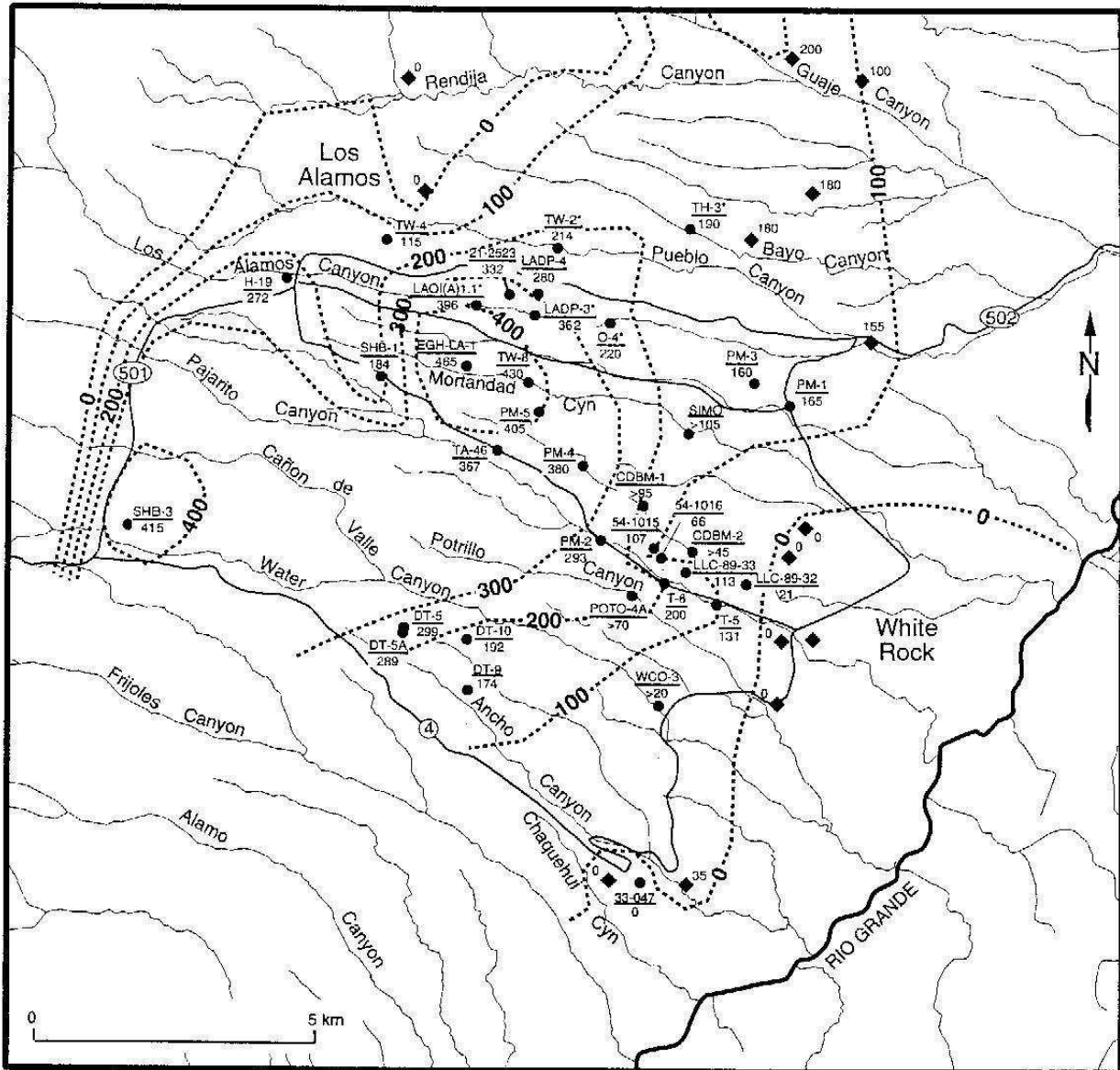


Figure 3.4. Pre-Otowi paleosurface as calculated by Broxton and Reneau (1996)

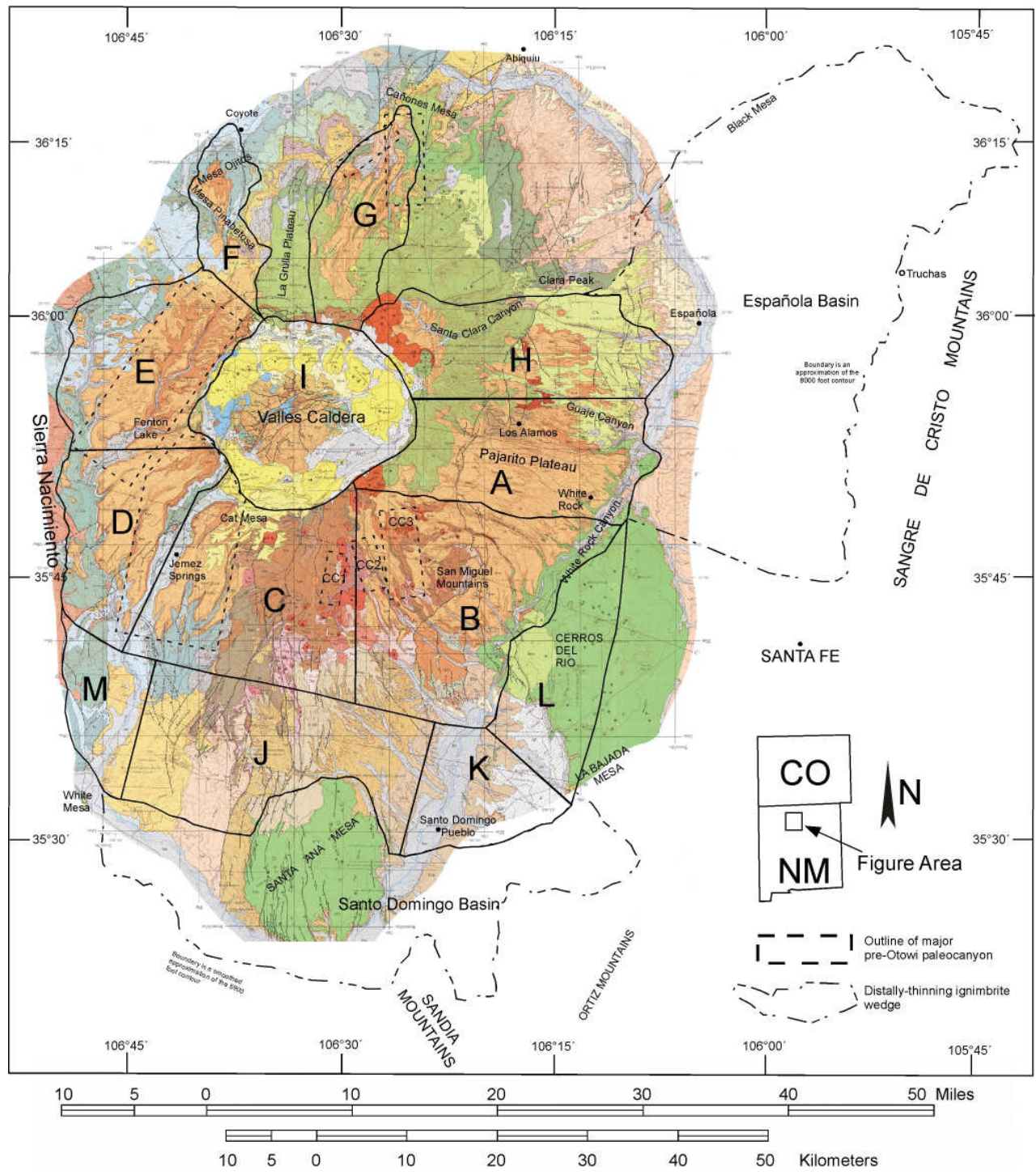


Figure 3.5. Individual zones and sections used in the calculation of the Otowi eruptive volume on the geologic map of Smith et al. (1970).

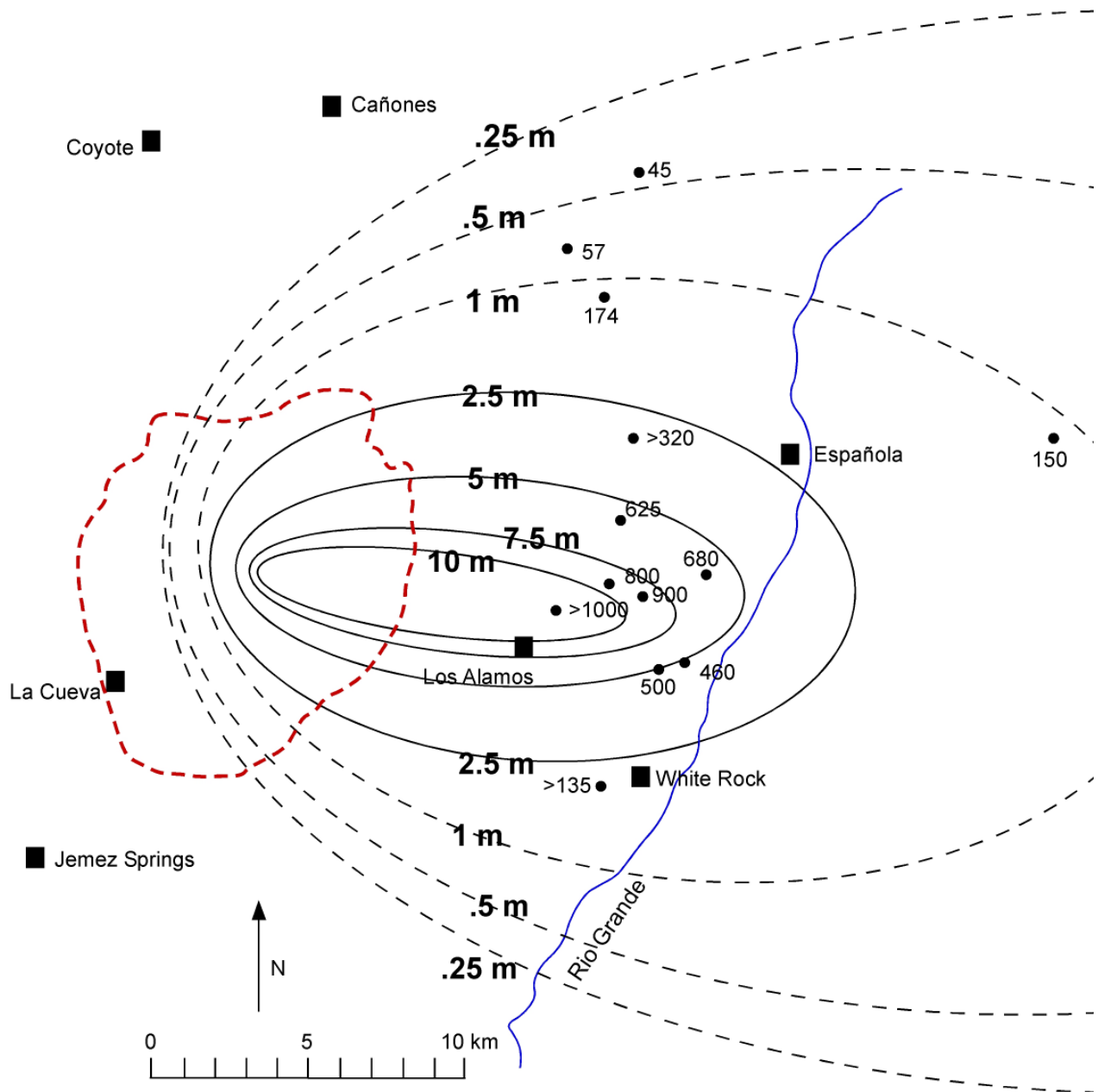


Figure 3.6. Reconstructed isopach map for Guaje plinian fall unit A using thickness data from Self et al. (1986) and Self et al. (1996).

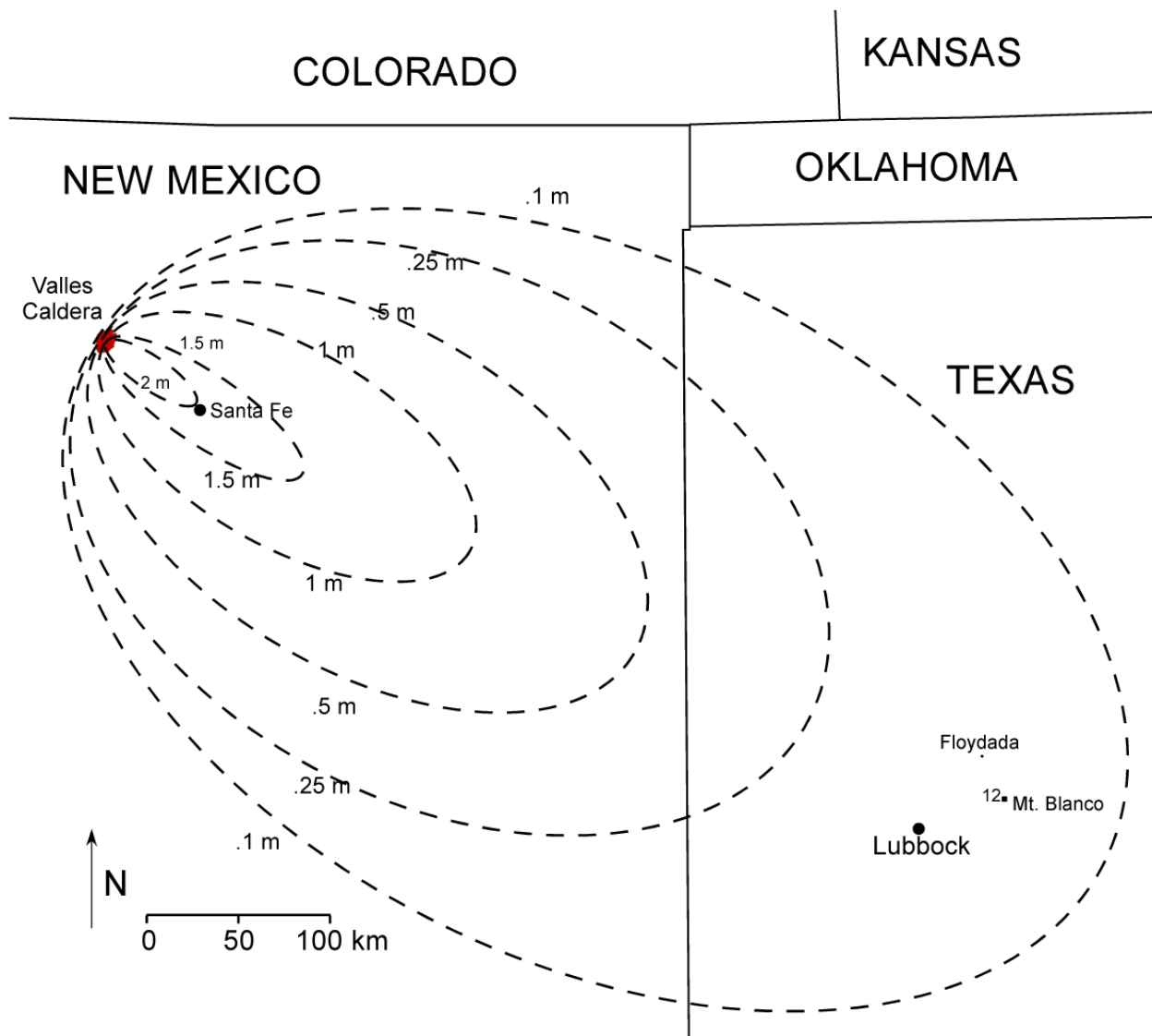


Figure 3.7. Reconstructed isopach map for plinian units B-E. Isopachs are represented with dashed lines as they are inferred using the spacing determined from an exponential thinning model.

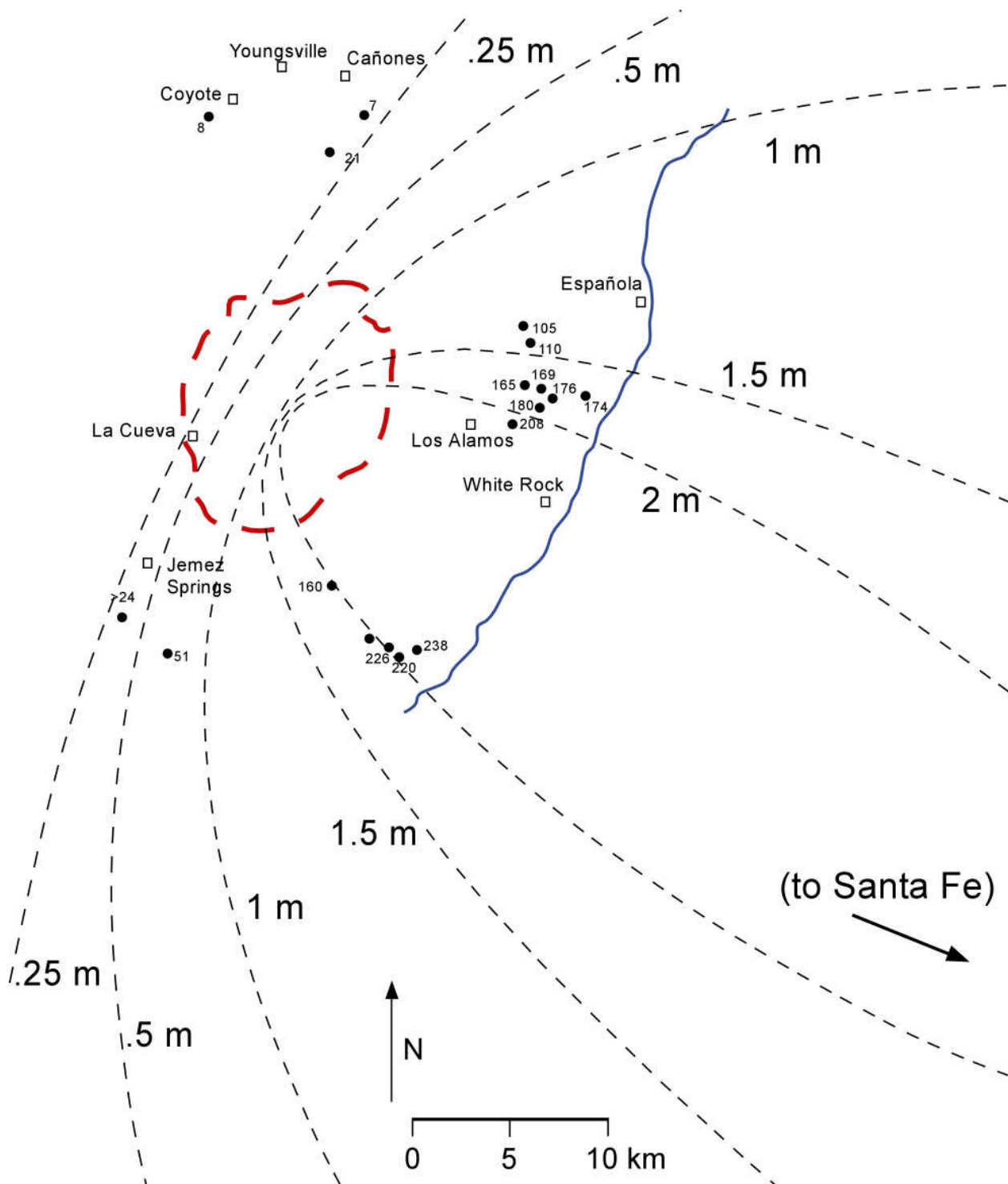


Figure 3.8. Close-up view of the isopach map for Guaje plinian units B-E. Thicknesses of fall deposits are from Self et al. (1996). The Valles Caldera is outlined in red.

Guaje Plinian

A

Thickness (cm)	long axis (km)	short axis (km)	area (km ²) A=Pi(L*S)	sq root A (km)	In thickness (cm)
1000	11.8	2.7	25.0	5.0	6.9
750	13.6	3.8	40.6	6.4	6.6
500	16.1	6.7	84.7	9.2	6.2
250	20.5	11.6	186.8	13.7	5.5
100	31.3	18.9	464.6	21.6	4.6
50	49.2	26.6	1027.9	32.1	3.9
25	63.7	34.4	1721.0	41.5	3.2
		1/2 distance	3.91		
		Volume	2.3		
		DRE (km³)	1.15		

Guaje Plinian

B-E

Thickness (cm)	long axis (km)	short axis (km)	area (km ²) A=Pi(L*S)	sq root A (km)	In thickness (cm)
200	60	18	848.2	29.1	5.3
150	130	38.4	3920.7	62.6	5.0
100	235	108	19933.4	141.2	4.6
50	335	187	49201.3	221.8	3.9
25	437	289	99190.3	314.9	3.2
10	600	380	179070.8	423.2	2.3
		1/2 distance	52.1		
		Volume	89		
		DRE (km³)	44		

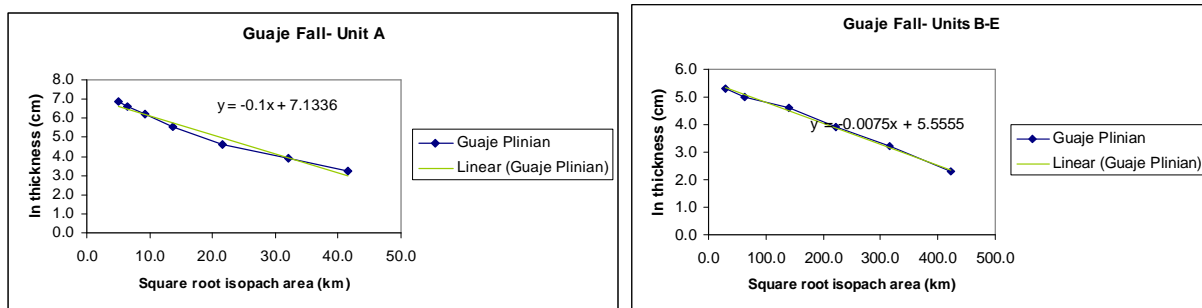


Figure 3.9. Calculations and plots used to determine plinian volumes, based on the methodology of Pyle (1989).

CHAPTER FOUR
A LITHIC STUDY OF THE OTOWI MEMBER

Background

Lithic counts have traditionally been an under-utilized method for determining characteristics of an ignimbrite-producing eruption, owing largely to the amount of time and labor involved in the process. Despite this, lithic counts remain perhaps the best method for identifying vent locations and shifts throughout the course of a large caldera-forming eruption. This is particularly true if the basement geology beneath a volcanic edifice is particularly well-constrained. However, since the 1970's, there have been only a handful of lithic count studies, focusing on eruptions in the United States, Europe, New Zealand, Japan, and Mexico.

Hildreth and Mahood (1986) used lithic counts from Long Valley in California (Bishop Tuff) to pinpoint the locations of eruptive vents across the caldera. They discovered that areal distributions of lithic fragments were an ideal indicator of vent locations. This is particularly true in the case of Long Valley because the pre-Bishop Tuff geology is particularly well-constrained and variable. Specifically, there are a series of narrow belts comprised of distinctive lithologies that are easily identified as lithics in the Bishop Tuff. In addition, there are pre-caldera domes that assist greatly to distinguish vents situated on the north side of the caldera from those on the south.

They concluded that the initial deposits of the Bishop Tuff (plinian and early flow deposits) emanated from a vent in the south-central portion of the caldera and that later flows represented a transition to vents associated with ring-faults on the periphery of the caldera (Hildreth and Mahood, 1986). Based on lithic data, they were able to ascertain that the vents

migrated around the caldera in a counter-clockwise direction and that the transition from a single, centrally-located vent to multiple, ring-fault vents took place after approximately 20% of the magma had been erupted (Hildreth and Mahood, 1986).

More recently, Wilson and Hildreth (1997) have reassessed the eruptive model for the Bishop Tuff, using lithic data from Hildreth and Mahood (1986) along with new lithic counts and a re-examination of stratigraphy. In this study, lithics with a diameter greater than 5 mm were collected from various points around the caldera and classified. This more robust and detailed lithic distribution data resulted in a determination that vent migrations, initially identified by Hildreth and Mahood, were actually far more complex than previously thought (Wilson and Hildreth, 1997). In addition, the authors discovered that the Bishop Tuff was intraplinian in nature, with coeval eruption of pyroclastic falls and flows.

Cole et al. (1998) used lithic proportions and chemistry to determine provenance for individual ignimbrites in the Taupo Volcanic Center, Taupo Volcanic Zone, New Zealand. The authors used distribution, petrologic, and density data derived from 1162 lithics greater than 32 mm to assist in correlating various ignimbrite units and to evaluate volcanic structures within the Taupo Volcanic Zone (Cole et al., 1998).

Browne and Gardner (2004) examined a small (3-4 km³ DRE) caldera situated in a stratovolcano (Volcan Ceboruco) located in the Trans-Mexican volcanic belt. Lithic assemblages were found to shift demonstrably across the collapse transition, from deep origin to progressively shallower origins. In this study, the authors were able to demonstrate the applicability of lithic data to the study of calderas other than those erupting only large volumes, such as Valles or Long Valley.

Lithic Studies in the JMVF

Potter and Oberthal (1987) produced the only study using lithic fragment data to delineate eruptive processes for the Bandelier Tuff. Their study proposes that at least seven vents, situated along the margin of the Toledo Caldera and coincident with ring-fractures, were involved in the 1.61 Ma eruption of the Otowi Member of the Bandelier tuff. They cite five key pieces of evidence in support of this determination: 1.) the overall broad radial distribution of large volumes of Otowi ignimbrite; 2.) areal variations in lithic fragments, 3.) contrasts in welding and zonation of the Otowi ignimbrite, 4.) paleotopography, 5.) flow directions of ignimbrite determined using measurements of elongated pumice and charred tree-casts.

Field techniques used by Potter and Oberthal include collection of lithic data, an assortment of stratigraphic observations (including observations of thicknesses, areal extent, degrees of welding, and zonation within the Otowi tuff), and an examination of pumice orientations for use as flow-direction indicators (Potter and Oberthal, 1987). Their field procedure employed two or three scientists at each outcrop making observations across a zone approximately 10 to 50 meters wide. Afterwards, their data was pooled. All visible lithic clasts in the face of the outcrop, ranging in size from .5 to 20 cm, were counted and identified. In all, a total of 5200 lithics from 54 localities were identified with approximately 88 (on average) from each site (Potter and Oberthal, 1987). Basalt and andesite lithics were lumped in a single group, as were rhyodacite and rhyolite. The data were presented in pie charts for comparison (Figure 4.1). Pumice orientations were mapped from 120 stations, 48 in the upper third of the Otowi, 28 in the middle third, and 43 in the lower third. Flow directions were inferred largely from the measurement of pumice orientations. The direction and magnitude of plunge of pumice fragments were recorded at all sites and from all stratigraphic levels. In addition to pumice, the

orientations of carbonized logs and groove-casts were used as flow-direction indicators.

Weathered outcrops were selected over hardened outcrops because the orientations of the pumice clasts are more easily measured in weathered outcrops.

Based on the field data, the authors assert that as many as seven vents, located on the caldera ring-fracture, were involved in the eruption of the Otowi ignimbrite (Potter and Oberthal, 1987). To assess the data, the authors subdivided the caldera into five regions, labeled A-E, starting in the southwest and running counter-clockwise around the caldera (Figure 4.1).

Physical data was evaluated in each region and compared to the other sections. The authors' first contention is that flow direction data derived from pumice orientations is significantly variable around the caldera, which supports multiple sources. In addition, they suggest that the broad radial distribution of huge volumes of Otowi ignimbrite represents direct evidence for multiple vents. Next, the asymmetrical distribution of welding throughout the Otowi tuff (prevalent throughout the western caldera, poorly-developed in the east) is identified as further evidence for multiple vents. Finally, contrasts in lithic distributions in areas A-E are used as evidence for multiple vents sampling varied source lithologies.

The authors propose that Otowi Member Tuff was derived primarily from vents within Paliza Canyon lavas which are dominated by andesite. The exception is the Pajarito Plateau, where lithic fragments are predominantly dacitic and thus were likely sampling Tschicomama lavas (Potter and Oberthal, 1987). Potter and Oberthal admit that they are "puzzled" by the presence of rhyolites, as they are not dominant in formations exposed near the caldera. They go on to suggest the possibility that their "rhyolites" may have been confused with hydrothermally-bleached volcanic rock (Potter and Oberthal, 1987).

Criticism of the findings of Potter and Oberthal (1987)

Self and Turbeville (1987) provide a useful criticism of the findings of Potter and Oberthal (1987) in which they evaluate the evidence presented for locations and numbers of eruptive vents. They question the validity of using paleotopographic data, distribution of Otowi ignimbrites, and flow indicators as evidence for multiple vents. Self and Turbeville point out that flow patterns and ignimbrite distribution observed in the Otowi could also be produced in an eruption emanating from a single, centrally-located vent. In this circumstance, the flow indicators observed by Potter and Oberthal would represent not multiple vents, but instead, funneling of pyroclastic flows into pre-existing paleovalleys in the pre-Otowi topography. They suggest that Potter and Oberthal did not consider the effects of erosion of the original, more substantive Otowi sheet and that current erosional remnants may not reflect original eruptive processes.

In addition, Self and Turbeville question flow direction indicators, citing that 40% of the flow direction data came from the basal portion of the Otowi ignimbrite. Flow directions obtained from the basal portion of a flow are heavily influenced by underlying topography and thus may have improperly skewed Potter and Oberthal's conclusions (Self and Turbeville, 1987).

Self and Turbeville also question the use of variations in welding zonation as an indicator for multiple vents. They suggest that many factors influence welding patterns, including deflection of hot pyroclastic flows by collapse events, asymmetric collapse of an eruption column, and even erosion (Self and Turbeville, 1987).

In the last segment of their criticism, the authors propose that the disparity discovered by Potter and Oberthal between lithics from the Pajarito Plateau (Area C of Potter and Oberthal, Figure 4.1) and the rest of the caldera may be attributed to the presence of thick Guaje fall

deposits. The deposition of 8-10 meters of pyroclastic fall early in the eruption would have prevented later entrainment of surface lithics by Otowi pyroclastic flows. They also point out that Potter and Oberthal seem to have had difficulty in the identification of lithic types. For example, andesite and basalt were lumped together; they did not provide any criteria for distinguishing latites, which in some of their sample localities constitute up to 80% of the lithics present; welded ignimbrites were not recognized, even though this lithic type is present in the Otowi, as discovered by Eichelberger and Koch (1979). Self and Turbeville go on to point out that the relative uniformity of lithologies around the Valles Caldera makes identification of vent sites based on lithic assemblage a tricky task.

Self and Turbeville do not discount the possibility that the Otowi eruption initially came from a large central vent, later migrating to peripheral, caldera ring-vents. In fact, precisely this scenario is presented in an earlier paper (Self et al., 1986). However, they submit that the evidence presented by Potter and Oberthal is insufficient to prove the case, and it is thus still open to alternative interpretation.

In a response published in the same volume, Potter and Oberthal defend their earlier interpretations. They re-assert that the broad distribution of the Otowi ignimbrite provides “ready explanation in multiple vents” and note that Self and Turbeville do not discuss this. In addition, they reiterate that the contrast in lithic signatures between east and west is their most important piece of evidence for multiple vents. The issue of lithic misidentification is addressed and Potter and Oberthal essentially plead ‘no-contest,’ stating that although their identification methodology (in-situ at the outcrop) may be unusual, they identified at a large number of widely separated stations (54), and despite the uncertainties inherent in identification of small fragments, they are confident their signatures are valid and show real contrasts. They summarize by stating

that they are not “dogmatic” about the number of vents (7) but they remain firm in their assertion that the Otowi was erupted from multiple ring vents.

The main issue with the lithic study of Potter and Oberthal is that although they do identify some legitimate contrasts in lithic distributions, the evidence provided is insufficient to substantiate a multiple ring-vent eruptive scenario. Self and Turbeville concur with this assessment and note that the evidence presented by Potter and Oberthal could also be used to support a single, centrally-located vent throughout the duration of the eruption. Another major shortcoming of the lithic fragment study of Potter and Oberthal (1987) is that the authors knew much less than we now know about pre-Otowi subsurface geology, particularly in the western part of the caldera. Since the late 1980’s, a number of important investigations of pre-Otowi volcanism have been published including Goff et al. (1989; 1990), Goff and Gardner (2004), Wolff et al. (2005), and Rowe et al. (2007). This new information has allowed for a much better understanding of subsurface geology in the Valles Caldera (see map in Figure 4.2). In turn, this has allowed lithic counts to become a more accurate tool for use in provenance studies of ignimbrites in the Jemez Mountains.

Why this lithic count study is superior to previous studies

In this study, a total of nine sample localities around the caldera were selected from various points in the Otowi ignimbrite (Figure 4.3). The lithic data obtained in this study is not only more comprehensive but more valuable for several reasons. For one, our understanding of pre-Otowi geology is now far more comprehensive. Pre-existing lavas and tuffs that may potentially be present as lithic fragments are well characterized chemically and petrographically. As a result, by using a combination of hand-sample identification, geochemistry, and

petrographic techniques, lithics are much more easily identified and associated with their source localities.

Next, Potter and Oberthal (1987) relied entirely on field-based identification of only exposed, in-situ lithics in the faces of outcrops. The problems inherent with this technique are obvious. First, count data may be skewed as it is only representative of what is present at the surface of an outcrop and not the entire deposit. Specifically, factors such as erosion, preferential weathering, or pyroclastic transport mechanisms may artificially affect the lithic population on the surface of an outcrop, thus introducing a bias in count data. Second, classification of mainly small (< 1 cm), aphanitic igneous rock in the field is a difficult proposition under even the best of circumstances. Consequently, in this study, bulk ignimbrite samples were collected from outcrops, sieved in the field, and taken back to the lab. In the lab, samples were further sieved to separate the various components, including pumice, lithics, and ash matrix. The lithics were then washed thoroughly. Identifying small, aphanitic rock fragments is difficult enough when the samples are pristine. It becomes far more difficult when the samples are weathered and covered with dirt, ash, and other assorted materials. Consequently, our experience is that a clean surface is vital for proper lithologic recognition. Lithic type identifications were made with the assistance of a binocular microscope, hand lens, and several strategically-positioned lamps that produced an exceptionally well-lit work area. Therefore, we believe our sampling and identification technique is superior to that of Potter and Oberthal (1987).

Finally, this work is one of the largest lithic count studies ever undertaken, involving the collection and identification of over 17,000 lithic fragments from all stratigraphic levels of the Otowi Member. The data set is not only robust, but it is three-dimensional in that it includes

vertical and lateral lithic distributions. In addition, geochemical analyses from the host tuff have allowed comparison of lithic distributions and magmatic processes. This has not before been attempted in the Bandelier Tuff.

Experimental Methods

Bulk Otowi Ignimbrite samples were collected from nine locations around the caldera (Figure 4.3) and placed in two-gallon Ziploc plastic bags. The samples were collected in the field during the summer of 2000 by W.L. Aubin, R.L. Winters, M.C. Rowe, P. Hartman, and J.A. Wolff. At each locality, multiple samples were taken from different stratigraphic heights. In addition, individual pumice and lithic samples were collected for geochemical analysis. The bulk samples were initially sieved in the field to separate larger material from ash-sized particles. Later, in the lab, samples were once again sieved to assist in separation of individual fractions including pumice, ash, and lithics. Large pumice and lithic fragments were picked out at this point and bagged. Bulk material was then placed in a five-gallon bucket and filled with water to assist in pumice separation. Pumice too dense to float was visually picked out by hand once the mixture had dried. The processed material was then run through a 5 millimeter sieve, and all lithic fragments greater than 5 mm were picked out by hand. Lithics were then washed thoroughly in order to aid in the identification process.

All lithics larger than 5 mm were identified, counted, and weighed. A binocular microscope and a hand-lens were used to assist in identifying smaller fragments. Lithics were divided into five categories based on known pre-caldera lithologies: andesite, dacite, rhyolite, ignimbrite, and miscellaneous lithologies. Miscellaneous lithologies include, but are not limited to, various plutonic igneous clasts, metamorphic rocks (amphibolites and quartzites), and a variety of sandstones and other clastic sedimentary rocks.

The data were organized using Microsoft Excel[®] spreadsheets. For each locality, individual pie graphs showing numbers of fragments and weight fractions were generated for each sample. The graphs were then placed in stratigraphic order for each sample locality. The resulting stratigraphic columns, complete with lithic distribution charts, were placed on a geologic map showing pre-Otowi lithologies in Figure 4.4

Lithologic Descriptions

Dacite lithic fragments encountered in this study were light grey to medium grey in color and aphanitic to porphyritic. Plagioclase, pyroxene, hornblende, biotite, and sparse quartz phenocrysts were observed in these fragments. The Paliza Canyon and Tschicoma Formations each contain significant quantities of dacitic lavas. The Tschicoma dacite is typically more coarsely porphyritic than the Paliza Canyon, with larger and more abundant plagioclase phenocrysts visible. Despite these differences, most samples were between 0.5-1 cm in size, and as a result it was difficult to accurately differentiate between Paliza Canyon and Tschicoma dacite in hand specimens. Consequently, determinations were made through geochemical analyses that will be discussed later in this chapter. Overall, the presence of the above-mentioned phenocrysts and the lighter color were sufficient to distinguish dacite as a lithic lithology.

Andesite lithic fragments encountered in this study were typically dark-grey in color and aphanitic to weakly porphyritic. Phenocrysts observed include plagioclase, pyroxene, and occasional olivine visible in a dark aphanitic matrix. Many fragments were vesicular with a spongy texture. In general, the darker color, presence of pyroxene and olivine phenocrysts, and the vesicular nature of some Paliza Canyon andesite was sufficient to distinguish andesite as a lithic lithology.

Rhyolite lithic fragments encountered in this study were typically light-grey in color and aphanitic, with occasional quartz and biotite phenocrysts visible. Most samples exhibited some degree of flow banding, with the majority of samples exhibiting conspicuous flow-banding. In light-colored lithic fragments that were not pyroclastic in origin, the presence of flow-banding and biotite phenocrysts were used to discriminate rhyolite fragments from dacite fragments. This seems reasonable, as many of the pre-caldera rhyolite units such as the Bearhead and El Rechuelos Formations are flow-banded.

Ignimbrite lithics encountered in this study were cream to buff colored and were typically small (< 1 cm) in size and strongly welded. Tiny pumices, phenocrysts, and occasional lithic fragments were observed within these tuff fragments. Most of these small samples were either altered hydrothermally or weathered significantly. Overall, they appear similar to the Bandelier Tuff. However, if they are recycled Otowi fragments, we would expect them to be much less weathered and/or altered than observed. Thus, the ignimbrite lithic fragments are more likely associated with the earlier La Cueva ignimbrites (formerly the San Diego Canyon Ignimbrites), which are chemically and petrographically similar to the Bandelier Tuff.

The other lithic fragment lithologies encountered were scarce in number, but include sedimentary rocks (sandstone and siltstone), metamorphic rocks (quartzites and amphibolites), and a variety of granitoid lithics. The sandstone and siltstone lithics were tan to beige in color, and appear arenitic with fine to very fine quartz grains visible with the aid of a binocular microscope. Quartzite lithics were observed as small cream-colored opaque to translucent fragments having a granular texture. Several small (< 0.8 cm) green to black metamorphic lithics were observed that have been tentatively identified as amphibolites. Granitoid lithic

fragments were the most abundant of the 'other' lithologies. They were typically found as small (< 1.0 cm) light-colored phaneritic fragments with feldspar, quartz, and biotite crystals visible.

Results

Lithic data obtained from the Otowi member is summarized in Table 1, the pie diagrams in Figure 4.5, and in the individual stratigraphic sections seen in Figures 4.6 through 4.10.

Overall, andesite (44%) and dacite (49%) were the most common lithics encountered. Rhyolite (4.8%), ignimbrite (1.4%), and "other" lithologies (0.8%) comprise the remainder of the count data.

Lithic abundances found at the nine individual sample locations are summarized in Figures 4.4 and 4.5. Upon close examination of all nine individual sample localities, andesite and dacite remain the most dominant lithologies. Combined abundances of andesite and dacite vary between 68.7% and 98.5% around the caldera. At six locations (including Cat Mesa, Pueblo Mesa, Cebolla Canyon, Wildcat Canyon, Upper Cochiti Canyon, and the Northeast #1 locality), the combined proportion of andesite and dacite is equal to or higher than 93.5%. In two locations (Dixon Ranch and the Airport Section), the combined proportion is 84.9% or greater. The exception is Guaje Canyon, where although still dominant, the overall percentage of andesite and dacite is somewhat lower (68.7%) due to the presence of larger quantities of rhyolite (20.2%) and densely-welded tuff (9.7%).

Rhyolite lithics are found at all localities with the exception of Cebolla Canyon, which is dacite-dominated. A striking feature of the data is that rhyolite lithics are found at similar points in stratigraphy around the caldera and are associated with the most evolved pumice concentrations (Figures 4.6-4.11). At nearly all localities, the largest quantities of rhyolite lithics are found in tuff with niobium (Nb) concentrations between 195-180 ppm, regardless of mode of

deposition (fall or flow). Moving upward in stratigraphy, beyond the ~180 ppm transition, rhyolite lithics decrease significantly in overall proportions.

Densely-welded ignimbrite lithics are found at four localities around the caldera: Wildcat Canyon, Cat Mesa, Guaje Canyon, and Dixon Ranch. Percentages of these lithics vary from 0.1% at Wildcat Canyon to 9.7% at Guaje Canyon. At Guaje Canyon, several samples (JMVF-00-09 and JMVF-00-10) actually contain ignimbrite as the dominant lithology (48% and 64% respectively). This is, however, the exception rather than the rule as ignimbrite is found only in minor quantities elsewhere.

Guaje Canyon

The stratigraphic section at Guaje Canyon (Figure 4.6) is a 15 m composite of two sections, one measured at the Copar pumice mine and the other measured at the White Eagle pumice mine. The two localities are within ½ mile of each other in Guaje canyon. Strata at both localities have thus been correlated to form a composite section. At Guaje Canyon, five fall units (A-E) are exposed in addition to a thin ash layer overlying fall unit E, followed by a layer of massive Otowi ignimbrite.

In this section (Figure 4.6), andesite and dacite comprise 68.7% of the total lithics encountered (38.3% and 30.4% respectively); rhyolite lithics, 20.2%; welded ignimbrite lithics, 9.7%; other lithics comprise 1.4% of the total. The total number of lithics encountered increases significantly from fall unit A to fall unit C, where the largest numbers of lithics are encountered (193 in sample JMVF-00-177). After fall unit C the number of lithics decreases steadily through fall units D and E, with only nine lithics encountered in fall unit E at 10.53 m above the base of the section. This would seem to correlate well with the hypothesis that the Otowi plinian column intensity peaked during deposition of unit C (Self et al., 1996).

Lithics increase in abundance in the overlying ignimbrite, but their numbers are more randomly distributed in stratigraphy. However, a pulse of welded ignimbrite lithics found between 12 and 12.75 m is noteworthy as these lithics are uncommon elsewhere.

The main lithologic trend observed in the Guaje section, is the dominance of andesite and dacite lithics and the regular fluctuation in the ratio between the two. A secondary trend begins with the appearance of rhyolite lithics in the upper portion of Fall Unit A. Rhyolite continues to increase in concentration upward until Fall Unit C where, in samples JMVF-00-03 and JMVF-00-177 it comprises 37.1% and 52.3% of the total lithics (respectively). Stratigraphically above Fall Unit C, and in the overlying ignimbrite, rhyolite lithics sharply decrease in concentration.

The emergence of rhyolite appears to coincide with Nb concentrations in the 195-180 ppm range. After fall Unit C, Nb concentrations drop significantly below the 180 ppm threshold, and rhyolite disappears as a major lithology. A third observed trend is the presence of densely-welded tuff lithics found within the ignimbrite above the plinian fall. Samples JMVF-00-09 and JMVF-00-10 contain 49% and 64% welded ignimbrite lithics, respectively. Other lithologies are minor in this section (1.4%) and appear randomly, if at all throughout stratigraphy.

Northeast Section

The Northeast exposure (so named because it is located the farthest north and east of all sample localities) consists of a small fall deposit and a 3 m ignimbrite sequence on Route 114. Only one bulk sample—JMVF-00-108 was taken from the ignimbrite. In this section (Figure 4.7), dacite is the dominant lithic (56.3%), followed by andesite (38.5%), and rhyolite (5.2%). Pumices analyzed from the host tuff at this location yielded Nb concentrations between 94 and 182 ppm.

Pueblo Mesa

Pueblo Mesa, located to the north of the present-day Valles Caldera is host to an approximately 45 m section (Figure 4.7) that contains a thin plinian unit and a massive ignimbrite. Four bulk samples were taken from the ignimbrite. Andesite (68.4%) and dacite (29.2%) comprise the majority of lithics encountered (97.7% overall) at the Mesa. Andesite is the dominant lithology, ranging from 55.2% at the bottom of the section to 94.3% at the top of the section. The andesite/dacite ratio shifts from nearly equivalent at the base of the section to overwhelmingly andesite-dominated (16.8 times as much andesite) at the top. Lithic numbers remain reasonably consistent throughout the section, ranging between 51 and 96 total fragments per sample.

Cebolla Canyon

One bulk sample was taken from Cebolla Canyon (Figure 4.7) in which dacite (89.2% of the total) is the dominant lithology encountered. Andesite comprises 9.2% and other lithologies 1.5% (one lithic).

Cat Mesa

Cat Mesa, located to the southwest of the present-day caldera, represents the largest sample site in the study in terms of stratigraphic breadth and abundance of lithics. Thirteen bulk samples were taken from the Otowi ignimbrite in a section (Figure 4.8) measuring 87.8 meters high. These samples yielded the largest number of lithics (9185 of the overall total) collected from any locality. In addition, some extraordinarily large (> 1 meter) lithic fragments are found in this outcrop. Particularly prominent in this section is a well-known lithic lag breccia, sampled as JMVf-00-83, located at approximately 73.7 m above the base. Bulk samples and pumice were taken from above, below, and within the lag breccia. In this section, dacite (50.9%) was

slightly more abundant than andesite (42.6%), with rhyolite (3.9%), tuff (1.6%), and other lithologies (1.0%) comprising the remainder of lithics observed. As in other sections, andesite and dacite are dominant in varying proportions. The section begins andesite-dominated (samples JMVf-00-42, 00-45, and 00-51) at the base; then, moving upward in stratigraphy the section switches to overwhelmingly dacite-dominated (samples JMVf-00-55, 00-57, 00-60, and 00-64), changes back to andesite-dominated (JMVf-00-66 and 00-69), shifts to heavily dacite-dominated within and just above the lag breccia (samples JMVf-00-83 and 00-85), then ends with andesite as the prevailing lithology (samples JMVf-00-88 and 00-90) at the top of the section.

Rhyolite lithics are found in samples at Cat Mesa that were sieved from tuff with Nb concentrations ranging from as low as 159 ppm to 200 ppm. The highest proportions of rhyolite lithics are found in samples taken from tuff with Nb concentrations between 189-195 ppm. This includes samples JMVf-00-51 (189 ppm) and JMVf-00-55 (191 ppm) where rhyolite lithics comprise 12.53% and 11.68% of the total lithics encountered respectively. At lower Nb concentrations the proportions of rhyolite lithics are smaller (< 5%). Rhyolite lithics are most prevalent beneath the lag breccia. The abundance of rhyolite lithics decreases upward in stratigraphy approaching the lag breccia, and they are completely absent within the lag breccia (sample JMVf-00-83). Above the breccia, they reappear in JMVf-00-85 (4.57%) and JMVf-00-88 (1.64%), and then disappear in sample JMVf-00-90.

Welded ignimbrite lithics are found in every sample except one but are most prevalent at the base of the section, below 12 meters, in samples JMVf-00-42 (10.09%) and JMVf-00-45 (6.41%). Immediately beneath the lag breccia at 73.7 meters, welded ignimbrite lithics are nearly absent (0.91% in sample JMVf-00-69), then return within the lag breccia (2.18% in sample JMVf-00-83) and above.

Other lithologies are not encountered in any significant quantities except for sample JMVF-00-66, where other lithologies comprise 3.4%. This includes quartzite and sandstone clasts, with several small plutonic lithics.

The number of lithics is very high in bulk samples from this section. At the base of the section 109 lithics were found in sample JMVF-00-42. Lithic numbers increase significantly up-section, with 1282 lithics counted in sample JMVF-00-66 at approximately 66 meters, and 964 lithics in sample JMVF-00-83 at 73.7 meters within the lag breccia. Above the lag breccia lithic numbers remain high until approximately 78 meters (1220 in sample JMVF-00-88). Above 78 meters the number of lithics declines.

Wildcat Canyon

At Wildcat Canyon seven bulk samples were taken from the Otowi ignimbrite in a stratigraphic section measuring 40 meters high. This section (Figure 4.9) is roughly correlative in stratigraphy with the section above the lag breccia at Cat Mesa. Dacite (51.5%) and andesite (46.0%) are the dominant lithic lithologies. Rhyolite (1.8%), other lithologies (0.6%), and welded ignimbrite (0.1%) were also encountered. Andesite and dacite lithics predominate throughout the section; although, the relative abundance of the two fluctuates between andesite-dominated and dacite-dominated. Rhyolite lithics are most prevalent at the base of the section in sample JMVF-00-150 (188 ppm Nb), where they comprise 3.9% of the lithic total. Both rhyolite lithic abundance and Nb concentration decrease upward in stratigraphy. An anomaly in this section is found in sample JMVF-00-171, where other lithologies comprise 17% of the total sample. Based on their texture and mineralogy, these nine lithics appear to be quartzite.

Dixon Ranch

The section measured at Dixon Ranch (Figure 4.10), located on the southeast side of the caldera, is a composite of two exposures approximately 400 m apart. The first outcrop contains fall units B-D (and possibly unit E) and an overlying massive ignimbrite. The second outcrop contains intra-plinian ignimbrite interbedded between sub-layers of fall unit C. Two bulk samples were collected from the plinian deposit (fall units B and D), and one sample was taken from the overlying ignimbrite. At this locality, dacite is the dominant lithic at 45.6%, followed by andesite (37.3%), rhyolite (9.7%), welded ignimbrite (4.8%), and other lithologies at 1.0%. Andesite and dacite ratios vary between the three samples, alternating between andesite and dacite-dominated in the plinian, then switching to dacite-dominated in the ignimbrite. The most conspicuous trend is the presence of rhyolite in greater proportions in the two samples taken from the plinian deposits. In JMVF-00-31, at 0.31 meters from the base (Nb = 182 ppm), rhyolite comprises 15.0% of the lithics. In JMVF-00-33, at 1.68 meters (Nb = 183 ppm), rhyolite comprises 17.8% of the lithics. Contrast this with the sample taken from the overriding ignimbrite (JMVF-00-40; at 4.75 m; Nb = 193 ppm), where rhyolite is 1.3% of the total lithics. Also significant is the relative abundance of welded ignimbrite lithics in the plinian (7.3% in JMVF-00-31, 10.3% in JMVF-00-33) compared to the complete absence in JMVF-00-40, taken from the ignimbrite.

Upper Cochiti Canyon

The stratigraphic section measured in Upper Cochiti Canyon (Figure 4.11) is a 64 meter exposure from which five bulk samples were collected in the Otowi ignimbrite. Overall, andesite (48.6%) and dacite (46.8%) are present in nearly equal quantities, with the remainder consisting of rhyolite (4.3%) and other lithologies (0.4%). As in the majority of other sample

localities, the combined proportions of andesite and dacite remain similar in each sample throughout the section, and it is the ratio between the two that changes between samples. Rhyolite is observed to increase in abundance dramatically moving upward in stratigraphy. In particular, samples JMVF-00-200 (6.3%) and JMVF-00-204 (19.4%) show significant quantities of rhyolite lithics.

Airport Section

The airport section (Figure 4.11) is located immediately to the east of the Los Alamos Airport and consists of a 39.9 meter stratigraphic section of massive Otowi ignimbrite. Lithic data was obtained from two bulk samples. In this section, andesite (45.3%) and dacite (42.8%) are the dominant lithics, with rhyolite (11.8%) and other lithologies (0.1%) also present. As in many of the other sections, the andesite-dacite ratio is variable throughout stratigraphy. At the base of the section, sample JMVF-00-70 is dacite-dominated (62.1%) with subordinate andesite (24.2%) and rhyolite (13.7%). Sample JMVF-00-74, taken midway up in the section (21.8 m), is significantly more andesite-dominated (74.7%) with lesser dacite (15.9%) and rhyolite (9.4%).

Geochemistry as a means of determining dacite lithic provenance

Two of the most significant pre-caldera units, in terms of overall volume and lithic presence within the Otowi member, are the Paliza Canyon Formation and the Tschicoma Formation (Figure 4.2). Each of these units constitutes a significant quantity of the lithics that were entrained within the explosive Otowi eruption at 1.61 Ma. The Paliza Canyon Formation is composed of a diverse series of volcanic rocks ranging in composition from basalt to dacite although it consists mainly of andesite and dacite lavas. The Tschicoma Formation consists primarily of dacite domes, found in the north and east portion of the JMVF.

Because the Paliza Canyon and Tschicoma Formations are the major pre-Otowi rocks beneath the caldera, geochemical identification of either or both as accidental fragments at a sample locality may be used to corroborate conclusions derived from the lithic distribution data. Both the Paliza Canyon and Tschicoma Formation contain dacite in relative abundance, which provides an opportunity to chemically fingerprint unknown dacite lithics in the count data and to use them for determination of provenance. This information may also confirm the location of vents. Consequently, twenty-eight dacite lithics from two localities, Cat Mesa and Guaje Canyon, were analyzed by XRF (Table 4.2 and 4.3) for major and trace element geochemistry. These specific localities were chosen because they represent the two most noteworthy stratigraphic columns in the study, and they are widely separated on either side of the caldera.

The differences between the Paliza Canyon and Tschicoma dacites are subtle but are significant enough to allow for differentiation between the two. Geochemistry for the Paliza Canyon and Tschicoma lavas used for comparison with the unknown samples was taken from Rowe et al. (2007). The most significant difference is that some Paliza Canyon dacites are weakly alkaline, thereby plotting as trachydacite on the TAS diagram of Le Bas et al. (1986) seen in Figure 4.12. In contrast, Tschicoma dacite do not contain high enough concentrations of total alkalis to plot as trachydacite. Other differences occur with the major element oxide Na_2O and the incompatible trace elements Nb and Zr. With these elements, the Paliza Canyon lavas exhibit higher average concentrations and a much greater spread of data (Gardner, personal communication). In contrast, the Tschicoma lavas tend to delineate a tighter grouping of data, typically with lower concentrations than the majority, but not all, of the Paliza Canyon samples.

Unknown dacite lithics were plotted on the TAS diagram of Le Bas et al. (1986) in Figure 4.12 along with representative Paliza Canyon and Tschicoma analyses from Rowe et al.

(2007). As only Paliza Canyon lavas are trachydacite, the unknown dacite samples that plot as such have been automatically attributed to the Paliza Canyon Formation. This includes fourteen samples from the list of unknowns. For the remaining fourteen samples (five from Cat Mesa and eight from Guaje Canyon), the plots of Na_2O vs. SiO_2 , Nb vs. SiO_2 , and Zr vs. SiO_2 , all of which show recognizable variation between Paliza Canyon and Tschicoma dacite, were used to distinguish the unknowns. Incompatible trace element ratio plots of Ba/Nb vs. Nb and Rb/Th vs. Rb were used to assist further in determinations. Each unknown sample was individually plotted on these diagrams; the full set of plots can be seen in Appendix A. Additionally, in Figure 4.13 the unknown samples are shown plotted on diagrams of Na_2O vs. SiO_2 , Nb vs. SiO_2 , Zr vs. SiO_2 , and Ba/Nb vs. Nb for easy comparison.

Based on the individual sample diagrams in Appendix A and the summary plots in Figure 4.13, the fourteen non-trachydacite samples were identified. Those that showed a clear relationship to either formation on at least four of the six plots were ascribed to that formation. Three samples were equivocal and thus were not attributed to either formation. Distributions are shown in Table 4. Paliza Canyon dacite is more prevalent, comprising 15 of the twenty-eight analyzed samples. Of these fifteen samples, fourteen plotted as trachydacite, and a single sample was assigned after analyzing the aforementioned discriminatory plots. Ten samples were determined to be of Tschicoma origin, and three were equivocal.

The most significant overall finding of the data is that both pre-Otowi dacite lavas are found as accidental lithics in the Otowi ignimbrite at two widely-separated localities on opposite sides of the caldera. This provides important information for the location of eruptive vents, which will be discussed in the following sections. More importantly, it casts doubt on the

contention of Self et al. (1986) that the lag breccias at Cat Mesa are evidence for a local vent, since there is no local source of Tschicoma lithics.

Discussion

Lithic fragment distributions in the Otowi Member are remarkably similar at most locations around the caldera, despite the fact that there are variations in lithic signatures within the vertical sections from each location. The summary data in Figure 4.4 shows a striking similarity between lithic fragment signatures at most locations with the exception of Pueblo Mesa and Cebolla Canyon where rhyolite lithics are not observed. Guaje Canyon is different to some extent in that it has a greater abundance of rhyolite lithics than any other locality, and in addition, it has welded ignimbrite lithics as a noteworthy constituent.

Overall, andesite and dacite lithic fragments predominate at all localities around the caldera. This suggests that most of the localities share a common source for erupted material. Vertical variations may simply be representative of pyroclastic transport processes or varying paleotopography. Other than the welded ignimbrite lithic fragments at Guaje Canyon, there are few distinctive lithic signatures. Additionally, there are few noteworthy transitions in lithic distributions with stratigraphic height.

Previous researchers have proposed that the Otowi eruption emanated from an initial central vent that later shifted to multiple vents located around the periphery of the caldera. If this hypothesis is correct, we would expect to see unique lithic signatures representative of local sources. Based on the lithic distributions seen in Figure 4.4 this hypothesis is not well-supported. Figure 4.14 is a hypothetical diagram illustrating lithic distributions that would be expected if the ring-vent transition hypothesis is valid. Two key examples from the diagram demonstrate the lack of support for this hypothesis. First, an eruptive vent situated along the

eastern ring fracture would sample mostly Tschicoma dacite. Andesite would not be expected as a significant lithic lithology. In actuality, ignimbrites found east of the caldera at Guaje Canyon, the Airport section, and the Northeast section contain significant proportions of andesite lithics—a lithology not in abundance in the Tschicoma formation—in addition to dacite. Therefore, it is unlikely that a local vent was responsible for the deposits in that region.

Similarly, the southwest side of the caldera is underlain by dominantly Precambrian basement rocks and Paleozoic sedimentary rocks. A vent located in this region would be expected to sample significant quantities of Precambrian and Paleozoic rocks. Despite this, these lithologies are not dominant lithic fragment types in the ignimbrites at Wildcat Canyon, Cat Mesa, and Cebolla Canyon. Consequently, it is doubtful that a local vent was involved in the eruption of these units.

Overall, if the eruption shifted from a centrally-located vent to a series of ring vents, we would not expect to see such homogeneity in the lithic data as is observed in Figure 4.4. In fact, even when comparing individual vertical sections, significant similarities are still present. Specifically, rhyolite lithics appear and disappear at correlative points in stratigraphy around the caldera (Figures 4.6-4.11) and are coincident with similarly evolved Nb compositions at nearly all localities. It is unlikely that this similarity is coincidental, and it serves to link different sample localities in an eruptive sense.

The chemical data used to determine lithic provenance for dacite fragments also supports a centrally-located vent hypothesis for the majority of the duration of the eruption. Paliza Canyon Formation and Tschicoma Formation dacite lavas and domes are well constrained in terms of their position beneath the Valles Caldera. Determinations of dacite provenance were conducted for two widely spaced sample localities, at Cat Mesa in the southwest and Guaje

Canyon in the northeast. Even though there is no local source for both Paliza Canyon and Tschicoma dacites at each locality, both dacite types have been found at each locality. This questions the likelihood that a local vent source was responsible for the ignimbrites found at either locality. In fact, the only area in which both Paliza Canyon and Tschicoma dacite can be entrained simultaneously is located roughly in the east-central portion of the present-day caldera.

Finally, it is important to note that at some localities lithic data are correlative with chemical variations in the host deposits. Two significant examples of this are the near disappearance of rhyolite lithics where Nb drops below 180 ppm around the caldera and the dramatic change in pumice chemistry at the same height as the lag breccias at Cat Mesa. In the following chapter, Nb chemical variations in stratigraphy (determined from analyses of pumices) will be evaluated and compared to the lithic data from this chapter. The combination of the two datasets will be evaluated with a specific emphasis on implications for eruptive events. The ultimate goal is to delineate a detailed event sequence for the Otowi eruption in Chapter 6.

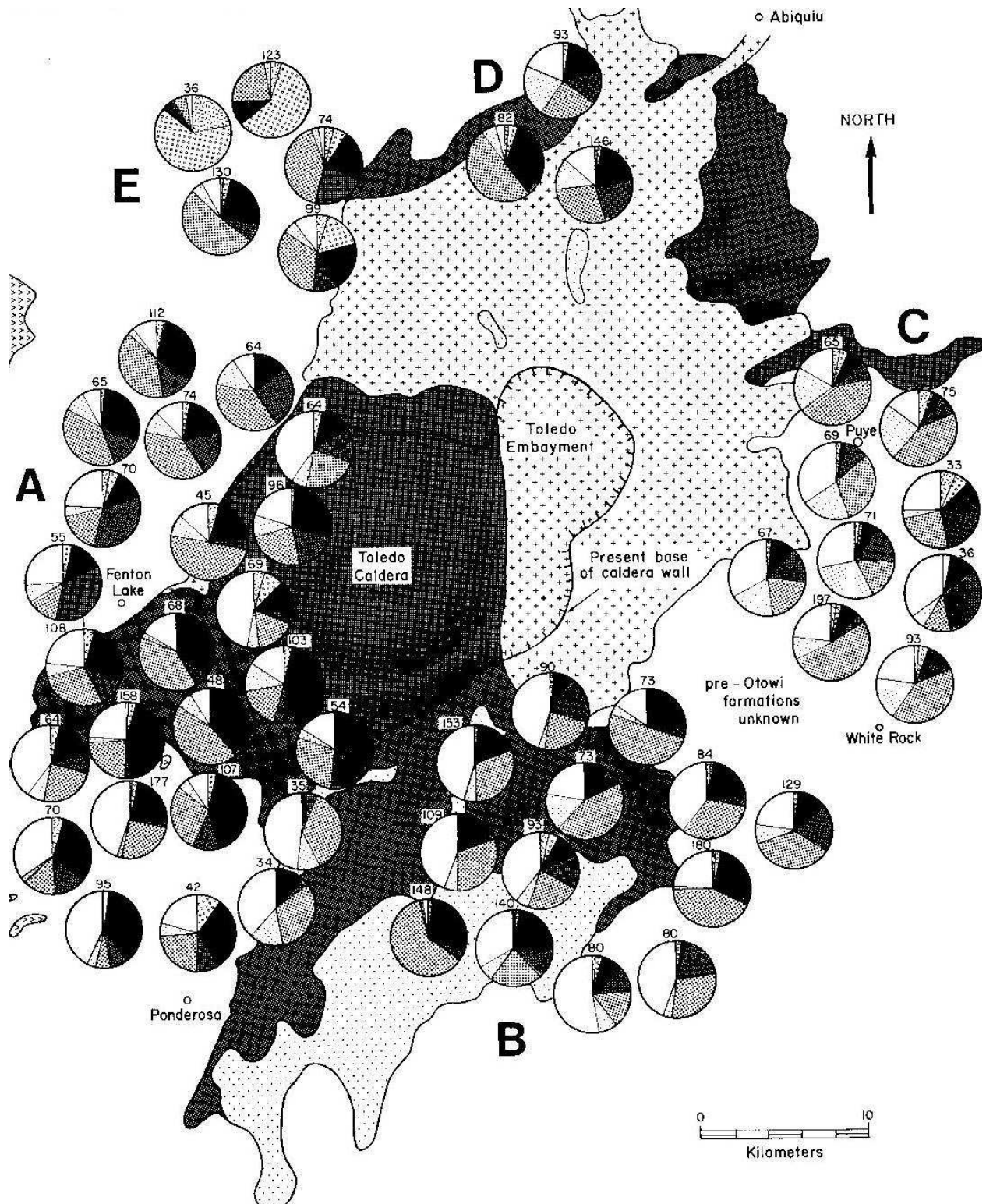


Figure 4.1. Map of Potter and Oberthal (1987) showing lithic distributions and abundances, including the regional breakdown (areas A-E) utilized.

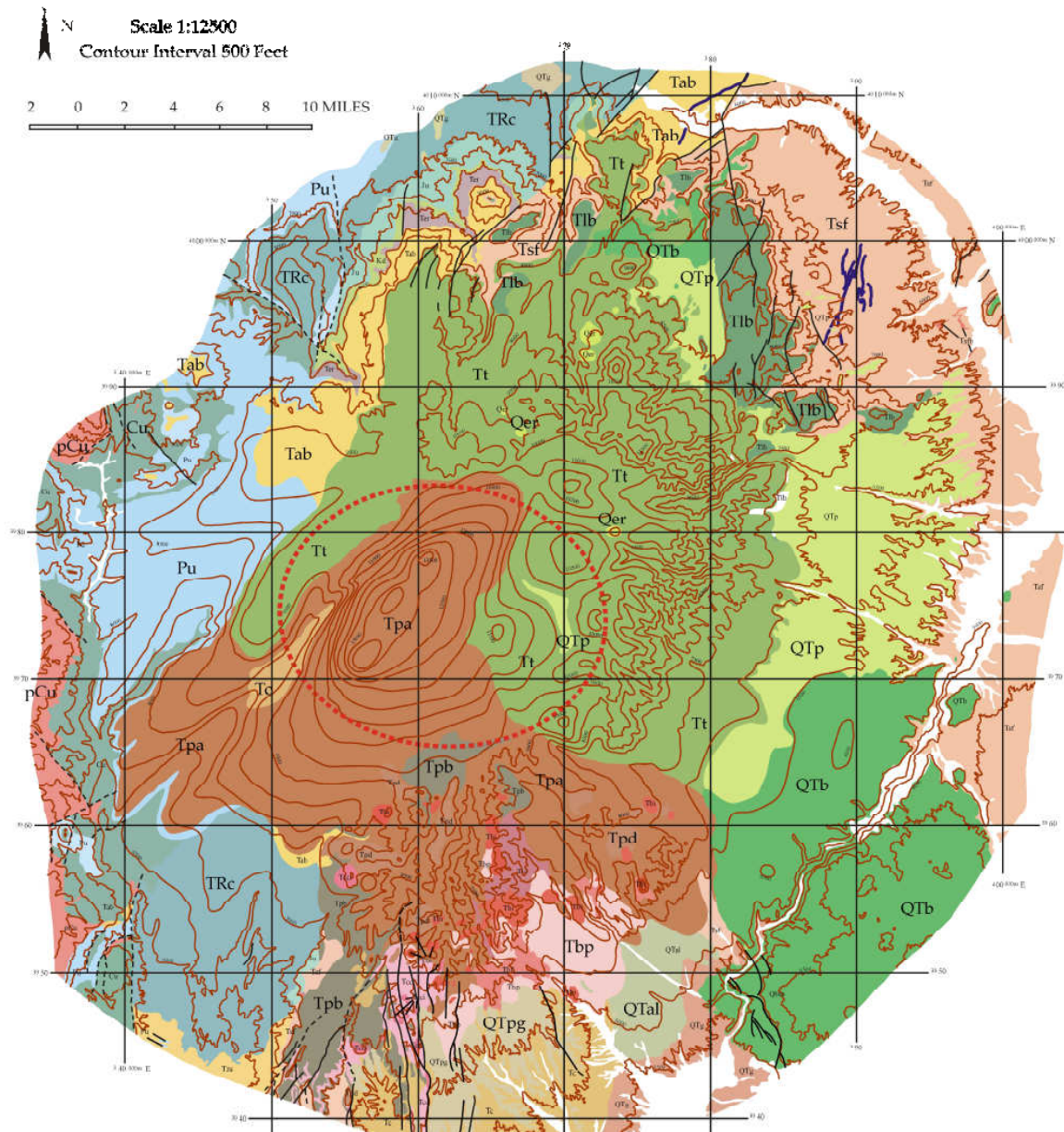
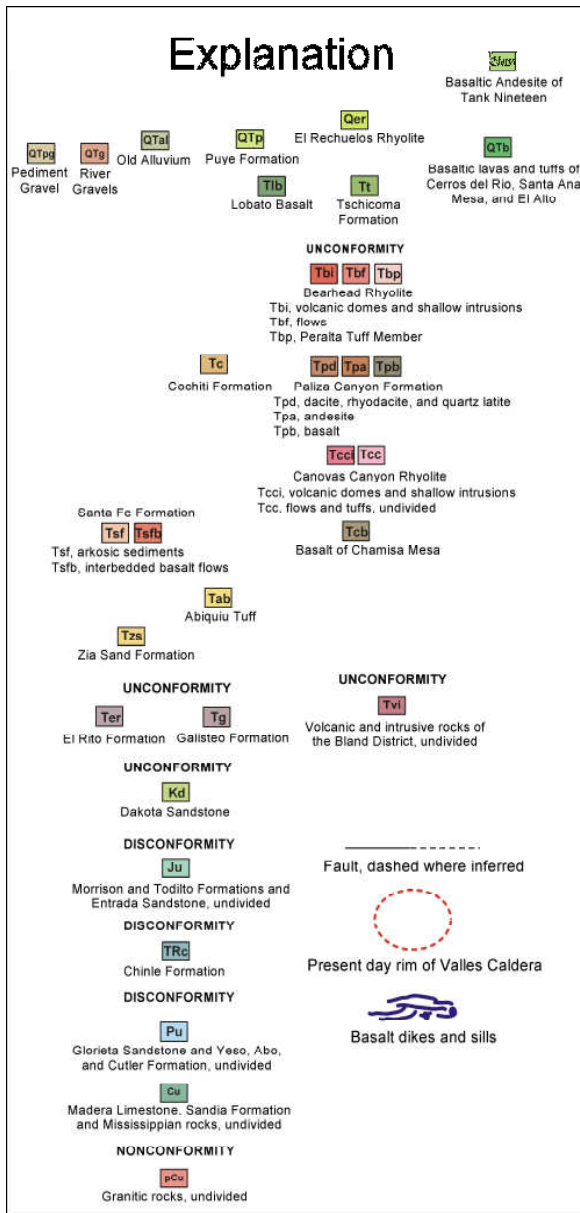


Figure 4.2. Map of the pre-Otowi geology

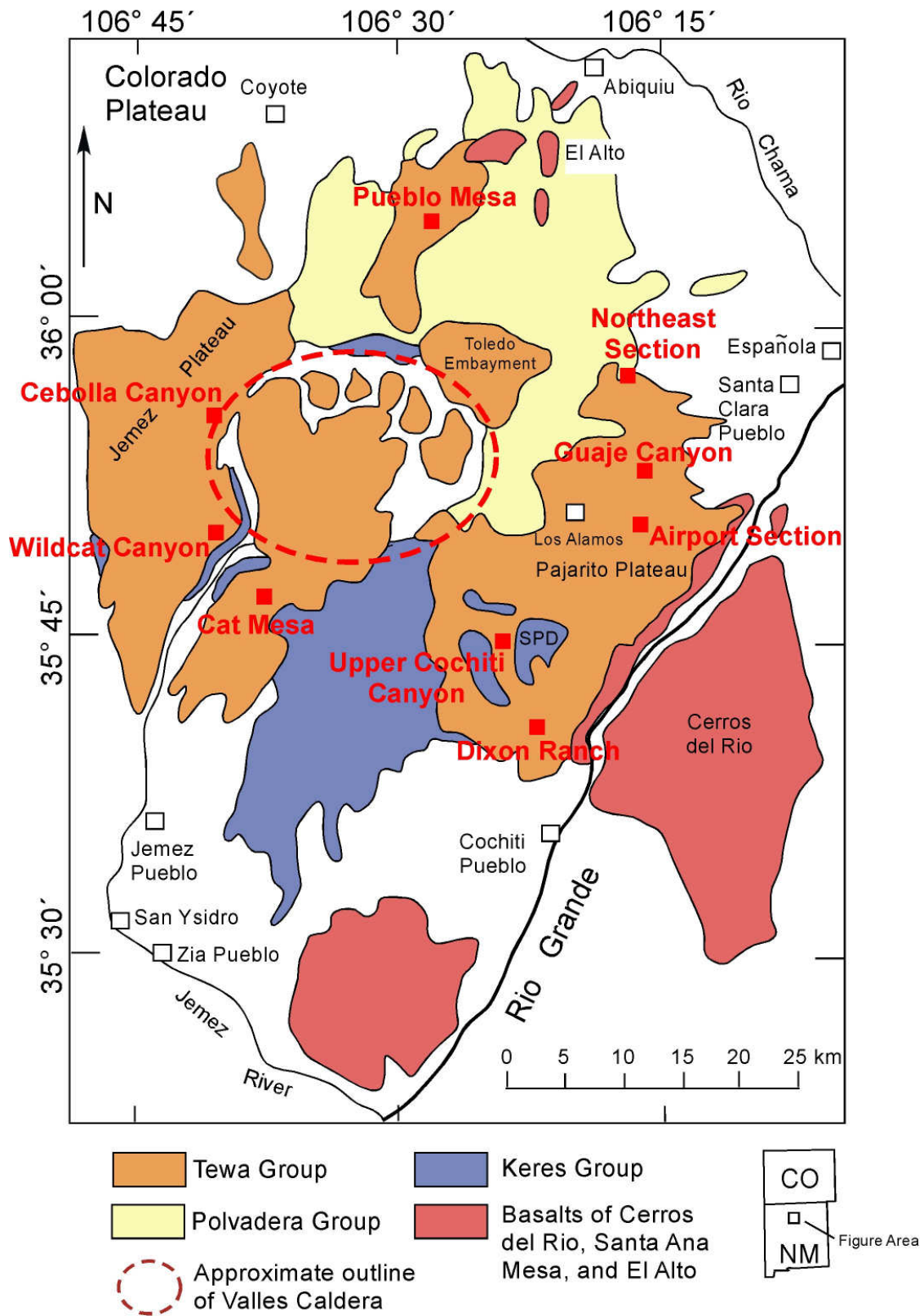


Figure 4.3. Map showing locations used for sample collection across the JMVF.

Table 4.1. Lithic count data summarized by sample locality

Guaje Canyon

<u>Sample</u>	<u>Dacite</u>	<u>Andesite</u>	<u>Tuff</u>	<u>Rhyolite</u>	<u>Other</u>	<u>Total</u>	<u>Andesite/Dacite</u>
JMVF-00-01	2	14	0	0	0	16	7.0
JMVF-00-02	14	24	0	3	1	42	1.7
JMVF-00-03	17	22	0	23	0	62	1.3
JMVF-00-04	10	15	0	0	0	25	1.5
JMVF-00-05	5	16	0	3	1	25	3.2
JMVF-00-08	15	12	1	2	0	30	0.8
JMVF-00-09	7	10	18	0	2	37	1.4
JMVF-00-10	16	14	56	0	1	87	0.9
JMVF-00-175	1	11	0	2	2	16	11.0
JMVF-00-176	86	39	0	19	3	147	0.5
JMVF-00-177	45	47	0	101	0	193	1.0
JMVF-00-178	10	52	0	4	1	67	5.2
JMVF-00-180	2	7	0	0	0	9	3.5
JMVF-00-183	6	14	0	0	0	20	2.3
Total Counts	236	297	75	157	11	776	
% Overall	30.4	38.3	9.7	20.2	1.4		

Northeast #1 Section

<u>Sample</u>	<u>Dacite</u>	<u>Andesite</u>	<u>Tuff</u>	<u>Rhyolite</u>	<u>Other</u>	<u>Total</u>	<u>Andesite/Dacite</u>
JMVF-00-108	98	67	0	9	0	174	0.7
Total	98	67	0	9	0	174	
%	56.3	38.5	0.0	5.2	0.0		

Pueblo Mesa

<u>Sample</u>	<u>Dacite</u>	<u>Andesite</u>	<u>Tuff</u>	<u>Rhyolite</u>	<u>Other</u>	<u>Total</u>	<u>Andesite/Dacite</u>
JMVF-00-215	43	53	0	0	0	96	1.2
JMVF-00-218	26	54	0	1	2	83	2.1
JMVF-00-219	15	32	0	0	4	51	2.1
JMVF-00-222	4	67	0	0	0	71	16.8
Total	88	206	0	1	6	301	
%	29.2	68.4	0.0	0.3	2.0		

Cebolla Canyon

<u>Sample</u>	<u>Dacite</u>	<u>Andesite</u>	<u>Tuff</u>	<u>Rhyolite</u>	<u>Other</u>	<u>Total</u>	<u>Andesite/Dacite</u>
JMVF-00-191	58	6	0	0	1	65	0.1
Total	58	6	0	0	1	65	
%	89.2	9.2	0.0	0.0	1.5		

Cat Mesa

<u>Sample</u>	<u>Dacite</u>	<u>Andesite</u>	<u>Tuff</u>	<u>Rhyolite</u>	<u>Other</u>	<u>Total</u>	<u>Andesite/Dacite</u>
JMVF-00-42	45	53	11	0	0	109	1.2
JMVF-00-45	105	137	18	13	5	278	1.3
JMVF-00-51	198	227	0	61	1	487	1.1
JMVF-00-55	336	183	28	73	5	625	0.5
JMVF-00-57	387	298	3	18	4	710	0.8
JMVF-00-60	488	354	8	14	12	876	0.7
JMVF-00-64	767	276	3	45	1	1092	0.4
JMVF-00-66	554	602	14	69	43	1282	1.1
JMVF-00-69	254	270	5	15	8	552	1.1
JMVF-00-83	642	296	21	0	4	963	0.5
JMVF-00-85	395	230	20	31	2	678	0.6
JMVF-00-88	353	841	1	20	6	1221	2.4
JMVF-00-90	148	149	13	0	1	311	1.0
Total	4672	3916	145	359	92	9184	
%	50.9	42.6	1.6	3.9	1.0		

Airport Section

<u>Sample</u>	<u>Dacite</u>	<u>Andesite</u>	<u>Tuff</u>	<u>Rhyolite</u>	<u>Other</u>	<u>Total</u>	<u>Andesite/Dacite</u>
JMVF-00-70	267	104	0	59	0	430	0.4
JMVF-00-74	49	230	0	28	1	308	4.7
Total	316	334	0	87	1	738	
%	42.8	45.3	0.0	11.8	0.1		

Wildcat Canyon

<u>Sample</u>	<u>Dacite</u>	<u>Andesite</u>	<u>Tuff</u>	<u>Rhyolite</u>	<u>Other</u>	<u>Total</u>	<u>Andesite/Dacite</u>
JMVF-00-135	10	18	0	0	0	28	1.8
JMVF-00-149	381	212	1	4	1	599	0.6
JMVF-00-150	385	383	3	32	3	806	1.0
JMVF-00-154	137	159	0	10	2	308	1.2
JMVF-00-156	88	187	0	4	0	279	2.1
JMVF-00-159	543	349	0	1	5	898	0.6
JMVF-00-161	57	132	0	5	0	194	2.3
JMVF-00-171	29	15	0	0	9	53	0.5
Total	1630	1455	4	56	20	3165	
%	51.5	46.0	0.1	1.8	0.6		

Dixon Ranch

<u>Sample</u>	<u>Dacite</u>	<u>Andesite</u>	<u>Tuff</u>	<u>Rhyolite</u>	<u>Other</u>	<u>Total</u>	<u>Andesite/Dacite</u>
JMVF-00-31	94	54	14	29	2	193	0.6
JMVF-00-33	34	42	11	19	1	107	1.2
JMVF-00-40	120	100	0	3	2	225	0.8
Total	248	196	25	51	5	525	
%	47.2	37.3	4.8	9.7	1.0		

Upper Cochiti Canyon

<u>Sample Name</u>	<u>Dacite</u>	<u>Andesite</u>	<u>Tuff</u>	<u>Rhyolite</u>	<u>Other</u>	<u>Total</u>	<u>Andesite/Dacite</u>
JMVF-00-196	353	330	0	4	3	690	0.9
JMVF-00-198	145	196	0	1	1	343	1.4
JMVF-00-199	148	259	0	7	0	414	1.8
JMVF-00-200	282	208	0	33	0	523	0.7
JMVF-00-204	114	89	0	50	5	258	0.8
Total	1042	1082	0	95	9	2228	
%	46.8	48.6	0.0	4.3	0.4		

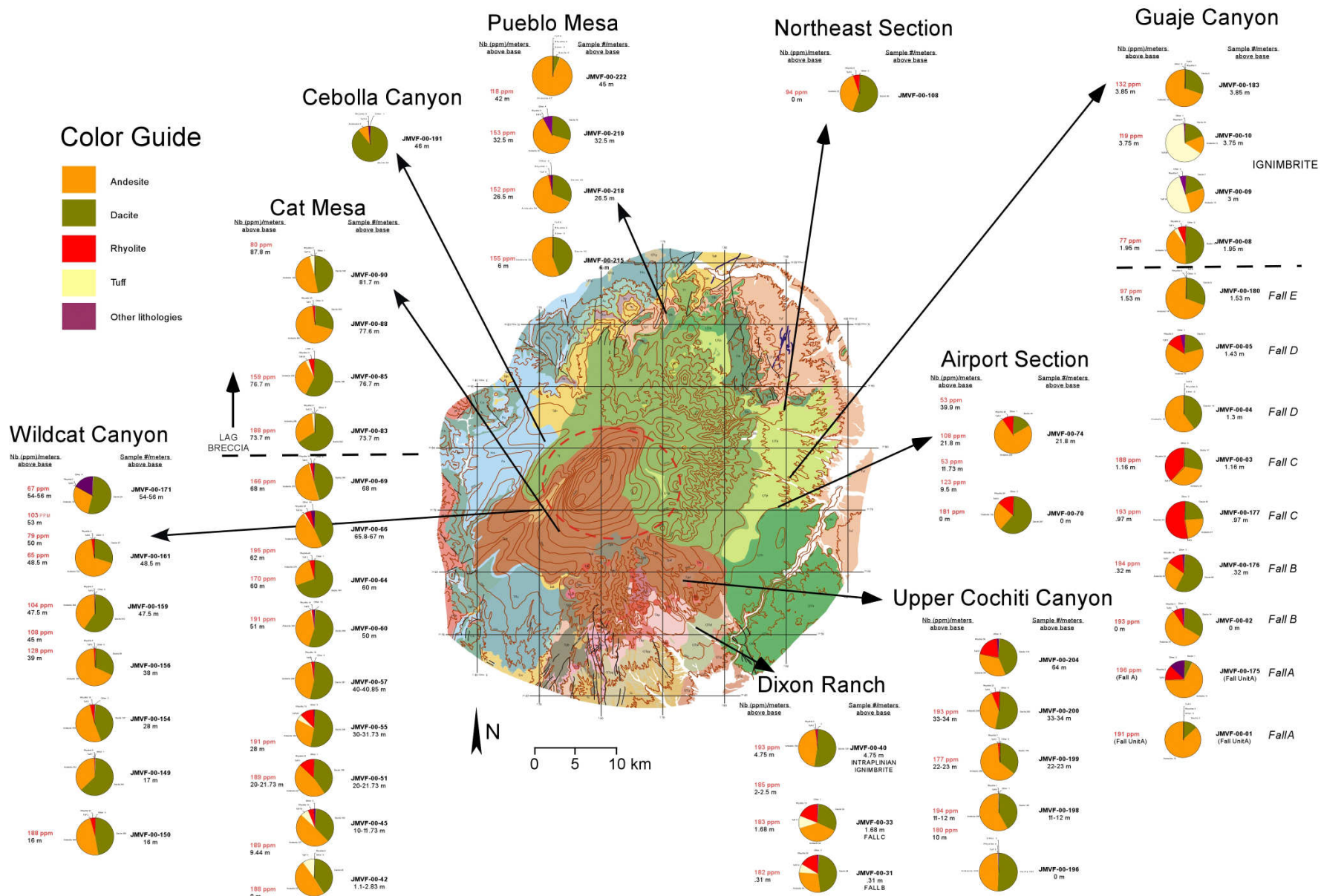


Figure 4.4. Distributions of lithics on pre-caldera geologic map

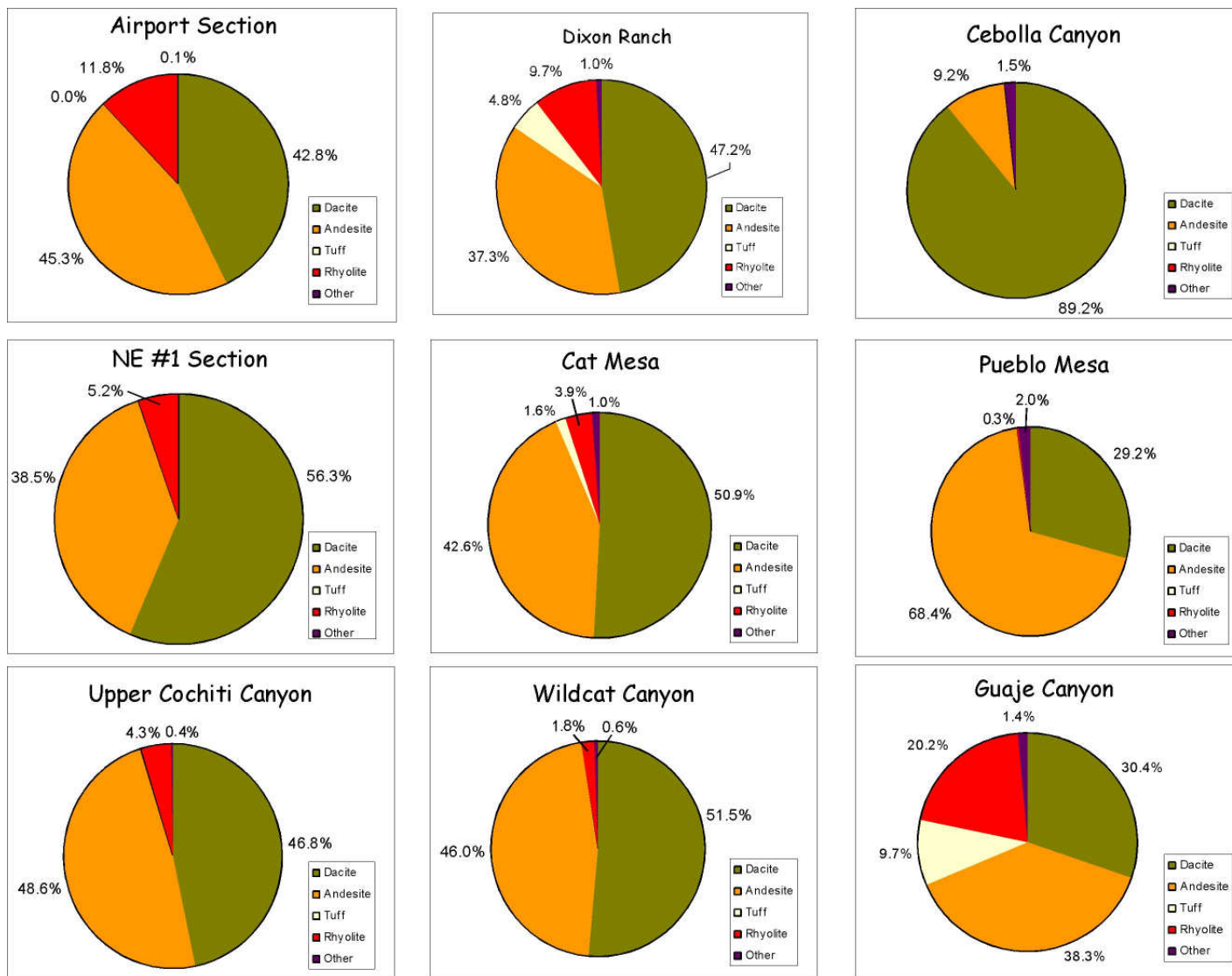


Figure 4.5. Pie charts showing overall lithic fragment proportions at each sample locality. Sample collection locations can be seen in Figures 2 + 3

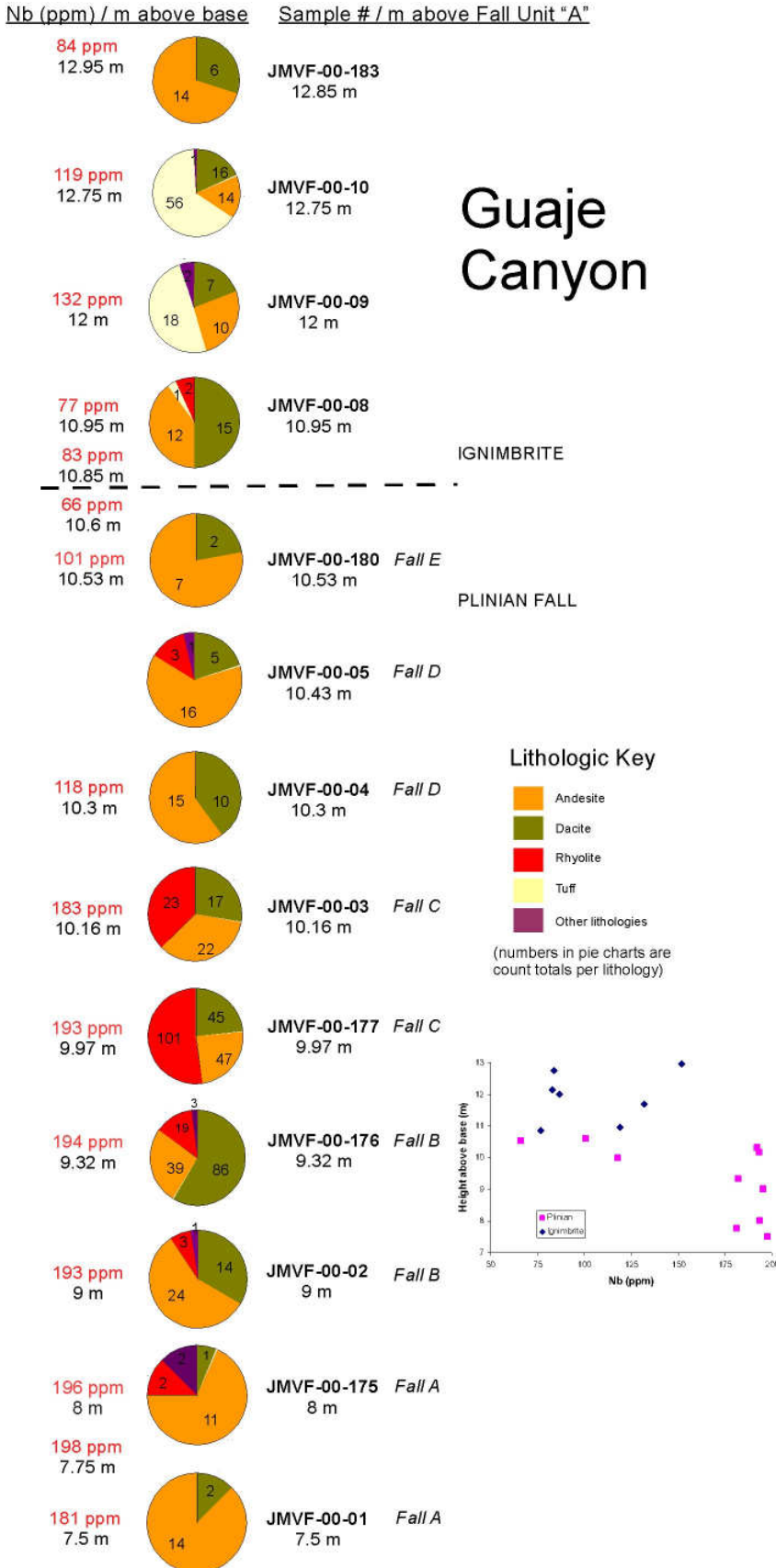
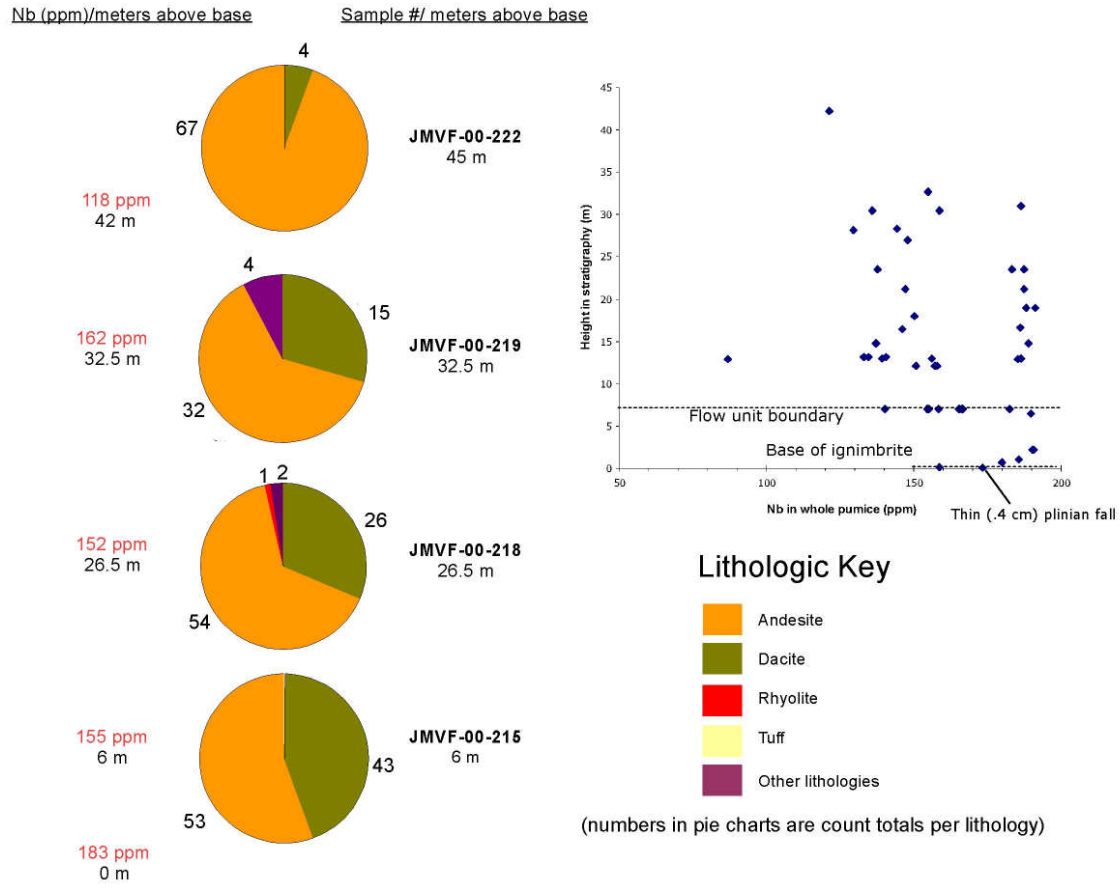
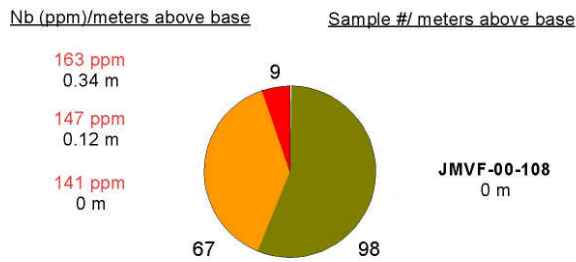


Figure 4.6. Stratigraphic column for Guaje Canyon showing lithic abundances and Nb data.

Pueblo Mesa



Northeast Section



Cebolla Canyon

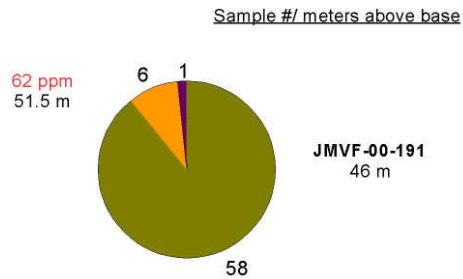


Figure 4.7. Stratigraphic column for three localities (Pueblo Mesa, Northeast Section, Cebolla Canyon) showing lithic abundances and Nb data.

Nb (ppm)/ m above base Sample #/ m above base

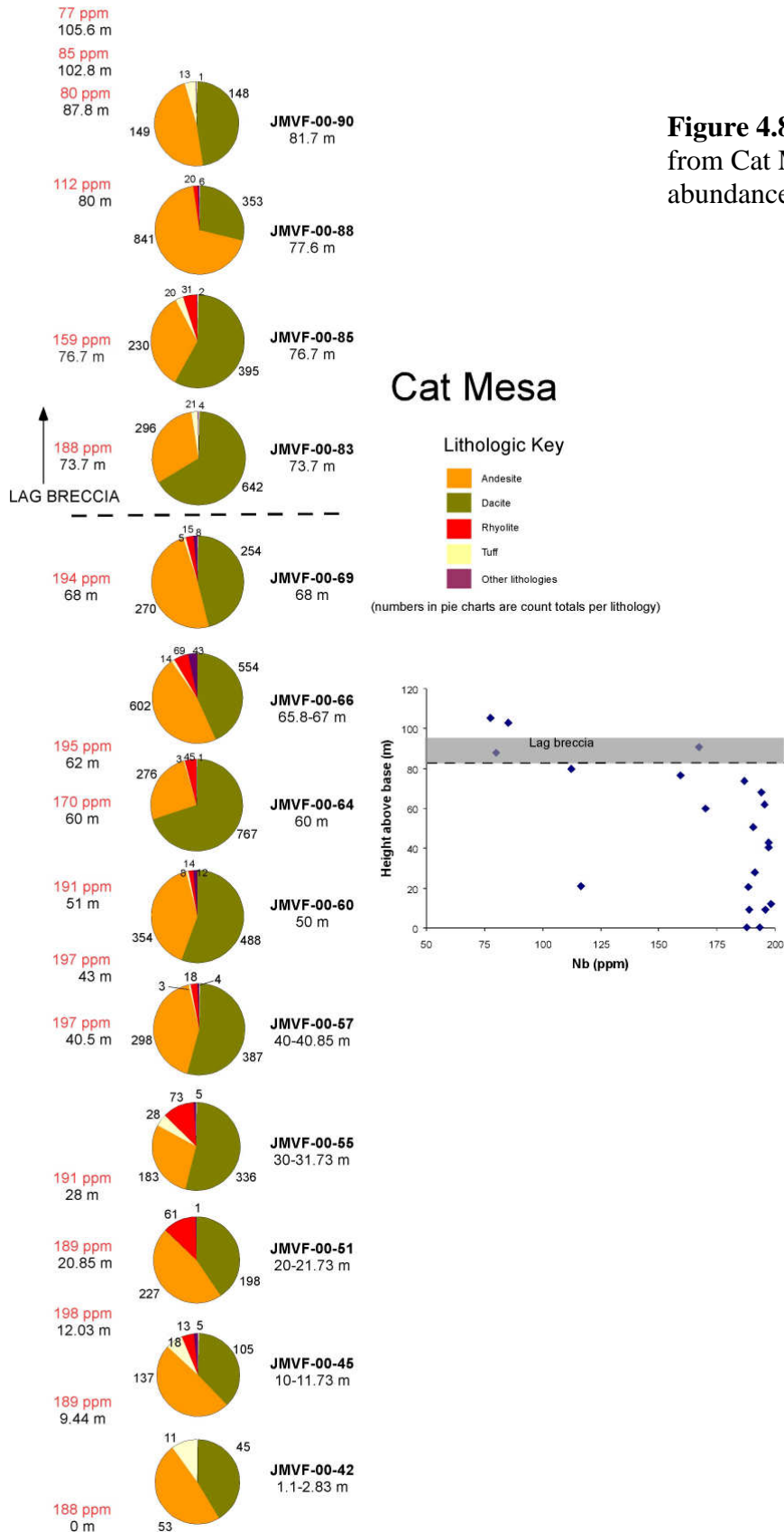


Figure 4.8. Stratigraphic column from Cat Mesa showing lithic abundances and Nb data.

Wildcat Canyon

Nb (ppm)/meters above base Sample #/ meters above base

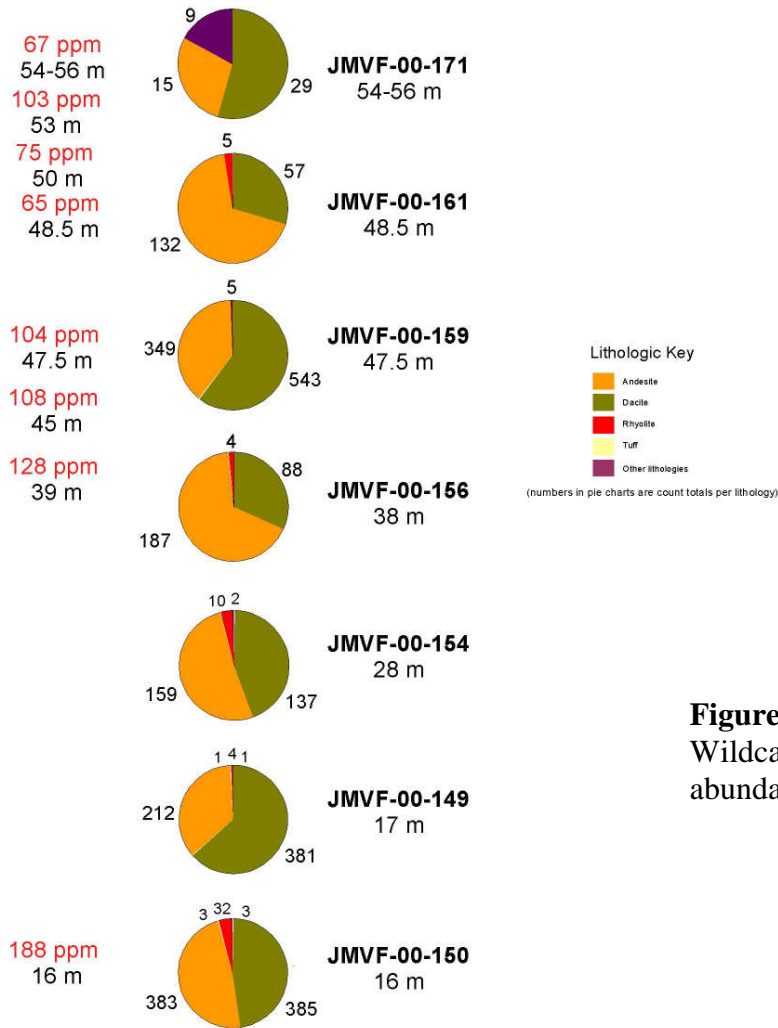
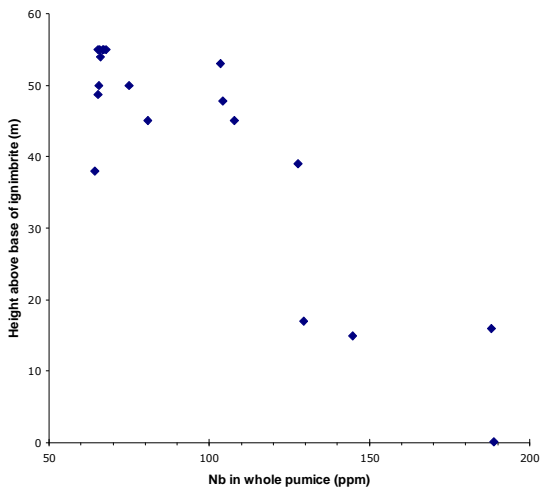
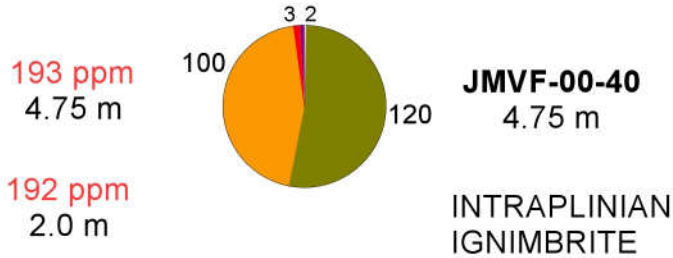


Figure 4.9. Stratigraphic column for Wildcat Canyon showing lithic abundances and Nb data.



Dixon Ranch

Nb (ppm)/meters above base Sample #/ meters above base



Lithologic Key



(numbers in pie charts are count totals per lithology)

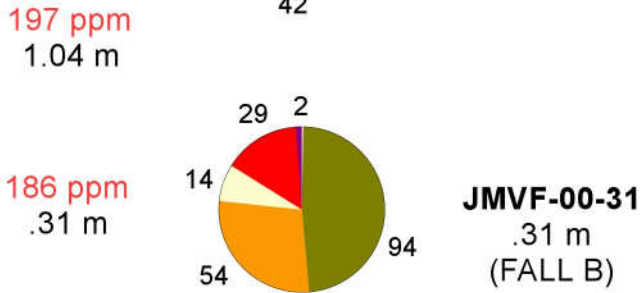
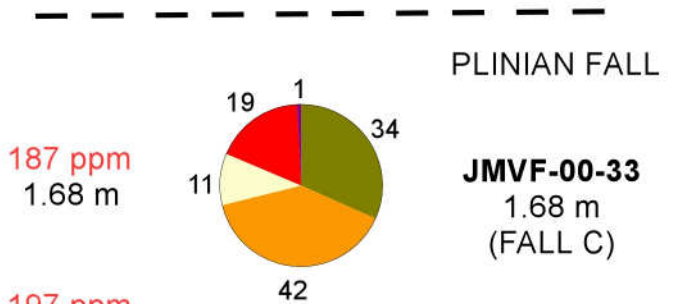
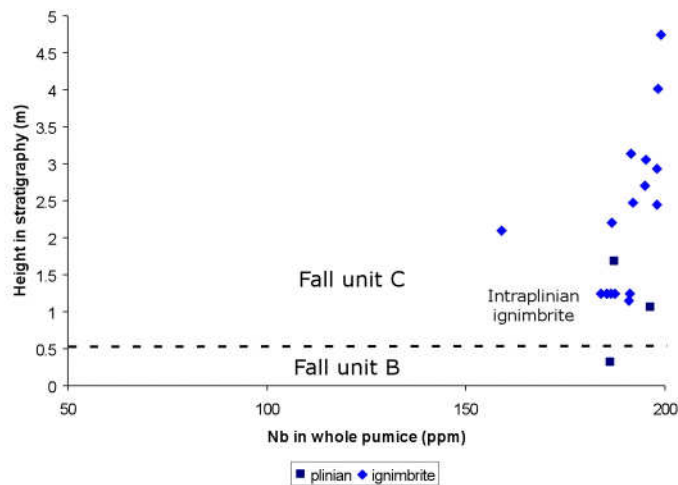
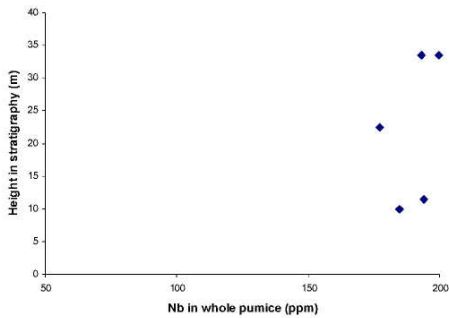
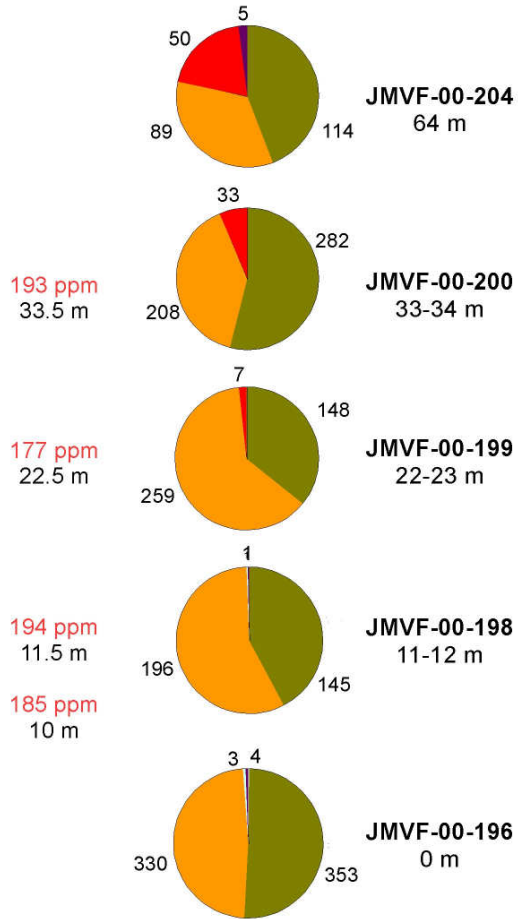


Figure 4.10. Stratigraphic column for Dixon Ranch showing lithic abundances and Nb data.



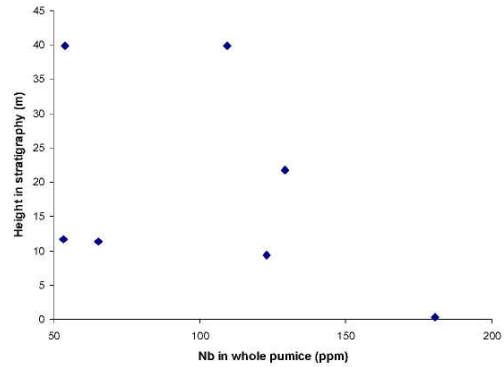
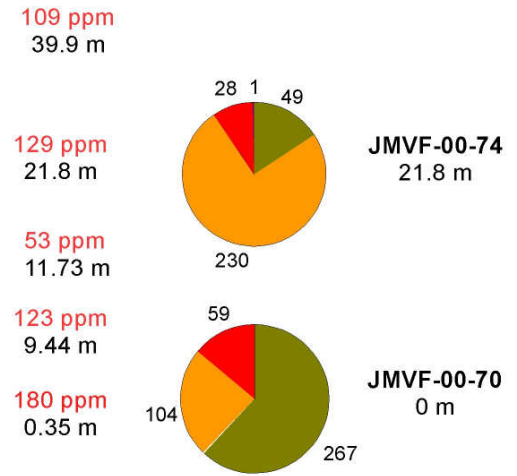
Upper Cochiti Canyon

Nb (ppm)/ m above base Sample #/ m above base



Airport Section

Nb (ppm)/ m above base Sample #/ m above base



Lithologic Key



(numbers in pie charts are count totals per lithology)

Figure 4.11. Stratigraphic columns for Upper Cochiti Canyon and the Airport section showing lithic abundances and Nb data.

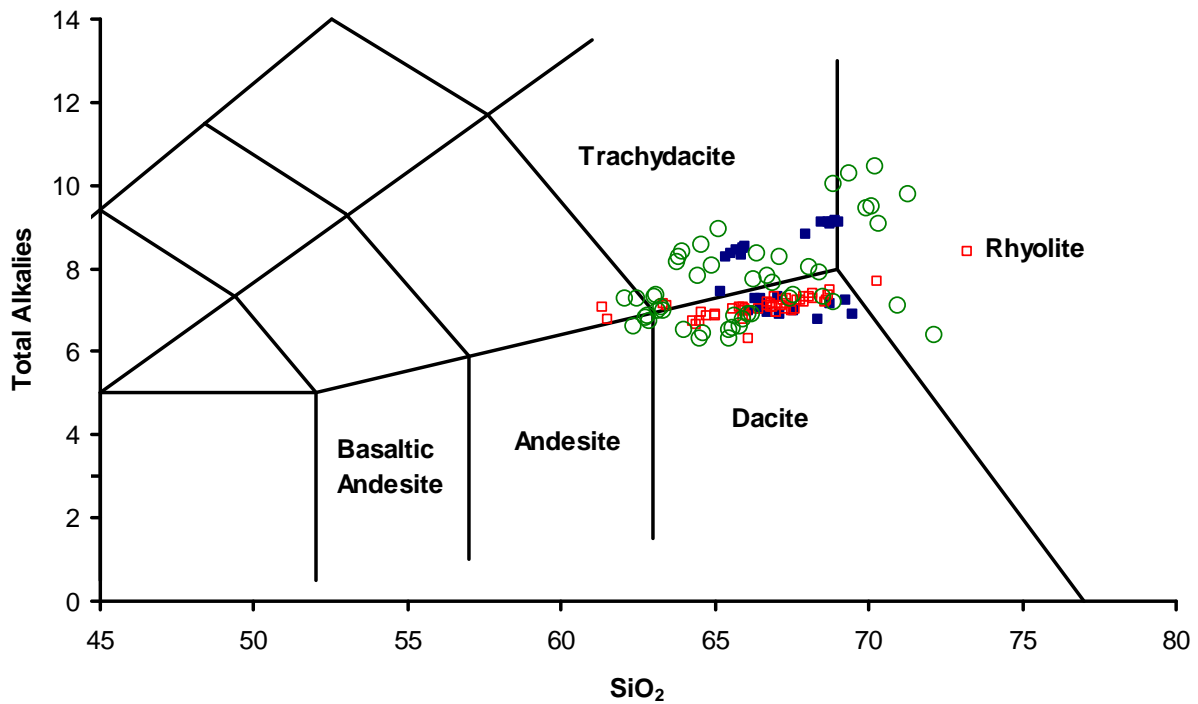


Figure 4.12. TAS diagram of Le Bas et al. (1986) showing unknown dacite lithic chemistry (dark blue squares) compared with analyses of Paliza Canyon (open green circles) and Tschicoma Formation lavas (open red squares). Note that some unknown lithic samples plot as trachydacite. These samples have been automatically assigned to the Paliza Canyon Formation specifically because trachydacite is not typically found in the Tschicoma lavas.

Sample	SiO₂	TiO₂	Al₂O₃	FeO*	MnO	MgO	CaO	Na₂O	K₂O	P₂O₅	TAS
CM 55-D1	68.72	0.638	15.76	2.82	0.075	0.78	1.97	5.10	3.95	0.174	9.050
CM 55-D2	65.87	0.821	16.22	4.04	0.104	1.27	3.03	4.88	3.46	0.318	8.335
CM 57-D1	65.91	0.807	16.25	4.03	0.086	1.16	2.95	4.95	3.56	0.305	8.503
CM 57-D2	66.46	0.710	15.77	4.06	0.063	1.68	3.72	4.13	3.15	0.249	7.274
CM 57-D3	65.50	0.827	16.37	4.21	0.083	1.08	3.26	4.90	3.45	0.326	8.345
CM 57-D4	65.97	0.833	16.34	4.09	0.078	1.00	2.83	4.97	3.56	0.320	8.535
CM 60-D1	67.93	0.646	16.25	3.03	0.083	0.80	2.25	5.12	3.72	0.176	8.833
CM 60-D2	68.49	0.608	16.32	2.65	0.065	0.44	2.15	5.18	3.92	0.175	9.097
CM 60-D3	69.46	0.787	16.12	3.70	0.065	0.49	2.16	3.33	3.55	0.336	6.887
CM 60-D4	68.71	0.607	15.98	2.80	0.072	0.57	1.96	5.18	3.94	0.172	9.122
CM 60-D5	66.09	0.798	17.40	3.51	0.063	0.83	4.03	4.46	2.53	0.286	6.993
CM 83-D1	67.08	0.771	16.89	3.61	0.030	0.48	3.55	4.47	2.85	0.282	7.316
CM 83-D2	65.38	0.812	16.39	4.23	0.090	1.17	3.36	4.88	3.39	0.308	8.263
CM 83-D4	65.68	0.810	16.36	4.09	0.084	1.16	3.09	4.97	3.45	0.314	8.421
CM 90-D1	68.93	0.616	16.07	2.75	0.052	0.42	1.86	5.53	3.62	0.156	9.144
CM 90-D2	66.49	0.705	15.78	4.10	0.067	1.72	3.86	4.34	2.67	0.267	7.012
CM 90-D3	65.16	0.771	16.61	4.61	0.068	1.47	3.60	4.58	2.85	0.278	7.426
G 04-D1	65.84	0.863	15.95	4.31	0.088	1.39	2.85	4.82	3.59	0.308	8.411
G 09-D1	68.36	0.471	15.47	3.39	0.062	1.76	3.53	4.13	2.66	0.175	6.789
G 09-D2	68.72	0.446	15.39	3.27	0.054	1.46	3.34	3.93	3.22	0.164	7.152
G 176-D1	69.04	0.625	15.73	2.63	0.080	0.75	1.88	5.10	4.00	0.177	9.097
G 183-D1	67.13	0.587	15.77	3.59	0.065	1.82	3.91	4.08	2.81	0.230	6.889
G 10-D1	66.73	0.534	16.31	3.43	0.065	1.68	4.09	4.23	2.69	0.247	6.917
G 10-D2	67.54	0.495	15.99	3.22	0.045	1.73	3.80	4.10	2.87	0.198	6.971
G 10-D3	66.31	0.665	15.95	3.86	0.069	1.70	3.92	4.18	3.10	0.241	7.281
G 10-D4	66.52	0.820	17.19	3.96	0.044	0.65	3.44	4.23	2.84	0.300	7.076
G 10-D5	69.25	0.448	15.07	3.07	0.056	1.53	3.18	3.88	3.35	0.163	7.234
G 10-D6	68.81	0.621	15.75	2.73	0.083	0.77	1.96	5.14	3.95	0.172	9.092

Table 4.2. XRF major element oxide geochemical data for unknown dacites. All data in wt %.

Sample	Ni	Cr	Sc	V	Ba	Rb	Sr	Zr	Y	Nb	Ga	Cu	Zn	Pb	La	Ce	Th	Nd
CM 55-D1	5	2	5	23	1353	76	317	307	30	40.2	18	2	55	19	54	98	13	40
CM 55-D2	11	3	5	47	1335	68	479	299	27	41.4	20	7	64	19	54	96	12	41
CM 57-D1	3	4	6	47	1322	71	471	319	25	40.2	18	3	64	15	55	91	10	36
CM 57-D2	18	26	8	66	1266	58	500	197	17	18.3	17	7	56	16	39	69	5	29
CM 57-D3	6	6	7	50	1304	67	515	307	25	37.7	21	6	64	17	53	92	10	37
CM 57-D4	5	3	5	48	1314	70	466	321	25	40.3	19	6	68	42	57	101	11	39
CM 60-D1	2	3	5	22	1375	76	383	305	29	40.1	19	2	63	20	55	99	9	39
CM 60-D2	2	4	5	24	1344	79	377	302	28	41.1	19	5	67	22	53	98	11	37
CM 60-D3	4	4	6	45	1326	76	426	291	49	42.1	19	7	46	25	48	94	10	35
CM 60-D4	2	3	5	21	1360	80	326	306	29	40.5	19	5	55	28	56	100	21	39
CM 60-D5	1	2	7	55	1405	57	716	186	22	18.9	19	6	58	31	40	79	7	32
CM 83-D1	1	2	7	48	1338	50	656	191	21	18.2	18	9	63	30	39	69	8	28
CM 83-D2	6	4	6	51	1296	65	519	305	24	37.3	20	9	78	19	52	93	8	36
CM 83-D4	2	3	7	47	1305	65	502	315	25	39.0	19	8	70	26	54	94	10	37
CM 90-D1	7	4	4	21	1357	64	325	296	26	38.8	18	3	60	91	55	95	22	40
CM 90-D2	27	21	9	81	1207	55	689	176	19	18.4	16	16	42	30	37	66	17	26
CM 90-D3	17	15	9	91	1209	63	828	206	19	23.9	19	16	59	27	40	74	7	28
G 04-D1	9	8	6	53	1317	68	439	320	27	41.0	20	9	63	23	54	88	21	36
G 09-D1	23	37	8	51	1250	61	459	172	17	11.1	18	10	57	18	37	63	4	25
G 09-D2	20	33	8	49	1266	62	448	168	16	11.9	19	16	55	21	34	57	5	22
G 176-D1	5	5	5	21	1354	73	277	293	29	37.8	21	4	59	24	58	101	27	41
G 183-D1	19	20	7	67	1291	47	608	142	17	14.6	18	10	57	26	37	62	7	27
G 10-D1	20	21	7	56	1328	33	659	131	16	14.8	19	10	53	23	36	55	7	23
G 10-D2	22	29	7	50	1249	46	615	139	15	12.8	20	17	44	15	32	55	6	20
G 10-D3	16	20	7	66	1242	56	518	187	18	16.1	19	15	60	17	39	68	6	28
G 10-D4	1	3	9	47	1321	55	649	191	25	19.5	19	7	59	24	47	76	17	33
G 10-D5	24	32	7	48	1302	63	400	167	17	11.1	18	9	52	24	32	66	19	28
G 10-D6	2	2	6	17	1382	73	317	307	27	39.3	18	3	56	19	53	99	11	37

Table 4.3. XRF trace-element geochemical data for unknown dacites. All data in ppm.

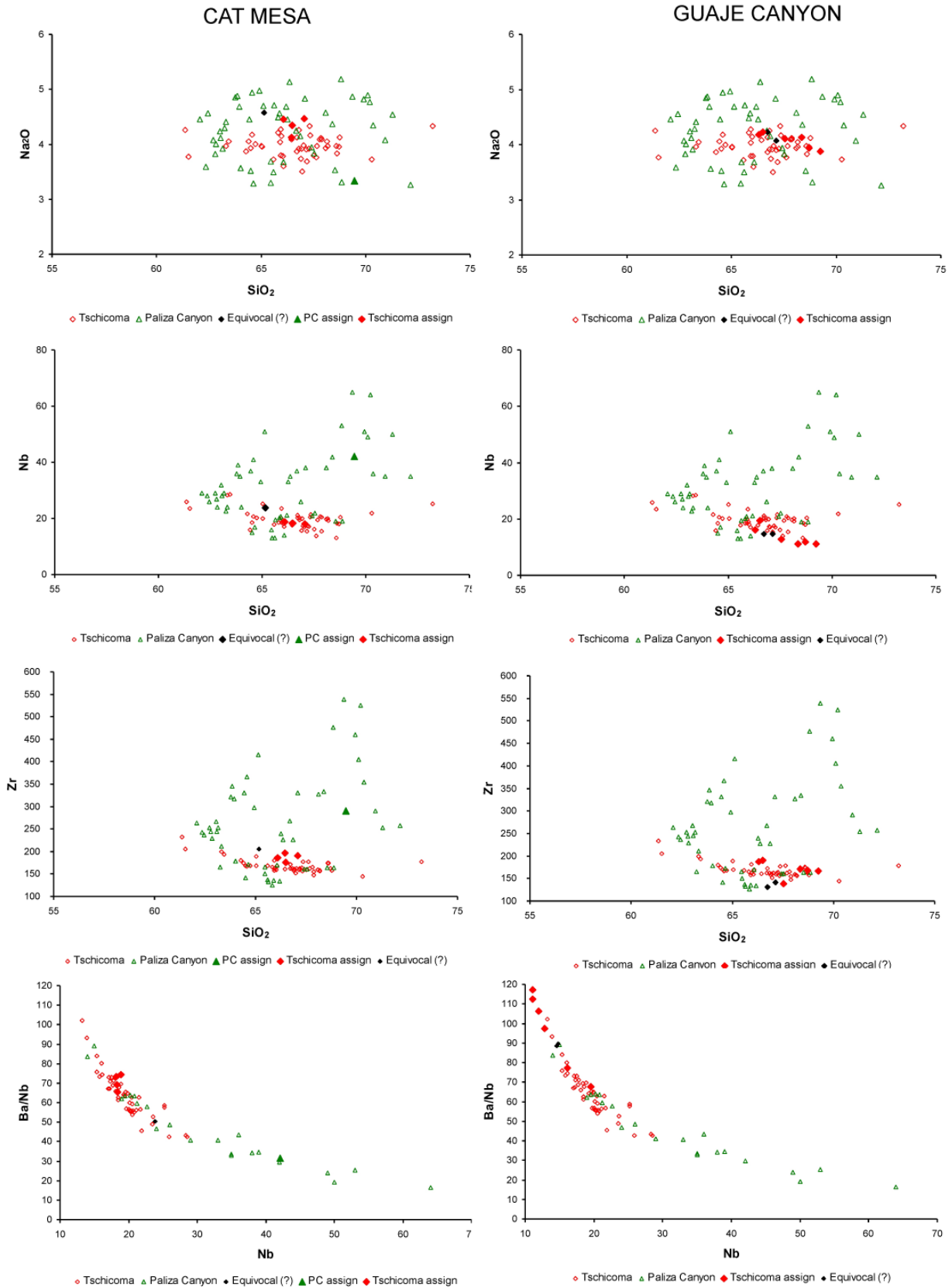


Figure 4.13. Selected geochemical data used in determining dacite lithic provenance.

CAT MESA

CM 90-D3	? (equivocal)
CM 90-D2	Tschicoma
CM 90-D1	PC (Trachydacite)
CM 83-D4	PC (Trachydacite)
CM 83-D2	PC (Trachydacite)
CM 83-D1	Tschicoma
CM 60-D5	Tschicoma
CM 60-D4	PC (Trachydacite)
CM 60-D3	PC
CM 60-D2	PC (Trachydacite)
CM 60-D1	PC (Trachydacite)
CM 57-D4	PC (Trachydacite)
CM 57-D3	PC (Trachydacite)
CM 57-D2	Tschicoma
CM 57-D1	PC (Trachydacite)
CM 55-D2	PC (Trachydacite)
CM 55-D1	PC (Trachydacite)

} Lag Breccia

GUAJE CANYON

G 183-D1	? (possibly Tschicoma)
G 10-D6	PC (Trachydacite)
G 10-D5	Tschicoma
G 10-D4	Tschicoma
G 10-D3	Tschicoma
G 10-D2	Tschicoma
G 10-D1	? (equivocal)
G 09-D2	Tschicoma
G 09-D1	Tschicoma
G 04-D1	PC (Trachydacite)
G 176-D1	PC (Trachydacite)

Table 4.4. Distribution of unknown dacite samples per sample locality. Samples are organized according to stratigraphic order at each locality. The lag breccia at Cat Mesa is represented by three samples: CM 83-D1, CM-83-D2, and CM-83-D4. Paliza Canyon samples are highlighted in red, Tschicoma samples are highlighted in black, and equivocal samples are highlighted in blue. Identifications were accomplished using the TAS diagram in Figure 4.12, and by plotting individual samples on the geochemical plots seen in Appendix A.

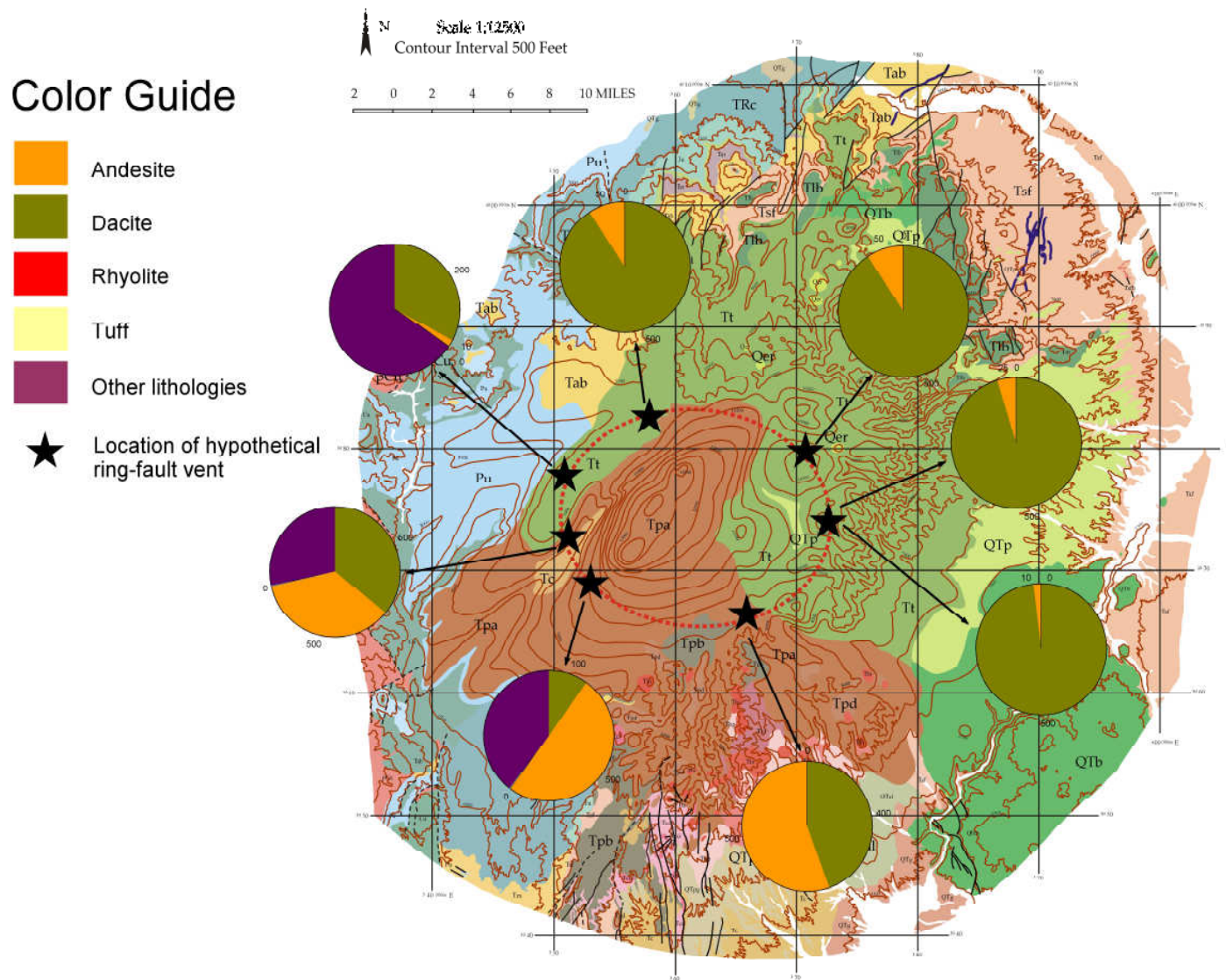


Figure 4.14. Expected lithic distributions based on the hypothesis that the Otowi eruption transitioned from a central vent to multiple ring-vents during the course of the eruption.

CHAPTER FIVE

CORRELATION OF LITHIC DISTRIBUTIONS AND NB CONCENTRATIONS

Purpose

In this chapter, chemical variations in pumices from the Otowi plinian and ignimbrite deposits are evaluated and compared with lithic data obtained in Chapter 4. In addition, chemical data have been used in conjunction with volume calculations from Chapter 3 to calculate approximate abundances of chemical types in the Otowi Member. This type of calculation has not been previously attempted for the Otowi Member. The cumulative goal of this exercise (found in Chapter 6) is to delineate a detailed event stratigraphy for the Otowi eruption based on the lithic and chemical data.

Smith and Bailey (1966) were the first to identify the Bandelier Tuff as a product of a zoned silicic magma body. Inherent in this finding is that the Bandelier eruptive products are compositionally-zoned in a systematic way as well, reflecting their extraction from a zoned magma system. For zoned high-silica rhyolitic magma suites such as the Bandelier, incompatible elements such as Nb are commonly used as an index of magmatic evolution. In the Otowi Member nearly fourfold increases in Nb concentration are observed between the least and most-evolved eruptive products (Kuentz, 1986; Dunbar and Hervig, 1992a; Dunbar and Hervig, 1992b; Hervig and Dunbar, 1992; Wolff et al., 1999). Consequently, previous studies on the Bandelier Tuff (Smith, 1979; Kuentz, 1986; Winters, 2002) have utilized Nb as a convenient differentiation index. The assumption is that juvenile (pumice) fragments containing the highest Nb concentrations are derived from the most chemically-evolved portions of the magma chamber.

Another possible use for Nb in zoned outflow sheets is as a chemostratigraphic marker. Studies have demonstrated that the chemistry of a zoned eruptive deposit can be strongly correlated with eruptive processes. In the Otowi Member, fall deposits and ignimbrite flow units are systematically zoned with respect to trace element chemistry. The early erupted units generally have higher Nb concentrations, and these deposits are taken to be associated with the most differentiated magmas, typically derived from the upper portion of the magma chamber. Later erupted units generally have progressively lower concentrations of Nb, and these are associated with less-differentiated magmas originating from lower levels in the chamber.

Consequently, in addition to serving as a useful petrogenetic indicator, Nb variations in stratigraphy can be used to correlate eruptive units and to discern physical eruptive processes. This may include identification of changing vent locations and geometries (such as widening), shifts in eruption dynamics (sustained versus collapsing plinian column), the timing of caldera collapse, and finally to link eruptive events with the host magma body.

In this study Nb data from the host tuff have been examined at 12 stratigraphic sections from 11 localities (Figure 5.1) around the caldera. Eight of these stratigraphic sections have corresponding lithic population data. Chemical variations in stratigraphy at each of the localities have been linked with lithic distributions and abundances from Chapter 4. The combination of the chemical data set with the lithic data set is significant because it allows for a more thorough evaluation of eruptive processes.

Chemical data are from several sources: the study of Kuentz (1986); the study of Winters (2001) in which pumices were collected by R.L. Winters, W.L. Aubin, P. Hartman, M.C. Rowe, and J.A. Wolff during the summer of 2000; and from samples collected by the author, J.A. Wolff, and K. Brunstad during the summer of 2003. Samples were cleaned and weathered rinds

were removed using a diamond lap. The bulk pumice samples were then processed and analyzed by XRF and ICP-MS at New Mexico Tech and Washington State University (Kuentz, 1986; Winters, 2001; present study). Detailed sample preparation and analytical procedures can be found at the WSU Geoanalytical Laboratory website (<http://www.sees.wsu.edu/Geolab>).

Background: Stratigraphy, Geochemistry and Zoning in the Otowi Member

The Otowi Member of the Bandelier Tuff is a mineralogically and compositionally-zoned high-silica rhyolitic ignimbrite (Smith and Bailey, 1966; Smith, 1979; Kuentz, 1986; Dunbar and Hervig, 1992; Wolff et al., 1999; Winters, 2001; Wolff and Ramos, 2003). The Bandelier magma chamber is thought to reside within Proterozoic basement rocks that are situated beneath the JMVF. This is based in part on borehole data (Nielson and Hulen, 1984) and on the presence of partially re-melted Proterozoic lithic fragments found within the Otowi ignimbrite (Eichelberger and Koch, 1979). These lithics include granitoid and amphibolite fragments found in the ignimbrite and rare garnet xenocrysts found in the basal portions of the Guaje fall deposits (Wolff et al., 2002).

The Otowi Member includes both plinian deposits and widespread non-welded to densely-welded ignimbrite deposits. The plinian deposit, known as the Guaje Pumice Bed, consists of five units (designated A through E) that are found primarily to the east and southeast of the present-day Valles Caldera. The fall deposits range from massive to well-bedded and consist primarily of well-sorted angular pumice clasts. The prevalence of bedding increases upward in stratigraphy due to a decrease in the number of large pumice fragments, and thus units B-D exhibit more stratification than the typically massive unit A. In addition, crystal concentrations generally increase upward in stratigraphy (Kuentz, 1986). Unit A is by far the

thickest plinian layer (up to 9 m in thickness) while units B-D are individually much thinner (< 1.0 meters) depending on location. The fall units have variable dispersal axes indicative of changing wind directions during the eruption. Unit A is found only to the east, while units B-D can be found along an arc stretching from east to southeast around the caldera. Dispersal axes were calculated by Self et al. (1986) using isopleth and isopach maps.

Fall unit A is a homogenous pumice fall deposit with weak stratification observed at Guaje Canyon towards the top of the unit. It is conspicuously absent to the south, west, and north of the caldera. Unit B is lithic rich (up to 25 wt. %) and found primarily to the east and south of the caldera. Fall unit C is coarse-grained and homogenous in nature and was associated with the highest plinian eruptive columns during fall deposition (Self et al., 1996). Fall units D and E are thin and can be found to the east and south of the caldera; however, they are more poorly exposed due to erosion by early pyroclastic flows (Self et. al, 1996). Distally, ashes have been found 550 km to the southeast of the Valles caldera in the Texas panhandle that are correlative with Otowi eruption (Izett et al., 1972; Holliday, 1988).

The Otowi ignimbrites are comprised of multiple flow units and are typically observed as white to pale pink or tan, non-bedded to weakly-stratified rhyolitic ash-flows with variable proportions of accidental (lithic) fragments. Welding is poor in most areas although the Otowi ignimbrites on the Jemez Plateau in the west are typically densely welded. In most areas to the south and east of the caldera, the ignimbrites sit above the plinian fall deposits A-E. However, intraplinian ignimbrites have been found situated between subunits of fall C in Lower Cochiti Canyon near Dixon Ranch, southeast of the caldera (Winters, 2001).

Chemically, the Otowi deposit is almost entirely made up of high-silica rhyolite and demonstrates a general internal upward decrease in the concentrations of incompatible trace

elements. Major element concentrations are uniform throughout, but large variations are observed in minor and trace elements. Phenocryst contents range from 7.5-19.5% (Self et al., 1996). Major phenocrysts present (>1%) are quartz and sanidine (Self et al., 1996). Other phases include clinopyroxene, fayalite, magnetite, zircon, allanite, and chevkinite (Winters, 2001). The plinian fall deposits become progressively less evolved moving upward in stratigraphy from first-erupted (fall unit A) to the last-erupted units (falls D and E). Otowi plinian unit A is thought to represent extraction of magma from a highly-differentiated zone in the upper portion of the Bandelier magma chamber. The bulk of the magma was erupted as voluminous pyroclastic flows that cover large areas of the JMVF. Compositions from pumices analyzed in the Otowi ignimbrites are typically less consistent, with variable ranges of chemistry scattered throughout flow units. Although, in some localities (such as at Cat Mesa) clear evidence of compositional zoning is evident in the ignimbrites.

Prior Otowi Member Geochemical Studies

Smith and Bailey (1966) conducted the first examination of Bandelier stratigraphy in which zoning and chemical variations were discussed. Preliminary data (chemical and mineralogical) were presented, and the study focused on chemical, mineralogical, and stratigraphic variations in the Tshirege (Upper) Member of the Bandelier Tuff than on the Otowi Member. An assumption of similarity between the Tshirege and Otowi was used to draw conclusions for the Otowi Member.

Smith (1979) examined zoning in magma chambers as part of a larger study on ash flows. In this study the relationships between ash-flow sheet volume, magma chamber size, and chemical zoning in magma chambers were examined, and the Bandelier Tuff was used as a primary example. Several conclusions are highlighted. Smith stated that all caldera-forming ash

flow sheets should show some evidence of zoning inherited from the magma chamber. He also emphasized that when examining various zoned outflow sheets, a spectrum of chemical gradients may be observed. For example, in some units the compositional gradients may be well-defined, while in others the gradients may be obscured partially by eruptive mechanisms. Finally some outflow sheets may exhibit compositional gaps between individual flow units (Smith, 1979). These gaps are interpreted in several ways. One simple explanation involves a scenario in which there exists unequal distribution of successive ash flows. In this circumstance, the missing compositions may be found in other areas of the outflow sheet. A second scenario proposed that ash flows may emanate from different vents creating compositional gaps and reversals. In this situation different levels of the magma chamber are tapped at the same time. Another explanation is that in some circumstances, a compositional gap in an outflow sheet can be correlated directly to a compositional gap in the magma chamber.

Smith (1979) also compared volumes and compositions of magmas erupted from known caldera systems and presented them in a basic model shown in Figure 5.2. The fundamental relationships between volumes and compositions in the model were used to make five observations: 1) chambers tend to be compositionally zoned and become more mafic with depth. 2) Erupted parts range from nearly uniform rhyolitic compositions to strongly-contrasting basalt-rhyolite compositions. 3) Small volume systems show stronger compositional contrasts than do large systems. 4) Successive ash-flow cycles from the same source tend to become more mafic in average composition than the preceding cycles. 5) Irrespective of starting composition, the volume of a magma chamber must control the depth at which successively more mafic magmas will reside during and after differentiation (Smith, 1979).

Sommer and Schramm (1983) used several techniques to determine volatile concentrations in melt inclusions from the Bandelier Tuff. Volatile measurements from melt inclusions were used to infer concentrations in the magma chamber, a practice that has since been identified by Wolff et al. (1999) as potentially misleading. Sommer and Schramm (1983) reported large differences between H₂O content in samples from the plinian and the ignimbrites for both the Otowi and Tshirege Members. The authors attributed the large differences in H₂O concentrations in melt inclusions from the plinian and ignimbrite units to the eruptive transition from plinian activity to large-scale ignimbrite deposition. This transition is referred to as “catastrophic column collapse” by the authors.

Kuentz (1986) conducted a study on the geochemistry of the Otowi Member in which chemical variations in the erupted units were examined; their implications for magma withdrawal and eruptive processes were then evaluated. The author suggested that although the Otowi Member pyroclastic deposit is not consistently zoned throughout its entirety (the plinian is well-zoned, while the ignimbrites are more intermittently zoned) the striking trace element variations found within the erupted units are indicative of a heterogeneous, zoned magma source. Analyses of trace elements in the plinian were found to show little variation, while analyses for the same elements from the ignimbrite were more variable. Chemical zonation was attributed to fractionation of a magma that resulted in density, volatile, and viscosity gradients within the magma chamber. Side-wall crystallization was proposed as the primary fractionation mechanism in which quartz, sanidine, pyroxene, magnetite, apatite, chevkinite, allanite, and zircon were the main phases crystallizing. The initial phase of the Otowi eruption (Guaje plinian unit) was proposed to have been erupted first from a highly evolved upper carapace in the magma chamber. Eruption of the main ignimbrite body then tapped progressively deeper levels within

the magma chamber. Kuentz suggested that magma withdrawal during the main phase of the eruption caused intermingling of magmas within the chamber, thus destroying pre-eruptive gradients and decreasing chemical zonation in the erupted ignimbrites (Kuentz, 1986).

Dunbar and Hervig (1992a) compared the systematics of trace element chemistry and volatiles from melt inclusions in the Bishop Tuff and the Otowi Member of the Bandelier Tuff. They noted that although the trace element data were not identical, some striking similarities could be drawn between the two units. Volatile zonation and density gradients were determined to be similar in the Bishop and Otowi magmas (Dunbar and Hervig, 1992a). Data from melt inclusions in the plinian and ignimbrite phases of the tuffs suggested that the Bishop and Otowi magmas were strongly zoned with respect to H₂O in the upper portions of the chambers but largely non-zoned for the majority of the magma body. Based on the trace-element and volatile concentration data, Dunbar and Hervig (1992a) suggested that a combination of fractionation and partial melting could produce the compositional zoning observed within the Bishop and Bandelier magmas.

Dunbar and Hervig (1992b) further examined volatile and trace element concentrations from melt inclusions in Otowi quartz, sanidine, and pyroxene phenocrysts using the electron and ion microprobes and XRF analysis. As did Kuentz (1986) before them, they observed significant trace element variations and inferred that large pre-eruptive volatile and density gradients existed. They echoed the observation of Kuentz (1986) that although the Otowi ignimbrite shows only partial compositional zoning, the large trace element variations are indicative of an ignimbrite erupted from a zoned magma chamber.

Wolff et al. (1999) examined Sr isotope disequilibrium in glasses from Otowi quartz and sanidine phenocrysts and from glasses in quartz/feldspar glomerocrysts. As in prior studies

(Kuentz, 1986; Dunbar and Hervig, 1992a; Dunbar and Hervig, 1992b; Hervig and Dunbar, 1992), it was noted that Otowi pumices show three-fold to five-fold coherent variation with incompatible trace elements that is consistent with fractionation of the phenocryst assemblage sanidine + quartz + clinopyroxene + magnetite \pm fayalite \pm zircon \pm chevkinite. An important conclusion of Wolff et al. (1999) is that melt inclusions from quartz and other phenocrysts may not necessarily be representative of bulk magma compositions. The concept of preferential derivation of melt-inclusion bearing phenocrysts from marginal environments along the periphery of a magma chamber may thus invalidate prior work that uses melt inclusions to determine pre-eruptive volatile contents. This includes prior studies conducted on the Otowi, such as that by Sommer and Schramm (1983) and Dunbar and Hervig (1992b).

Winick et al. (2001) conducted $^{40}\text{Ar}/^{39}\text{Ar}$ studies on glass melt inclusions in quartz from the Bishop and Bandelier Tuffs. The overall goal was to use the K-Ar system to study the controversial topic of magma residence time in large silicic systems. The study found unreasonably high apparent ages for melt inclusions in quartz phenocrysts from both the Bishop and Bandelier Tuffs. For the Otowi Member, an age of 14.60 ± 1.50 Ma was calculated. This exceeds realistic chamber residence times for quartz by a factor of two to five (Winick et al., 2001). These unrealistic ages were attributed to excess ^{40}Ar present in the melt inclusions. It was therefore concluded that apparent ages derived from melt-inclusion bearing quartz phenocrysts are not necessarily representative of crystallization or eruption ages. Another significant corollary of this finding was the recognition by the authors that excess ^{40}Ar may also be found in melt inclusions from sanidine phenocrysts. This has the potential to shift sanidine apparent ages for the Bishop and Bandelier Tuffs back in time anywhere from thousands to tens of thousands of years. Based on this assumption, for the Otowi Member, single-crystal laser

fusion ages were estimated to be up to 27,000 years younger than the age cited by Izett and Obradovich (1994) of 1.61 Ma (Winick et al., 2001). Ages for the Bandelier Members are still being refined, however, with new ages of 1.68 Ma for the Otowi Member and 1.21 Ma for the Tshirege Member reported by Phillips et al. (2006).

Winters (2001) investigated the behavior of REE and trace elements in the Otowi Member. The chemical data were used to assist in identification of petrogenetic and magma withdrawal processes and to define an eruptive sequence. Much of the chemical data in this study is taken from Winters (2001).

Wolff et al. (2002) conducted a study of oxygen isotopes in quartz and feldspar phenocrysts from Bandelier plinian and ignimbrite deposits. This included samples from the Otowi and Tshirege Members and the Cerro Toledo Rhyolite. However, the majority of samples were taken from the Upper Bandelier. All samples analyzed had $\delta^{18}\text{O}$ values between 6.3‰ and 8.3‰. For the Otowi samples, $\delta^{18}\text{O}$ values in both quartz and feldspar ranged between 7.16‰ and 7.91‰. None of the samples analyzed were representative of a low $\delta^{18}\text{O}$ rhyolite.

Wolff and Ramos (2003) provided the first high-precision Pb isotope data for a high-silica rhyolite. In addition, they expanded the Sr isotope data set from Wolff et al. (1999). Within the Otowi Member, Pb isotope ratios were found to be variable between the Guaje pumice unit A, the Otowi ignimbrite, the Upper Guaje pumice units, and in the glomerocrysts. Wolff and Ramos (2003) concluded that this observed variation could not result from in situ ingrowth and that open system processes must have been responsible for generating Pb isotope variations.

Nb variations and comparisons to lithic data

In Figures 5.3 through 5.13, Nb concentrations in whole pumices have been plotted versus height in stratigraphy at eleven sampling localities. Chemical variations will be discussed for each locality, and lithic distributions will be compared to the chemical data for each locality. Additionally, an evaluation of potential eruptive processes will be made where applicable for each locality based on the chemical and lithic data.

Some general observations include the following: to the north of the caldera, at Pueblo Mesa, sections show initial highly-evolved compositions that shift weakly towards less-evolved compositions with height in stratigraphy. To the southwest of the caldera, compositions are observed to shift more suddenly and span a wider range. The highest Nb concentrations are in the plinian fall deposits found to the east and southeast of the present-day caldera. The lowest Nb concentrations are found in the ignimbrites, particularly in those found on the Jemez Plateau in the west and in the stratigraphically-highest ignimbrites deposited at Wildcat Canyon to the southwest. In addition, pumices with very low Nb (~ 50 ppm) are found in ignimbrites on the Pajarito Plateau at the Airport Section and at Locations 17 and 27 of Kuentz (1986).

Guaje Canyon

At Guaje Canyon (Figure 5.3) the most evolved material is found in the plinian fall units, with Nb concentrations decreasing up-section; the overlying ignimbrite is less evolved than the majority of the plinian. In the plinian, Nb is consistently high in fall units A-C, with concentrations ranging between 181 to 198 ppm. In fall Unit D, Nb decreases from 160 ppm to 118 ppm. Fall Unit E is the least evolved plinian layer, with Nb concentrations dropping to 66 ppm at 10.6 m above the base of the section. Above fall unit E there is a fine ash layer that is equivalent in chemistry (Nb concentrations of 83 and 57 ppm) to fall unit E. Stratigraphically

above 11 meters in the ignimbrite, Nb concentrations randomly fluctuate with height between 152 and 84 ppm.

By comparing lithic distributions to chemical variations, several patterns are evident at Guaje Canyon. First, it is immediately evident that the largest proportions of lithics are in fall units B and C where Nb concentrations are some of the highest in the section. The largest proportions of lithics are encountered in unit C, after which the number of lithic fragments present decreases significantly in fall units D and E. The decrease in lithic abundance coincides directly with the abrupt decrease in Nb chemistry above fall unit C. Rhyolite lithics are present in significant quantities in fall units B and C where Nb concentrations are very high; after fall unit C, rhyolite lithics decrease considerably in numbers and are absent within the ignimbrite above 11 meters. Finally, welded ignimbrite lithics are observed as a dominant lithic type between 12-12.75 meters in the ignimbrite. These are associated with intermediate Nb concentrations (119-132 ppm) and do not appear to correspond to any significant shifts in chemistry.

The lithic data presented here support the hypothesis of Self et al. (1996) that the plinian phase increased in intensity through deposition of fall units A-C and peaked during deposition of fall C. Crystal concentration data (Self et al. (1996) support this, as enrichment factors increase from 0.8 in fall unit A to 3.8 in fall unit C. After fall unit C, enrichment factors decrease to 3.4 in fall D and 2.0 in Fall E. In addition, the high Nb concentrations found in the early to middle fall units suggest that that magma was being extracted from the highly differentiated, upper portion of the Otowi magma chamber. Chemical data from this study also imply similarity between fall unit E and the first ignimbrite at Guaje Canyon. Later ignimbrites show intermediate compositions that fluctuate more randomly in stratigraphy.

The increasing lithic abundances, crystal enrichment factors, and sudden decrease in Nb above fall unit C likely represent a progressive widening of the vent system early in the eruption. Vent widening could facilitate higher eruption rates which would, in turn, allow larger quantities of magma to be extracted from the chamber. With continued eruption, deeper, more primitive magmas with lower Nb concentrations would be extracted. This may help to explain why fall units D and E and the ignimbrites at Guaje Canyon have significantly lower Nb concentrations than fall units A-C.

In the ignimbrites, Nb concentrations fluctuate as ‘bulk’ composition Otowi magmas were erupted. The appearance of densely-welded ignimbrite lithics in major quantities is a phenomenon that is only observed at Guaje Canyon (see Appendix A for easy comparison of lithics between all sampling localities). Two explanations can be invoked for the presence of these lithics: first, they may simply represent remobilized fragments of Otowi ignimbrite; second, they may suggest a more localized lithic signature common to Guaje Canyon and thus imply a vent shift towards the northeast and the vicinity of Guaje Canyon. The remobilization hypothesis is not supported by this study; the ignimbrite lithics in question are densely welded, weathered in many cases, and do not appear similar to ‘typical’ Bandelier ignimbrite. Therefore it is unlikely that they represent pieces of Otowi pyroclastic deposits incorporated into later flows. A vent shift is the only reasonable explanation for such a unique lithic signature to be found at Guaje Canyon.

Cat Mesa

At Cat Mesa two sections were measured (Figures 5.4 and 5.5), Cat Mesa A and Cat Mesa B. In both sections a similar trend is observed beneath the prominent lag breccia in which Nb concentrations in the ignimbrite are typically high (> 180 ppm). Starting within the lag

breccia and continuing stratigraphically above it, pumice compositions shift dramatically to < 90 ppm Nb within a span of approximately 14 meters.

Several significant observations can be made with respect to the chemical and lithic data at Cat Mesa. First, the striking change in pumice chemistry corresponds directly with the appearance of the lag breccia in stratigraphy. Lithic abundances increase up-section and remain extraordinarily high through the lag breccia until approximately 78 meters, above which abundances decrease significantly. Second, rhyolite lithics are most prevalent in the lower ignimbrites associated (as at Guaje Canyon) with the most evolved pumice compositions (> 180 ppm Nb). Finally, the lower ignimbrites at Cat Mesa contain highly evolved pumices with high Nb concentrations (> 180 ppm).

The lag breccias at Cat Mesa were described by Self et al. (1986) as being vent-proximal and thus were used to support the theory that vents had migrated during the Otowi eruption to ring fractures around the caldera. Conversely, the data from this study proposes a single vent hypothesis for the duration of the eruption. This is based on the overall similarity of the lithic signatures at all sampling localities around the caldera, the determination of provenance for dacite fragments in Chapter 4, and the appearance of rhyolite lithics where Nb > 180 ppm at similar locations in stratigraphy at the majority of sampling sites. This is in contradiction to the multiple ring vent hypothesis, and thus the origin of the lag breccias at Cat Mesa must be addressed.

Chemical analyses of dacite lithics in Chapter 4 showed that both Paliza Canyon and Tschicoma dacite fragments are present at Cat Mesa at various levels in stratigraphy, including the lag breccia. Based on current knowledge of the pre-caldera geology, Tschicoma dacite is not known to underlie the Cat Mesa sampling locality. Therefore, it is impossible that the

ignimbrites there, and in particular the lag breccia, were erupted locally from a ring vent. Thus, it is proposed that the lag breccias at Cat Mesa represent a widening of the centrally-located vent, rather than a vent shift. The sudden drop in Nb chemistry and the increase in abundance and size of lithic fragments being deposited in the ignimbrites could just as easily correspond to an increase in the eruption rate brought about by widening of the vent. In addition, the region around Cat Mesa lies in a significant pre-Otowi paleovalley. Pyroclastic flows from the collapsing column were undoubtedly funneled down this paleocanyon. In this circumstance, the lag breccias could represent dense lenses of lithics associated with deposition of pyroclastic flows. Based on the evolved nature of pumices analyzed from the lower portions of the Cat Mesa sections, it is likely that these ignimbrites were emplaced earlier on in the eruption sequence.

Wildcat Canyon

The stratigraphic section at Wildcat Canyon (Figure 5.6) is roughly correlative with the upper portions of the Cat Mesa sections. In this section, Nb is observed to decrease fairly consistently with increasing height in stratigraphy. Nb concentrations range from highly evolved (189 ppm) at the base of the section to depleted (66 ppm) at 55 meters. Between 45 and 50 meters, several reversals are observed in which Nb fluctuates, going as high as 108 ppm and as low as 65 ppm; above 54 meters in the section Nb concentrations cluster between 66-68 ppm.

At Wildcat Canyon rhyolite lithics are slightly more abundant at the base of the section where Nb concentrations are more evolved. Minor quantities of rhyolite lithics (less than 3% of each bulk ignimbrite sample) are found up-section associated with more primitive Nb concentrations. Lithics are prevalent in number throughout the section but decrease above 54 meters.

The section at Wildcat Canyon is similar to that at Cat Mesa above the lag breccia. Decreasing Nb concentrations most likely represent deposition of ignimbrites associated with more primitive magmas derived from deeper levels in the chamber. These ignimbrites were deposited during the mid to late phase of the eruption based on their stratigraphic position and decreasing Nb chemistry.

Pueblo Mesa

Nb data from Pueblo Mesa (Figure 5.7) show considerable spread throughout the section. At the base of the section, a very thin layer of the Otowi plinian is exposed with a Nb concentration of 173 ppm. Above this, a fine ash overlying the plinian has a more intermediate composition of 159 ppm Nb. Immediately above this, the first ignimbrites have higher Nb concentrations (~ 180-190 ppm). Pumices analyzed from just beneath a flow unit boundary in the ignimbrite at 7 meters have a range of compositions between 140-190 ppm Nb. Moving upward in stratigraphy, two groupings of pumice are present at all levels of stratigraphy between 10-35 meters: an intermediate grouping where Nb = 130-160 ppm and a more evolved grouping where Nb = 180-200 ppm.

There does not appear to be any significant correlation between lithic distributions and Nb chemistry at Pueblo Mesa. Lithics at Pueblo Mesa are dominated by andesite and dacite with extremely small quantities of rhyolite (1 of 301 total) and other lithologies (6 of 301 total). Andesite and dacite lithic proportions fluctuate in stratigraphy, with andesite the dominant lithic lithology at the top of the section. Numbers of lithics are fairly consistent throughout the section. Most likely, the ignimbrites at Pueblo Mesa are the result of the eruption coring downward through Paliza Canyon Formation andesite and dacite and Tschicoma Formation dacite beneath

the centrally-located vent. The multiple groupings of pumice chemistries indicate extraction of magma from multiple levels of the magma chamber simultaneously.

Seven Springs and Cebolla Canyon

At Seven Springs (Figure 5.8) Nb concentrations from the densely-welded ignimbrite are considerably lower (≤ 90 ppm) when viewed in comparison with data from stratigraphic columns from other parts of the JMVF. The data exhibit a slight negative trend with increasing stratigraphic height. Bulk ignimbrite samples were not collected from this locality so a comparison of Nb chemistry and lithic distributions is not possible. However, a bulk sample was collected at Cebolla Canyon (Figure 4.5 in Chapter 4), located slightly to the northeast of Seven Springs. At this sample locality the dominant lithics were andesite and dacite. A single pumice analyzed from this bulk sample yielded a Nb concentration of 62 ppm, which is consistent with the chemical data obtained at Seven Springs. In general, the Nb concentrations (generally < 100 ppm) on the Jemez Plateau are lower than anywhere else around the caldera. Therefore, these ignimbrites represent less-evolved magmas derived from lower in the chamber and were probably erupted later in the overall eruption sequence.

Dixon Ranch

The composite section at Dixon Ranch (Figure 5.9) exposes fall units B and C and intraplinian ignimbrites. The intraplinian ignimbrite is situated between subunits of fall unit C. Fall unit A is not exposed in this area, having been deposited to the east of the caldera. The vast majority of the material analyzed at this location is highly evolved, with Nb concentrations > 180 ppm. Fall units B and C contain pumices with Nb ≥ 180 ppm; likewise, the intraplinian ignimbrites all contain evolved pumices with Nb between 173-199 ppm. Sample JMVF-00-40,

taken several meters into the upper ignimbrite at 4.75 meters, yielded a highly evolved pumice composition of 199 ppm.

At Dixon Ranch rhyolite lithics are present in relative abundance in fall units where Nb concentrations are high (> 180 ppm). This is a reiteration of the trend where rhyolite lithics are found in plinian and ignimbrite units around the caldera associated with the most evolved pumice chemistry.

The highly evolved chemical signature found in the deposits at Dixon Ranch suggests that these materials were erupted from the upper, highly-differentiated portion of the Otowi magma chamber. The presence of the intraplinian ignimbrite is evidence that fall and flow deposition were simultaneous during the plinian phase. Self et al. (1996) proposed that the Otowi plinian phase peaked in intensity during deposition of fall unit C—a conclusion that is supported by lithic data from this study. Thus, the intraplinian ignimbrites likely represent instability in the plinian column, with smaller-scale pyroclastic flows being deposited during a partial column collapse. These flows were funneled down the paleocanyon in what is now Cochiti Canyon. Given the highly-evolved chemical makeup of the ignimbrites at Dixon Ranch, it is likely that they represent some of the first ignimbrites to be deposited from the eruption.

Upper Cochiti Canyon

The five pumice samples collected for analysis at Upper Cochiti Canyon are highly evolved (Figure 5.10); Nb compositions range between 177-200 ppm. Lithic fragments found in this section are dominantly andesitic and dacitic; proportions of the two are variable with stratigraphic position. Beginning at 22.5 meters and continuing to the top of the section at 64 meters, rhyolite lithics become increasingly abundant and are associated with high Nb concentrations. The ignimbrites at this locality contain pumices with some of the highest Nb

readings collected (~ 200 ppm) in this study. Based on their highly-evolved chemistry, these ignimbrites, like those at Dixon Ranch to the south, are associated with magmas from the upper, more differentiated portion of the magma chamber. Accordingly, as with the Dixon Ranch ignimbrites, they are most-likely intraplinian in nature.

Airport Section

The graph in Figure 5.11 shows that Nb compositions at this locality are highly variable in stratigraphy, ranging from highly evolved at the base of the section (180 ppm) to more primitive (54 ppm) at 40 meters. Based on Nb chemistry Winters (2001) noted that two chemically distinctive pumice populations are present in the massive ignimbrite at this locality. The more evolved grouping is unaltered with fewer phenocrysts, and the less evolved grouping is more phenocryst-rich and has a “yellowish tint throughout” (Winters, 2001). Despite the two distinct groupings, it was noted that the mineralogy is similar with quartz, sanidine, hedenbergite, and magnetite phenocrysts present in each group (Winters, 2001).

Lithics at the Airport Section were measured from two bulk samples (JMVf-00-70 and JMVf-00-74) at zero meters and 21.8 meters respectively. Rhyolite lithics are more abundant where Nb concentrations are high, in this case at the base of the measured section. Curiously, however, at 21.8 meters where Nb is lower (129 ppm) rhyolite lithics are still prevalent. Most likely, the highly variable nature of the Nb chemistry suggests that these ignimbrites were erupted with the bulk of the ignimbrite volume later in the eruption.

Location 13 and Location 27

Locations 13 and 27 represent two stratigraphic sections measured by Kuentz (1986) from a road cut on N.M. Route 4 at the base of Otowi Mesa on the Pajarito Plateau. Location 13 includes fall unit A only, and Location 27 includes only massive Otowi ignimbrite. The graphs

in Figure 5.12 show chemical variations for each of these locations. At Location 13, three samples were collected from fall unit A, each of which contains (perhaps unsurprisingly) high Nb concentrations between 193-196 ppm. At Location 27, eight samples from the ignimbrite have low Nb concentrations between 52-93 ppm. Nb does generally increase from the base to the top of the section. No lithic data is associated with either of these locations.

Location 17

Location 17 is east-southeast of the Copar Mine in Guaje Canyon. The section was measured in massive non-welded Otowi ignimbrite exposed above the plinian and contains two flow units separated by a poorly-defined boundary (Kuentz, 1986). The graph in Figure 5.13 shows that Nb concentrations range between 51-136 ppm. From the base of the section, Nb initially increases to 135 ppm, then decreases back to 88 ppm and stays in this range up to the flow unit boundary. Above the flow boundary, Nb concentrations show first a positive reversal, then a negative reversal, and finally a positive reversal at the top of the section to a value of 145 ppm. No lithic data is associated with this section. The Nb chemistry here is fairly typical of what has been observed within the bulk Otowi ignimbrite at other localities—moderate fluctuation within flows that range between low and mid-range concentrations (50-150 ppm).

Volume calculations of Otowi chemical types

In addition to being extremely useful as a petrogenetic tracer, the Nb data has been used to determine the abundance of various chemical groupings present in the eruptive products of the Otowi Member. Dunbar and Hervig (1992b) suggested that the Otowi may be divided into three major chemical divisions that delineate an early, middle, and late phase of evolution. To test this hypothesis, Nb concentrations from eight sampling localities (Figure 5.1) have been used to estimate proportions of ignimbrite chemical types as percentages of height in stratigraphy. Three

ranges of chemical types have been identified: 170-200 ppm for the most evolved compositions, 90-170 ppm for intermediate compositions, and < 90 ppm for the least evolved compositions. In each of the eight stratigraphic columns abundances of the three chemical ranges have been estimated as both a thickness in meters and as a percentage of the total stratigraphic height. Table 5.1 shows the percentages determined for each chemical group at each of the eight columns in the Otowi ignimbrite.

Next, the proportions of each chemical group were applied to the volumes calculated in Chapter 3 to determine the amount of each chemical type present in km³ DRE. For volume zones containing a stratigraphic column (A-E, G, and H) the proportions from that column were used. For those zones not containing a stratigraphic column (F, I, J, K, L, M, and the distal zones in the adjacent rift basins) data from an adjacent segment or an average of multiple adjacent segments have been used. The intracaldera fill, which is represented by zone I, was calculated using averages from stratigraphic sections in all of the adjacent zones A-H. For the Española Basin distal wedge, an average of the chemical proportions from zones A and H was used. For the Santo Domingo Basin, an average of the chemical proportions from zones B and C (the areas from which the ignimbrites in the basin presumably came from) was used. Using this methodology, a total volume has been calculated (in km³ DRE) for the three ignimbrite chemical groupings in each zone. The results of these calculations, including totals for the entire Otowi ignimbrite deposit, are shown in Table 5.2.

Two stratigraphic localities, Dixon Ranch and Guaje Canyon, contain Otowi plinian deposits. For the chemical volume calculations in this chapter, the plinian phase has been considered as a separate entity from the ignimbrite. Proportions of chemical types in the five plinian fall units were estimated using the stratigraphic columns from Guaje Canyon and Dixon

Ranch. The data sets from the two localities were averaged in Table 5.3 to determine the overall proportions of chemical types in each of the five plinian fall units.

As was done for the ignimbrite, the plinian chemical proportions have been applied to the volumes calculated in Chapter 3. Fall unit A is estimated as 1.2 km³ DRE, and fall units B-E are estimated to collectively represent 44 km³ DRE. Table 5.4 shows the quantity (in km³ DRE) of the three chemical types for fall unit A and fall units B-E. Unsurprisingly, the data show that the Guaje is dominantly (90%) evolved composition (170-200 ppm Nb).

For the Otowi ignimbrite, three chemical types are present in roughly equal quantities. The most evolved grouping (170-200 ppm Nb) comprises 119.7 km³ DRE, which is 41% of the deposit. The intermediate grouping (90-170 ppm) constitutes 85.8 km³ DRE or approximately 30% of the deposit, while the least evolved chemical grouping comprises 84.4 km³ DRE, which equates to approximately 29% of the deposit. Figure 5.14a is a pie chart illustrating the relative proportions of the three chemical groupings in the ignimbrite.

Plinian fall units A-C are comprised of 100% of the 170-200 ppm Nb compositional grouping. Fall unit D is comprised of 70% of the 170-200 ppm Nb grouping and 30% of the 90-170 ppm Nb grouping. Fall unit E is comprised of 50% of the 90-170 ppm Nb grouping and 50% of the < 90 ppm Nb grouping. Overall in the plinian, a total of 73.2 km³ DRE (90%) is made up of 170-200 ppm Nb. The remaining 8 km³ DRE (10%) is comprised of the intermediate (90-170 ppm Nb) grouping. Figure 5.14b is a pie chart illustrating the relative proportions of the three chemical groupings in the plinian.

Summary

Data from this study and from previous geochemical studies support the concept that chemical zonation in the Otowi Member results from the eruption of magma from a zoned

Bandelier magma chamber. The most evolved compositions (as determined by Nb concentrations) are found in plinian fall units A-C and in intraplinian ignimbrites exposed to the east-southeast of the caldera. Stratigraphically above fall unit C, Nb concentrations decrease significantly through fall units D and E and into the lower, post-plinian ignimbrites.

Intraplinian ignimbrites exposed at Lower Cochiti Canyon (Dixon Ranch) and Upper Cochiti Canyon contain highly evolved pumice with high Nb concentrations. Their presence interspersed between sub-units of fall unit C proves that fall and pyroclastic flow deposition were simultaneous during the plinian phase. This is most likely attributed to column instability during the plinian phase with associated partial column collapses that resulted in deposition of the intraplinian ignimbrites in Cochiti Canyon. This phenomenon was suggested by Self et al. (1996).

Within the Otowi ignimbrites, zoning is more random and a greater spread of Nb chemistry exists depending on the locality and height in stratigraphy; although, at several localities (Cat Mesa, Wildcat Canyon, Seven Springs) the ignimbrites do show general decreases in Nb with height in stratigraphy as would be expected in a zoned outflow deposit. At the majority of other localities positive and negative shifts in Nb chemistry are observed at varying heights in stratigraphy.

Kuentz (1986) proposed that much of the compositional zoning present in the Otowi magma has been obscured and overprinted in the eruptive units. It was noted that zoning is not as well preserved in the Otowi plinian and tuff deposits as it is in other zoned ignimbrites such as the Bishop Tuff. In the Otowi Member chemical zonation is best exhibited between the plinian and ignimbrite deposits. However, many of the ignimbrites are unzoned.

These unzoned ignimbrites, as well as fluctuation of Nb within the outflow units both in stratigraphy and with geographic locality, can be attributed to shifts in eruptive dynamics and also to processes operating within the magma chamber. Physical changes during an eruption, such as widening of vents, the onset and progression of caldera collapse, and funneling of pyroclastic flows via pre-existing topography can all influence deposition and thus affect chemical patterns in the erupted material. In addition, beneath the surface several magmatic processes may have influenced the composition of magmas that were extracted during the Otowi eruption. Chiefly, this includes mixing and perturbation of the magma chamber before and during the eruption. Disruption of magmas (and thus chemical zonation) during the Otowi eruption was suggested by Kuentz (1986) to be one reason why the Otowi ignimbrites do not reflect compositional zoning as well as some other tuffs.

Spera (1984) and Spera (1986) showed with numerical models that magma can be erupted from different levels of a zoned magma chamber simultaneously and that compositional gaps may exist within outflow units. Kuentz (1986) suggested that in the case of the Otowi Member, chaotic caldera collapse may have caused independently sinking blocks to function as pistons which allowed for magmas with different compositions from multiple depths to be sampled simultaneously. This phenomenon can adequately explain random fluctuations in Nb chemistry at some localities and the unzoned nature of ignimbrites at others. It is also a plausible explanation for the chemical variability at Pueblo Mesa; there, pumices from the ignimbrite show two simultaneous and distinctive compositional groupings throughout a large part of the stratigraphic section.

Mixing of bulk Otowi magmas with the evolved and altered carapace of material on the periphery of the chamber, as suggested by Wolff et al. (1999) and Wolff et al. (2002) may have

also affected the compositions of erupted materials throughout the course of the eruption. The first magmas erupted as the plinian fall and intraplinian ignimbrites could represent highly evolved liquids stored in the upper portion of the chamber. Later, disruption of the carapace and subsequent mixing led to various other compositions being extracted.

Finally, volume calculations of chemical types appear to delineate a tri-part division within the Otowi ignimbrite. Roughly equal quantities of evolved (> 170 ppm Nb), intermediate (90-170 ppm Nb), and depleted (<90 ppm Nb) are present. The evolved magmas are slightly more represented (40%), while the intermediate and depleted types are nearly equal in quantity (30% and 29% respectively). In the plinian, approximately 90% of the deposit is comprised of the most evolved Nb compositions, while the remaining 10% is of intermediate composition. It is intriguing that the chemical quantities within the ignimbrites are roughly equal. The volume calculations presented are enough to warrant future work on this subject with an expanded dataset, perhaps including isotopic analyses.

Based on the information ascertained in chapters one through five, the next chapter (Chapter 6) will provide a cumulative synthesis of the eruption sequence. The eruption has been broken down into a series of stages with interpretations.

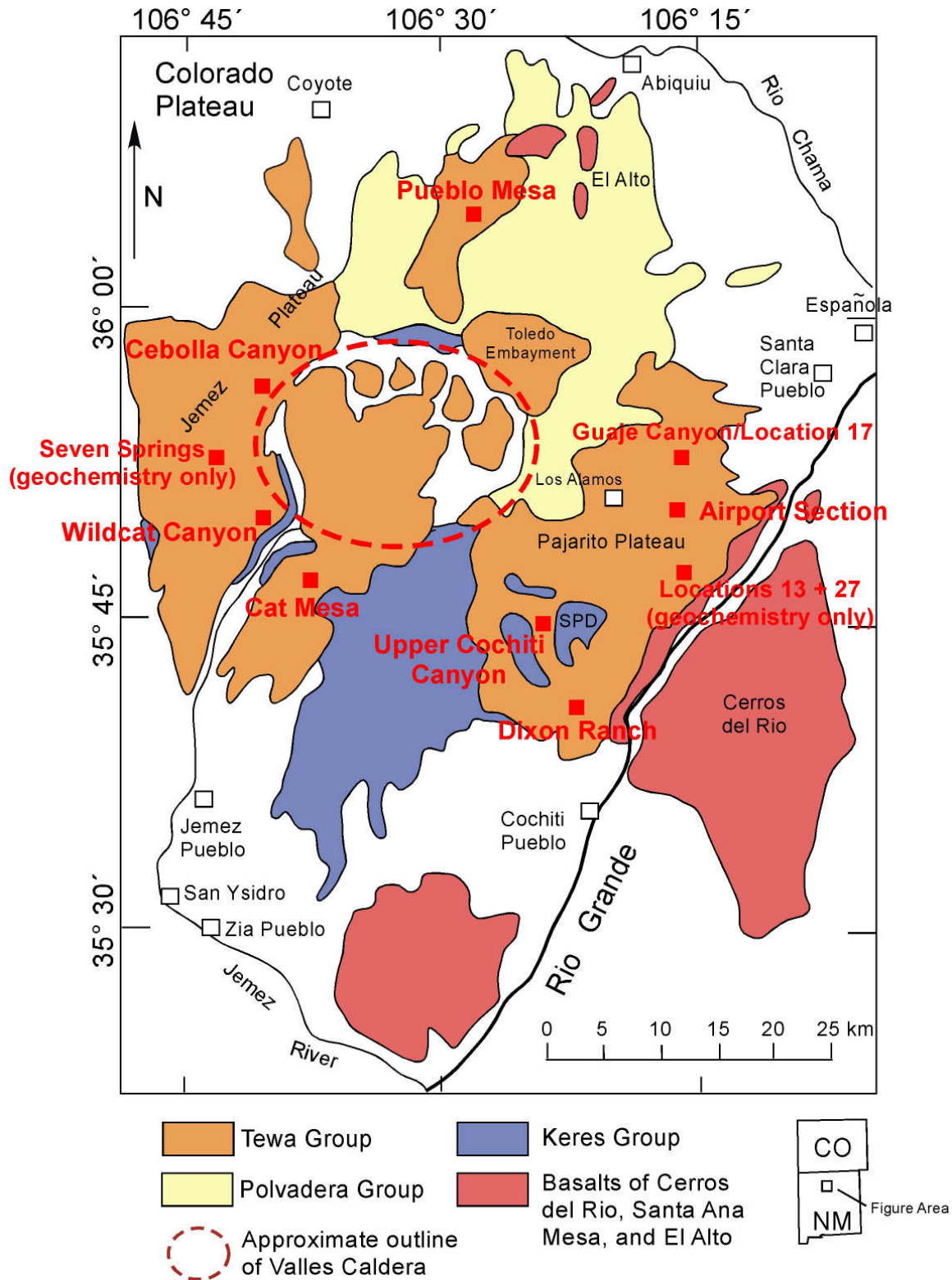


Figure 5.1. Sample locations for geochemical analyses of whole pumices from Otowi plinian and ignimbrite deposits. Locations that do not have corresponding lithic population data are labeled 'geochemistry only'.

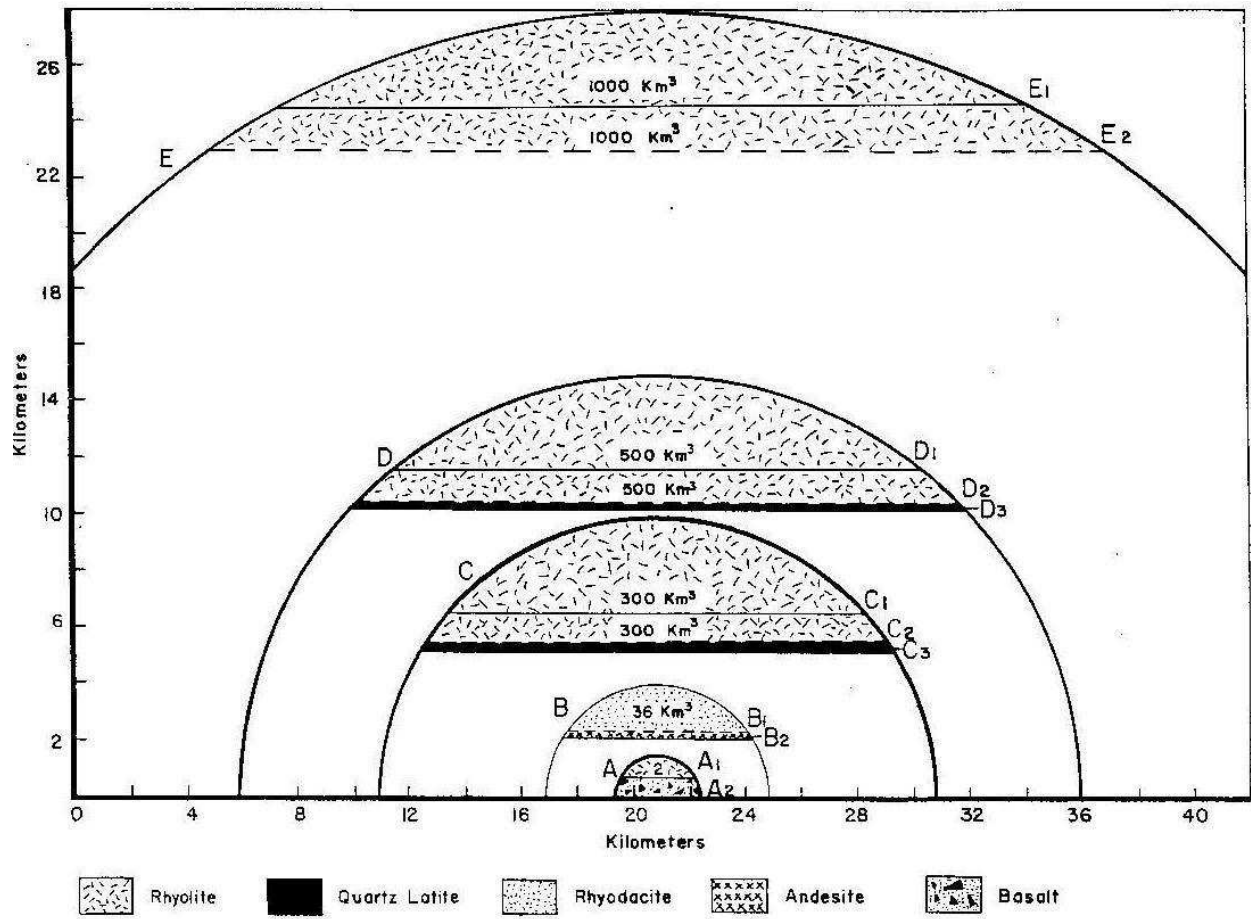


Figure 5.2. Basic comparison of volumes and compositions of magma erupted from known caldera systems, from Smith (1979). Cross-sections are drawn to scale and are based on the assumption that caldera-forming magma resided in the upper portions of a hemisphere having the diameter of the caldera. Cross sections are labeled as follows: A = Askja, Iceland. A₁ is the Knebel caldera; A₂ represents basalt presumed to underlie erupted silicic compositions. Data are from Bemmelen and Rutten (1955). B = Crater Lake, Oregon. B₁ is rhyolite-rhyodacite; B₂ is andesite. Data are from Williams (1942) and Williams and Goles (1969). C = Bandelier Tuff, New Mexico. C₁ is the Otowi Member; C₂ is the Tshirege Member; C₃ is the Cerro Toledo rhyolite. D = Timber Mtn. caldera, Nevada. D₁ is a high-SiO₂ rhyolite from the Rainier Mesa Member of the Timber Mountain Tuff; D₂ is rhyolite; D₃ is quartz latite. Data are from Byers et al. (1976) and Christiansen et al. (1977). E = Yellowstone, Wyoming from approximately 6×10^5 years ago. E₁ is the volume erupted during caldera formation; E₂ is the post-caldera magma that has been extruded since.

GUAJE CANYON

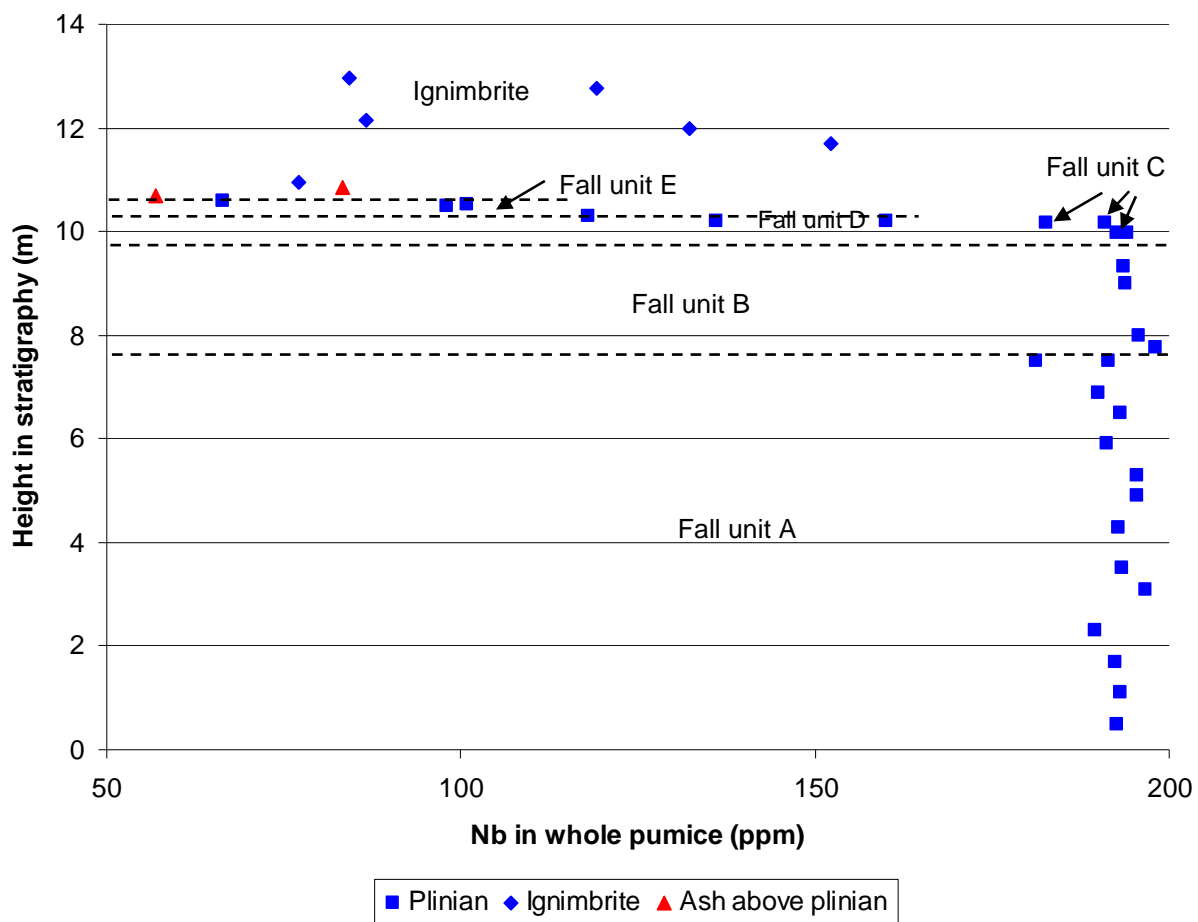


Figure 5.3. Graph showing Nb chemical variations with height in stratigraphy at Guaje Canyon.

CAT MESA A

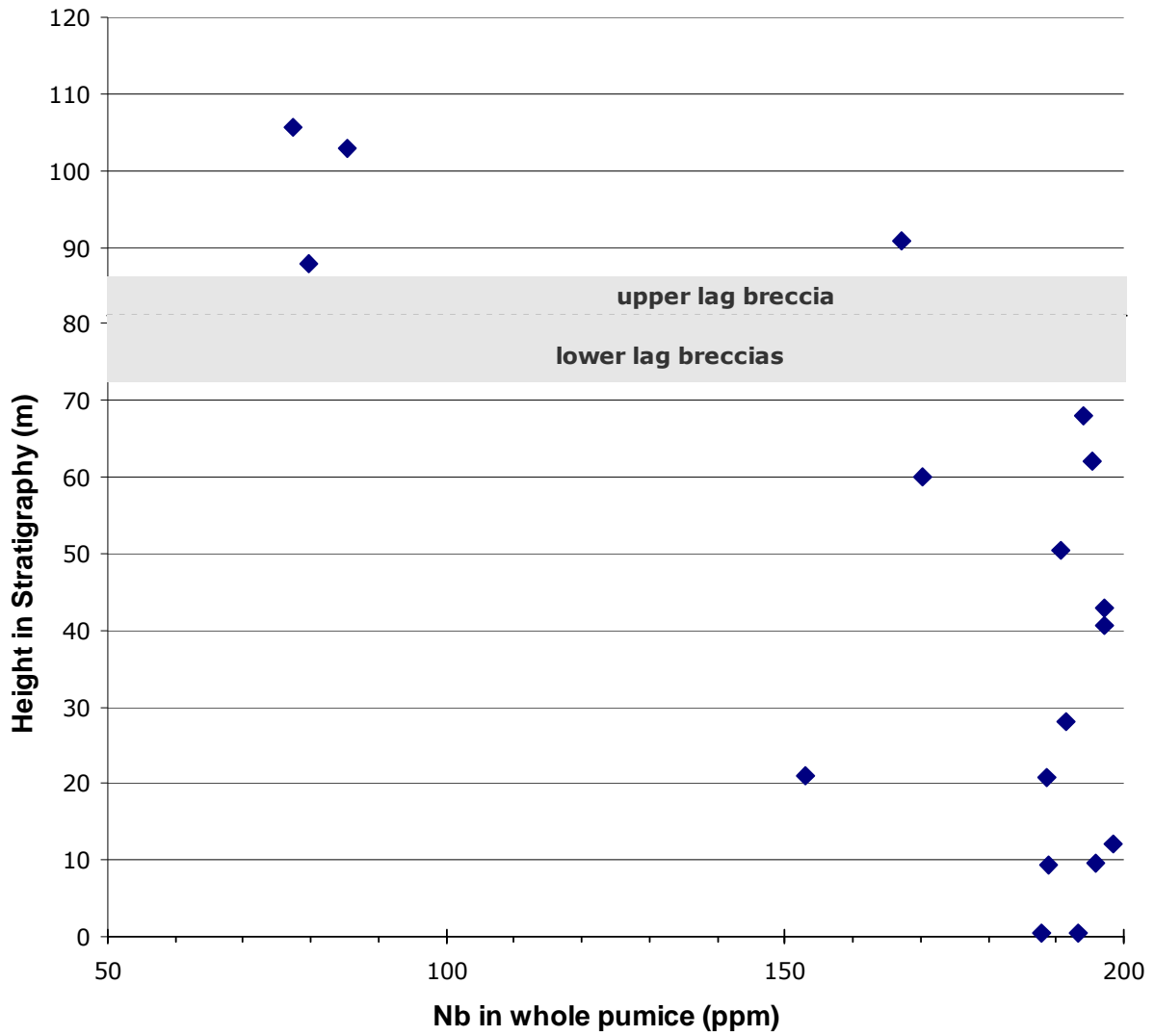


Figure 5.4. Graph showing Nb chemical variations with height in stratigraphy at Cat Mesa A.

CAT MESA B

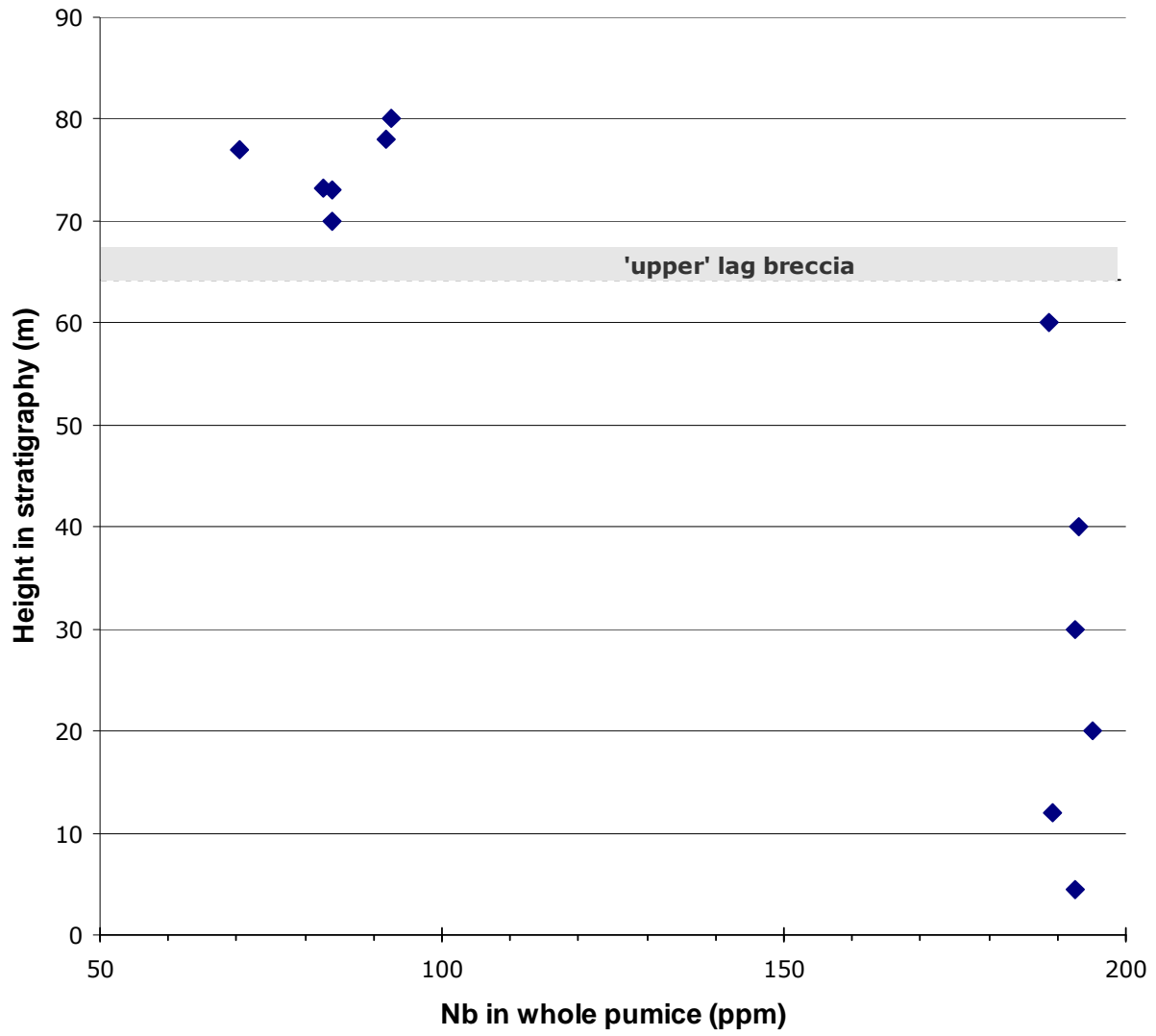


Figure 5.5. Graph showing Nb chemical variations with height in stratigraphy at Cat Mesa B.

WILDCAT CANYON

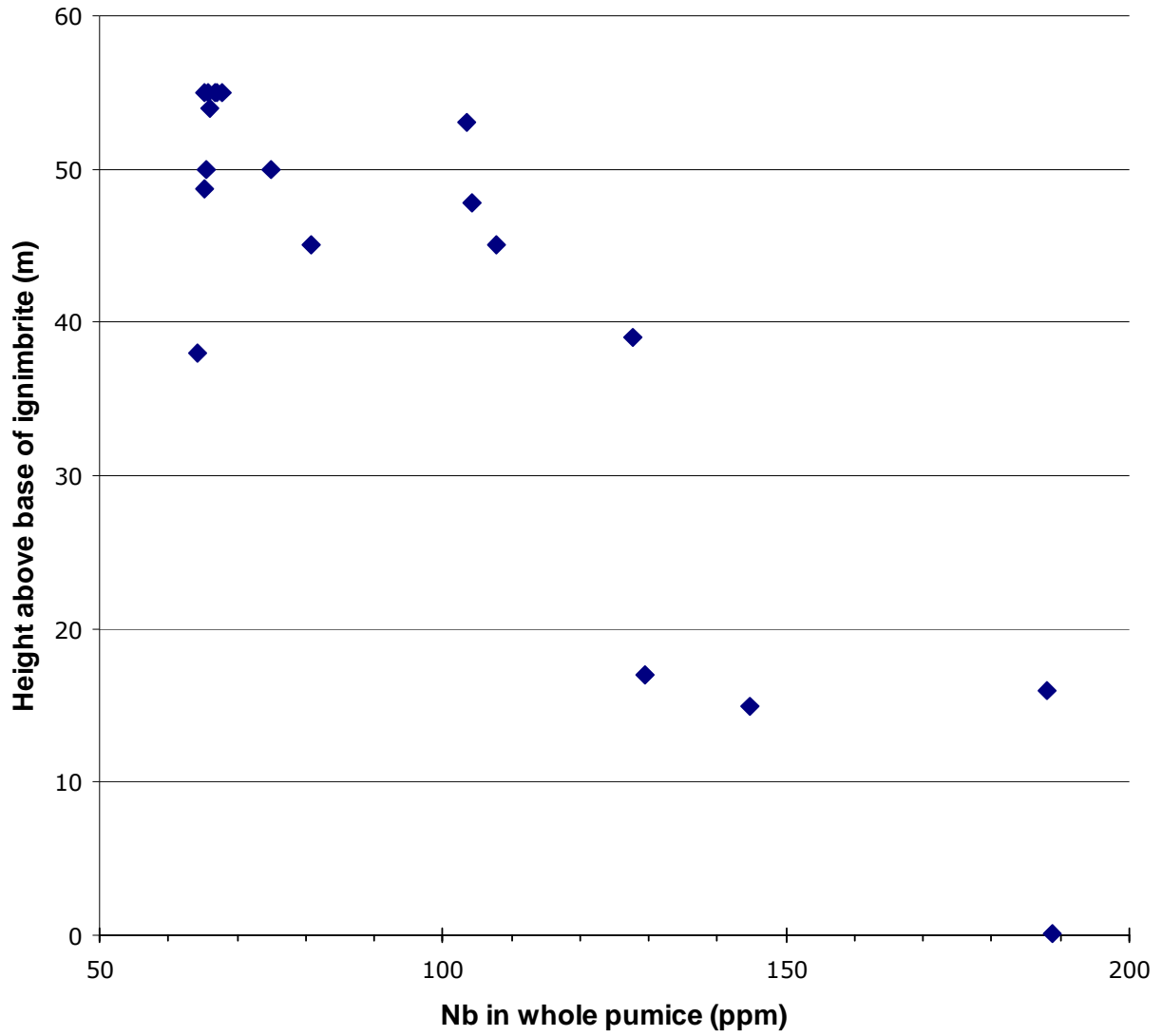


Figure 5.6. Graph showing Nb chemical variations with height in stratigraphy at Wildcat Canyon.

PUEBLO MESA

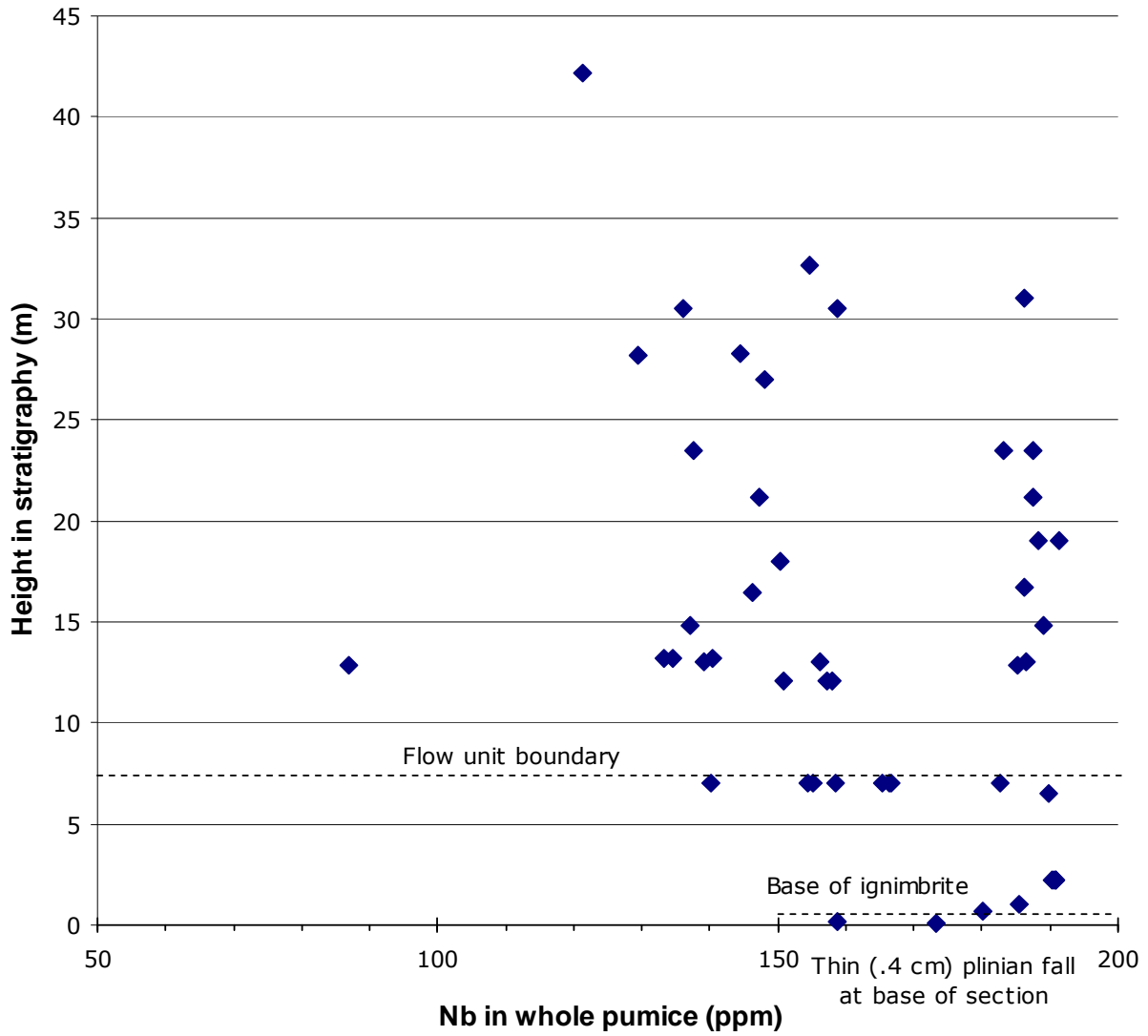


Figure 5.7. Graph showing Nb chemical variations with height in stratigraphy at Pueblo Mesa.

SEVEN SPRINGS

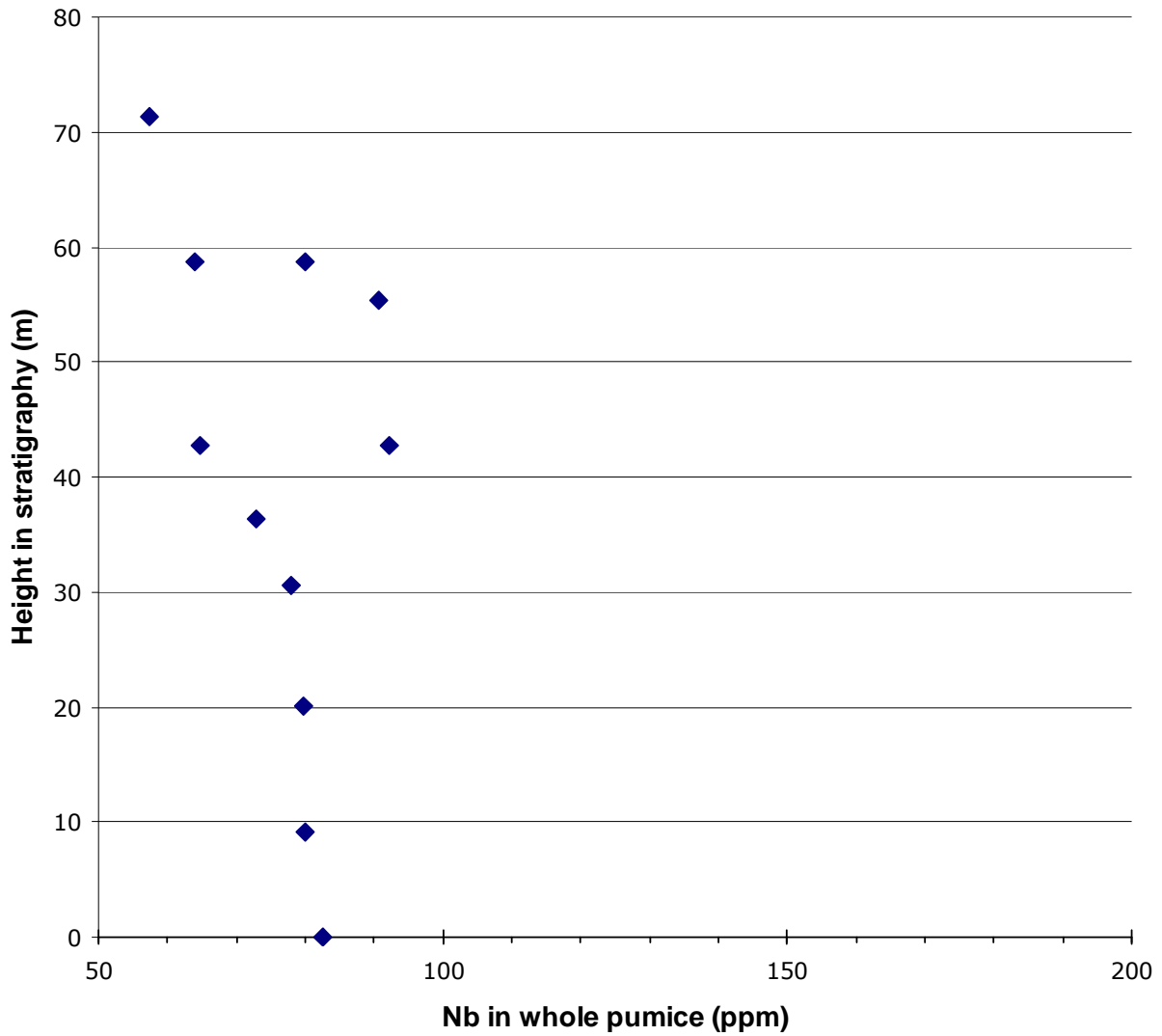


Figure 5.8. Graph showing Nb chemical variations with height in stratigraphy at Seven Springs.

DIXON RANCH (LOCATION 14)

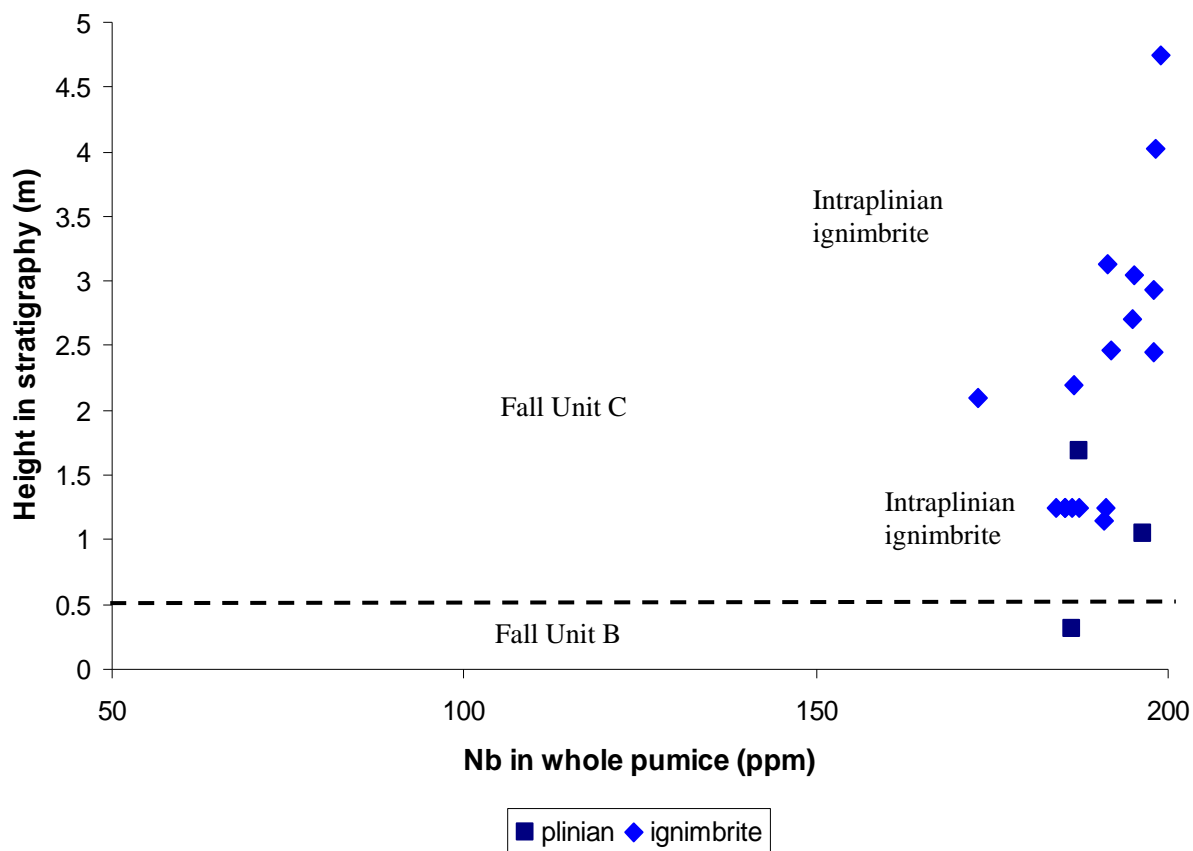


Figure 5.9. Graph showing Nb chemical variations with height in stratigraphy at Dixon Ranch (Location 14).

UPPER COCHITI CANYON

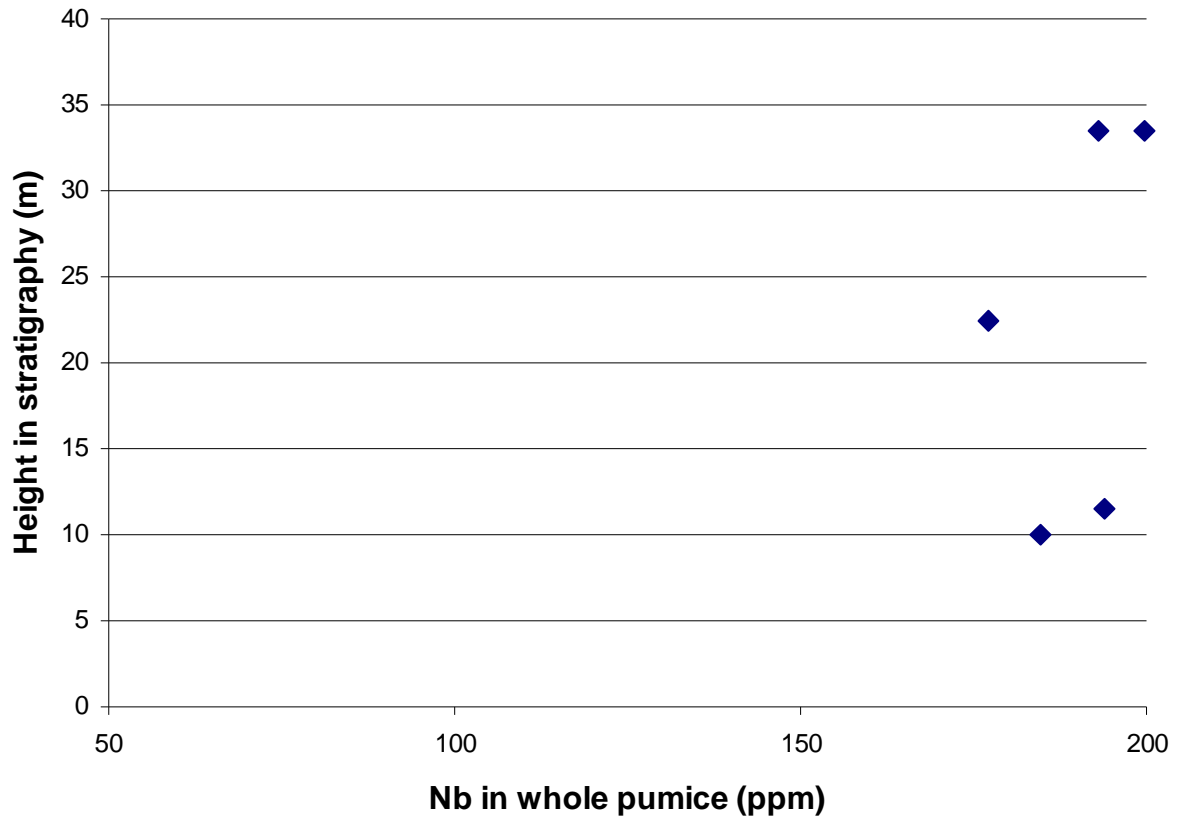


Figure 5.10. Graph showing Nb chemical variations with height in stratigraphy at Upper Cochiti Canyon.

AIRPORT SECTION

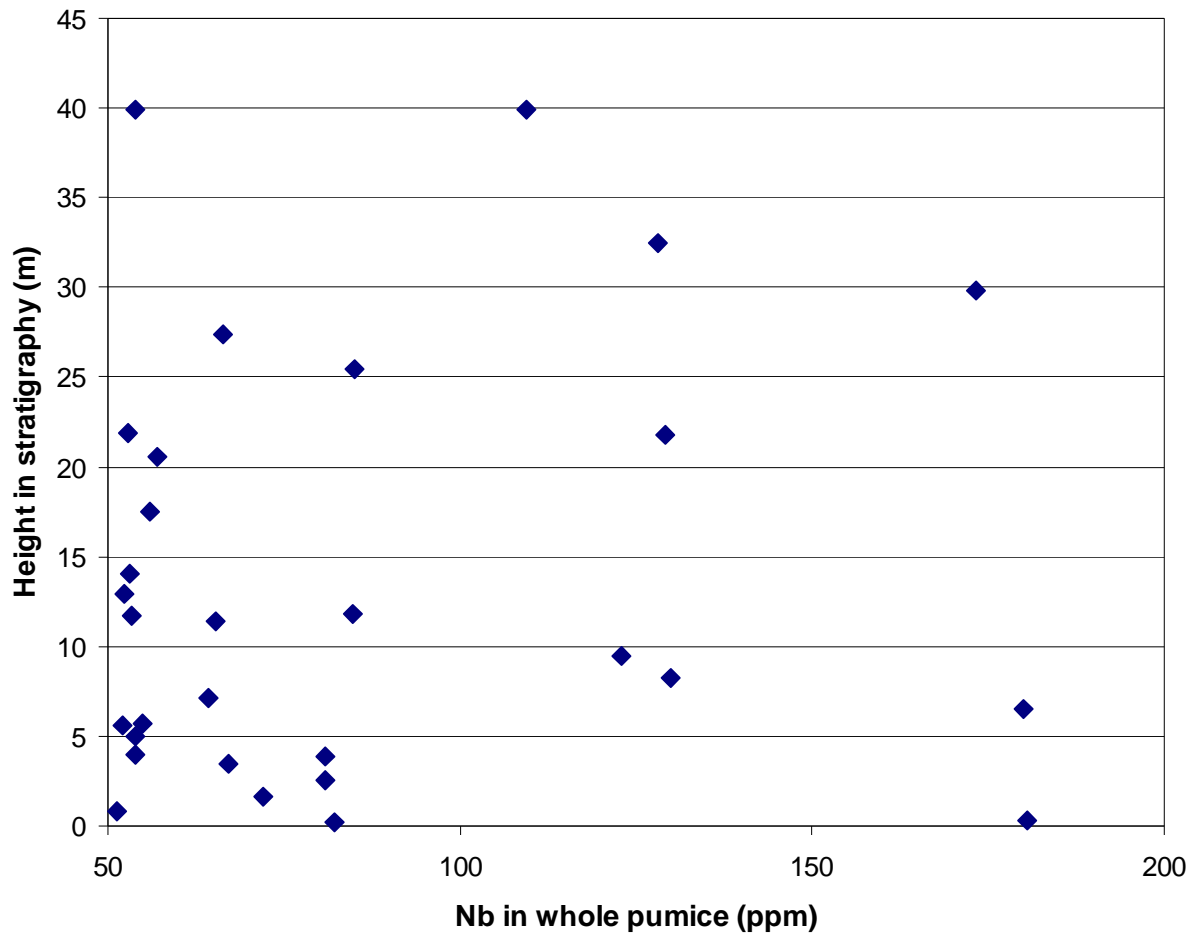
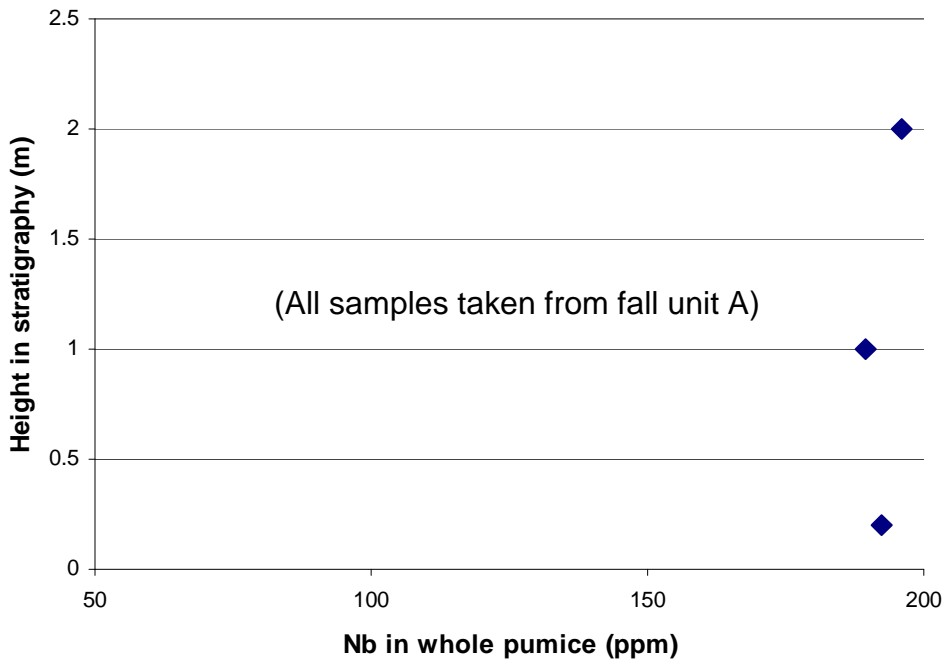


Figure 5.11. Graph showing Nb chemical variations with height in stratigraphy at the Airport Section.

LOCATION 13



LOCATION 27

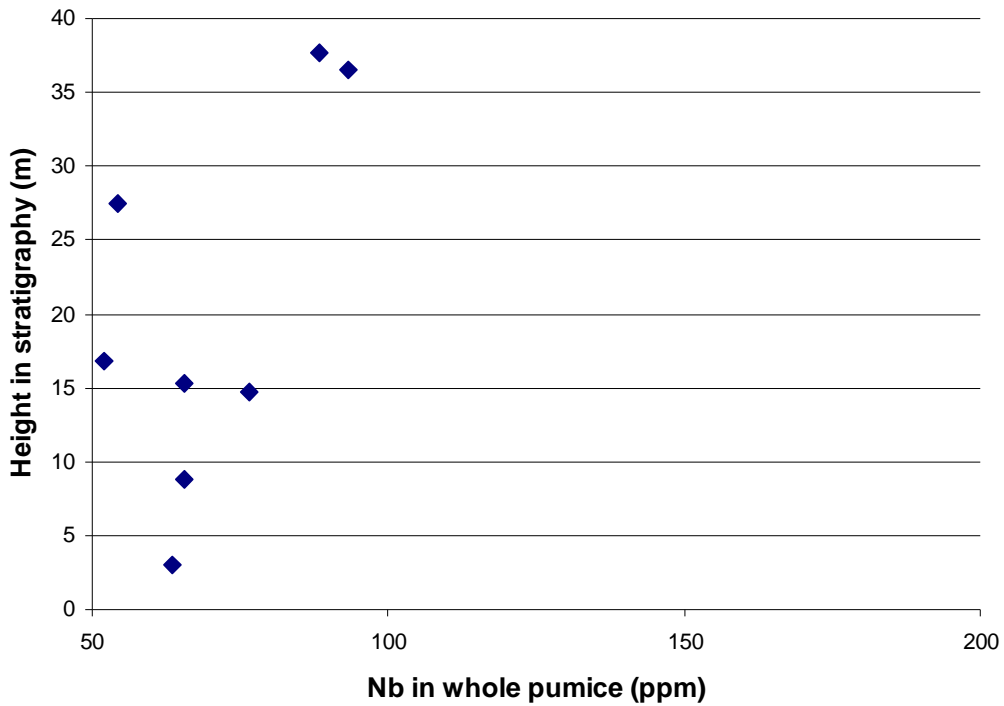


Figure 5.12. Graph showing Nb chemical variations with height in stratigraphy at Locations 13 and 27.

LOCATION 17

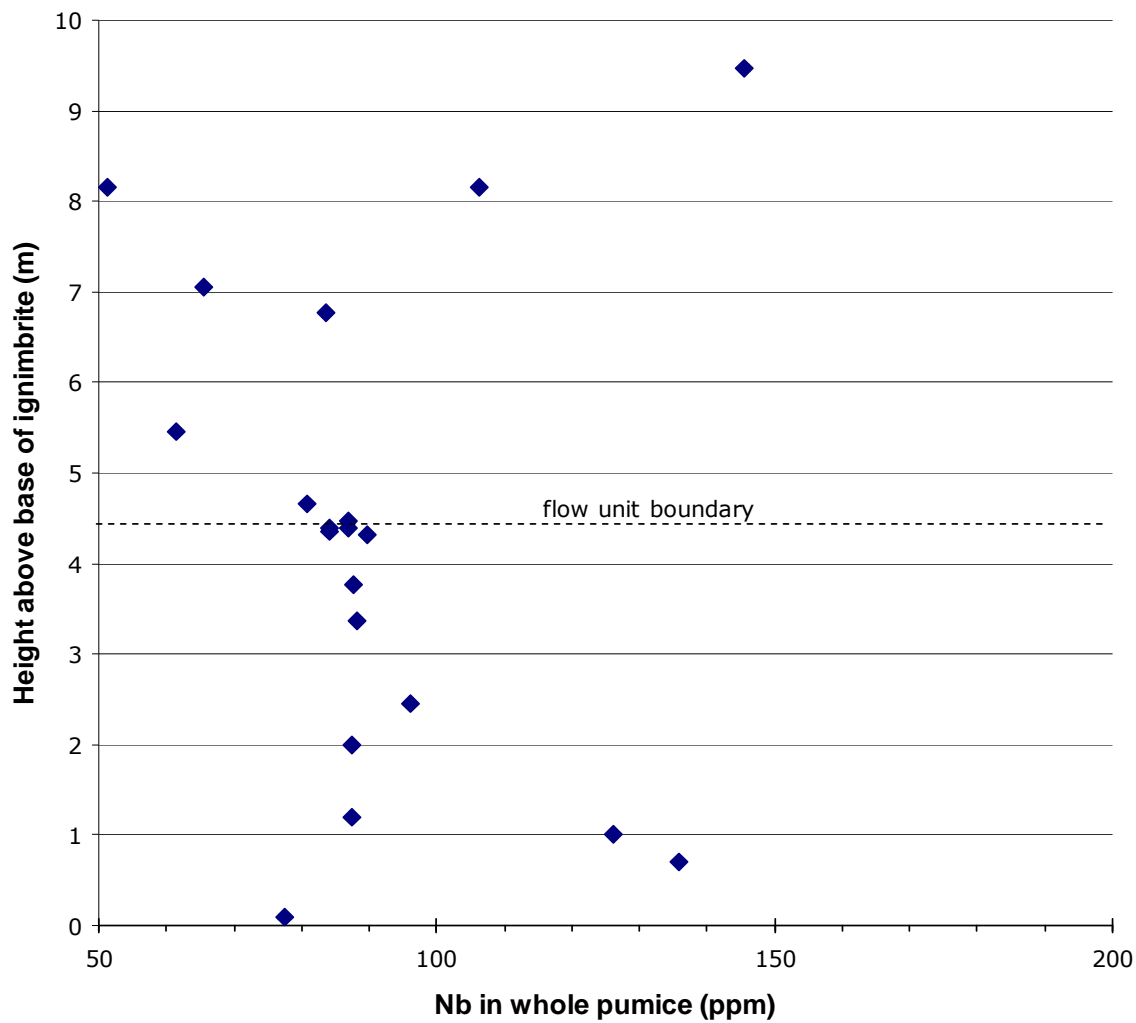


Figure 5.13. Graph showing Nb chemical variations with height in stratigraphy at Location 17.

<u>Locality</u>	Height of section (m)	% of Stratigraphic height = 170-200 ppm Nb	% of Stratigraphic height = 90-170 ppm Nb	% of Stratigraphic height < 90 ppm Nb
Cat Mesa	105.6	71.2	8.3	20.5
Wildcat Canyon	56	41.1	44.6	14.3
Seven Springs	71.3	0	19.6	80.4
Pueblo Mesa	42	7.1	92.9	0
Guaje Canyon	2.25	0	67	33
Airport	39.9	3.8	81.2	15
Upper Cochiti	33.5	100	0	0
Dixon Ranch	2.85	100	0	0

Table 5.1. Proportions of Otowi chemical types expressed as percentages of height in stratigraphy for eight stratigraphic sections from the Otowi ignimbrite.

<u>Area Segment</u>	Total Volume (km³ DRE)	Volume of 170-200 ppm Nb (km³ DRE)	Volume of 90-170 ppm Nb (km³ DRE)	Volume of <90 ppm Nb (km³ DRE)
A	8.8	0.33	7.15	1.32
B	19.9	19.9	0	0
C	18.7	13.31	1.55	3.83
D	4.8	1.97	2.14	0.69
E	38.5	0	7.55	30.95
F	2.5	0	0.49	2.01
G	6.4	0.45	5.95	0
H	1.2	0	0.80	0.40
I	148.6	58.55	50.67	39.38
J	4.4	3.46	0.27	0.67
K	2.5	2.5	0	0
L	10.9	10.9	0	0
M	1.5	0.91	0.31	0.27
Santo Domingo Wedge	3.99	3.42	0.17	0.41
Española Basin Wedge	7.11	0.27	5.77	1.07
 <u>Paleocanyons</u>				
Jemez Plateau	2.96	0.00	0.58	2.38
San Diego	6.05	3.40	1.60	1.05
CC1	0.09	0.06	0.01	0.02
CC2	0.12	0.12	0	0
CC3	0.3	0.12	0	0
Pueblo Mesa (west)	0.25	0.02	0.23	0
Pueblo Mesa (east)	0.57	0.04	0.53	0
 <u>Total (km³ DRE)</u>	290.14	119.7	85.8	84.4
<u>% of Total</u>		41	30	29

Table 5.2. Chart showing volumes (in km³ DRE) and proportions (in %) of chemical types in the Otowi ignimbrite from each area segment used in volume calculations from Chapter 3.

<u>Guaje Cyn.</u> <u>(plinian)</u>	Thickness(m)	% of Stratigraphic height = 170-200 ppm Nb	% of Stratigraphic height = 90-170 ppm Nb	% of Stratigraphic height < 90 ppm Nb
Fall E	0.1	0	50	50
Fall D	0.3	0	100	0
Fall C	0.7	100	0	0
Fall B	1	100	0	0
Fall A	8.5	100	0	0
Total	10.6			

<u>Dixon Ranch</u> <u>(plinian)</u>	Thickness(m)	% of Stratigraphic height = 170-200 ppm Nb	% of Stratigraphic height = 90-170 ppm Nb	% of Stratigraphic height < 90 ppm Nb
Fall E	0	-	-	-
Fall D	0.7	100	0	0
Fall C	0.6	100	0	0
Fall B	0.7	100	0	0
Fall A	0	-	-	-
Total	2			

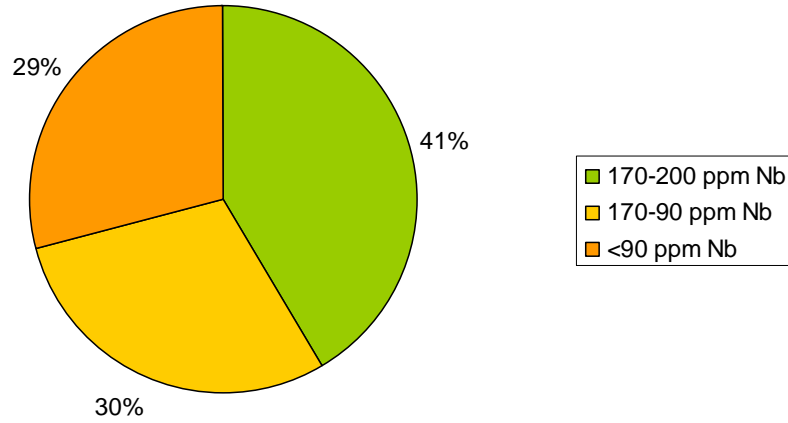
<u>Averaged Plinian</u>	Total Thickness (m)	% of Stratigraphic height = 170-200 ppm Nb	% of Stratigraphic height = 90-170 ppm Nb	% of Stratigraphic height < 90 ppm Nb
Fall E	0.1	0	50	50
Fall D	1	70	30	0
Fall C	1.3	100	0	0
Fall B	1.7	100	0	0
Fall A	8.5	100	0	0
Total	12.6			

Table 5.3. Proportions of Otowi chemical types present in the plinian phase. Data from the Guaje Canyon section and Dixon Ranch section has been averaged to determine overall chemical proportions for each of the five fall units (A-E).

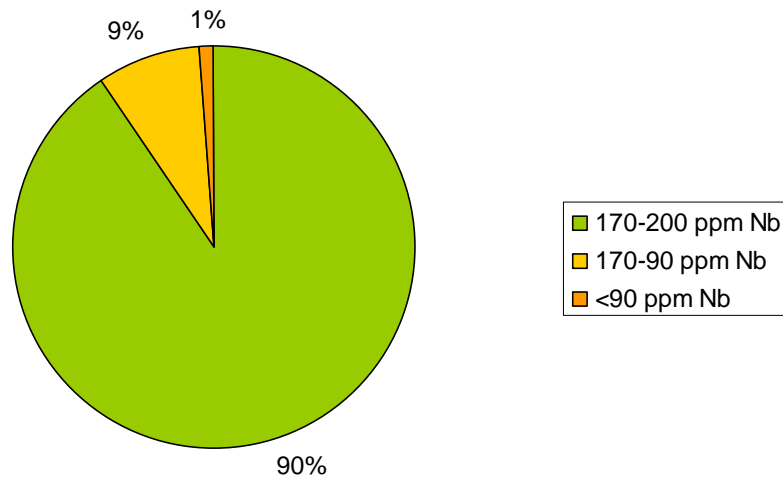
<u>Plinian Unit</u>	<u>Volume (km³ DRE)</u>	<u>Volume of 170- 200 ppm Nb (km³ DRE)</u>	<u>Volume of 90- 170 ppm Nb (km³ DRE)</u>	<u>Volume of <90 ppm Nb (km³ DRE)</u>
Fall unit A	1.2	1.2	0	0
Fall units B-E	44	39.7	3.8	0.5
Total (km³ DRE)	45.2	40.9	3.8	0.5
% of Total		90.5	8.5	1.0

Table 5.4. Chart showing volumes (in km³ DRE) of chemical types in the plinian phase of the Otowi eruption. Note: The total volume used for the Otowi plinian phase is 45.2 km³, as determined in Chapter 3 based on the plinian isopach reconstructions. Volume proportions for individual fall units (B-E) have been determined using stratigraphic sections from Self et al. (1986) and from this study.

**Otowi Ignimbrite
(Fig. 5.14a)**



**Otowi Plinian
(Fig. 5.14b)**



Figures 5.14a and 5.14b. Pie charts showing overall proportions of Otowi chemical types in both the Otowi ignimbrite and plinian phases.

CHAPTER SIX

ERUPTIVE SEQUENCE AND CONCLUSIONS

In this chapter the eruptive sequence for the Otowi Member has been constructed based on the data and conclusions in the preceding chapters and from previous studies. The eruption has been subdivided into five phases. Figures 6.1 through 6.5 are a series of diagrams illustrating the proposed stages and distribution of the eruptive units.

Eruptive Sequence

I. Initial plinian phases: fall units A-C

The Otowi eruption began (Figure 6.1) with a plinian phase that emanated from a vent located roughly in the center of the present-day caldera. A thick pumice fall (fall unit A) was dispersed to the east by the prevailing winds; fall unit A is not found to the southeast of the caldera. Up to 9 meters of predominantly massive and coarse pumice was deposited along a fairly narrow dispersal axis on the Pajarito Plateau, including sampling localities at Guaje Canyon and Location 13. Fall unit A is highly evolved chemically ($\text{Nb} \geq 180$ ppm) and thus was most likely extracted from the upper portion of the zoned Otowi magma chamber. The majority of fall unit A (~6 meters) is massive, and numbers of lithics do not change significantly within the unit. In addition maximum pumice and lithic diameters do not change demonstrably through unit A (Self et al., 1996). This evidence strongly suggests that the eruption column was steady and constant during deposition of fall unit A. Self et al. (1996) proposed a relatively low eruption column of approximately 20 km or less. This was based upon low crystal concentrations (enrichment factor of ~1.0), relatively small maximum grain sizes, and application of the fallout model of Carey and Sparks (1986). The small volume and limited

dispersal area calculated for fall unit A in Chapter 3 support the hypothesis that the early eruptive column was subplinian in nature.

Following deposition of fall unit A, fall units B and C were deposited to the east and southeast of the caldera. The prevailing winds must have shifted during this time as the dispersal axes (Self, 1986) for fall units B and C are oriented more to the southeast than for fall A. The intensity of the eruption increased through deposition of fall units B and C and likely peaked during deposition of fall C. This is based on two lines of evidence: one, crystal enrichment factors (which can indicate the intensity of an eruption) increase significantly through fall units A-C and are then observed to decrease significantly after fall unit C (Self, 1996); two, lithics increase in number significantly in falls B and C, then decrease in number in fall units D and E at Guaje Canyon and at Dixon Ranch.

The increasing intensity of the eruption and increase in numbers of lithics through fall unit C are interpreted to coincide with a sudden vent widening. After fall unit C, numbers of lithics are observed to decrease significantly, and Nb concentrations drop considerably in fall units D and E. A sudden vent widening and a corresponding increase in eruption rates can account for the increase in the proportions of lithics in falls B and C. Additionally, increased eruption rates would result in magma extraction from lower levels in the magma chamber where compositions are more primitive than those erupted in the early stages (fall unit A). As a consequence, following a peak in eruption intensity, Nb concentrations would be expected to decrease in response to the tapping of progressively deeper magmas. This decrease is observed in fall units D and E.

Fine ashes were reported by Self et al. (1996) lying between plinian units B-D at Guaje Canyon and Dixon Ranch. This indicates that deposition of the plinian units B-D was not

necessarily continuous and that slight pauses may have occurred between each fall unit. These ashes are most likely co-ignimbrite ashes.

II. *Plinian column instability: deposition of intraplinian ignimbrites*

The first ignimbrites were deposited concomitantly with fall unit C to the southeast of the caldera in Cochiti Canyon and to the southwest of the caldera at Cat Mesa in Cañon de San Diego (Figure 6.2). These intraplinian ignimbrites have highly evolved compositions (> 180 ppm Nb) and are likely associated with magmas extracted from the upper differentiated portion of the magma chamber. Deposition was heavily influenced by paleotopographic features; specifically, paleocanyons were instrumental in funneling pyroclastic flows (Figure 6.2). At Cochiti Canyon southeast of the caldera, intraplinian flow units associated with high Nb concentrations are exposed between subunits of fall unit C at Dixon Ranch; in the upper portion of Cochiti Canyon ignimbrites with high Nb content (≥ 170 ppm Nb) are also exposed. Southwest of the caldera in the paleo-Cañon de San Diego at Cat Mesa, the lower ignimbrites (from beneath the lag breccia) contain dominantly high Nb content. Additionally, these intraplinian ignimbrites contain Nb concentrations that are consistently higher than those found in fall units D and E. The conclusion is that these flow units are associated with the same evolved magmas that were deposited as the early to middle fall units, and that they were erupted prior to fall units D and E.

A noteworthy lithic trend observed in the intraplinian ignimbrites is that rhyolite lithics are found in abundance and are associated with high Nb concentrations—very similar to the distribution of rhyolite lithics in the plinian deposits. This suggests a single vent operating throughout the plinian phase of the eruption.

The presence of these intraplinian pyroclastic deposits (Figure 6.2) is evidence for instability in the plinian column. Portions of the convecting column collapsed and consequently pyroclastic flows were funneled down paleocanyons in what is present-day Cochiti Canyon and Cañon de San Diego.

III. Lithic lag breccias: evidence for a vent widening and possible timing for caldera collapse

The prominent lithic lag breccias at Cat Mesa and Wildcat Canyon to the southwest of the caldera (Figure 6.3) were previously identified by Self et al. (1986) as evidence for vents shifting to the periphery of the caldera along ring fractures. However, the lithic evidence from this study presented in Chapter 4 does not support a local source for these deposits. In the absence of any evidence for a local vent associated with these lag deposits, several explanations can be invoked to explain their presence.

One, they may simply represent preferential deposition of lithics in paleocanyons brought about by changing depositional conditions. Two, they are associated with a major vent widening event. Increased eruption rates and increased rates of downward coring through the pre-caldera lavas can adequately explain the voluminous lithics at the locality. Furthermore, the conspicuous drop in Nb chemistry at the lag breccias at Cat Mesa can be explained by greater magma extrusion rates brought about by vent widening—deeper and more varied magma compositions were extracted from the magma chamber. The pyroclastic flows associated with this vent widening were violently deposited in the paleo-Cañon de San Diego and the lithic lag breccias are thus more likely associated with depositional processes rather than proximity to a vent.

Three, the lithic lag breccias may potentially indicate the onset of caldera collapse. As the magma chamber depressurized and collapse ensued, new eruptive pathways were formed and magma extrusion rates increased significantly. The lag breccias at Cat Mesa and Wildcat

Canyon and the sudden decrease of Nb chemistry higher in stratigraphy at Cat Mesa are evidence for a significant shift in the eruption; this could possibly be explained by a major change in the vent morphology such as collapse and breakup of the caldera floor. However, lithic proportions stayed the same around the caldera, so it is unlikely that a new vent opened. This fact may damage the argument that caldera collapse began during this phase of the eruption.

IV. Late intraplinian ignimbrites and fall units D-E

At Pueblo Mesa, located to the north of the caldera, Nb chemistry is generally high; consequently, the ignimbrites there were likely deposited concurrently with fall units D and E (Figure 6.4). At Pueblo Mesa, massive flow deposits with varying Nb chemistry were deposited on top of a thin plinian ash layer. These flows, which represent different portions of the magma body, were deposited through paleocanyons on either side of topographic barriers—the Tschicoma dacite domes on the La Grulla Plateau and domes located to the northeast. Also at this time, fall units D and E were deposited to the east and southeast of the caldera (Figure 6.4). Lithic abundances are significantly decreased in these units, and Nb chemistry falls considerably to lower concentrations at the top of fall E. These fall units are thin and poorly exposed, most likely because they have been significantly eroded by overriding pyroclastic flows. At Guaje Canyon, fall unit E, which is composed of pumice, is chemically similar to an ash layer immediately above it and to the overriding ignimbrite; this thin ash may be a co-ignimbrite ash associated with the first ignimbrites deposited in Guaje Canyon.

V. Main deposition of ignimbrites

The ignimbrites at Guaje Canyon contain pumice dunes at their base which suggests that they were violently emplaced soon after deposition of fall E and the ash overlying fall E. These ignimbrites show moderate variability in Nb concentrations. In addition, they exhibit a unique

lithic signature that may imply a local source. At this locality, an unusual abundance of welded tuff lithics are found within the ignimbrite. These lithics are weathered, and densely-welded, and do not appear similar to Otowi ignimbrite—it is unlikely that they represent remobilized Otowi flows.

The presence of weathered ignimbrite lithics at Guaje Canyon may be significant for multiple reasons. First, it may provide a more plausible timing for the onset of caldera collapse. The change in lithic signature and the chemically incoherent ignimbrites that erupted in Guaje Canyon could signify the onset of collapse and subsequent voluminous eruption of ignimbrites with heterogeneous composition.

Second, as it is a unique lithic signature not observed elsewhere, it supports the hypothesis that at least one new vent opened up to the northeast of the caldera late in the eruption sequence. Certainly, a vent shift is plausible at this time, particularly if it occurred concurrently with the onset of collapse.

If caldera collapse did occur at this point in the eruption, the preferred scenario is a significant increase in eruption rate with associated widening of the vent followed by depressurization of the magma chamber and the onset of caldera collapse. Collapse was complicated: prior studies (Nielson and Hulen, 1984); Heiken et al., 1986) have shown that the caldera floor is asymmetric to the southeast which suggests a trapdoor-type collapse. Additionally, during collapse the caldera floor was likely broken into numerous fragments in a piecemeal-style collapse. The inconsistent nature of the collapse likely provided new pathways for magmas to reach the surface and thus allowed for larger quantities of magmas to be erupted as the main, voluminous Otowi ignimbrites observed around the JMVF.

In this stage (Figure 6.5), wholesale deposition of pyroclastic flows ensued around the caldera. At Cat Mesa the upper, more primitive composition pyroclastic deposits were emplaced. Nearby, at Wildcat Canyon weakly zoned pyroclastic flows that correlate stratigraphically with the upper portion of Cat Mesa were deposited around the same time.

Caldera collapse and chaotic breakup of the intracaldera floor was likely responsible for the removal of topographic barriers to the northwest and northeast. With these barriers removed, the thick Otowi ignimbrites found on the Jemez Plateau were funneled out of a breach in the northwest wall of the caldera and into a fairly deep paleocanyon co-located approximately with present-day Cebolla Canyon and the Seven Springs/Fenton Lake area. The ignimbrites are different in this region from other Otowi ignimbrites—they are thick, have comparatively low Nb concentrations, and they are densely welded. Simultaneous opening of the large central vent and the onset of caldera collapse can explain the voluminous nature of the Jemez Plateau ignimbrites. Furthermore, their low Nb chemistry suggests that they were derived from deeper portions of the magma chamber. A consequence of this is that they were likely at a higher temperature when erupted. This may explain why the Otowi ignimbrites on the Jemez Plateau are so densely welded—they were thicker and hotter when deposited and thus were more susceptible to post-depositional welding.

At the same time, pyroclastic flows likely spilled out onto the Pajarito Plateau, depositing massive ignimbrite thicknesses. At the Airport Section, Location 17, and Guaje Canyon tuffs show variable Nb concentrations and are indicative of a heterogeneous magma source erupted from the vent system.

Number of eruptive vents

The lithic data from this study strongly support a single vent hypothesis for the majority of the duration of the Otowi eruption. There is noteworthy uniformity in the distributions and numbers of lithics between sampling localities from around the caldera. No compelling evidence exists to suggest a local source for lithics at any of the localities except for the welded ignimbrite lithics at Guaje Canyon. In addition, the best evidence for earlier vent migration—the lithic lags at Cat Mesa and Wildcat Canyon—has been questioned based on the comparison of dacite lithic lithologies.

Consequently, there is no hard evidence to support the hypothesis that the Otowi eruption transitioned from a large central vent to numerous ring vents as was illustrated in Self et al., 1986. Potter and Oberthal (1987) proposed as many as seven ring vents based on their lithic study and determination of flow directions from pumice orientations. However, the lithic work conducted in this study is far more comprehensive for a variety of reasons: significantly greater numbers of lithics (3.5 times) were counted and the sampling techniques were improved; the pre-Otowi geology is now much better understood; lithologic identifications of fragments were more accurate (as explained in Chapter 4); and perhaps most importantly, the lithic data has been supported with chemical data from the host tuff. Therefore, the conclusions from this study represent an improvement over those of Potter and Oberthal (1987). In their reply to the conclusions of Potter and Oberthal (1987), Self and Turbeville (1987) pointed out that the flow directions and distributions of lithics reported by Potter and Oberthal could just as easily have been produced by an eruption from a central vent. The results from this study validate that statement. The exception is the pulse of welded ignimbrite lithics at Guaje Canyon, which represent one piece of evidence for at least some type of vent shift in the later stages of the

eruption sequence. This shift most likely took place after caldera collapse ensued later in the eruption. However, the lithic evidence is not sufficient to determine the numbers of new vents formed.

Conclusions

Three significant conclusions are derived from this study. First, the minimum calculated total volume of the Otowi plinian and ignimbrite deposit (335 km^3 DRE) represents a significant improvement on prior volume calculations, and is considerably greater than previously thought (Smith and Bailey, 1966). Furthermore, as it is a solid minimum estimate, it suggests that the actual erupted volume for the Otowi Member could be greater than 500 km^3 . The plinian/distal ash reconstruction (45.2 km^3 DRE) is admittedly a rough estimate and will undoubtedly continue to be refined in the future; however, the overall number validates the volumes reported by Self et al. (1996).

Second, the 1.61 Ma Otowi Member of the Bandelier Tuff most likely emanated from a central vent for the majority of the duration of the eruption. Several flaring or widening events are supported by the lithic and chemical data both in the plinian and ignimbrite, but evidence does not support a major shift from a central vent to numerous ring-fault vents. Prior evidence (Self et al., 1986; Potter and Oberthal, 1987) for multiple ring-vents has been questioned based on the lithic and supporting chemical data from this study. There is some data, however, that suggests that new vents may have opened during the late stages of the eruption, thus producing the more unique lithic signature at Guaje Canyon. Additionally, two features present in the eruption sequence—the lag breccias at Cat Mesa earlier in the eruption and the shift in lithic proportions at Guaje Canyon later in the eruption—have been identified as potential timing

events for caldera collapse. Based on the evidence, it appears that the latter is the more likely candidate.

Third, a tri-part distribution of chemical types is present in the Otowi ignimbrite, including an evolved (> 180 ppm Nb), intermediate (90-170 ppm Nb), and primitive (< 90 ppm Nb) component. The proportions of these three types are in roughly equal quantities (41%, 30%, and 29% respectively). Volume-constrained chemical data are useful to petrogenetic studies and may thus prove extremely useful in future geochemical investigations on the Otowi Member.

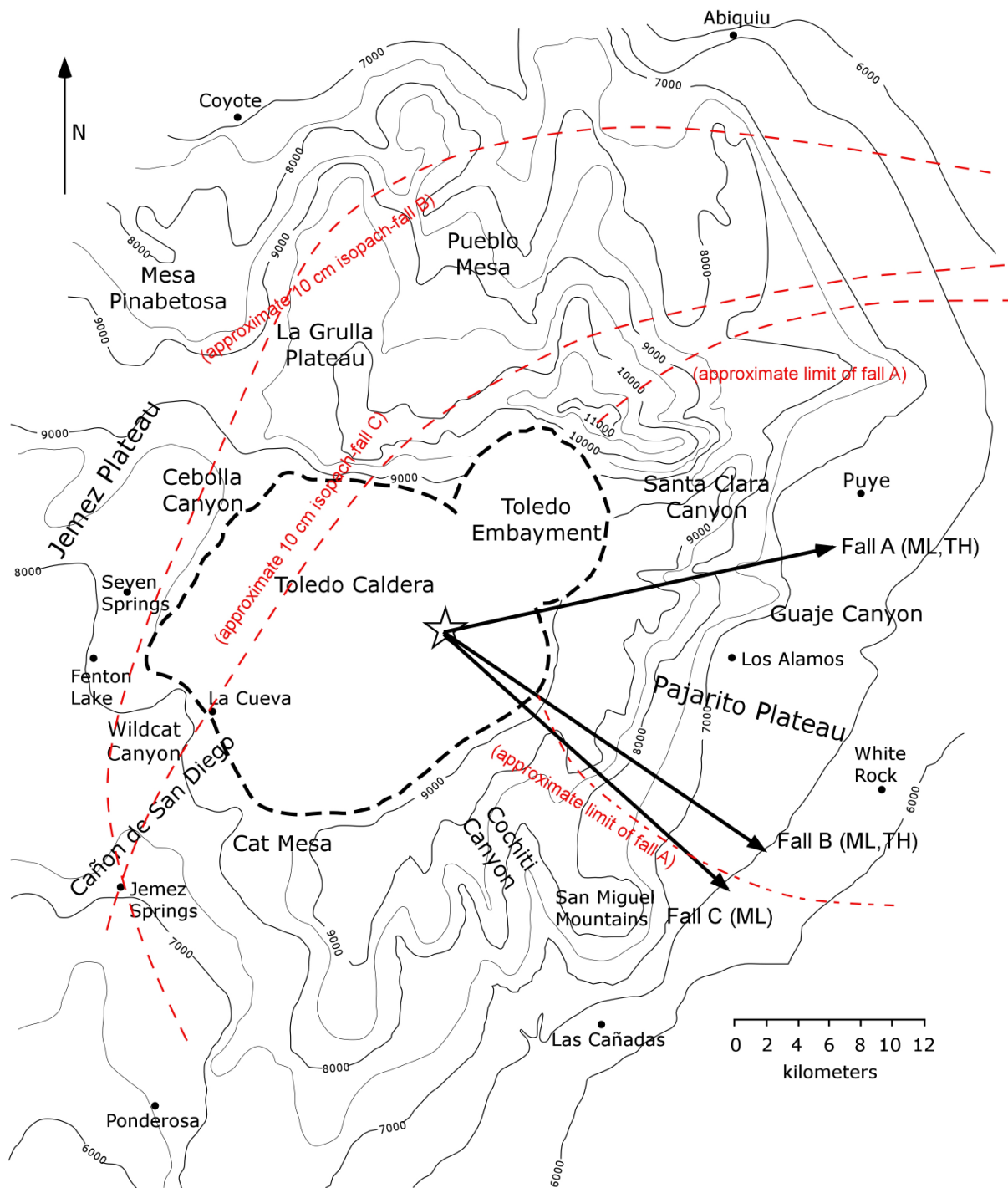


Figure 6.1. Eruptive sequence stage one: Initial plinian emanated from a vent (denoted with star) and was deposited to the east-southeast of the caldera by the prevailing winds as fall units A-C. Vent location, plinian dispersal axes (black arrows) and 10 cm plinian isopachs are from Self et al. (1986). The diagram shows that Fall unit A was dispersed in a more easterly direction and is not found to the southeast of the caldera; fall units B and C were deposited across a wider region than fall unit A as indicated by their dispersal axes and thicknesses around the caldera. Contour interval = 500 ft; contour data from Potter and Oberthal (1987)

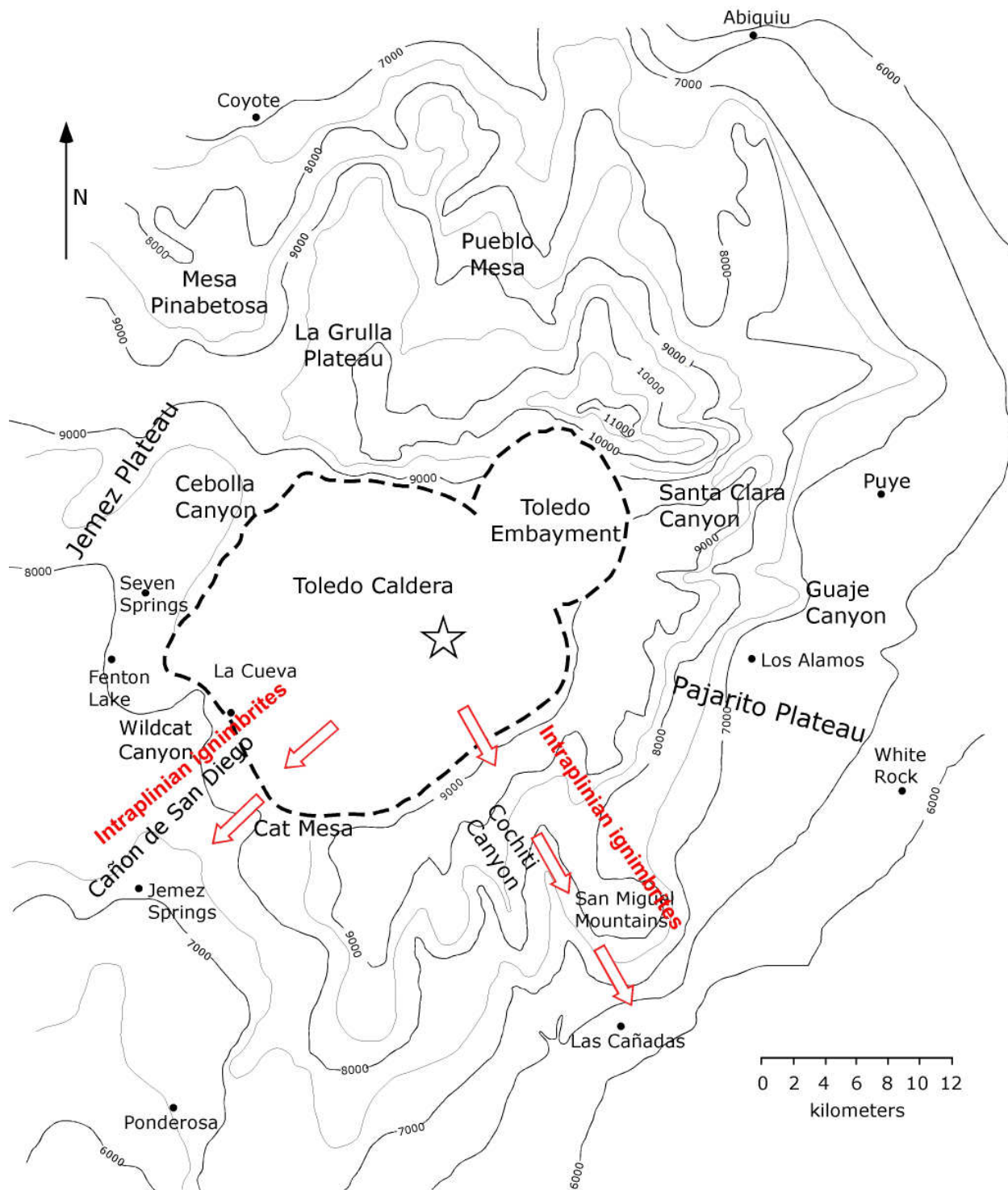


Figure 6.2. Eruptive sequence stage two: Instability in the plinian column leads to partial collapse, which deposits intraplinian pyroclastic flows in Cochiti Canyon to the southeast of the caldera and Cañon de San Diego in the southwest. Vent location (star) remains the same. Contour interval = 500 ft; contour data from Potter and Oberthal (1987)

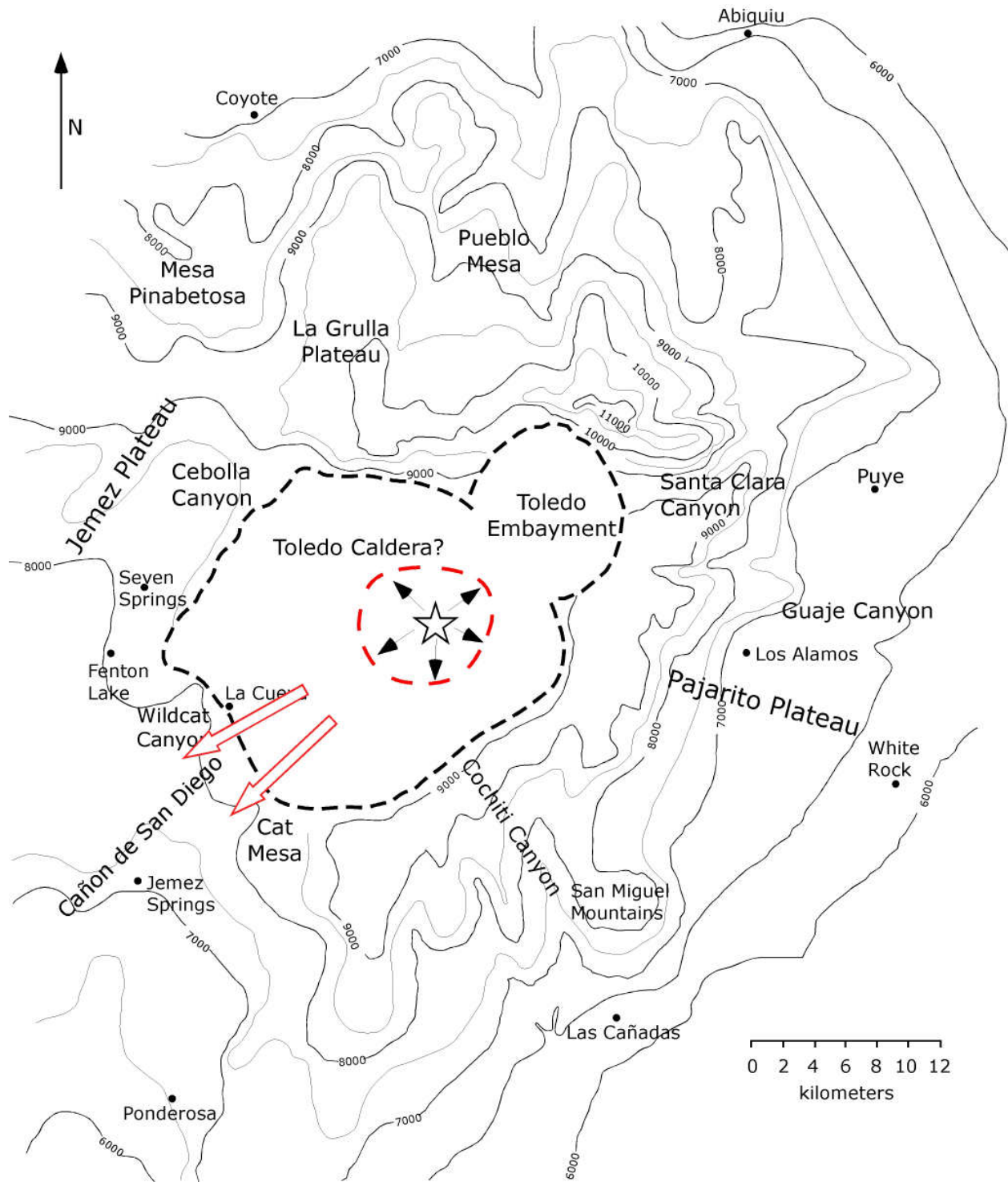


Figure 6.3. Eruptive sequence stage three: Vent widening and potential onset of caldera collapse results in an increased eruption rate. Increase in eruption rate is recorded by an increase in lithic abundance and later decrease in Nb chemistry at Cat Mesa. Lithic lag breccias are deposited at Cat Mesa and Wildcat Mesa as density currents within pyroclastic flows at the bottom of deep paleocanyons. Contour interval = 500 ft; contour data from Potter and Oberthal (1987)

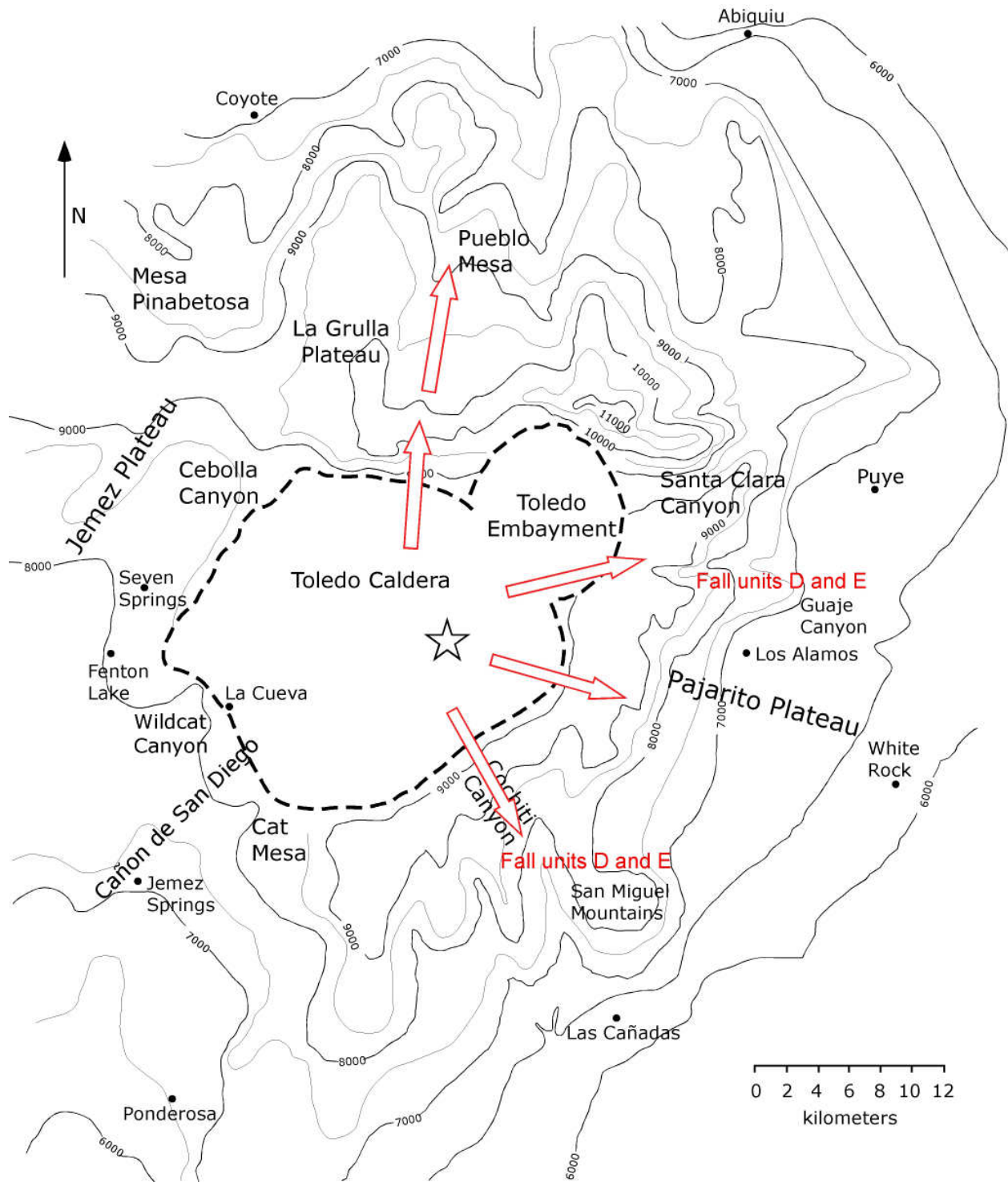


Figure 6.4. Eruptive sequence stage four: In this stage, ignimbrites are deposited at Pueblo Mesa to the north of the caldera. Plinian deposition of fall units D and E continues following deposition of fall units A-C and intraplinian ignimbrites. Contour interval = 500 ft; contour data from Potter and Oberthal (1987)

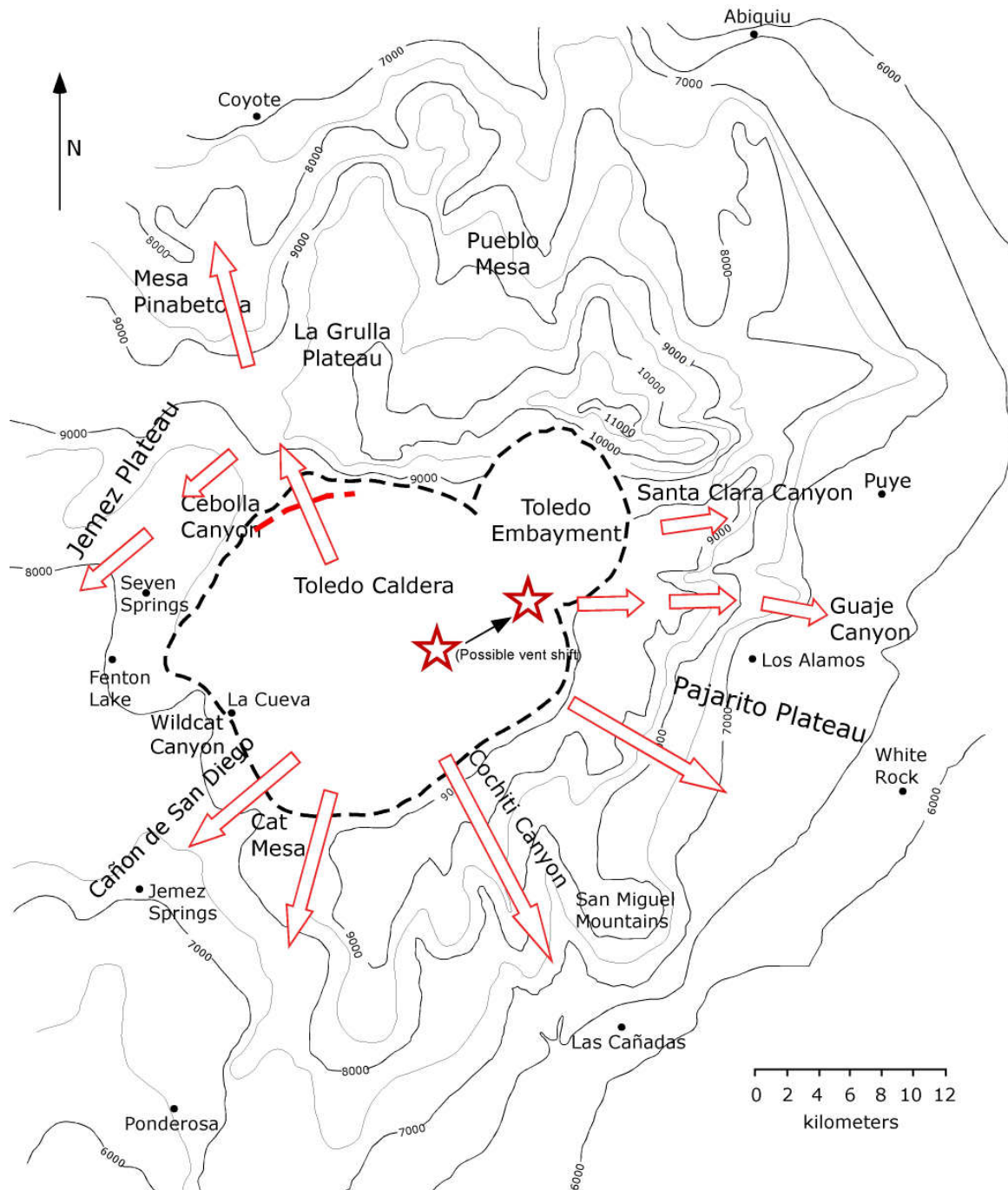


Figure 6.5. Eruptive sequence stage five: The possible onset of caldera collapse allows for greater quantities of magma to be erupted. The majority of pyroclastic flows are deposited around the caldera during this stage. Removal of topographic barriers to the northwest (red dashed line) allows voluminous pyroclastic flows to travel down a large paleocanyon in what is now the Jemez Plateau; to the northeast pyroclastic flows are funneled down Santa Clara Canyon and Guaje Canyon. A vent shift may have occurred during this stage, as indicated on the diagram. Contour interval = 500 ft; contour data from Potter and Oberthal (1987)

REFERENCES

- Aldrich, M.J. and Laughlin, A.W., 1984. A Model for the Tectonic Development of the Southeastern Colorado Plateau Boundary. *Journal of Geophysical Research* **89**, 10,207-10,218.
- Aldrich, M.J., Chapin, C.E. and Laughlin, A.W., 1986. Stress history and tectonic development of the Rio Grande rift, New Mexico. *Journal of Geophysical Research* **91**, 6199-6211.
- Aldrich, M.J., and Dethier, D., 1990. Stratigraphic and tectonic evolution of the northern Espanola Basin, Rio Grande Rift, New Mexico. *Geological Society of America Bulletin*, **102**, 1695-1705.
- Aramaki, S., 1984. Formation of the Aira caldera, southern Kyushu, ~ 22,000 years ago. *Journal of Geophysical Research* **89**, 8485-8501.
- Bailey, R.A., Smith, R.L., and Ross, C.S., 1969. Stratigraphic nomenclature of volcanic rocks in the Jemez Mountains, New Mexico, *USGS Bulletin* **1274-P**, 19 p.
- Baldrige, W.S., Damon, P.E., Shafiqullah, M., and Bridwell, R.J., 1980. Evolution of the central Rio Grande rift, New Mexico: new potassium-argon ages. *Earth and Planetary Science Letters* **51**, 309-321.
- Bemmelen, R.W. Van, 1929. Het Caldera probleem. *De Mijningénieur* **4**.
- Bemmelen, R.W. Van, 1939. The volcano-tectonic origin of Lake Toba (north Sumatra). *Ing. Ned. Indie* **6**, 126-140.
- Boyd, F.R., 1961. Welded Tuffs and Flows in the Rhyolite Plateau of Yellowstone Park, Wyoming. *Geological Society of America Bulletin* **72**, 387-426.
- Branney, M.J. and Kokelaar, P., 1994. Volcanotectonic faulting, soft-state deformation, and rheomorphism of tuffs during development of a piecemeal caldera, English Lake District. *Geological Society of America Bulletin* **106**, 507-530.
- Branney, M.J., 1995. Downsag and extension at calderas: New perspectives on collapse geometries from ice-melt, mining and volcanic subsidence. *Bulletin of Volcanology* **57**, 303-318.
- Branney, M.J. and Gilbert, J.S., 1995. Ice-melt collapse pits and associated features in the 1991 lahar deposits of Volcán Hudson, Chile: criteria to distinguish eruption-induced glacial melt. *Bulletin of Volcanology* **57**, 293-302.

- Brookins, D. and Laughlin, A.W., 1983. Rb-Sr geochronological investigation of Precambrian samples from deep geothermal drill holes, Fenton Hill, New Mexico. *Journal of Volcanology and Geothermal Research*, **15**, 43-58.
- Broxton, D. and Reneau, S., 1995. Stratigraphic nomenclature of the Bandelier Tuff for the restoration project at Los Alamos National Laboratory. Los Alamos National Laboratory, Report **LA-13010-MS**, 21 p.
- Broxton, D. and Reneau, S., 1996. Buried early Pleistocene landscapes beneath the Pajarito Plateau, Northern New Mexico. In: Goff, F., Kues, B.S., Rogers, M.A., McFadden, L.D., and Gardner, J.N., (eds) *The Jemez Mountains Region. New Mexico Geological Society 47th Field Conference Guidebook*, 325-334.
- Browne, B.L. and Gardner, J.E., 2004. The nature and timing of caldera collapse as indicated by accidental lithic fragments from the AD ~ 1000 eruption of Volcán Ceboruco, Mexico. *Journal of Volcanology and Geothermal Research* **130**, 93- 105.
- Bryan, K., 1938. Geology and Groundwater conditions of the Rio Grande depression in Colorado and New Mexico, p. 197-225 in Regional Planning, Pt. 6, Upper Rio Grande: Washington, National Resources Commission, v. 1, pt. 2, sec. 1.
- Buch, L. Von, 1820. Über Die Zusammensetzung der basaltischen Inseln und über Erhebungskrater. Kg. Preuss. Akad. Wiss. Berlin, 51-68.
- Burbank, W.S., 1933. Vein systems of the Arrastre Basin and regional geologic structure in the Silverton and Telluride quadrangles, Colorado. *Colorado Scientific Society Proceedings* **13**, 135-214.
- Chapin, C.E., 1971, The Rio Grande Rift, Part 1: Modifications and Additions: New Mexico Geological Society, **22nd** Field Conference Guidebook, 191-202.
- Chapin, C.E. and Seager, W.R., 1975. Evolution of the Rio Grande rift in the Socorro and Las Cruces areas. New Mexico Geological Society Guidebook **26**, 297-391.
- Chapin, C.E., and Elston, W.E., 1979. Introduction. In: Chapin, C.E. and Elston, W.E. (Eds) *Ash-flow tuffs: Geological Society of America, Special Papers* **180**, 1-4.
- Chamberlin, R.M., 2007. Evolution of the Jemez Lineament: connecting the volcanic “dots” through late Cenozoic time. New Mexico Geological Society Guidebook **58**, 80-82.
- Chamberlin, R.M., Pazzaglia, F., Wegmann, C., and Smith, G.A., 1999. Preliminary geologic map of the Loma Creston Quadrangle, Sandoval County, New Mexico. New Mexico Bureau of Mines and Mineral Resources Map **OF-DM-25**, scale 1:24,000.

- Chester, D.K., Duncan, A.M., Guest, J.E., and Kilburn, C.R.J., 1985. *Mount Etna, the anatomy of a volcano*: Stanford, California, Stanford University Press, 404 p.
- Clough, C.T., Mauff, H.B. and Bailey, E.B., 1909. The cauldron subsidence of Glen Coe, and the associated igneous phenomena. *Geological Society of London Quarterly Journal* **65**, 611-678.
- Cole, J.W., Brown, S.J.A., Burt, R.M., Beresford, S.W., Wilson, C.J.N., 1998. Lithic types in ignimbrites as a guide to the evolution of a caldera complex, Taupo volcanic centre, New Zealand. *Journal of Volcanology and Geothermal Research* **80**, 217-237.
- Cole, J.W., Milner, D.M., and Spinks, K.D., 2005. Calderas and caldera structures: a review. *Earth Science Reviews* **69**, 1-26.
- Cordell, L., 1982. Extension in the Rio Grande Rift. *Journal of Geophysical Research* **87**, 8561-8569.
- Dalrymple, G.B., Cox, A., Doell, R.R., and Grommé, C., 1967. Pliocene geomagnetic polarity epochs. *Earth and Planetary Science Letters* **2**, 163-173.
- Daly, R.A., Iddings, J.P., and Lindgren, W., 1914. *Igneous rocks and their origin*. Xxii: New York, McGraw-Hill, 563 p.
- Daly, R.A., 1933. *Igneous rocks and the depths of the earth; containing some revised chapters of "Igneous rocks and their origin" (1914)*. Xvi: New York, McGraw-Hill, 508 p.
- De Beaumont, J.B.E., 1837. From a memoir on the origin of Mt. Etna. *American Journal of Science and Arts* **31**, 168-170.
- Dethier, D.P., Aldrich, M.J., and Shafiquallah, M., 1986. New K-Ar ages for Miocene volcanic rocks from the northeastern Jemez Mountains and Tejana Mesa, New Mexico. *Isochron West* **47**, 12-14.
- Dethier D.P., and Aldrich, M.J., 1988. Late Cenozoic rates of erosion in the western Espanola basin, New Mexico; evidence from geologic dating of erosion surfaces. *Geological Society of America Bulletin* **100**, 927-937.
- Diller, J.S. and Patton, H.B., 1902. Geology and petrology of Crater Lake National Park. *United States Geological Survey Professional Paper* **3**, 167 pages.
- Doell, R.R. and Dalrymple, G.B., 1966. Geomagnetic polarity events- A new polarity event and the age of the Brunhes-Matuyama boundary. *Science*, **152**, 1060-1061.

- Doell, R.R., Dalrymple, G.B., Smith, R.L., and Bailey, R.A., 1968. Paleomagnetism, potassium-argon ages, and geology of rhyolites and associated rocks of the Valles caldera, New Mexico. *Geological Society of America Memoir*, **116**, 211-248.
- Druitt, T.H. and Sparks, R.S.J., 1984. On the formation of calderas during ignimbrite eruptions. *Nature* **310**, 679-681.
- Duecker, K., Yuan, H., and Zurek, B., 2001. Thick-structured Proterozoic lithosphere of the Rocky Mountain Region. *GSA Today* **11**(12), 4-9.
- Dunbar, N.W., and Hervig, R.L., 1992a. Petrogenesis and volatile stratigraphy of the Bishop Tuff: Evidence from melt inclusion analysis. *Journal of Geophysical Research* **97**, 15,129-15,150.
- Dunbar, N.W., and Hervig, R.L., 1992b. Volatile and trace element composition of melt inclusions from the lower Bandelier Tuff: implications for magma chamber processes and eruptive style. *Journal of Geophysical Research* **97**, 15,151-15,170.
- Duncker, K.E., Wolff, J.A., Harmon, R.S., Leat, P.E., Dickin, A.P and Thompson, R.N., 1991. Diverse mantle and crustal components in lavas of the NW Cerros del Rio volcanic field, Rio Grande Rift, New Mexico. *Contributions to Mineralogy and Petrology* **108**, 331-345.
- Dungan, M.A., Muehlberger, W.R., Leininger, L., Peterson, C., McMillan, N.J., Gunn, G., Lindstrom, M., and Haskin, L., 1984. Volcanic and Sedimentary Stratigraphy of the Rio Grande gorge and the late Cenozoic geologic evolution of the southern San Luis valley. *New Mexico Geological Society 35th Field Conference Guidebook*, 157-178.
- Dutton, C.E., 1884. Hawaiian Volcanoes, in *Fourth Annual Report, U.S. Geological Survey, Washington D.C.*, 75-219.
- Eichelberger, J.C., and Koch, F.G., 1979. Lithic fragments in the Bandelier Tuff, Jemez Mountains, New Mexico. *Journal of Volcanology and Geothermal Research*, **5**, 115-134.
- Escher, B.G., 1929. On the formation of calderas. *Leidsche Geol. Meded.*, **3**, 183-219
- Fenner, C.N., 1920. The Katmai region, Alaska, and the great eruption of 1912. *Journal of Geology* **28**, 569-606.
- Fouqué, F., 1879. Santorin et ses eruptions. Masson, Paris, 39 + 440 pp.
- Galusha, T., and Blick, J.C., 1971. Stratigraphy of the Santa Fe Group, New Mexico: *Bulletin of the American Museum of Natural History*, **144**, 127 p.

- Gardner, J.N., 1985. Tectonic and petrologic evolution of the Keres Group: Implications for the development of the Jemez volcanic field, New Mexico [PhD Dissertation]: Davis, University of California, 293 p.
- Gardner, J.N., 2008. Personal communication: Jemez dacite geochemistry.
- Gardner, J.N., and Goff, F. 1984. Potassium-argon dates from the Jemez volcanic field: Implications for tectonic activity in the north-central Rio Grande rift. *New Mexico Geological Society 35th Field Conference Guidebook*, 75-81.
- Gardner, J.N. and Goff, F., 1986. Stratigraphic Relations and Lithologic Variations in the Jemez Volcanic Field, New Mexico. *Journal of Geophysical Research*, **91**, 1763-1778.
- Gardner, J. N., Kolbe, T., and Chang, S., 1993, Geology, drilling, and some hydrologic aspects of Seismic Hazards Program core holes, Los Alamos National Laboratory; *Los Alamos National Laboratory report, LA-12460-MS*, 19 p.
- Gardner, J.N. and Goff, F., 1996. Geology of the northern Valles Caldera and Toledo embayment, New Mexico. In: Goff, F., Kues, B.S., Rogers, M.A., McFadden, L.D., and Gardner, J.N., (eds) *The Jemez Mountains Region. New Mexico Geological Society 47th Field Conference Guidebook*, 225-230.
- Gardner, J.N., S.L. Reneau, C.J. Lewis, A. Lavine, D.J. Krier, G. Woldegabriel, and G.D. Guthrie, 2001. Geology of the Pajarito fault zone in the vicinity of S-site (TA-16), Los Alamos National Laboratory, Rio Grande Rift, New Mexico. Rep. LA-13831-MS. Los Alamos Natl. Lab., Los Alamos, NM.
- Gay, K.R. and Smith, G.A., 1993. Eruptive history for two volcanic vents as recorded in the Peralta Tuff; Jemez Mountains, New Mexico. *New Mexico Geology* **15**, 75.
- Geologic Map of New Mexico, New Mexico Bureau of Geology and Mineral Resources, 2003, Scale 1:500,000, ISBN: 1-883905-16-8.
- Gibson, S.A., Thompson, R.N., Leat, P.T., Morrison, M.A., Hendry, G.L., Dickin, A.P., and Mitchell, J.G., 1993. Ultrapotassic magmas along the flanks of the Oligo-Miocene Rio Grande Rift, USA; monitors of the zone of lithospheric mantle extension and thinning beneath a continental rift. *Journal of Petrology* **34**, 187-228.
- Goff, F., and Kron, A., 1980. Geologic map of Canon de San Diego, Jemez Springs, New Mexico and Lithologic log of Jemez Springs geothermal well, scale 1:12,000. *Los Alamos National Lab Report LA-8276-MAP*.
- Goff, F., and Grigsby, C., 1982. Valles Caldera geothermal systems, New Mexico, USA. *Journal of Hydrology* **56**, 119-136.

- Goff, F., and Gardner, J.N., 1994. Evolution of a mineralized geothermal system, Valles caldera, New Mexico. *Economic Geology* **89**, 1803-1832.
- Goff, F., and Gardner, J.N., 2004. Late Cenozoic geochronology of volcanism and mineralization in the Jemez Mountains and Valles caldera, north central New Mexico. In: Mack, G.H., and Giles, K.A. (Eds) *The Geology of New Mexico: A Geologic History*: New Mexico Geological Society Special Publication **11**.
- Goff, F., Grigsby, C.O., Trujillo, P.E., Counce, D., and Kron, A., 1981. Geology, water chemistry, and geothermal potential of the Jemez Springs area, Cañon de San Diego, New Mexico. *Journal of Volcanology and Geothermal Research* **10**, 227-244.
- Goff, F., Rowley, J., Gardner, J.N., Hawkins, W., Goff, S., Charles, R., Wachs, D., Maassen, L., and Heiken, G., 1986. Initial results from VC-1, first Continental Scientific Drilling Program core hole in Valles Caldera, New Mexico. *Journal of Geophysical Research* **91**, 1742-1752.
- Goff, F., Gardner, J.N., Baldrige, W.S., Hulen, J.B., Nielson, D.L., Vaniman, D., Heiken, G., Dungan, M.A., and Broxton, D., 1989. Excursion 17B: Volcanic and hydrothermal evolution of Valles Caldera and Jemez volcanic field. *New Mexico Bureau of Mines and Mineral Resources Memoir* **46**, 381-434.
- Goff, F., Gardner, J.N., and Valentine, G., 1990. Geologic map of the St. Peter's Dome area, Jemez Mountains, New Mexico. New Mexico Bureau of Mines and Mineral Resources, Map 69, scale 1:24,000.
- Golombek, M.P., 1983. Geology, structure, and tectonics of the Pajarito fault zone in the Española Basin of the Rio Grande rift, New Mexico. *Geological Society of America Bulletin* **94**, 192-205.
- Golombek, M.P., McGill, G.E., and Brown, L., 1983. Tectonic and geologic evolution of the Espanola Basin, Rio Grande rift: Structure, rate of extension, and relation to the state of stress in the western U.S. *Tectonophysics* **94**, 483-507.
- Griggs, R.F., 1922. *The Valley of Ten Thousand Smokes*. National Geographic Society
- Griggs, R., 1964. Geology and groundwater resources of the Los Alamos area, New Mexico. *U.S. Geological Survey Water Supply Paper* **1753**, 107 p.
- Gudmundsson, A., 1988. Formation of collapse calderas. *Geology* **16**, 808-810.
- Heiken, G. and McCoy, F., 1984. Caldera development during the Minoan eruption, Thira, Cyclades, Greece. *Journal of Geophysical Research* **89**, 8441-8462.

- Heiken, G., Goff, F., Stix, J., Tamanyu, S., Shafiqullah, M., Garcia, S., and Hagan, R., 1986. Intracaldera volcanic activity, Toledo Caldera and Embayment, Jemez Mountains, New Mexico. *Journal of Geophysical Research* **91**, 1799-1815.
- Hervig, R.L. and Dunbar, N.W., 1992. Cause of chemical zoning in the Bishop (California) and Bandelier (New Mexico) magma chambers. *Earth and Planetary Science Letters* **111**, 97-108.
- Hildreth, W., 1979. The Bishop Tuff: evidence for the origin of compositional zonation in silicic magma chambers. In: Chapin, C.E., and Elston, W.E. (eds) Ash Flow Tuffs. *Geological Society of America, Special Paper* **180**, 43-75.
- Hildreth, W., 1981. Gradients in silicic magma chambers: implications for lithospheric magmatism. *Journal of Geophysical Research* **86**, 10153-10192.
- Hildreth, W., and Mahood, G.A., 1986. Ring-fracture eruption of the Bishop Tuff. *Geological Society of America Bulletin* **97**, 396-403.
- Hildreth, W., and Wilson, C.J.N., 2007. Compositional zoning of the Bishop Tuff. *Journal of Petrology* **48**, 951-999.
- Holliday, V.T., 1988. Mt. Blanco revisited: soil-geomorphic implications for the ages of the upper Cenozoic Blanco and Blackwater Draw formations. *Geology* **16**, 505-508.
- Holohan, E.O., Troll, V.R., van Wyk de Vries, B., Walsh, J.J and Walter, T.R., 2008. Unzipping Long Valley: An explanation for vent migration patterns during an elliptical ring fracture eruption. *Geology* **36**, 323-326.
- Hulen, J.B., and Nielson, D.L., 1986. Hydrothermal alteration in the Baca geothermal system, Redondo dome, Valles caldera, New Mexico. *Journal of Geophysical Research* **91**, 1867-1886.
- Hulen, J.B., and Gardner, J.N., 1989. Field geologic log for Continental Scientific Drilling Program Corehole VC-2B, Valles Caldera, New Mexico. *DOE report ER/13196-4, ESL-89205-TR*, 92 pages.
- Hulen, J.B., Nielson, D.L., and Little, T.M., 1991. Evolution of the Western Valles Caldera complex, New Mexico: evidence from intracaldera sandstones, breccias and surge deposits. *Journal of Geophysical Research* **96**, 8127-8142.
- Iddings, J.P., 1890. On a group of rocks from the Tewan Mountains, New Mexico, and on the occurrence of primary quartz in certain basalts. *U.S. Geological Survey, Bulletin* **66**, 34 p.

- Ingersoll, R.V., Cavazza, W., Baldrige, W.S. and Shafiqullah, M., 1990. Cenozoic sedimentation and paleotectonics of north-central New Mexico: Implications for initiation and evolution of the Rio Grande rift. *GSA Bulletin* **102**: 1280-1296.
- Izett, G.A., and Obradovich, J.D., 1994. $^{40}\text{Ar}/^{39}\text{Ar}$ age constraints for the Jaramillo normal subchron and the Matayama-Brunhes geomagnetic boundary. *Journal of Geophysical Research* **99**, 2925-2934.
- Justet, L., 1996. The geochronology and geochemistry of the Bearhead Rhyolite, Jemez volcanic field, New Mexico [MS Thesis] Las Vegas, University of Nevada, 152 p.
- Justet, L. and Spell, T.L., 2001. Effusive eruptions from a large silicic magma chamber: the Bearhead Rhyolite, Jemez volcanic field, N.M. *Journal of Volcanology and Geothermal Research* **107**, 241-264.
- Karlstrom, K.E., Bowring, S.A., and Chamberlain, K.R., 2002. Structure and evolution of the lithosphere beneath the Rocky Mountains: initial results from the CD-ROM experiment. *GSA Today*, **12/3**, 4-10
- Keller, G.R., Khan, M.A., Morgan, M., Wendlandt, R.F., Baldrige, W.S., Olsen, K.H, Prodehl, C. and Braile, L.W., 1991. A comparative study of the Rio Grande and Kenya Rifts. *Tectonophysics* **197**, 355-371.
- Keller, G.R. and Cather, S.M., 1994. Introduction, in Keller, G.R. and Cather, S.M., eds., Basins of the Rio Grande Rift: Structure, Stratigraphy and Tectonic Setting: Boulder, Colorado, *Geological Society of America, Special Paper* **291**.
- Kelley, V.C., 1952. Tectonics of the Rio Grande depression of central New Mexico. New Mexico Geological Society Guidebook, **3rd** field conference, October, 1952, 93-105.
- Kelley, V.C., 1956. The Rio Grande depression from Taos to Santa Fe. New Mexico Geological Society Guidebook, **7th** field conference, October, 1956, 109-114.
- Komuro, H., Fujita, Y. and Kodama, K., 1984. Numerical and experimental models on the formation mechanism of collapse basins during Green Tuff orogenesis of Japan. *Bulletin of Volcanology* **47**, 649-666.
- Komuro, H., 1987. Experiments on cauldron formation: A polygonal cauldron and ring fractures. *Journal of Volcanology and Geothermal Research* **31**, 139-149.
- Komuro, H., Aoyama, M and Arayashiki, T., 2006. Collapse mechanism of the Paleogene Sakurae cauldron, SW Japan. *Bulletin of Volcanology* **68**, 631-640
- Kuentz, D.C., 1986. The Otowi Member of the Bandelier Tuff: a study of the petrology, petrography, and geochemistry of an explosive silicic eruption, Jemez Mountains, New Mexico. M.S. Thesis: University of Texas at Arlington, 168 p.

- Lipman, P.W., Doe, B.R., Hedge, C.E. and Steven, T.A., 1978. Petrologic evolution of the San Juan Volcanic field, southwestern Colorado: Pb and Sr isotopic evidence. *GSA Bulletin* **89**, 59-82
- Lipman, P.W., 1981. Volcano-tectonic setting of Tertiary ore deposits, southern Rocky Mountains, Relation of Tectonics to Ore Deposits in the Southern Cordillera. Edited by W.R. Dickinson and W.D. Payne. *Arizona Geological Society Digest* **15**, 199-213.
- Lipman, P.W., 1984. The roots of ash flow calderas in western North America: Windows into the tops of granite batholiths. *Journal of Geophysical Research* **89**, 8801-8841.
- Lipman, P.W., Self, S. and Heiken, G., 1984. Introduction to calderas special issue. *Journal of Geophysical Research* **89**, 8219-8221.
- Lipman, P.W., Legatchev, N.A., Zorin, Y.A., Chapin, C.E., Kovalenko, V. and Morgan, P., 1989. Intracontinental rift comparisons, Baikal and the Rio Grande rift systems. *EOS, Transactions of the American Geophysical Union* **70**, 578-579
- Lipman, P.W., 1997. Subsidence of ash-flow calderas: relation to caldera size and magma-chamber geometry. *Bulletin of Volcanology* **59**, 198-218.
- Lipman, P.W., 2000a. Calderas. In: Sigurdsson, H. (Ed.), *Encyclopedia of Volcanoes*. Academic Press, San Francisco, pp. 643-662.
- Lipman, P.W., 2000b. The central San Juan caldera cluster: regional volcanic framework. *Geological Society of America, Special Papers* **346**, 9-71.
- Loeffler, B.M., Vaniman, D.T., Baldrige, W.S., and Shafiqullah, M., 1988. Neogene rhyolites of the northern Jemez volcanic field, New Mexico. *Journal of Geophysical Research*, **93**, 6157-6168.
- Lucas, S.G., 1984. Correlation of Eocene rocks of the northern Rio Grande rift and adjacent areas: implications for Laramide tectonics. N.M. Geological Society Field Conference Guidebook **34**, 123-128.
- Luedke, R. and Smith, R.L., 1978. Map showing distribution, composition, and age of late Cenozoic volcanic centers in Arizona and New Mexico. U.S. Geological Survey, Miscellaneous Investigation Map **I-1091-A**, scale 1:1,000,000.
- Lyell, C., 1830. *Principles of Geology*: London, J. Murray, 385 p.
- Macdonald, G.A., 1972. *Volcanoes*: Englewood Cliffs, N.J., Prentice-Hall, 510 p.
- Magnani, M.B., Miller, K.C., Levander, A. and Karlstrom, K., 2004. The Yavapai-Mazatzal boundary: A long-lived tectonic element in the lithosphere of southwestern North America. *GSA Bulletin* **116** n. 7/8, 1137-1142.

- Mahood, G.A., 1984. Pyroclastic rocks and calderas associated with strongly peralkaline magmatism. *Journal of Geophysical Research* **89**, 8540-8552.
- Manley, K., 1982. Geologic map of the Cañones quadrangle. *US Geological Survey Miscellaneous Field Studies Map MF-1440*, scale 1:24,000.
- Marsh, B.D., 1984. On the mechanics of caldera resurgence. *Journal of Geophysical Research* **89**, 8245-8251.
- Marti, J., Ablay, G.J., Redshaw, L.T. and Sparks, R.S.J., 1994. Experimental study of collapse calderas. *Journal of the Geological Society, London* **151**, 919-929.
- Mason, B.G., Pyle, D.M., and Oppenheimer, C., 2004. The size and frequency of the largest explosive eruptions on Earth. *Bulletin of Volcanology* **66**, 735-748.
- McBirney, A.R., 1990. An historical note on the origin of calderas. *Journal of Volcanology and Geothermal Research* **42**, 303-306.
- McCall, H.G., 1963. Classification of “Krakatoan” and “GlenCoe” types. *Nature* **197**, 136-138.
- McIntosh, W. and Quade, J., 1995. $^{40}\text{Ar}/^{39}\text{Ar}$ geochronology of tephra layers in the Santa Fe Group, Espanola Basin, New Mexico: N.M Geological Society 46th field Conference Guidebook, 279-287.
- Moore, I. and Kokelaar, P., 1998. Tectonically controlled piecemeal caldera collapse: A case study of Glencoe volcano, Scotland. *Geological Society of America Bulletin* **110**, 1448-1466.
- Morgan, L.A., Doherty, D.J., and Leeman, W.P., 1984. Ignimbrites of the Eastern Snake River Plain: Evidence for major caldera-forming eruptions. *Journal of Geophysical Research* **89**, 8665-8678.
- Muehlberger, W.R., 1979. The Embudo fault between Pilar and Arroyo Hondo, New Mexico: An active intracontinental transform fault. *New Mexico Geological Society 30th Field Conference Guidebook*, 77-82.
- Nielson, D.L., and Hulen, J.B., 1984. Internal geology and evolution of the Redondo Dome, Valles Caldera, New Mexico. *Journal of Geophysical Research* **89**, 8695- 8711.
- Phillips E.H., Goff, F., Kyle, P.R., McIntosh, W.C., and Dunbar, N.W., 2006. Data repository for $^{40}\text{Ar}/^{39}\text{Ar}$ age constraints on the duration of resurgence at the Valles Caldera, New Mexico: New Mexico Bureau of Geology and Mineral Resources, Open File Report OF-AR-26, 46 p.

- Pittari, A., Cas, R.A.F., Edgar, C.J., Nichols, H.J., Wolff, J.A., and Marti, J., 2005. The influence of palaeotopography on facies architecture and pyroclastic flow processes of a lithic-rich ignimbrite in a high gradient setting; the Abrigo Ignimbrite, Tenerife, Canary Islands. *Journal of Volcanology and Geothermal Research*. **152**, 273-315
- Potter, D.B., and Oberthal, C.M., 1987a. Vent sites and flow directions of the Otowi ash flows (lower Bandelier tuff), New Mexico. *Geological Society of America Bulletin*, **98**, 66-76
- Potter D.B., and Oberthal, C.M., 1987b. Vent sites and flow directions of the Otowi ash flows (lower Bandelier Tuff), New Mexico: Discussion and reply. *Geological Society of America Bulletin* **99**, 601-603.
- Powell, J., 1961. The exploration of the Colorado River and its canyons. Dover Publications, New York, 400 p. (Republication of Canyons of the Colorado, Flood and Vincent, 1885).
- Pyle, D.M., 1989. The thickness, volume and grainsize of tephra fall deposits. *Bulletin of Volcanology* **51**, 1-15.
- Ramberg, H., 1981. *Gravity, Deformation and the Earth's Crust. In Theory, Experiments, and Geological Application*, 2nd ed., 452 p.
- Reck, H., 1928. Zur Deutung der vulkanischen Geschichte und der Calderabildung auf der Insel La Palma. *Zeitschr. F. Vulk.* **11**, 217-243.
- Reck, H., 1936. *Santorin, der Werdegang eines Inselvulkans und sein Ausbruch 1925-1928*. Berlin: 3 vols.
- Roberts, J.L., 1963. Source of the Glen Coe ignimbrites. *Nature* **5**, 901
- Roberts, J.L., 1966. Ignimbrite eruptions in the volcanic history of the Glencoe cauldron subsidence. *Geological Journal* **5**, 173-184.
- Roberts, J.L., 1974. The evolution of the Glen Coe Cauldron. *Scottish Journal of Geology* **10**, 269-282.
- Roche, O., Druitt, T.H., and Merle, O., 2000. Experimental study of caldera formation. *Journal of Geophysical Research* **105**, 395-416
- Rose, W.I., and Chesner, C.A., 1987. Dispersal of ash in the great Toba eruption, 75 ka. *Geology* **15**, 913-917.
- Ross, C.S., 1938. Valles Volcano, New Mexico. *Journal of the Washington Academy of the Sciences*, **28**, 417 p.

- Ross, C.S., and Smith, R.L., 1961. Ash-flow tuffs: Their origin, geologic relations, and identification: *U.S. Geological Survey Professional Paper* **366**, 81 p.
- Ross, C.S., Smith, R.L., and Bailey, R.A., 1961. Outline of the geology of the Jemez Mountains, New Mexico. *New Mexico Geological Society 12th field conference guidebook*, 139-143.
- Rowe, M.C., Wolff, J.A., Gardner, J.N., Ramos, F.C., Teasdale, R., and Heikoop, C.E., 2007. Development of a Continental Volcanic Field: Petrogenesis of Pre-caldera Intermediate and Silicic Rocks and Origin of the Bandelier Magmas, Jemez Mountains (New Mexico, USA). *Journal of Petrology* **48**, 2063-2091.
- Scandone, R., 1990. Chaotic collapse of calderas. *Journal of Volcanology and Geothermal Research* **42**, 285-302.
- Scrope, George P., 1825. *Considerations on Volcanos: The probable causes of their phenomena, the laws which determine their march, the disposition of their products, and their connection with the present state and past history of the globe; leading to the establishment of a new theory of the earth*. London: W. Phillips, George Yard, Lombard Street
- Seager, W.R. and Mack, G.H., 1986. Laramide paleotectonics of in southern New Mexico. In: J.A. Peterson (Editor), *Paleotectonics and Sedimentation in the Rocky Mountain Region*. *AAPG Memoir* **41**, 669-685
- Self, S., Goff, F., Gardner, J.N., Wright, J.V. and Kite, W.M., 1986. Explosive rhyolitic volcanism in the Jemez Mountains: Vent locations, caldera development and relation to regional structure. *Journal of Geophysical Research* **91**, 1779-1798.
- Self, S., and Turbeville, B.N., 1987. Vent sites and flow directions of the Otowi ash flows (lower Bandelier Tuff), New Mexico: Discussion and reply. *Geological Society of America Bulletin* **99**, 601-603.
- Self, S. and Lipman, P.W., 1989. Large ignimbrite and caldera-forming eruptions; IAVCEI Working Group on Explosive Volcanism and its Products. 124 p.
- Self, S., Wolff, J.A., Spell, T.L., Skuba, C.E., and Morrissey, M.M., 1991. Revisions to the stratigraphy of and volcanology of the post-0.5 Ma units and volcanic section of VC-1 core hole, Valles Caldera, New Mexico. *Journal of Geophysical Research* **96**, 4107-4116.
- Self, S., Heiken, G., Sykes, M. L., Wohletz, K., Fisher, R.V., and Dethier, D.P., 1996. Field excursions to the Jemez Mountains, New Mexico. *Bulletin of the New Mexico Bureau of Geology & Mineral Resources* **134**, 72 pages.

- Shaw, C.A., and Karlstrom, K.E., 1999. The Yavapai-Mazatzal crustal boundary in the southern Rocky Mountains. *Rocky Mountain Geology* **34**, 37-52.
- Singer, B.S., and Kudo, A.M., 1986. Assimilation-fractional crystallization of Polvadera Group rocks in the northwestern Jemez Volcanic Field, New Mexico. *Contributions in Mineralogy and Petrology* **94**, 374-386.
- Smith, G.A. and Abitz, R.J., 1989. Stratigraphy of the Peralta Tuff; implications for the volcanic and structural evolution of the southeastern Jemez volcanic field. *New Mexico Geology* **11**, 65.
- Smith, G.A. and Kuhle, A.J., 1998. Geology of the Santo Domingo Pueblo and Santo Domingo SW 7.5-minute Quadrangles, Sandoval County, New Mexico. New Mexico Bureau of Mines and Mineral Resources Map **OF-GM 15 & 26**, scale 1:24,000.
- Smith, R.L. and Bailey, R.A., 1966. The Bandelier Tuff: A study of ash-flow eruption cycles from zoned magma chambers. *Bulletin of Volcanology* **29**, 83-104.
- Smith, R.L. and Bailey, R.A., 1968. Resurgent Cauldrons. *Memoirs of the Geological Society of America* **116**, 613-662.
- Smith, R.L., Bailey, R.A., and Ross, C.S., 1961. Structural evolution of the Valles caldera, New Mexico, and its bearing on the emplacement of ring dikes. *U.S. Geological Survey Professional Paper* **424-D**, 145-149.
- Smith, R.L., Bailey, R.A., and Ross, C.S., 1970. Geologic map of the Jemez Mountains, New Mexico, scale 1:125,000. *Geological Investigation Map I-571*, USGS, Reston, Va.
- Smith, R.L., 1960a. Ash Flows. *Geological Society of America Bulletin* **71**, 795-842.
- Smith, R.L., 1960b. Zones and zonal variations in welded ash flows. *U.S. Geological Survey Professional Paper* **354-F**, 159 p.
- Smith, R.L., 1979. Ash-flow magmatism. In: Chapin, C.E. and Elston, W.E. (Eds) *Ash-flow tuffs: Geological Society of America, Special Papers* **180**, 5-28.
- Sparks, R.S.J., Walker, G.P.L., 1977. The significance of vitric-enriched air-fall ashes associated with crystal-enriched ignimbrites. *Journal of Volcanology and Geothermal Research*, **2**, 329-341.
- Spell, T.L., Harrison, T., and Wolff, J.A., 1990. $^{40}\text{Ar}/^{39}\text{Ar}$ dating of the Bandelier Tuff and San Diego Canyon ignimbrites, Jemez Mountains, New Mexico: temporal constraints on magmatic evolution. *Journal of Volcanology and Geothermal Research*, **43**, 175-193

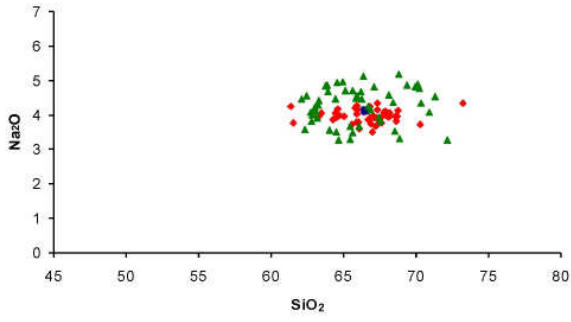
- Spell, T.L., Kyle, P.R., and Baker, J., 1996a. Geochronology and geochemistry of the Cerro Toledo rhyolite. In: Goff, F., Kues, B.S., Rogers, M.A., McFadden, L.D., and Gardner, J.N., (eds) *The Jemez Mountains Region. New Mexico Geological Society 47th Field Conference Guidebook*, 263-268
- Spell, T.L., McDougall, L., and Doulgeris, A., 1996b. Cerro Toledo Rhyolite, Jemez Volcanic Field, New Mexico: Ar geochronology of eruptions between two caldera-forming events. *Geological Society of America Bulletin* **108**, 1549-1566.
- Stix, J., Goff, F., Gorton, M.P., Heiken, G., and Garcia, S.R., 1988. Restoration of compositional zonation in the Bandelier silicic magma chamber between two caldera-forming eruptions: geochemistry and origin of the Cerro Toledo Rhyolite. *Journal of Geophysical Research* **93**, 6129-6147.
- Streck, M.J., and Grunder, A.L., 1995, Crystallization and welding variations in a widespread ignimbrite sheet—The Rattlesnake Tuff, eastern Oregon: *Bulletin of Volcanology*, v. 57, p. 151–169.
- Tanakadate, H., 1930. The problem of calderas in the Pacific region. *Proceeds of the 4th Pacific Scientific Congress, Batavia* **2b**, 730-744.
- Troll, V.R., Emeleus, C.H., Donaldson, C.H., 2000. Caldera formation in the Rum central igneous complex, Scotland. *Bulletin of Volcanology* **62**, 301-317.
- Troll, V.R., Walter, T.R., and Schmincke, H.U., 2002. Cyclic caldera collapse: piston or piecemeal subsidence? Field and experimental evidence. *Geology* **30**, 135-138.
- Turbeville, B., and Self, S., 1988. San Diego Canyon Ignimbrites: Pre-Bandelier Tuff ignimbrite explosive rhyolitic volcanism in the Jemez Mountains, New Mexico. *Journal of Geophysical Research* **93**, 6148-6156.
- Verbeek, R.D.M., 1885. *Krakatau*. Imprimerie l'Etat, Batavia, Indonesia 495 p.
- Walker, G.P.L., 1980. The Taupo pumice: product of the most powerful known (ultraplinian) eruption? *Journal of Volcanology and Geothermal Research* **8**, 6-94.
- Walker, G.P.L., 1984. Downsag calderas, ring faults, caldera sizes and incremental caldera growth. *Journal of Geophysical Research* **89**, 8407-8416.
- Walker, G.P.L., Heming, R.F., and Wilson, C.J.N., 1980. Low aspect-ratio ignimbrites. *Nature* **283**, 286-287.
- Walker, R.T., 1928. Mineralized volcanic explosion pipes. *Eng. And Min. Journal* **126**, 895-898, 939-942, 976-984.

- Walter, T.R., and Troll, V.R., 2001. Formation of caldera periphery faults: an experimental study. *Bulletin of Volcanology* **63**, 191-203.
- Waresback, D., Turbeville, B., 1990. Evolution of a Pliocene volcanogenic-alluvial fan: The Puye Formation, Jemez Mountains, New Mexico. *Geological Society of America Bulletin* **102**, 298-314.
- Williams, H., 1941. Calderas and their origin. *Bulletin of the Department of Geological Sciences, University of California* **25**, 239-346.
- Williams, H., 1942. Geology of Crater Lake national park. Carnegie Institution of Washington Publication Number 540, 162 pages.
- Williams, H. and McBirney, A.R., 1979. *Volcanology*: San Francisco, Freeman, 397 p.
- Wilson, C.J.N., 1991. Ignimbrite morphology and the effects of erosion; a New Zealand case study. *Bulletin of Volcanology* **53**, 635-644.
- Wilson, C.J.N., and Walker, G.P.L., 1981. Violence in pyroclastic flow eruptions. In: Self, S. and Sparks, R.S.J. (eds) *Tephra Studies*. D. Reidel, Dordrecht: 441-448.
- Wilson, C.J.N., Rogan, A.M., Smith, I.E.M., Northey, D.J., Nairn, I.A. and Houghton, B.F., 1984. Caldera volcanoes of the Taupo Volcanic Zone, New Zealand. *Journal of Geophysical Research* **89**, 8463-8484.
- Wilson, C.J.N., and Hildreth, W., 1997. The Bishop Tuff: New insights from eruptive stratigraphy. *The Journal of Geology* **105**, 407-439.
- Winick, J.A., McIntosh, W.C., and Dunbar, N.W., 2001. Melt-inclusion-hosted excess ⁴⁰Ar in quartz crystals of the Bishop and Bandelier magma systems. *Geology* **29**, 275-278.
- Winters, R.L., 2001. A geochemical study on the behavior of rare earth and trace elements in the Otowi Member of the Bandelier Tuff, Jemez Mountains, New Mexico. M.S. Thesis: Washington State University, 75 p.
- Woldegabriel, G., and Goff, F., 1989. Temporal relations of volcanism and hydrothermal systems in two areas of the Jemez volcanic field, New Mexico. *Geology* **17**, 986-989.
- Woldegabriel, G., and Goff, F., 1992. K/Ar dates of hydrothermal clays from corehole VC-2B, Valles caldera, New Mexico and their relation to alteration in a large hydrothermal system. *Journal of Volcanology and Geothermal Research* **50**, 207-230.
- Woldegabriel, G., Warren, R.G., Cole, G., Goff, F., Broxton, D., Vaniman, D., Peters, L., and Naranjo, A., 2003. Periodicity and distribution of volcanism in the Pajarito Plateau, Rio Grande rift, north-central New Mexico. *US Geological Survey Open-File Report* **03-369**, 7.

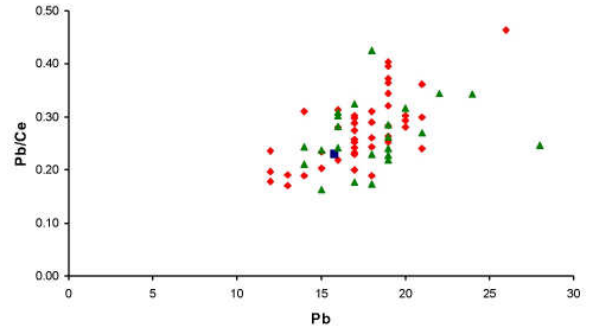
- Woldegabriel, G., Laughlin, A.W., Dethier, D.P., and Heizler, M., 1996. Temporal and geochemical trends of lavas in White Rock Canyon and the Pajarito Plateau, Jemez volcanic field, New Mexico, USA. In: Goff, F., Kues, B.S., Rogers, M.A., McFadden, L.D., and Gardner, J.N., (eds) *The Jemez Mountains Region. New Mexico Geological Society 47th Field Conference Guidebook*, 251-261.
- Wolff, J.A. and Gardner, J.N., 1995. Is the Valles Caldera entering a new cycle of activity? *Geology* **23**, 411-414.
- Wolff, J.A., Ramos, F.C., and Davidson, J.P., 1999. Sr isotope disequilibrium during differentiation of the Bandelier Tuff: constraints on the crystallization of a large rhyolitic magma chamber. *Geology*, **27**, 495-498.
- Wolff, J.A., Balsley, S.D., and Gregory, R.T., 2002. Oxygen isotope disequilibrium between quartz and sanidine from the Bandelier Tuff, New Mexico, consistent with a short residence time of phenocrysts in rhyolitic magma. *Journal of Volcanology and Geothermal Research*, **116**, 119-135.
- Wolff, J.A. and Ramos, F.C., 2003. Pb isotope variations among Bandelier Tuff feldspars no evidence for a long-lived silicic magma chamber. *Geology*, **31**, 533-536.
- Wolff, J.A., Rowe, M.C., Teasdale, R., Gardner, J.N., Ramos, F.C., and Heikoop, C.E., 2005. Petrogenesis of Pre-caldera mafic lavas, Jemez Mountains Volcanic Field, New Mexico, USA. *Journal of Petrology*, **46**, 407-439.
- Yokoyama, I., 1963. Structure of caldera and gravity anomaly. *Bulletin of Volcanology* **26**, 67-72.
- Yokoyama, I., 1981. A geophysical interpretation of the 1883 Krakatau eruption. *Journal of Volcanology and Geothermal Research*, **9**, 359-378.
- Yokoyama, I., 1983. Gravimetric studies and drilling results at the four calderas in Japan. In: Shimozuru, D. and Yokoyama, I., (eds) *Arc Volcanism: Physics and Tectonics*, 29-41.

APPENDIX A: DACITE LITHIC GEOCHEMISTRY

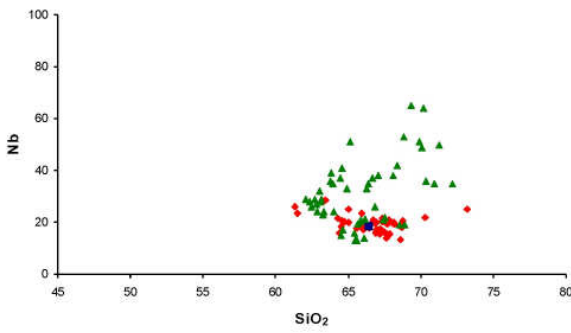
CM57D2



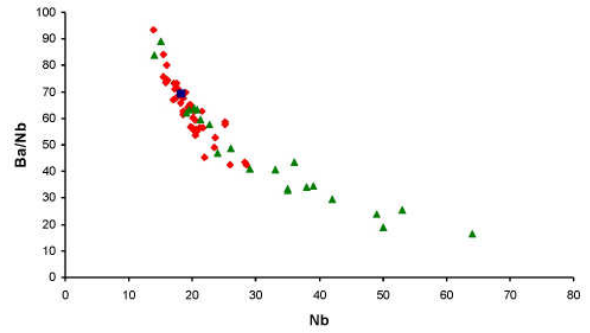
◆ Tschicoma ■ CM 57D2 ▲ Paliza Canyon



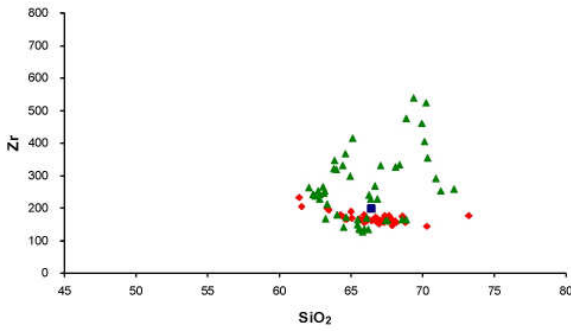
◆ Tschicoma ■ CM 57D2 ▲ Paliza Canyon



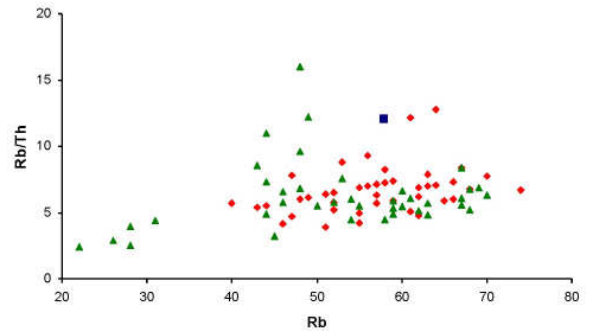
◆ Tschicoma ■ CM 57D2 ▲ Paliza Canyon



◆ Tschicoma ■ CM 57D2 ▲ Paliza Canyon

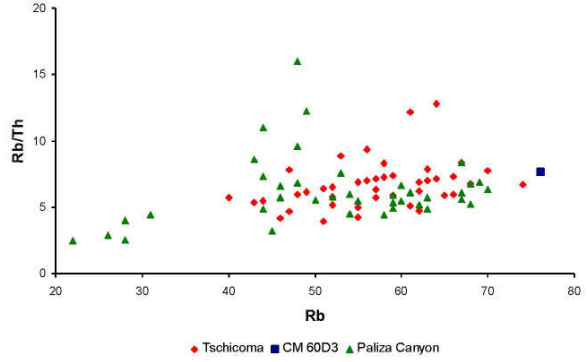
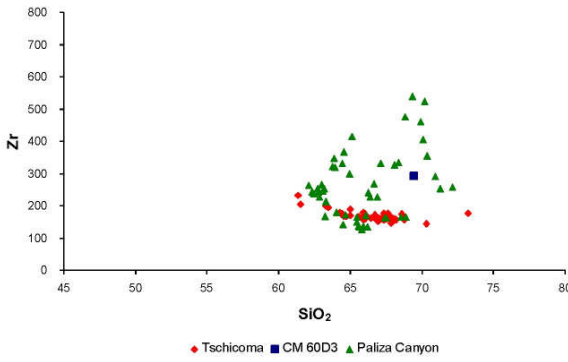
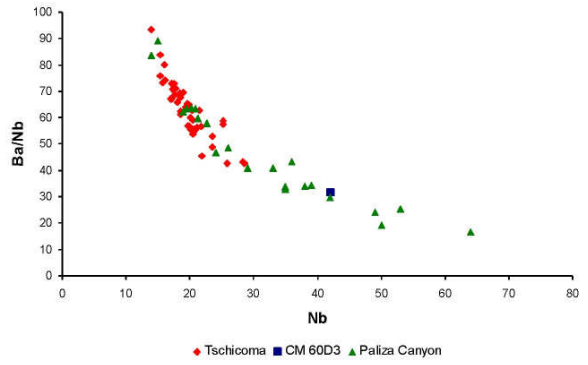
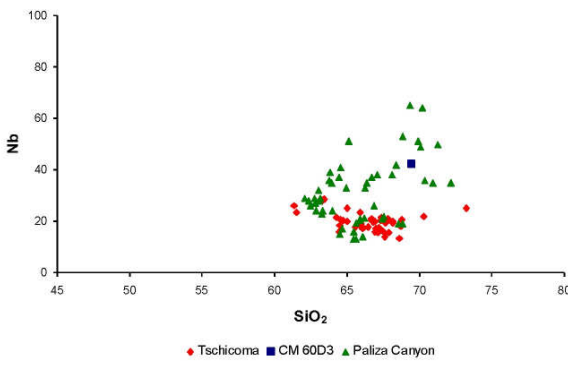
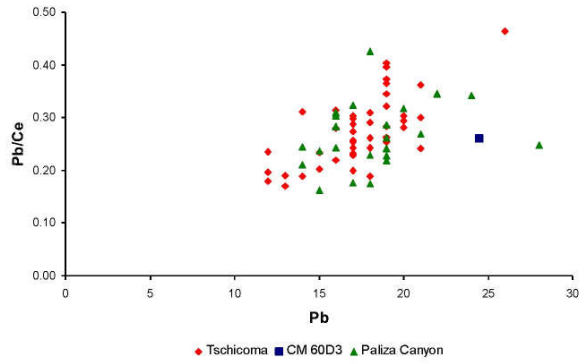
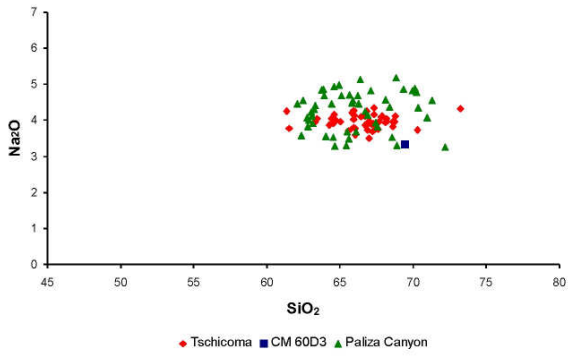


◆ Tschicoma ■ CM 57D2 ▲ Paliza Canyon

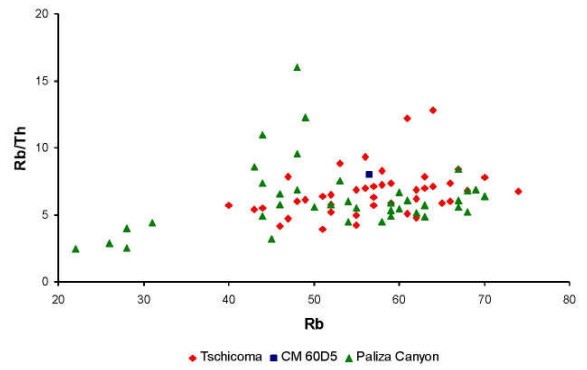
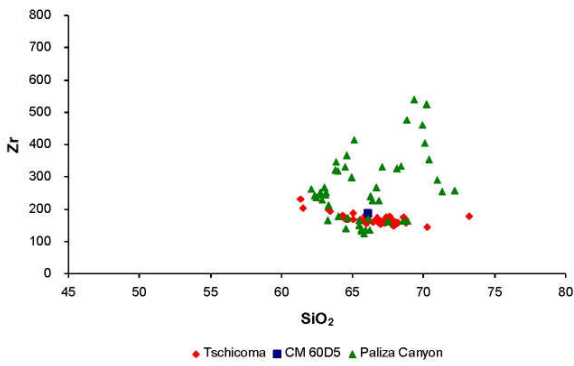
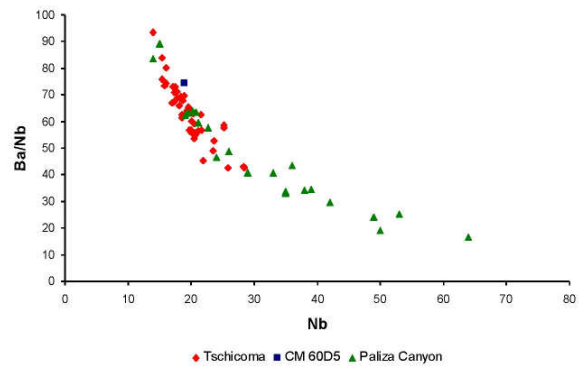
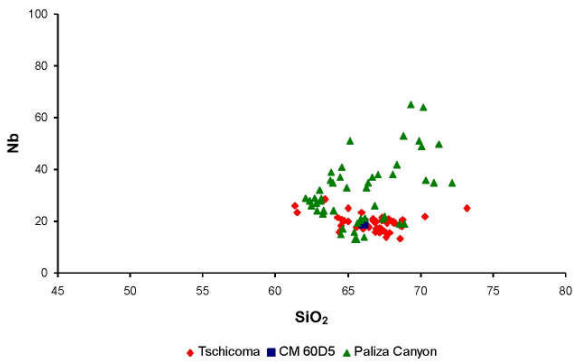
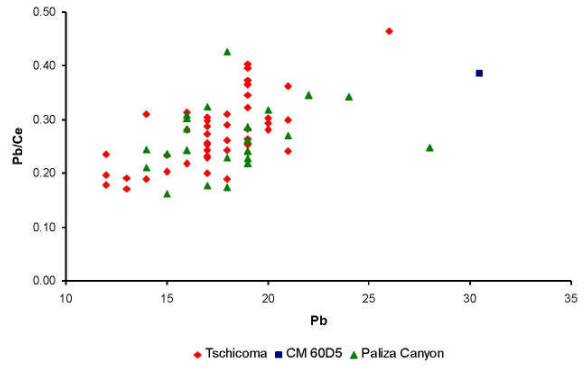
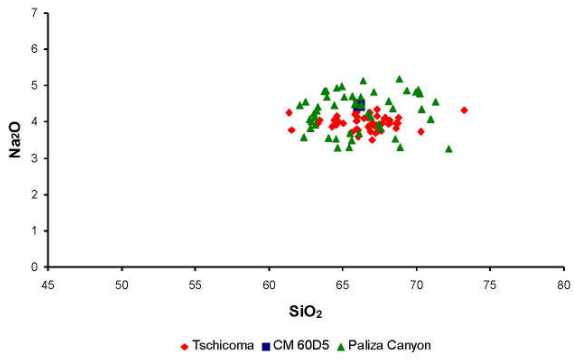


◆ Tschicoma ■ CM 57D2 ▲ Paliza Canyon

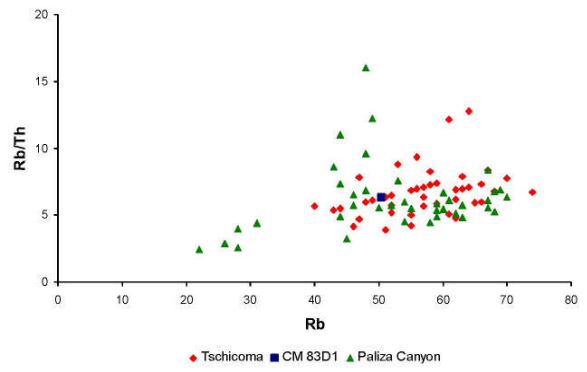
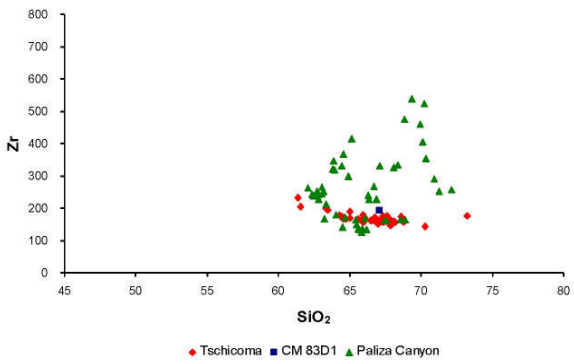
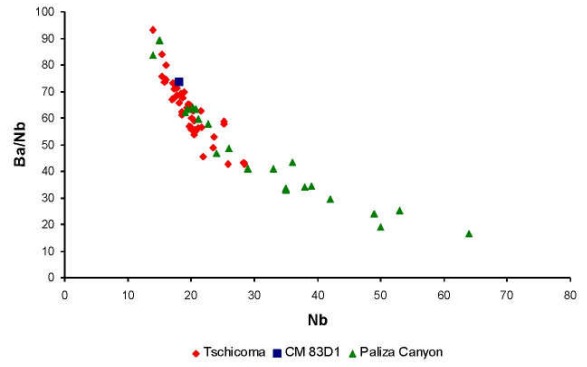
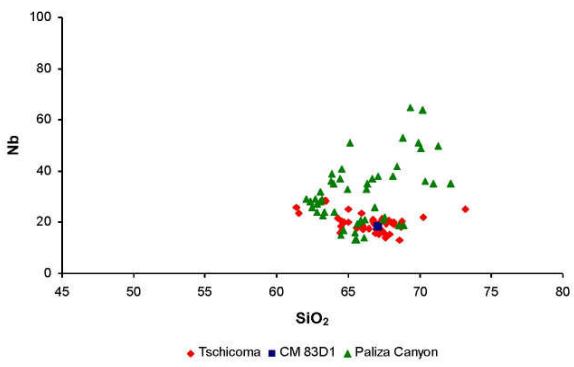
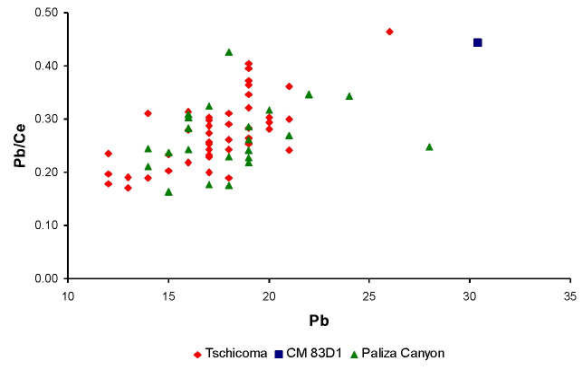
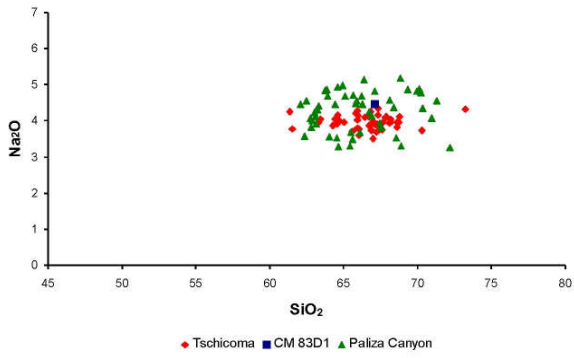
CM60D3



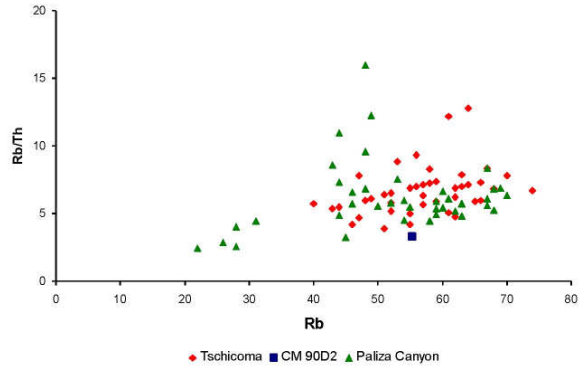
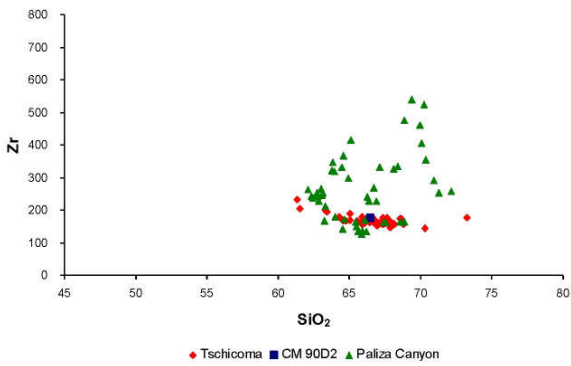
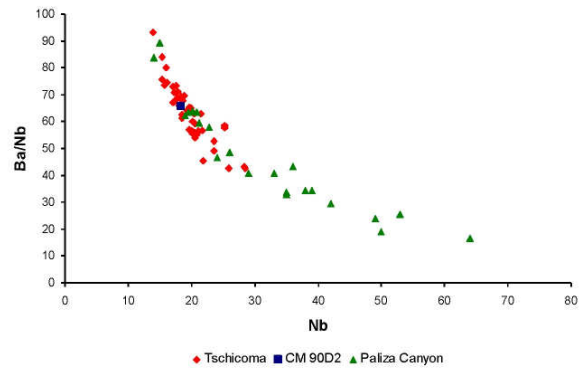
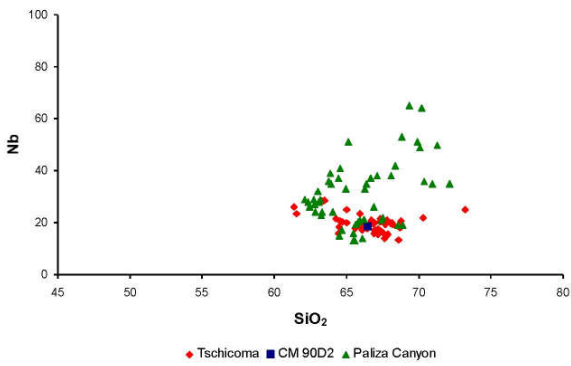
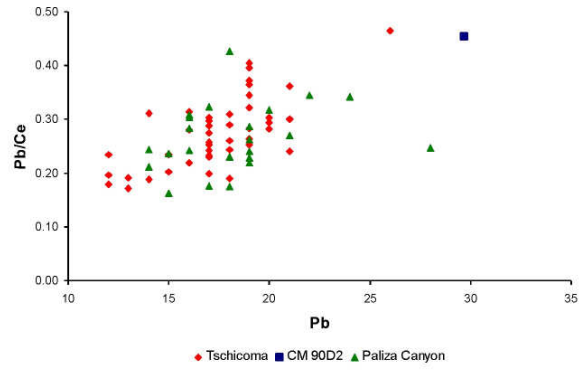
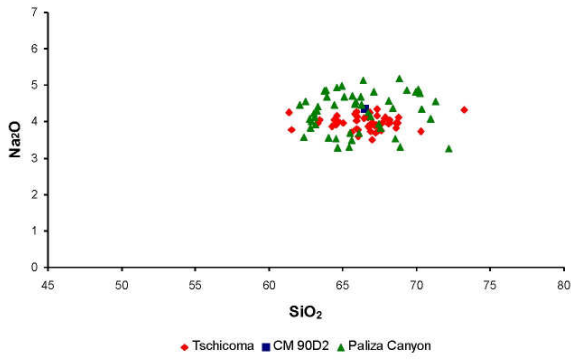
CM60D5



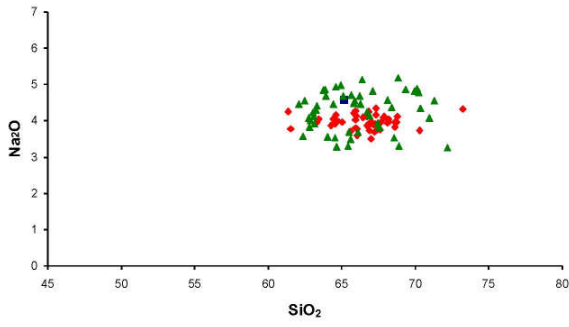
CM83D1



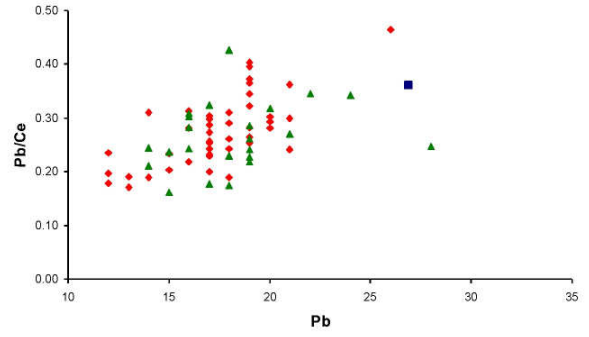
CM90D2



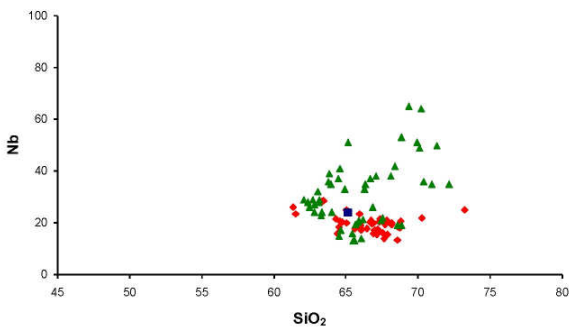
CM90D3



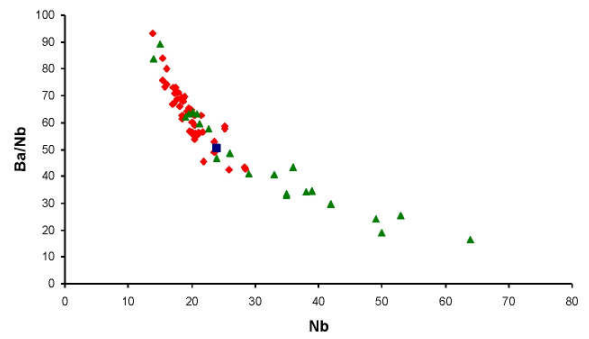
◆ Tschicoma ■ CM 90D3 ▲ Paliza Canyon



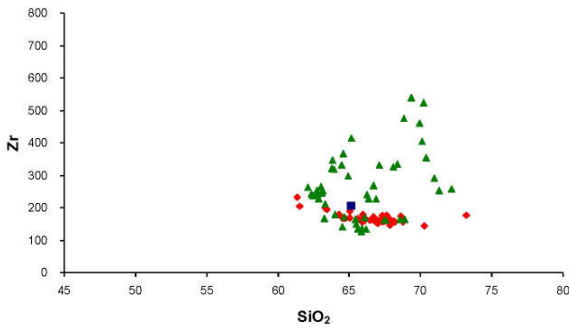
◆ Tschicoma ■ CM 90D3 ▲ Paliza Canyon



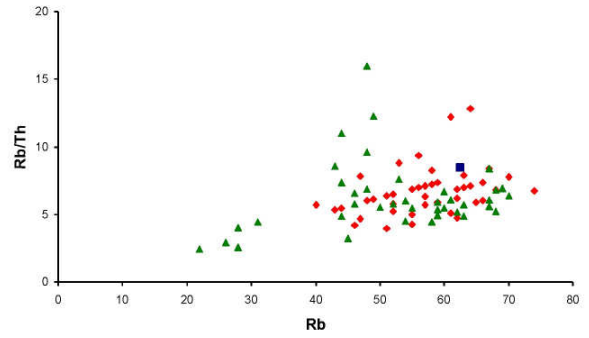
◆ Tschicoma ■ CM 90D3 ▲ Paliza Canyon



◆ Tschicoma ■ CM 90D3 ▲ Paliza Canyon

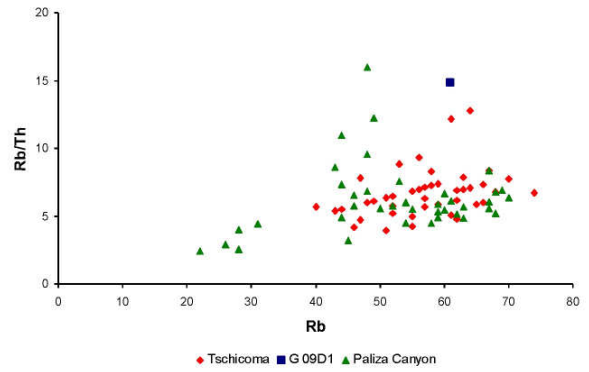
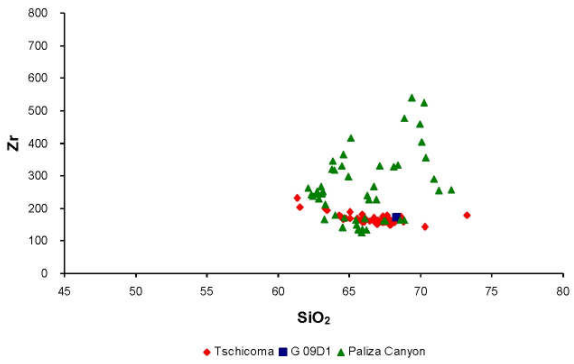
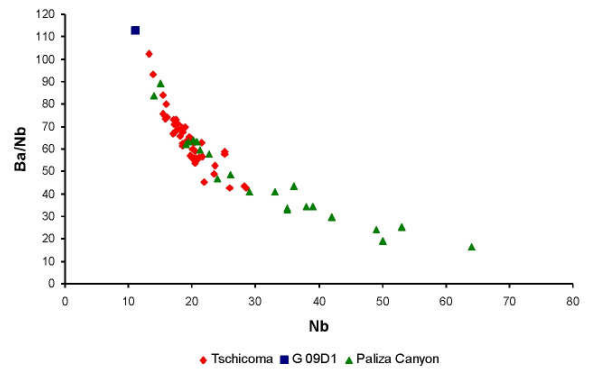
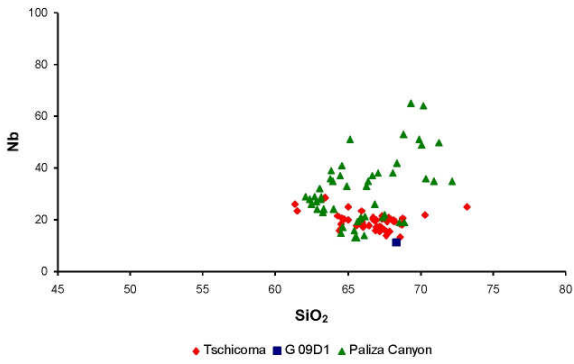
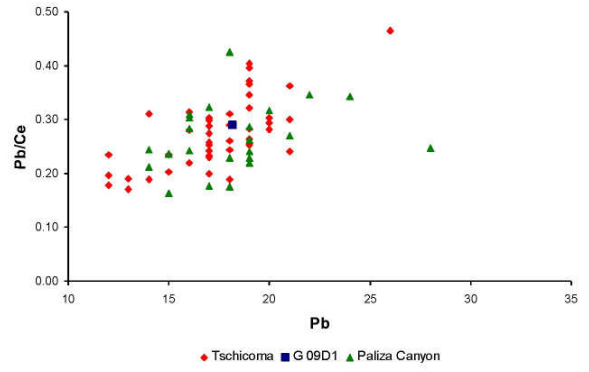
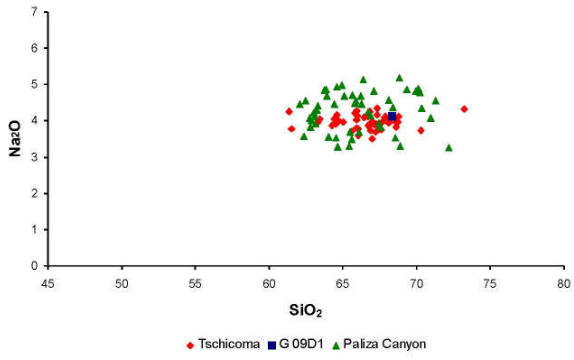


◆ Tschicoma ■ CM 90D3 ▲ Paliza Canyon

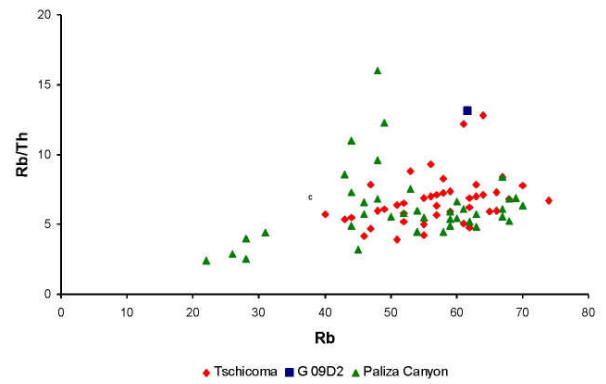
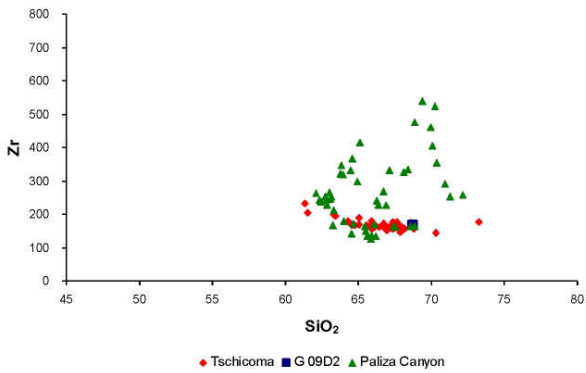
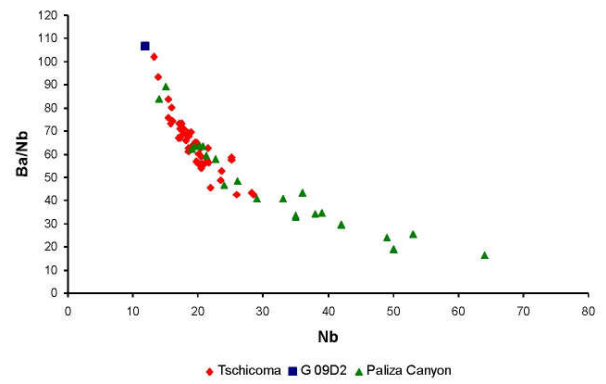
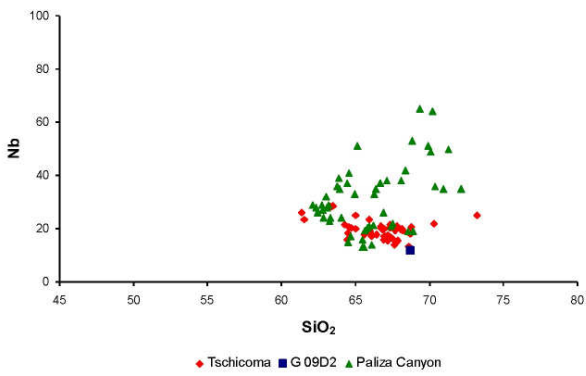
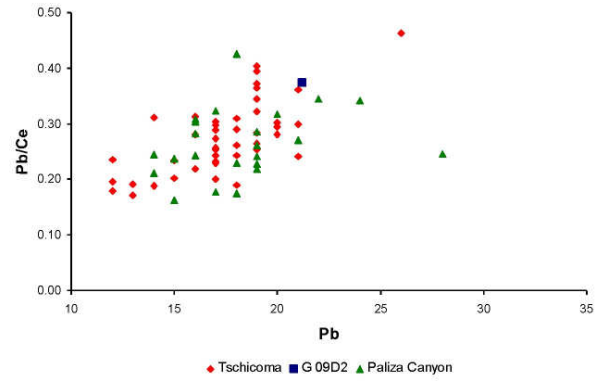
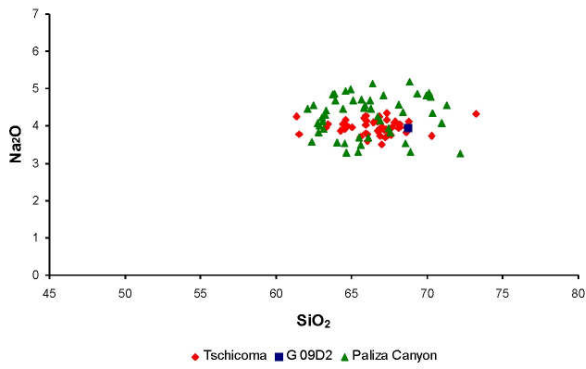


◆ Tschicoma ■ CM 90D3 ▲ Paliza Canyon

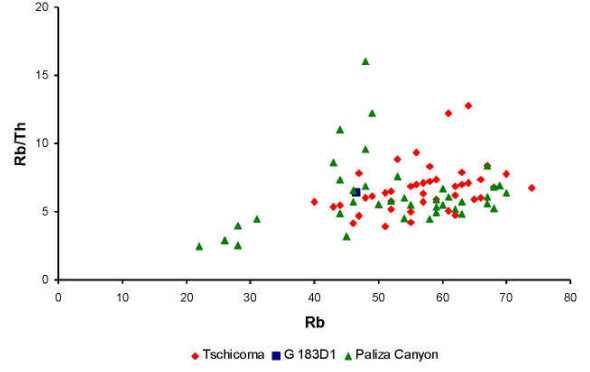
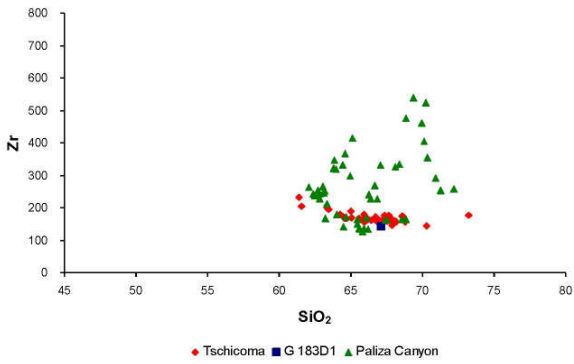
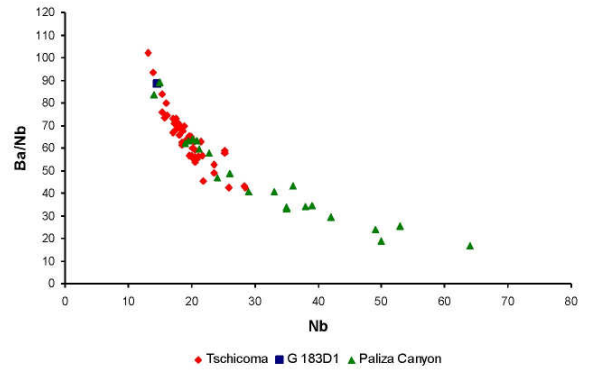
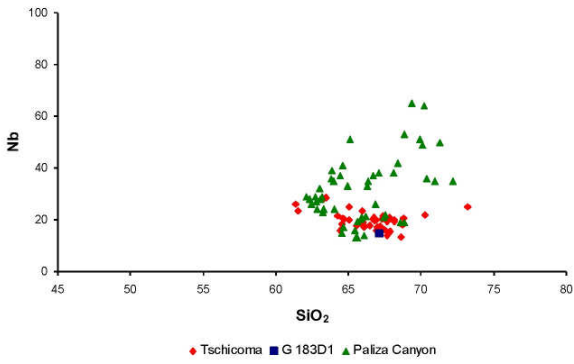
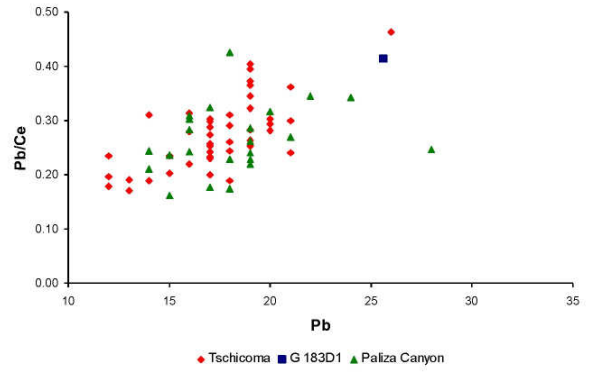
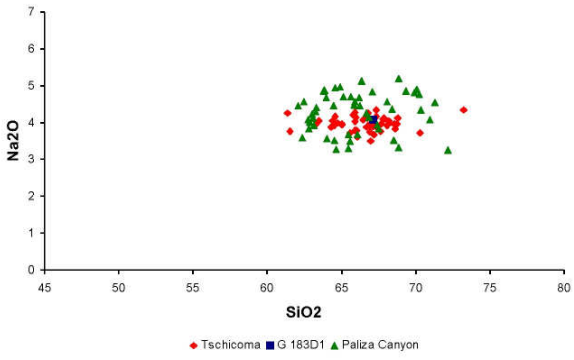
G09 D1



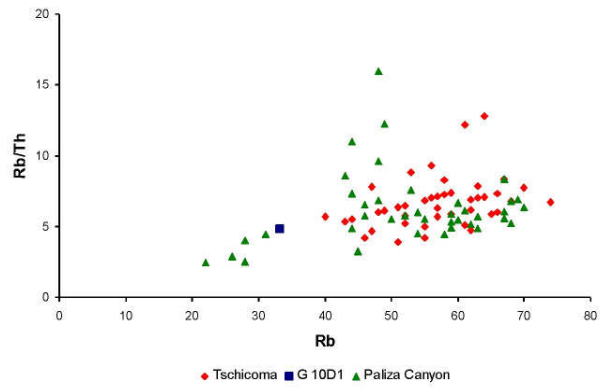
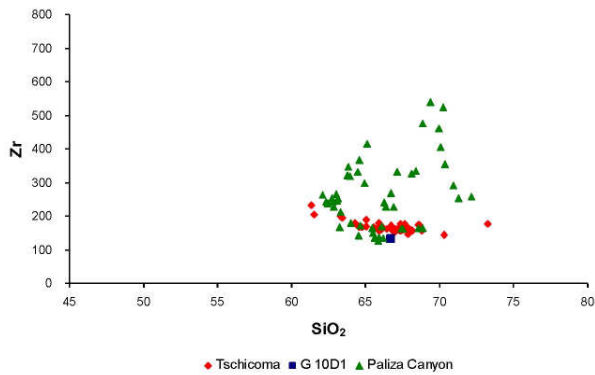
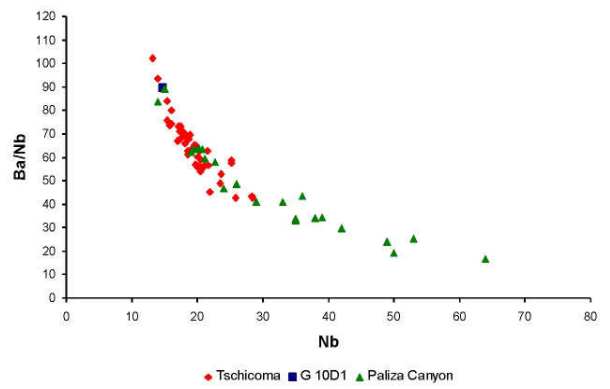
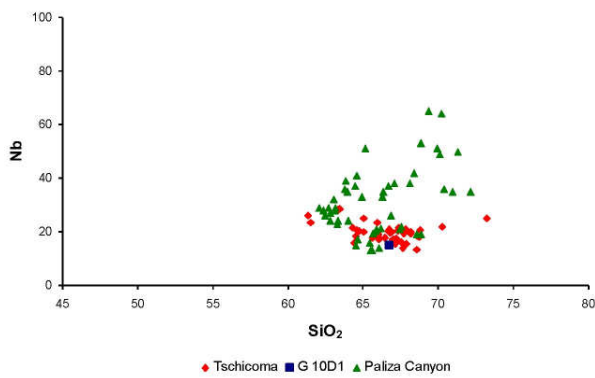
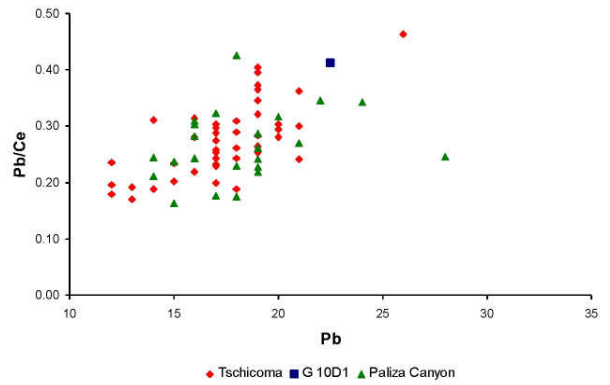
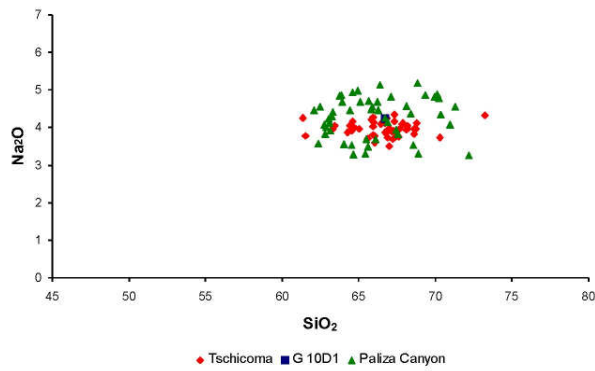
G09 D2



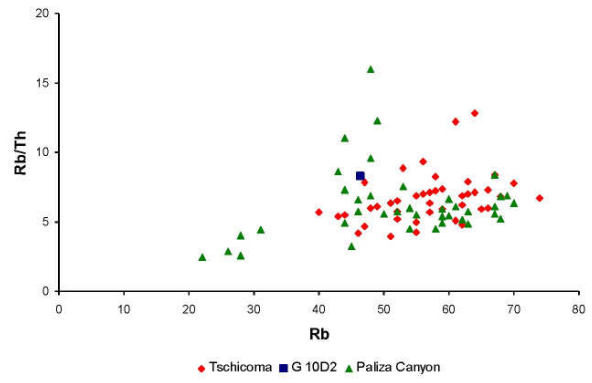
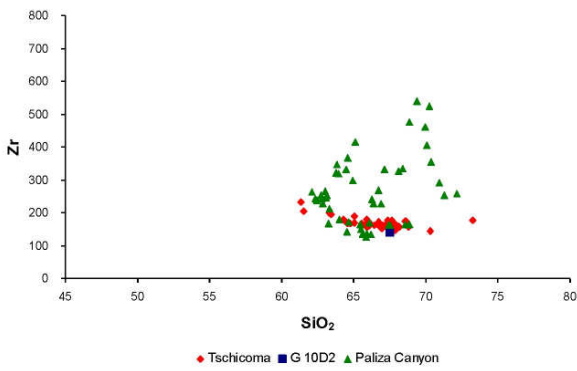
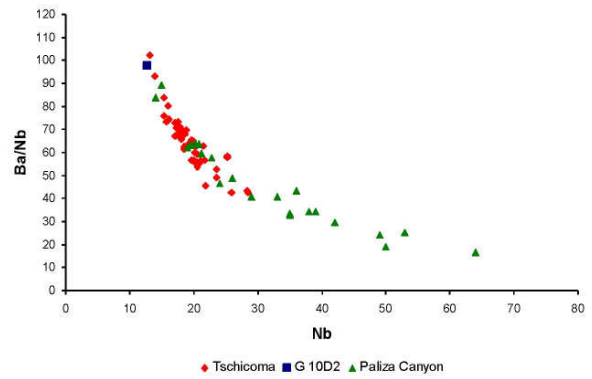
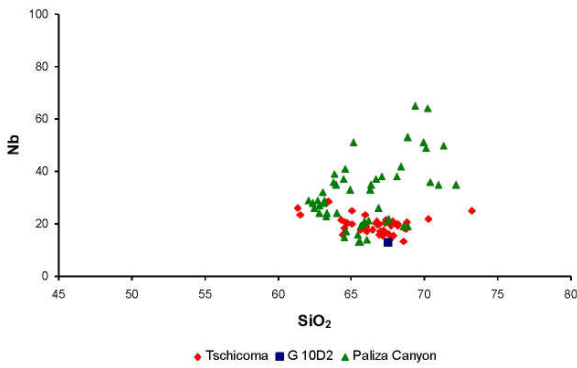
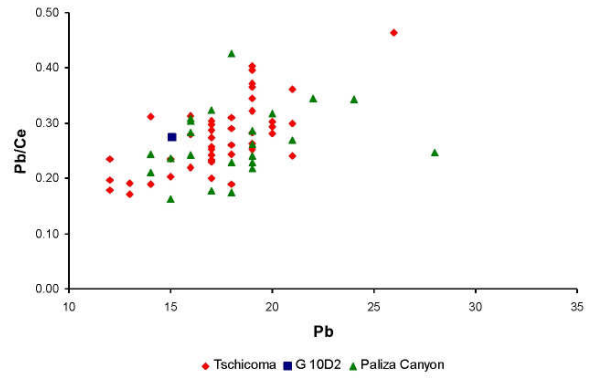
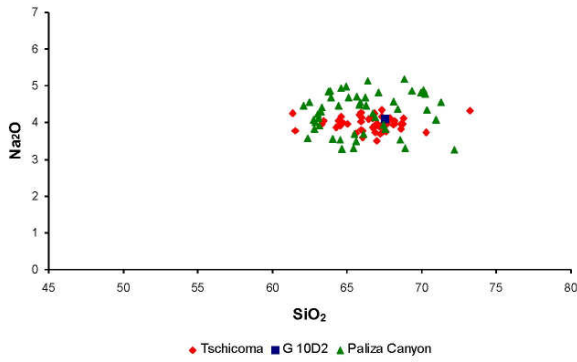
G183 D1



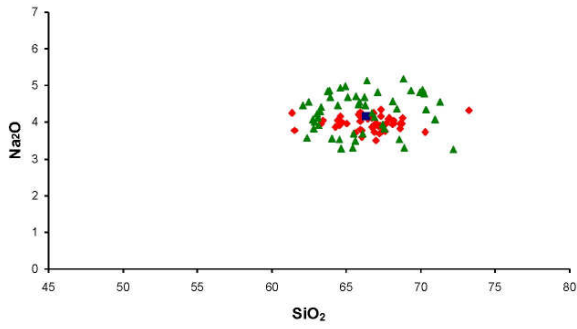
G10 D1



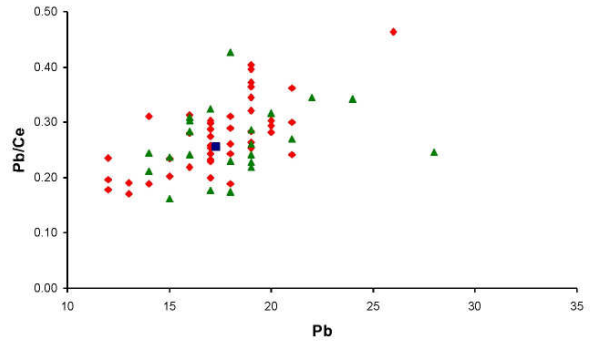
G10 D2



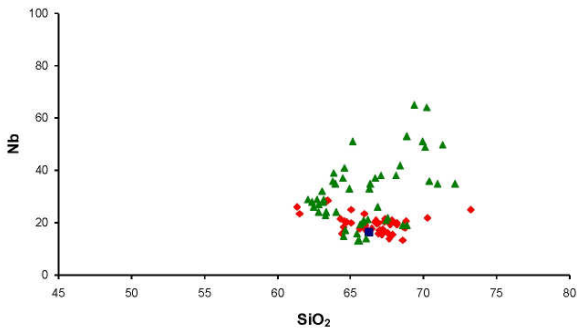
G10 D3



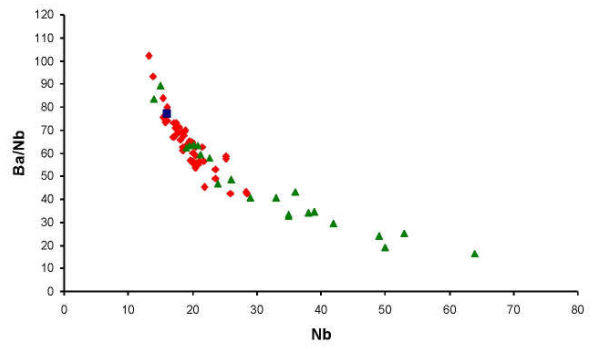
◆ Tschicoma ■ G 10D3 ▲ Paliza Canyon



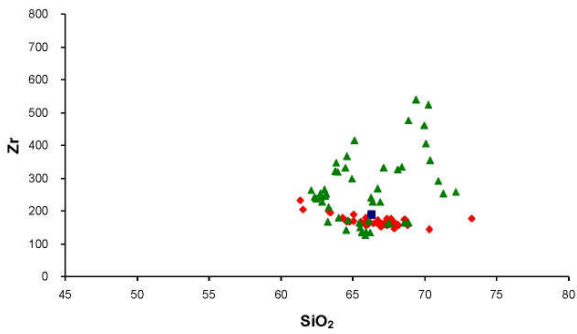
◆ Tschicoma ■ G 10D3 ▲ Paliza Canyon



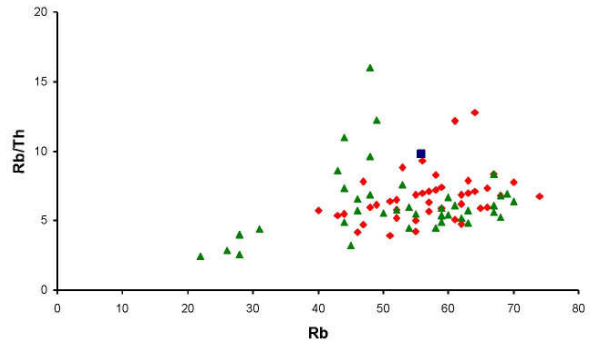
◆ Tschicoma ■ G 10D3 ▲ Paliza Canyon



◆ Tschicoma ■ G 10D3 ▲ Paliza Canyon

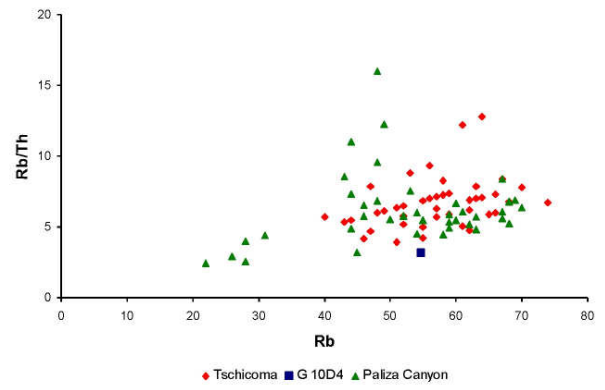
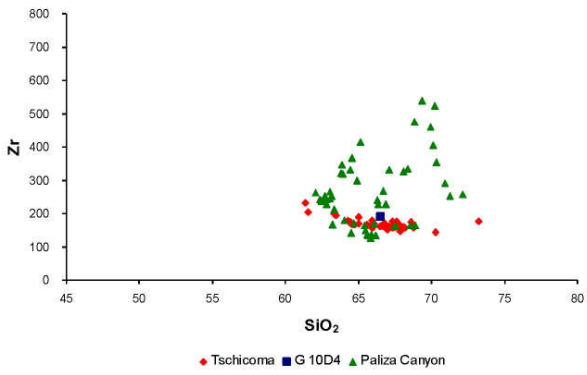
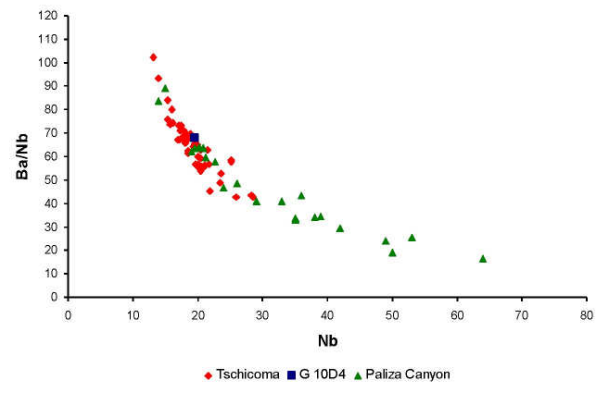
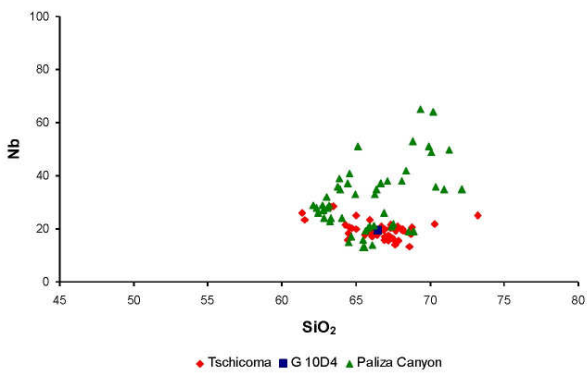
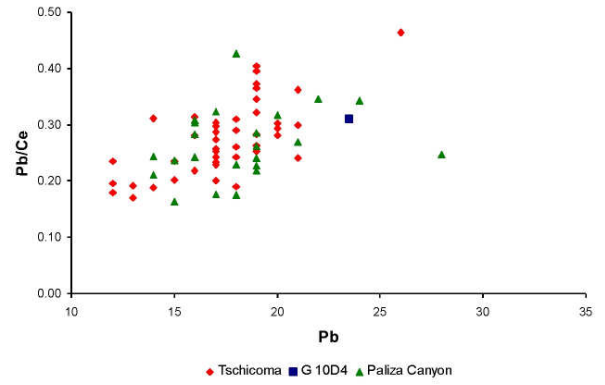
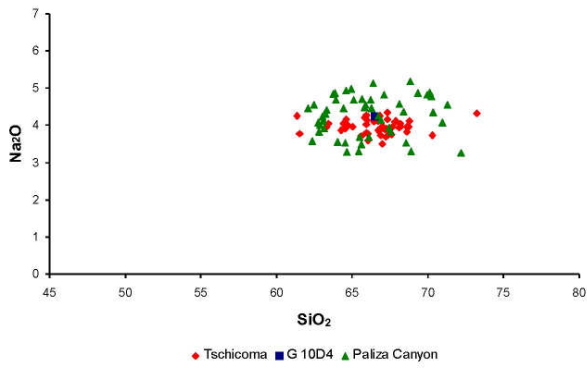


◆ Tschicoma ■ G 10D3 ▲ Paliza Canyon



◆ Tschicoma ■ G 10D3 ▲ Paliza Canyon

G10 D4



G10 D5

